

Interaction of cyclic antimicrobial hexapeptides with model lipid membranes

Dissertation

zur Erlangung des Doktorgrades der Naturwissenschaften
(Dr. rer. nat.)

der

Naturwissenschaftlichen Fakultät II
Chemie, Physik und Mathematik

der Martin-Luther-Universität
Halle-Wittenberg

vorgelegt von

Herrn Sebastian Finger
geboren am 13.06.1982 in Frankenberg / Eder

Gutachter:

1. Prof. Dr. Alfred Blume
2. Prof. Dr. Heiko Heerklotz

Tag der Verteidigung: 30.09.2021

Table of content

1 INTERACTION OF CYCLIC ANTIMICROBIAL HEXAPEPTIDES WITH MODEL LIPID MEMBRANES	1
1 INTRODUCTION	1
1.1 Lipids	1
1.1.1 History of cell membrane models	2
1.1.2 Lipid structures and membrane composition	5
1.1.2.1 Structure of lipids	5
1.1.2.2 Lipid membranes of prokaryotes	7
1.1.2.3 Membrane composition of eukaryotes	8
1.1.3 Lipids - building blocks of cell membranes	9
1.1.3.1 The critical packing parameter (cpp)	10
1.2 Antimicrobial peptides	13
1.2.1 Classes and representatives of AMPs	14
1.2.2 Mechanisms of antimicrobial action	15
1.2.2.1 Lipid clustering model	18
1.2.3 Bacteria resistance strategies towards antimicrobial peptides	20
1.3 Aim of work	21
2 THE PHASE BEHAVIOUR OF BINARY AND TERNARY MIXTURES OF DMPG, DMPE AND TMCL	23
2.1 Introduction	23
2.1.1 Ideal and non-ideal miscibility	23
2.1.2 Electrostatic interactions – general overview	27
2.1.2.1 Gouy-Chapman	28
2.1.3 The effect of electrostatic energy on lipid mixing behaviour	31
2.2 Single lipid components	36
2.2.1 DMPG and DMPE	36
2.2.2 Cardiolipin	38
2.2.2.1 DSC	38
2.2.2.2 ATR-IR	41
2.3 Binary mixtures	45
2.3.1 DMPG/DMPE	45
2.3.1.1 DSC	46
2.3.2 DMPG/TMCL	47
2.3.2.1 DSC	47
2.3.3 DMPE/TMCL	51
2.3.3.1 DSC	51
2.4 Ternary mixtures of DMPG/DMPE/TMCL	53
2.4.1 DSC	53

3 INTERACTION OF CYCLIC ANTIMICROBIAL HEXAPEPTIDES WITH MODEL LIPID MEMBRANES

59

3.1 Introduction

59

- 3.1.1 Cyclic hexapeptides as antimicrobial peptides 59
- 3.1.2 Cyclic peptide secondary structure 61
- 3.1.3 Specific lipid-peptide interactions 69
 - 3.1.3.1 Lipid interaction with lysine and arginine 71
 - 3.1.3.2 Lipid interaction with hydrophobic amino acid residues 72

3.2 Differential Scanning Calorimetry (DSC)

76

- 3.2.1 The impact of cyclic hexapeptides on the phase transition of pure lipid membranes 76
- 3.2.2 Peptide interaction with PG/PE mixed membranes 80
 - 3.2.2.1 Spermine binding to DMPG/DMPE bilayers 80
 - 3.2.2.2 PG/PE mixtures –chain length dependence 81
 - 3.2.2.3 PG/PE mixtures –dependence on chain length difference 87
 - 3.2.2.4 PG/PE mixtures –dependence on lipid mixing ratio 88
 - 3.2.2.5 Comparison of clustering efficacy of c-RWRWRW and c-RRRWWW 90
- 3.2.3 Peptide interaction with Cardiolipin/PE mixed membranes 93
- 3.2.4 Peptide interaction with the ternary lipid mixtures 97
- 3.2.5 Summary 99

3.3 Attenuated Total Reflection Infrared (ATR-IR) Spectroscopy

102

- 3.3.1 Peptide interaction with pure lipid membranes 102
 - 3.3.1.1 Peptide interaction with pure DMPG membrane 102
 - 3.3.1.2 Peptide interaction with pure TMCL membrane 107
 - 3.3.1.3 Comparison of peptide interaction with pure DMPG and pure TMCL membrane 111
- 3.3.2 PG/PE mixtures 113
 - 3.3.2.1 Analysis of the CH₂, CD₂ and lipid carbonyl vibrational band 114
 - 3.3.2.2 Analysis of the guanidinium and indole bands 117
 - 3.3.2.3 Comparison of relative changes in CH₂, CD₂, amide I and guanidinium bands 119
- 3.3.3 TMCL/DMPE mixtures 121
 - 3.3.3.1 Analysis of the CH₂, CD₂ and lipid carbonyl vibrational band 121
 - 3.3.3.2 Analysis of the amide I, guanidinium and indole bands 124
 - 3.3.3.3 Changes in lipid and peptide band frequencies and intensities from first to second upscan 126
 - 3.3.3.4 Effect of lipid mixture on the peptide indole vibrational peak maximum 127
- 3.3.4 Ternary lipid mixture 128
- 3.3.5 Summary 129

3.4 Isothermal Titration Calorimetry

131

- 3.4.1 Pure lipid-peptide interaction 131
 - 3.4.1.1 Peptide interaction with DPPG 131
 - 3.4.1.2 Peptide interaction with TMCL 139
- 3.4.2 PG/PE mixtures 143
- 3.4.3 TMCL/DMPE mixture 154
- 3.4.4 Summary 156

4 CONCLUSIONS

159

4.1 Lipid clustering mechanism

159

- 4.1.1 The stress release model 160
- 4.1.2 The model of macroion induced lipid clustering 161
- 4.1.3 Direct lipid-peptide and peptide-peptide interactions that induce lipid demixing 163

4.2 Consequences for lipid clustering as a model of antimicrobial action

164

5 SUMMARY/ ZUSAMMENFASSUNG	167
5.1 English version	167
5.2 German version	169
6 MATERIAL AND METHODS	173
6.1 Material	173
6.1.1 Chemicals	173
6.1.1.1 Lipids	173
6.1.1.2 Peptides	173
6.1.1.3 Polyamines	173
6.1.2 Vesicle preparation	174
6.2. Methods	174
6.2.1 Differential Scanning Calorimetry (DSC)	174
6.2.2 Isothermal Titration Calorimetry (ITC)	175
6.2.3 Attenuated Total Reflection Infrared (ATR-IR) spectroscopy (Bio-ATR)	175
7 SUPPLEMENTARY	177
7.1 Supplementary to Chapter 1	177
7.2 Supplementary to Chapter 2	179
7.2.1 Supplementary to Chapter 2.3	179
7.2.2 Supplementary to Chapter 2.4	182
7.3 Supplementary to Chapter 3	184
7.3.1 Supplementary to Chapter 3.1	184
7.3.2 Supplementary to Chapter 3.2	186
7.3.3 Supplementary to Chapter 3.3	188
7.3.4 Supplementary to Chapter 3.4	192
8 BIBLIOGRAPHY	201
9 ACKNOWLEDGEMENT	225
10 CURRICULUM VITAE	227
10.1 Personal data	227
10.2. Education and research experience	227
10.2.1 Scientific Publications	228
10.2.2 Patents published	229
11 STATEMENT OF ORIGINALITY	231

Abbreviations

A_L	Area per lipid
AMP	Antimicrobial peptide
A_P	Area per peptide
ATR FT-IR	Attenuated Total Reflection Fourier Transform Infrared Spectroscopy
<i>B. subtilis</i>	<i>Bacillus subtilis</i>
c-	cyclo-
cpp	Critical packing parameter
cryo-TEM	cryo-Transmission Electron Microscopy
δ	Deformation vibration
ΔC_p	Heat capacity difference
ΔG	Free energy change
ΔH	Enthalpy change
DPPE	1,2-dipalmitoyl-sn-glycero-3-phosphoethanolamine
DMPE	1,2-myristoyl-sn-glycero-3-phosphoethanolamine
DPPG	1,2-dipalmitoyl-sn-glycero-3-phosphoglycerol
DMPG	1,2-myristoyl-sn-glycero-3-phosphoglycerol
DPPE-d62	DPPE with perdeuterated acyl chains
DMPE-d54	DMPE with perdeuterated acyl chains
DPPG-d62	DPPG with perdeuterated acyl chains
DMPG-d54	DMPG with perdeuterated acyl chains
$\Delta R C_p$	Heat capacity change upon reaction
ΔS	Entropy change
DSC	Differential Scanning Calorimetry
<i>E. coli</i>	<i>Escherichia coli</i>
F, Phe	Phenylalanine
f_c	Clustering efficiency
GIXD	Grazing incidence X-ray diffraction
θ	Ratio of surface bound peptide to maximal possible surface bound peptide
IRE	Internal Reflection Element (ATR crystal)
IRRAS	Infrared Reflection Absorption Spectroscopy
ITC	Isothermal Titration Calorimetry
K, Lys	Lysine
L_α	Lamellar liquid crystalline phase
L_β, L_β'	Lamellar gel phase, tilted lamellar gel phase
L_c	Lamellar crystalline phase
LC	Liquid condensed
LE	Liquid expanded
LUV	Large unilamellar vesicle
MIC	Minimal Inhibitory Concentration
MLV	Multilamellar vesicle
vas	Anti-symmetric stretching vibration
NMR	Nuclear Magnetic Resonance
ν_s	Asymmetric stretching vibration
P	Power
π	Surface pressure
P_β	Ripple phase
Q	Heat
R, Arg	Arginine

R	Dichroic ratio
R_c	Ratio of peptide to lipid charges
r_{cc}	Critical clustering ratio
S	Order parameter
S	Solid analogues phase
σ_A	Peptide-Lipid area ratio
S.aureus	Staphylococcus aureus
SAXS	Small angle X-ray Scattering
SUV	Small unilamellar vesicle
T_m	Main transition temperature
TMCL	Tetramyristoylcardiolipin (1',3'-bis[1,2-dimyristoyl-sn-glycero-3-phospho]-glycerol)
T_p	Pre transition temperature
W, Trp	Tryptophan
WAXS	Wide angle X-ray scattering
X	Molar ratio
ϕ_P	Lipid volume fraction of clustered lipid in the "peptide area"
ϕ_L	Lipid volume fraction of the remaining lipid mixture.
χ	non-ideality parameter
Ψ_0	Surface potential
z	Charge number

1 Interaction of cyclic antimicrobial hexapeptides with model lipid membranes

Introduction

The smallest functional unit in living organisms is a cell. All cells possess cell membranes that confine the cell from its environment. This compartmentalisation is thought to be an important step in the origin of life when simple amphiphiles assembled and formed microreactors with limited volume that enabled molecules to react by increasing the chance of collision (1-3). During evolution, compartmentalisation by membranes has been used to achieve multi-functionality in a cell. These cells are called eukaryotes and build up all multicellular organisms.

The membrane is a lipid bilayer with embedded or peripherally bound proteins that enable a communication with the environment and account for about half of the membrane mass (4). About one-third of the human genome encodes for membrane proteins (5). Some diseases are connected to a dysfunction of membrane proteins like channelopathies, e.g. epilepsy, cystic fibrosis and myotonia (6). Also some evidence point into the direction that Alzheimer disease is connected to alteration in lipid membrane (7-9). Therefore, the interplay of proteins and lipids is of fundamental interest to understand and treat diseases or to specifically target infected or uncontrolled proliferating cells by smarter drug delivery systems (10).

Proteins span the membranes by alpha-helical or beta-sheet like secondary structures that often assemble into functional clusters. To fundamentally understand these processes, the interplay of peptides, as short protein mimics, with lipid membranes is a topic of interest.

1.1 Lipids

In biological systems, where polymers from carbohydrate, nucleic acids and amino acids build the living matter, lipids form the non-polymeric class of substances that build physiologically essential structures. The resulting structures like e.g. the lipid bilayer, cannot be deduced from the genome, as only the proteins for lipid synthesis are encoded and the properties of the resulting structures need to be actively controlled by the cell (10) to adjust the physical state to the ambient environmental

conditions. For example, lipid membranes of bacteria grown at different temperatures vary in lipid composition to maintain membrane fluidity (4).

Although the membrane is still widely considered as the barrier between the inner and outer cell, a more complex role in physiological processes is meanwhile in focus of research.

1.1.1 History of cell membrane models

The cell membrane first existed as a functional idea since the middle of the 19th century. It was first a hypothesis of an existing barrier between a cell and its environment. In 1877 Wilhelm Pfeffer named the thin layer surrounding the protoplast the “plasma membrane”. In 1895 Charles Ernest Overton found that the ability for different substances to pass a cell membrane increased with increasing partition coefficient of the respective substances between oil and water. He concluded that the membrane must be lipophilic in nature (4).

Ernest Langmuir published in 1917 a technique to measure changes in surface pressures of different liquids, the so-called Langmuir-trough. Eight years later Gorter and Grendel spread extracted lipids of red blood cells on a water surface of this trough. They found that the surface area occupied by the lipid extract is about double the size of the red blood cell surface determined by microscopy. Therefore, the two scientists from Leiden concluded that the cell membrane must be a lipid bilayer with lipophilic parts oriented towards each other and shielded from the surrounding water by a hydrophilic molecule part.

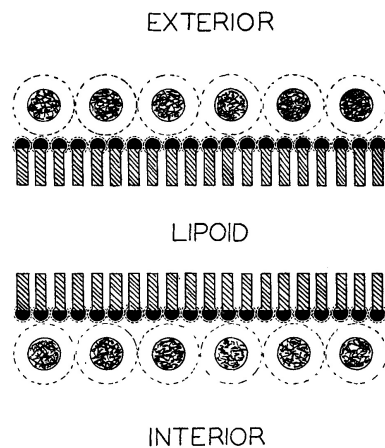


Figure 1-1-1 Membrane model by Danielli and Davson (1935). Taken from (11).

The knowledge that also proteins are amphipathic and that although diluted in the cytosol they interact with the plasma membrane led to the question of how these different classes of molecules can be attached to each other. The first model of adsorbed protein on a lipid bilayer developed by Danielli and Davson occurred in 1935 (Figure 1-1-1).

This model included peripheral bound proteins onto the lipid membrane surface. Experiments in the 60s and 70s pointed to the presence of integral proteins that span the lipid bilayer matrix (12). This

knowledge was included within the fluid-mosaic model by Singer and Nicolson. Figure 1-1-2 shows the drawings published by the authors in 1972 (13), later on often referred to as the “cartoon”.

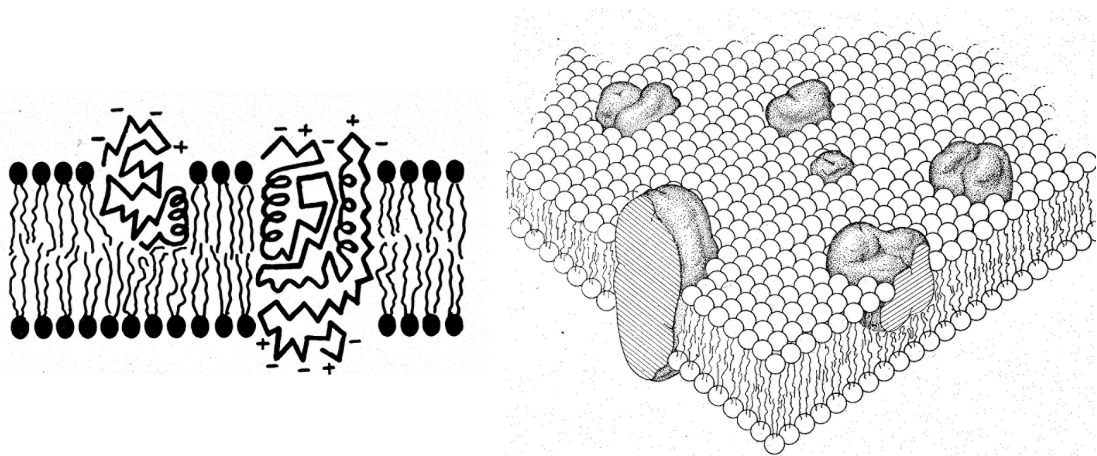


Figure 1-1-2 The fluid-mosaic model by Singer and Nicolson from 1972 showing peripheral and transmembrane proteins embedded in the lipid matrix in cross-section (left) and a 3D-drawing (the “cartoon”, right). Taken from (13).

The novelty of the model is the concept of lateral free diffusion of lipids and proteins within the lipid bilayer matrix, meaning that both perform rotational movements (lipids 10^8 - 10^9 s⁻¹ and proteins 10^3 - 10^5 s⁻¹) and translational movements (the diffusion coefficient of lipids is 10^{-8} - 10^{-9} cm² s⁻¹ and proteins 10^{-9} - 10^{-11} cm² s⁻¹) but no transbilayer movements. Another property of the Singer-Nicolson membrane is the asymmetry, referring here to the different lipid compounds, of the two single lipid monolayers.

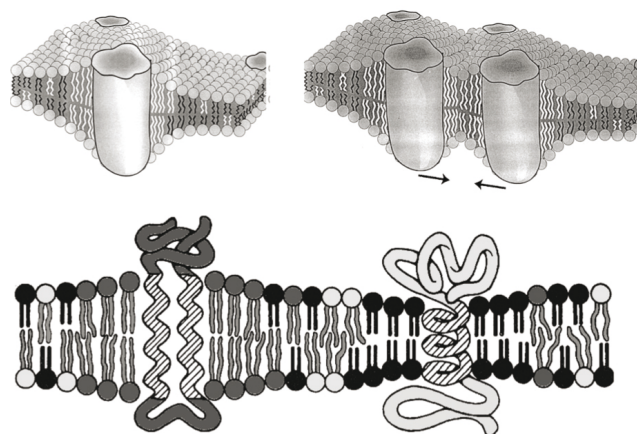


Figure 1-1-3 The Mouritsen Bloom mattress model of cell membranes. Taken from (10).

With increasing data about different membrane protein structures and a variety of data referring to the relation between different lipid composition and membrane protein function led to a new concept: the mattress model of cell membranes. Mouritsen and Bloom presented this model in 1984 to explain the functionality dependence of proteins on lipid membrane composition using the concept of hydrophobic mismatch (14). To avoid water contact of hydrophobic surfaces, the lipids

are sorted into domains around the proteins to match the hydrophobic thickness and to accomplish protein functionality. The energy penalty due to the entropy loss of the lipid mixture is regulated by the energy increments mainly due to the entropy win of water at the lipid-water interface. In biological membranes, a variety of lipid lengths are believed to mediate the different hydrophobic length of proteins, which can lead to protein aggregation and crystallisation as well as to lipid demixing (10).

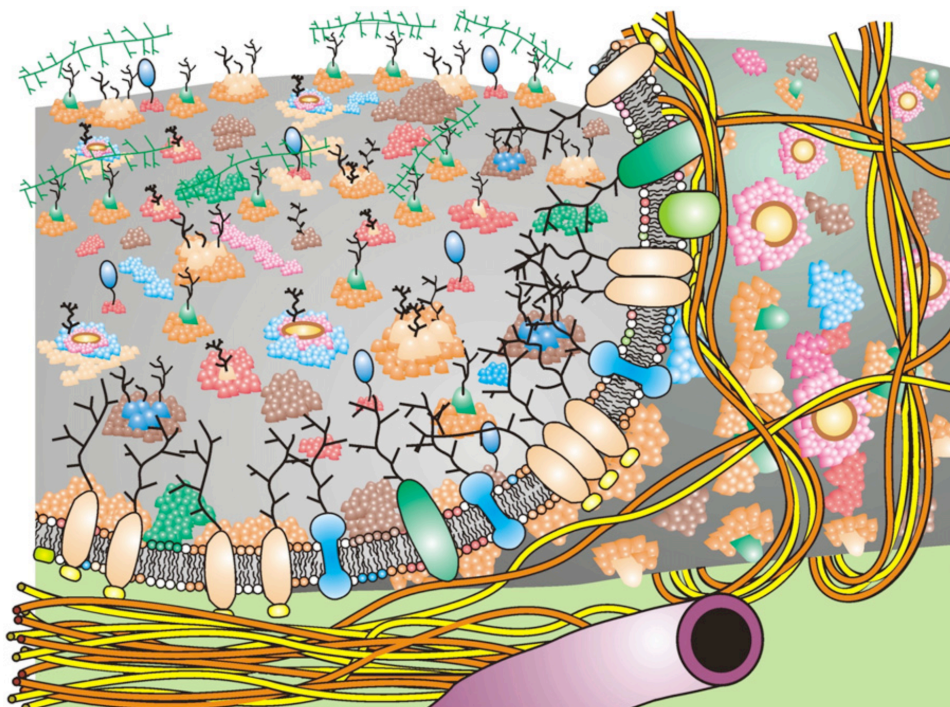


Figure 1-1-4 The updated Fluid-Mosaic Membrane Model by Nicolson. Different integral proteins, glycoproteins, lipids and oligosaccharides are represented by different colours. The membrane has been peeled-up to view the inner membrane surface cytoskeletal fencing is apparent that restricts the lateral diffusion of some but not all trans-membrane glycoproteins. Other lateral diffusion restriction mechanisms are also represented, such as lipid domains, integral membrane glycoprotein complex formation (seen in the membrane cut-away), polysaccharide–glycoprotein associations (at the far top left) and direct or indirect attachment of inner surface membrane domains to cytoskeletal elements (at lower left). Although this figure suggests some possible integral membrane protein and lipid mobility restraint mechanisms, it does not accurately present the sizes or structures of integral membrane proteins, cytoskeletal structures, polysaccharides, lipids, submicro- or nano-sized domains or membrane-associated cytoskeletal structures or their crowding in the membrane. Taken from (15).

The mattress model focuses on the effect of protein or peptide on the lipid mixing behaviour of lipids with varying chain length. The lipid research of the recent years focussed on the effect of mixtures of different lipids on the protein functionality, including the effect of lipid composition on protein motions like conformational transitions, protein assembly (e.g. gramicidin channel (16)) and a possible role of lipid domains to facilitate lateral membrane organisation (5). The focus on translational motion of proteins revealed that for some proteins the translational motion is decelerated or the translational freedom is hindered. One reason is that proteins partitioned in lipid domains are confined in translational freedom within this domain and move along the cell surface with the velocity of the aggregate structure. Larger aggregate structures also result from protein

aggregates, glycoprotein aggregates or polysaccharide-mediated glycoprotein associations. Another reason for confinement in translational mobility is that membrane proteins are attached to the cytoskeleton. They either move along the filaments and therefore relative to the cytoskeleton and the membrane or they are fixed to the cytoskeleton and the protein motion is relative to the membrane they insert into. These findings are included in the updated Fluid-Mosaic Model by Nicolson from 2014 which is shown in Figure 1-1-4.

1.1.2 Lipid structures and membrane composition

The term “lipid” includes different classes of molecules like oils, fats, waxes, terpenes, some vitamins, sterols, phospholipids and sphingolipids. Many of these molecules play an important role in metabolism, but only few of them are main components of cell membranes. In this work we only focus on membrane phospholipids where a short introduction into different lipid classes will be given.

A typical cell membrane contains between hundreds to thousands different lipid species (10) which occur apart from sterols as variations from fatty acids linked to various headgroups forming ester or amide bonds (4, 17, 18).

1.1.2.1 Structure of lipids

The most abundant class are phospholipids, as evolutionary conserved molecules of cell membranes. They are found in all domains of life. Phospholipids acyl chains can be linear and vary in saturation and length or can be branched or even contain alicyclic rings. The majority of unsaturated chains occur in *cis*-form (19) and mostly contain up to three double bonds. Fatty acid chains with more than three double bonds are not found in microorganism but can be found in fungi.

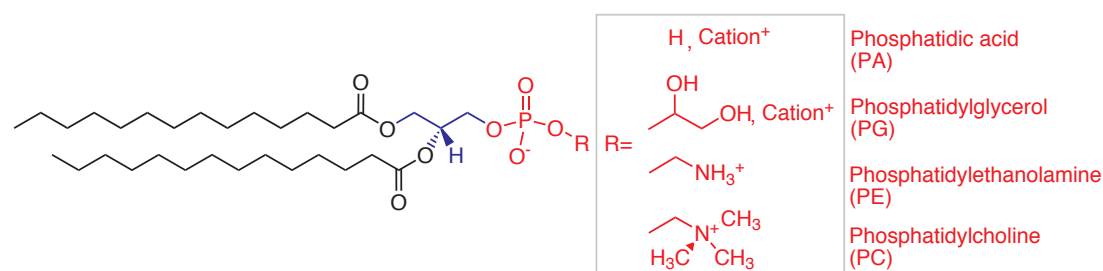


Figure 1-1-5 Structure of phospholipids. The acyl chains (black) are bound to the glycerol (blue). The length and saturation of the chains vary (myristoyl chains are displayed). The lipid headgroup (red) is bound via the phosphate at the glycerol backbone. Four typical membrane lipid headgroup structures are depicted: Phosphatidic acid (PA), Phosphatidylglycerol (PG), Phosphatidylethanolamine (PE) and Phosphatidylcholine (PC).

Figure 1-1-5 exemplifies the structure of phospholipids. In phospholipids, the two fatty acids (here myristic acid in black) form an ester bond with a glycerol molecule (blue) at *sn*-1 and *sn*-2 position, the chiral carbon atom. The third carbon at *sn*-3 position is esterified with a phosphate group to which different molecules can be bound to build different headgroup structures (red). The L-form is the most abundant form in nature. If a glycerol moiety is esterified with the phosphate group, the resulting molecule is called 1,2-dimyristoyl-*sn*-glycero-3-phosphoglycerol, which is abbreviated with DMPG.

Lipoaminoacids are a group of phospholipids containing amino acids, e.g. phosphatidylserine (PS) with a serine bound to the phosphate group. Molecules abundant in bacteria are aminoacyl esters of phosphatidylglycerols (PG), e.g. lysyl-, ornithyl-, or alanyl-PG (19). The amino acid binds to the *sn*-3 hydroxy group of the glycerol headgroup.

Another important lipid class are glycolipids. Glycolipids include various types of lipids containing sugar groups. Mono- or disaccharides bound to phospholipid headgroups are called glycerophospholipids. A widespread representative is the phosphatidylinositol, which plays in different phosphorylation states a major role in lipid mediated cell signalling.

Mono and disaccharides directly esterified by fatty acids are called glycosides. Also acylated diols and polyols (other than glycerol) are found in various organisms (20, 21). Smaller representatives, mostly acyl glycoses, are found in actinomycetes (19).

Other important lipid classes beside phospholipids are sphingolipids and sterols. In sphingolipid structure, a fatty acid is bound by N-acylation of the 2-aminogroup to the backbone molecule sphingosine, forming a ceramide. When the headgroup binds sugar derivatives via an ether bond at the 1-hydroxy group, the molecules are named carbohydrate-ceramides, e.g. glucosyl-, galactosyl- and lactosylceramide. If the headgroup is bound via a phosphate group to the sphingosine, the resulting molecules are sphingolipids, e.g. sphingomyelin (sphingophosphocholin).

Steroids are rigid structures with four rings, three six-membered rings and one five-membered ring in specific molecular configuration which are shown to modulate the membrane miscibility and fluidity. The most abundant steroid in eukaryotes is cholesterol whereas lanosterol, the precursor of cholesterol (22), is also found in prokaryotes (23). The most abundant cyclic structure in prokaryotes that is known to modulate membrane miscibility and fluidity are hopanoids.

1.1.2.2 Lipid membranes of prokaryotes

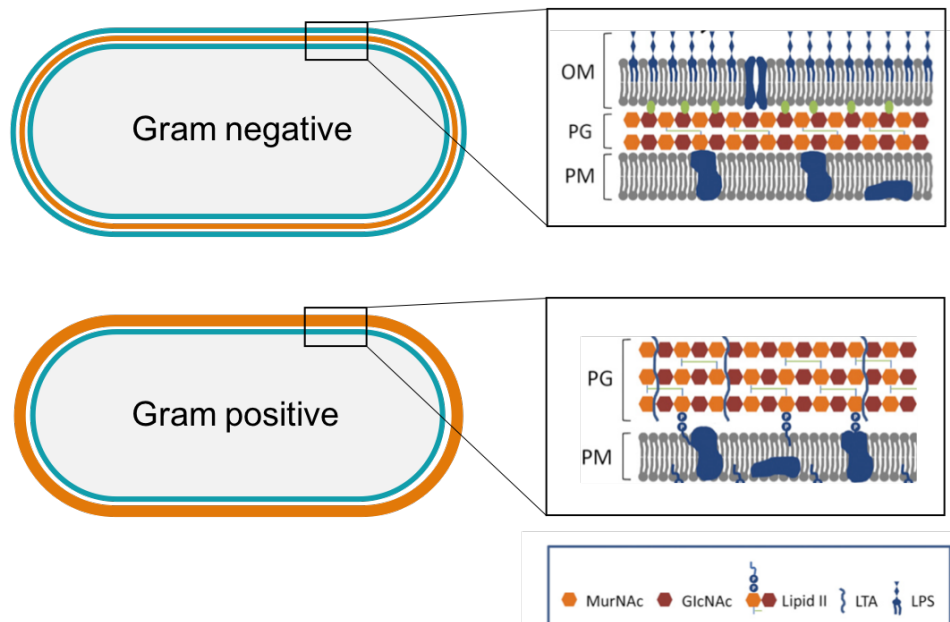


Figure 1-1-6 Bacteria cell wall. In gram positive bacteria the plasma membrane (PM) is surrounded by a thick peptidoglycan layer (PG) that mainly consists of N-Acetylmuramic acid (MurNAc) and N-acetyl-D-glucosamine (GlcNAc). In gram negative bacteria the peptidoglycan layer is much thinner. But a second outer membrane containing lipopolysaccharides (LPS) on the outer monolayer (OM) is present. Also, Lipid II and lipoteichoic acid (LTA) are depicted. Adapted from (24).

Gram-positive bacteria have a cytoplasmic membrane surrounded by peptidoglycan mesh. Gram-negative bacteria possess additionally a second lipid layer surrounding the peptidoglycan mesh (see Figure 1-1-6) with high amounts of lipopolysaccharides present in the outer monolayer which provide certain functionalities like e.g. cell signalling. In bacteria, the Lipopolysaccharides (LPS) are glycosides with a huge oligosaccharide headgroup where the backbone sugars are anchored in the membrane via the acyl chains. The main structural feature is called Lipid A. The headgroup polysaccharide can be structured into a core domain that is similar in many molecules and in the O-specific chain. Depending on this O-specific structure, lipopolysaccharides are responsible for the O-antigenic and endotoxic properties of bacteria.

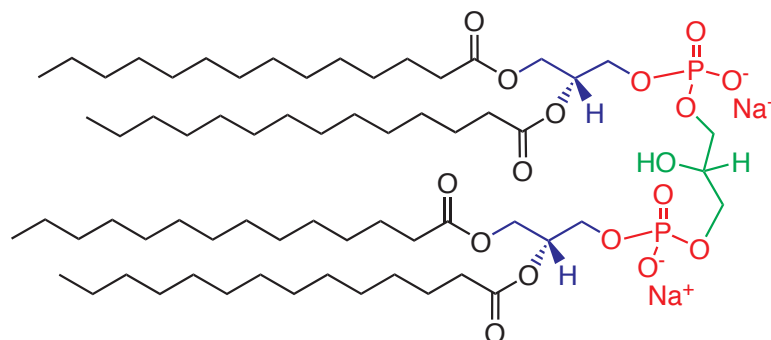


Figure 1-1-7 Structure of cardiolipin (1,3-bis(phosphatidyl)glycerol). Two phosphate groups (red) are linked by a glycerol molecule (green). The acyl chains can vary in length and saturation.

However, phospholipids are the major component of prokaryotic cytoplasmic membranes. The lipid dimer cardiolipin (CL) occurs in high amounts in bacteria. Cardiolipin consists of two phosphatidic acids bridged by a glycerol molecule (see figure 1-1-7). Gram-positive bacteria membranes often contain aminoacylated PG lipids. The most frequent one is LysylPG, which is one of the rare positively charged lipids in nature.

Species	PG	PE	CL	LysylPG	others
<i>Escherichia coli</i> outer membrane	3	91	6	-	
<i>Escherichia coli</i> cytoplasmic membrane	6	82	12	-	
<i>Bacillus subtilis</i>	11	29	47	7	6 (Phosphoglycolipids)
<i>Bacillus flavothermus</i>	39	42	11		8
<i>Bacillus polymyxa</i>	3	60	8		29
<i>Pseudomonas aeruginosa</i> *	21	60	11		8
<i>Salmonella typhimurium</i> outer membrane	17	81	2		
<i>Salmonella typhimurium</i> cytoplasmic membrane	33	60	7		
<i>Yersinia pestis</i> (outer and cytoplasmic membrane)	18	55	15		12

Table 1-1-1 Phospholipid headgroup composition of various bacteria membranes in weight percent. PG = Phosphatidylglycerol, PE = Phosphatidylethanolamine, CL = Cardiolipin, LysylPG = Lysylphosphatidylglycerol. Adapted from (19) and *(25).

As discussed above, some species contain additionally hopanoids or lanosterol with a cholesterol-like effect (22, 23, 26).

Sphingolipids occur in prokaryotes only in a few species: *Bacteroides*, *Sphingobacterium*, *Acetobacter*, *Pseudomonas paucimobilis*, *Bdellovibrio bacteriovorus*, *cystobacter fulvus*.

Table 1 gives some examples of bacteria phospholipid membrane headgroup composition. Please note that the lipid composition not only varies with the bacteria species but also with the respective growth state.

1.1.2.3 Membrane composition of eukaryotes

The variety of lipids in cell membrane increases with the complexity of organisms. As myelin sheets mostly contain sphingolipids, they are the most abundant lipid in higher animal organisms with developed nerve systems (10). They show the highest phase transition temperature of natural occurring lipids (27) as the highest occurrence is with long and saturated chains.

Besides sphingolipids, mainly zwitterionic phospholipids together with cholesterol constitute eukaryotic membranes. Some examples of plasma membrane composition of different eukaryotes are given in Table 1-1-2.

Membrane	PC	PE	PS	PI	SM	CL	Glycolipid	Chol.	Others
Erythrocyte	20	18	7	3	18	-	3	20	11
Plasma membrane (rat liver)	18	12	7	3	12	-	8	19	21
Nuclear membrane	44	17	4	6	3	1	-	10	15
Mitochondria	38	29	0	3	0	14	-	3	13
Neurons	48	21	5	7	4		3	11	1

Table 1-1-2 Lipid head group composition of different eukaryotic cell membranes in weight percent. PC = Phosphatidylcholine, PE = Phosphatidylethanolamine, PS = Phosphatidylserine, PI = Phosphatidylinositol, SM = Sphingomyelin, CL = Cardiolipin, Chol. = Cholesterol. Adapted from (4).

1.1.3 Lipids - building blocks of cell membranes

Lipids show lyotropic and thermotropic phase behaviour. At low water content, where the hydration of the headgroup is less pronounced, cubic and hexagonal phases are observed (28, 29). Here, only the phase behaviour in excess of water is further discussed. The lamellar phase at high water content shows a thermotropic behaviour for most double-chain phospholipids. For exemplification, Figure 1-1-8 displays the lyotropic and thermotropic phase behaviour of DPPC suspension at high water content. At low temperatures a lipid gel phase (L_{β}) bilayer is formed containing mostly all-trans lipid chain configurations. Under certain conditions, even crystalline phases (L_c) with densely packed all-trans chain lattice in three-dimensional order are observed. The all-trans chains can also be tilted with respect to the membrane normal to compensate for increased lipid headgroup area which is denoted by the prime in the L_c' or L_{β}' phase. With increasing temperature, the ripple phase (P_{β}') with periodic one-dimensional ripples is formed above the pretransition temperature (T_p). These periodic one-dimensional ripples are discussed to result from periodic arrangements of coexisting gel (L_{β}') and liquid crystalline (L_{α}) domains with opposing signs of curvature (30, 31). At the lipid main transition temperature T_m , the lipid bilayer undergoes a transition into the liquid crystalline (L_{α}) phase, where a “melting” of lipid chains is observed. This means that the all-trans chain lattice order is lost as the chains form gauche conformers leading to an increased lipid chain area but a decreased membrane thickness.

Details of the phase morphology of the lipids DMPG, DPPG, DMPE, DPPE and TMCL used in this study are discussed in Section 2.2 for the single components and in Section 2.3 for the binary mixtures thereof.

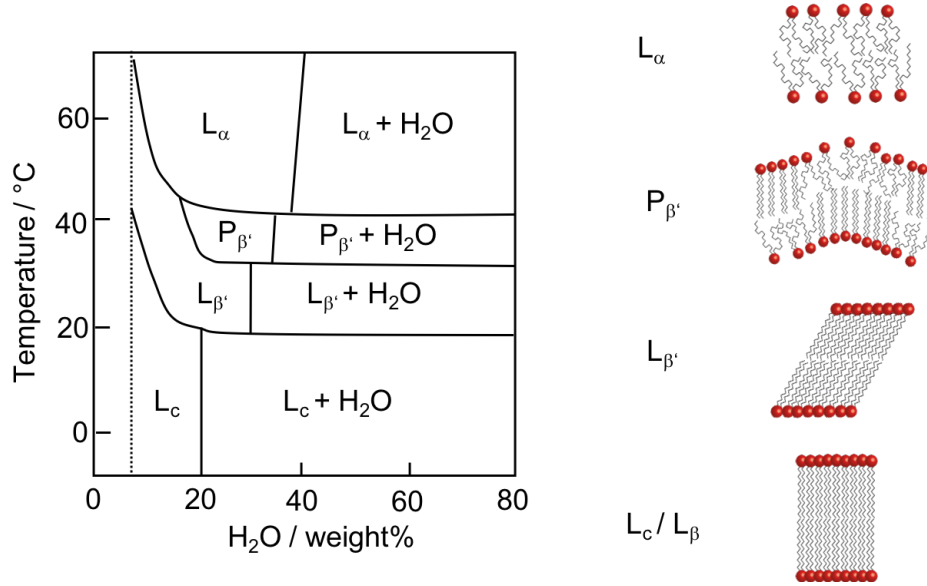


Figure 1-1-8 is an extract of a DPPC-water phase diagram with the lyotropic in x and the thermotropic behaviour in y direction. For simplicity the phases at low water content is not shown. Adapted from (4, 32, 33).

1.1.3.1 The critical packing parameter (*c_{pp}*)

The molecular form concept from Jacob N. Israelachvili from 1985 introduces a theory to predict the structures formed by amphiphiles. The formed aggregates are a result of the thermodynamics and two opposing intraaggregate forces tending to increase and decrease the molecular area, respectively, as schematically depicted in Figure 1-1-9.

The attractive force (F_γ) arises mainly from the interfacial tension at the hydrophobic-hydrophilic interphase with an approximate surface energy of 20 to 50 mJ m⁻² (34). In some cases, another contribution might result from lipid headgroup interaction, like ion mediated dipole or hydrogen bonding interactions. The repulsive force contributions are more complex and result on the one hand from rotational motion of lipid chains, summarized in chain forces (F_c). On the other hand, lipid headgroup hydration force, steric contribution and electrostatic repulsion in case of charged lipids build up the lipid headgroup forces (F_h). The interfacial energy μ_N can be described by

$$\mu_N = 2\gamma a_0 + \frac{\gamma}{a_0}(a - a_0)^2 \quad (1.1)$$

where γ denotes the interfacial free energy per unit area, a the interfacial area per amphiphilic molecule and a_0 the optimal area per molecule at which μ_N reaches a minimum.

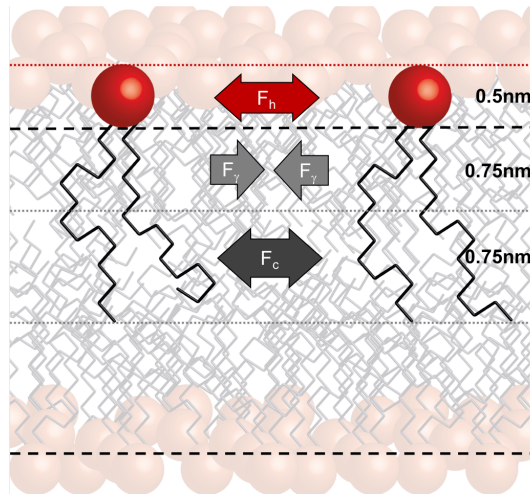


Figure 1-1-9 displays the lateral pressure distribution of a lipid bilayer. F_c is the repulsive lateral force resulting from rotational motions of lipid chains. F_γ in the interphase region results from the reducing surface tension γ by reducing the hydrophobic area in contact with hydrophilic molecules. F_h is the lipid headgroup lateral pressure resulting from steric, hydrational and electrostatic effects. It can, however, contain attractive forces, resulting from e.g. hydrogen bonding between lipid headgroups. Adapted from (29, 34).

This means the membrane adapts a state in which the attractive and repulsive interactions balance each other. The free energy is minimal with respect to the membrane area and the derivative of the free energy with respect to the area, i.e. the surface tension of a lipid bilayer, is zero (35).

The existence of an optimal area leads in return to the structure concept in which the amphiphiles can obtain an optimal packing depending on the molecular shape, the *critical packing parameter* c_{pp} . The critical packing parameter is a ratio of hydrophobic volume divided by the headgroup area and the molecular length.

$$c_{pp} = \frac{V_{hc}}{a_0 l_{hc}} \quad (1.2)$$

Where V_{hc} is the volume of the hydrocarbon chains, l_{hc} the maximum effective length of the hydrocarbon chain and a_0 is the optimal interfacial area. Some structures which are formed by amphiphiles of different c_{pp} are depicted in Figure 1-1-9. From X-ray data the overall bilayer thickness d_{hh} and the headgroup area a_0 can be obtained. The length of the hydrocarbon chain can be calculated by subtracting the headgroup length from the overall bilayer thickness.

$$l_{hc} = \frac{1}{2} d_{hh} - \left(\frac{V_{hg}}{a_0} \right) + 1.5 \text{ \AA} \quad (1.3)$$

The added 1.5 Å accounts for the carbonyl bond which is subtracted with the headgroup area. A comprehensive review on the chain packing of various lipids is given by Derek Marsh (36). Examples of c_{pp} values for different lipids is given in Table S1-1-1. Small values, as obtained for surfactants like e.g. sodium dodecyl sulphate (SDS), form micelles which can be spherical or obtain

prolongated cylindrical or rod-like shapes. An increased cpp value leads to extension of cylindrical structures that assemble into a hexagonal phase (H_I phase). By reaching a cpp value of about 1 for cylindrical or truncated cone shapes, the molecules assemble into planar bilayers which themselves can form vesicles to reduce the entropy contribution of the hydrophobic part in contact with water at the bilayer edges. Typical examples are the here discussed double chain phospholipids and dimers thereof as in case of cardiolipin. For molecules with increased cpp values above 1, like monogalactosyl diglyceride (MGDG), cubic and inverted hexagonal phases are observed. However, lipid phase morphology also depends on other parameters like temperature or ionic strength in case of charged lipids. Temperature influences the cpp value as lipid chains become more “fluid” with increasing temperature, resulting in a hydrophobic volume increase. Ions in solution influence the optimal headgroup size of lipids by screening headgroup charges and influence hydration forces. These effects will be discussed in more detail in Section 2.2 for the lipids used in this study.

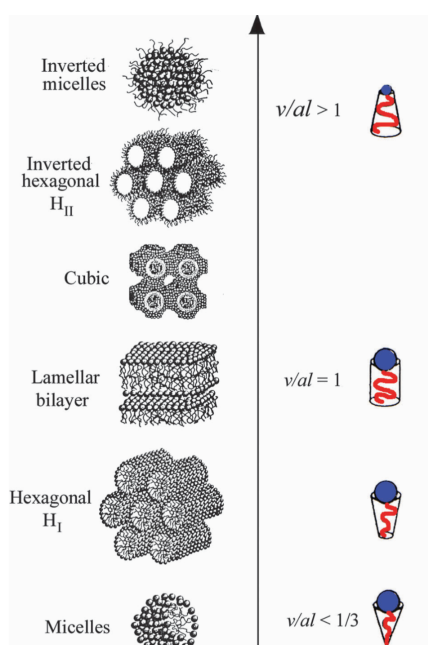


Figure 1-1-10 displays a schematic illustration of structures of aggregated amphiphiles in aqueous solutions in dependence of their critical packing parameter, $cpp = v/al$. Taken from (10).

In ideal lipid mixtures the mean intermediate cpp of the individual components governs the resulting aggregate properties (34). For example, insertion of molecules resulting in a larger mean cpp value can transform a bilayer into inverted hexagonal or cubic lipid phases. The insertion of detergents with small packing parameters ($cpp < 1$) can transform a lipid bilayer into hexagonal or micellar phases (37). For example, mixtures of Dilinoleoylphosphatidylethanolamine (DLPE) and Palmitoyloleoylphosphatidylcholine (POPC), one preferring the hexagonal H_{II} phase and one the bilayer phase, adopt a bilayer phase if the mixture contains more than 20 mol% of the bilayer-preferring lipid (38).

1.2 Antimicrobial peptides

Some peptides are evolutionary ancient molecules for innate immune response, therefore named antimicrobial peptides (AMPs). As we are facing a post-antibiotic era (39) mostly generated by the misuse of antibiotics in human and animal healthcare, especially in meat mass production (40-42), the research of new antimicrobial substances focussed, besides other topics, on antimicrobial peptides.

The discovery of penicillin in the ascomycetus fungi *penicillium rubens* by Alexander Fleming in 1928 was followed by numerous attempts to produce synthetic antibiotics. However, the creation of a systematic knowledge about the variety of naturally occurring antimicrobial substances for innate immune response and their respective action mechanism is still in progress.

Perhaps, a first systematic approach to understand evolutionary strategies of antimicrobial peptide host defence goes back to Pierre Joly. He advised Jules Hoffmann during his research stay in the group of professor Joly, based on his experience during organ transplantations of insects, to focus on the phenomenon of the immunity of grasshoppers (43):

“Professor Joly proposed to me the study of antimicrobial defences in grasshoppers. In fact, as he explained, his laboratory had over decades transplanted endocrine organs and even whole brains from one insect to another without ever taking antiseptic precautions, but they had never observed the appearance of opportunistic infections. To Professor Joly, this could only be explained if efficient antimicrobial defences existed in these insects.”

Since the first discovery of antimicrobial peptides, more than 3000 antimicrobial peptides have been found to date (<http://aps.unmc.edu/AP/class.php> (44)). In mammals, antimicrobial peptides are for example synthesised in skin epithelium, in the mucosa of the intestinal tract, as well as in respiratory and reproductive organs.

Up to now, computational analyses and synthetic combinatorial libraries (45-47) of natural occurring antimicrobial peptide structures succeeded to predict sequences of small artificial model peptides with high antimicrobial potency that found their way into clinical trials (48). The most common feature of AMPs is their amphipathic structure; therefore, the synthesized small artificial peptides contain mostly the charged residues arginine, histidine and lysine and the hydrophobic amino acids tryptophane, isoleucine, leucine and phenylalanine (49).

1.2.1 Classes and representatives of AMPs

Antimicrobial peptides mostly contain less than 100 amino acids. Key elements of antimicrobial peptides are the high net positive charge at physiological pH and the content of about 30% or more hydrophobic amino acid residues (50). Different classifications exist in literature. Some classifications sort AMPs by the biological source in bacterial AMPs (bacteriocins (51)), plant AMPs, animal AMPs including subclasses like e.g. insect, amphibian, fish, reptile, mammal AMPs etc. Another classification is based on the biological activity against certain organism e.g. antibacterial, antiviral, antifungal, wound healing, etc. Here, the minimal inhibitory concentrations, i.e. the lowest concentration of an antimicrobial peptide at which growth of a bacterium, virus or fungus is inhibited, are used for classification. Typical values for antimicrobial peptides range from 1 to 500 $\mu\text{g mL}^{-1}$. Some values for antimicrobial peptides that are subject of several publications referenced within this work are summarised in Table S1-2-1. Another classification, which is related to the mechanism of action is based on peptide properties, e.g. the net charge and the amphiphilicity. At current state, for about 13% of the known AMPs the 3D secondary structure is identified (52) which gives an additional opportunity for classification. Depending on the primary sequence antimicrobial peptides often adopt a secondary structure by the interaction with lipid membranes. This classification varies between different authors but four major classes are common (53). One class contains linear and α -helical peptides of which bombin, LL-37, magainin and melittin are famous examples. A second class contains β -sheet peptides like protegrin-1. A third class includes all circular antimicrobial peptides of which polymyxin B is a prominent example. The minimal inhibitory concentrations of these examples can be found in Table S1-2-1. A fourth class contains all “non-regular” peptides (50) that cannot be included in one of the three classes.

A different approach is to classify antimicrobial peptides by the encoding genome. The two major families are defensins and cathelicidins. Defensins are antimicrobial peptides mostly occurring in mammals and predominantly expressed in neutrophils and epithelial cells (54, 55). They are rich in β -sheet structures and contain disulphide bonds that are crucial for the secondary structure but not for antimicrobial activity.

The cathelicidin family encompasses all antimicrobial peptides that are encoded in a highly variable cathelicidin peptide domain as a precursor to the highly conserved cathelin protein domain (56) including examples like magainin, protegrin or LL-37. From the interspecies homology among different vertebrates the first appearance of cathelicidins in evolution can be estimated to 300 to 500 million years ago (57).

Besides the antimicrobial peptides targeting the cell membrane, antimicrobial peptides with different antimicrobial action exists. Lantibiotics like nisin target lipid II of the outer membrane and precursors for cell wall synthesis. Some proline-rich antimicrobial peptides have been shown to kill

bacteria by inhibiting the protein synthesis. These classes of antimicrobial peptides will not be further discussed within this work.

1.2.2 Mechanisms of antimicrobial action

Many different models describe the mechanism of antimicrobial action, most of them explaining a higher permeability of the lipid membrane after peptide binding (see Figure 1-2-1). Each different model explains features found for few peptides, to what Wimley and Hristova (58) referred to as the blind men describing an elephant (from “The blind men and the elephant” by John Godfrey Saxe), meaning that due to some observed effects different models were proposed, but a comprehensive explanation of antimicrobial peptide action is still missing. To shed some light on the relations of different models, the topical interest is to quantify the observed effects to be able to make predictions of antimicrobial activity and specificity of a given peptide sequence.

AMPs generally consist of charged residues, often with a positive net charge, to distinguish between the mostly negatively charged membranes of bacteria from membranes of the host organism (see Section 1.1.2 for more details). The hydrophobic amino acid residues are thought to contribute to the binding constant to anchor the peptide in the membrane. Nevertheless, this contribution is not only due to the “classical” entropy driven hydrophobic effect, i.e. the entropy increase by release of organized water molecules around the hydrophobic moiety, but also depends on “non-classical” enthalpic and entropic contributions occurring from formation of peptide secondary structures and membrane effects (59-62).

In all the different models one can distinguish between the peptide stabilizing a pore formation, which is mainly described for amphipathic α -helices but also β -sheet peptides like protegrin-1 (63, 64) and the models in which the peptide disrupts the membrane integrity and activity.

For the pore forming peptides the steps of initial surface binding, insertion and aggregation (pore formation) are critical for the antimicrobial action. The free energy of the transition from surface bound to membrane spanning has been simulated to be 13.2 ± 0.8 kcal mol⁻¹ for melittin in a POPC bilayer (100mM NaCl) with a P/L ratio below the ratio of antimicrobial activity (65). Above a critical ratio, when a certain surface concentration is exceeded the free energy is reduced to 9.6 ± 1.9 kcal mol⁻¹ for this transition. This cooperative effect results from a deeper penetration of water molecules into the hydrophobic bilayer region with higher membrane surface concentration of peptides (65). The hydrophobic surface accessed by water is reduced by transition to the transmembrane state. This transition was earlier discussed as threshold ratio for antimicrobial activity (66). If one peptide is already arranged perpendicular, the free energy for the transition for the second melittin is reduced to 5.1 ± 0.8 kcal mol⁻¹ (67, 68). Another contribution to the gibbs free energy of this process comes from the caused hydrophobic mismatch, i.e. a difference in length of hydrophobic lipid chain region and hydrophobic amino acids of peptide or protein sequence inserting into the membrane. The lipid

or the protein equals the difference in length by either stretching or tilting (69) or by a change in protein conformation to reduce the water accessible hydrophobic surface. This model has been supported by numerous studies investigating the effect of membrane insertion of proteins and peptides (5, 70-72) into membranes of different thickness and might also be a decisive parameter for the peptide selectivity towards the target bacteria membrane.

The *barrel stave model* is discussed since the early 70s (73-76). After initial membrane binding the peptides insert into the membrane and aggregate into a pore structure. One extensively studied example for a barrel stave pore is the alamethicin pore (77-82) for which the oligomeric α -helices assemble into an octameric structure (83). For dermcidin, a human skin antimicrobial peptide secreted by sweat glands (84), the peptide assembly in the bacteria membrane is stabilized via electrostatic interactions of charged amino acids incorporated into hydrophobic membrane region. The hexameric peptide assembly is stabilized by the presence of zinc ions already in solution and bound to the membrane surface before it subsequently inserts into the membrane, triggered by transmembrane voltage. In the *toroidal pore model*, the membrane spanning peptides do not interact with each other but are loosely associated with interdigitating lipid headgroups shielding the hydrophobic membrane core. Here, polar and charged residues found in the hydrophobic face of the amphipathic peptides, referred to as “imperfect amphipathicity”, are discussed to drag the lipid headgroup into the membrane centre and therefore stabilising the high curvature membrane resulting in a pore that is lined by peptides and lipid headgroups (63). The toroidal pore was first described for magainin interacting with model lipid membranes in 1996. Matsuzaki et al. (85) observed higher lipid flip-flop rates of fluorescently labelled lipids by the addition of peptides which could be explained by interconnecting both lipid monolayer leaflets via pore formation resulting in one continuous monolayer. This is in line with the observation that magainin and the short chain derivative MSI-78 mainly interacts with the lipid headgroup (86-88) and was soon after supported by neutron scattering measurements showing a pore formation of larger size than expected for a barrel stave model (89).

More recent simulation studies show that the pore formation takes place after a certain threshold peptide surface concentration is reached as a result of local tension induced by the peptide (90).

Furthermore, the peptides are more disordered than initially assumed which leads to a refined *disordered toroidal pore model* which was shown for magainin (90) and melittin (91). The acquired helix orientations are not only 0° and 90° with respect to the membrane normal as initially assumed by the toroidal pore model but obtain also angles between 45° and 90° along the formed channel and $5-20^\circ$ at the channel rim. Recently, also LL-37 was shown to induce toroidal pores or act in a carpet model manner (76, 92).

The *carpet model* (93) is an extreme case of the (disordered) toroidal pore model in which the pore formation leads to separation of micellar or bicellar lipid-peptide aggregates (78). The action of the antimicrobial peptides is often compared to the solubilisation of lipid membranes by detergents

where detergent molecules with low *c_{pp}* insert into the membrane until saturation occurs and the membrane is in equilibrium with saturated micelles (37, 94-96). Here, the detergent like manner refers to the intercalation of the peptide into the interphase region of the outer monolayer acting like a wedge, comparable to the low *c_{pp}* value of the detergent and resulting in a curvature strain (97, 98). According to this concept, phase diagrams can be obtained where the model of action can be deduced from the *c_{pp}* values of the membrane forming lipids and the peptide concentration. The micelle formation occurs for membranes containing mainly lipids with a *c_{pp}* value of about 1 and higher and high peptide concentration which is confirmed by using combined optical and mass-measuring methods in real time biosensor technologies (99).

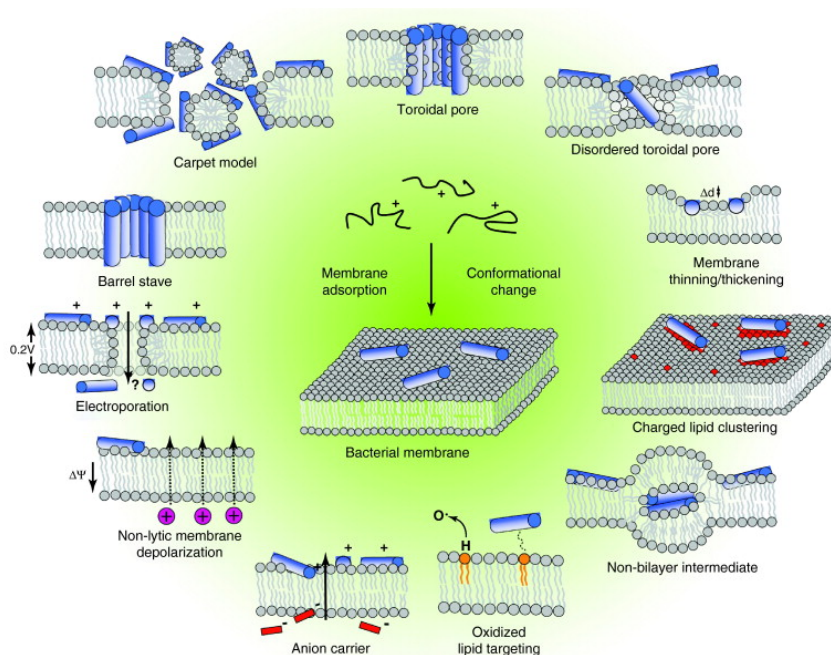


Figure 1-2-1 Events occurring at the bacterial cytoplasmic membrane following initial antimicrobial peptide (AMP) adsorption. These events are not necessarily exclusive of each other. In the classical models of membrane disruption, the peptides lying on the membrane reach a threshold concentration and insert themselves across the membrane to form either peptide-lined pores in the barrel-stave model, solubilize the membrane into micellar structures in the carpet model, or form peptide-and-lipid-lined pores in the toroidal pore model. In the revised disordered toroidal pore model, pore formation is more stochastic and involves fewer peptides. The thickness of the bilayer can be affected by the presence of the peptides, or the membrane itself can be remodelled to form domains rich in anionic lipids surrounding the peptides. In more specific cases, non-bilayer intermediates in the membrane can be induced; peptide adsorption to the membrane can be enhanced by targeting them to oxidized phospholipids; a peptide may couple with small anions across the bilayer, resulting in their efflux; the membrane potential can be dissipated without other noticeable damage; or conversely, in the molecular electroporation model, the accumulation of peptide on the outer leaflet increases the membrane potential above a threshold that renders the membrane transiently permeable to various molecules including the peptides themselves. Taken from (63).

Another antimicrobial mechanism targeting membranes with oxidized lipids results from the finding that the antimicrobial peptides temporin B and L intercalate more efficiently into lipid bilayers with oxidized lipid chains (100). Inherent in many of the previously discussed models are also impacts on the lipid membrane that might be side effects or by itself already lead to antimicrobial action like

electroporation (see discussion above), changes in membrane potential, e.g. by accumulation of the charged peptide on the lipid membrane or coupled peptide-ion transport by peptides with cell penetrating activity, as well as membrane thinning upon lipid binding or lipid clustering.

1.2.2.1 Lipid clustering model

Some molecules induce lipid segregation upon binding to a lipid membrane. This phenomenon is called “clustering”. The term is widely used when positively charged antimicrobial peptides induce lipid segregation of anionic lipids and non-charged or zwitterionic lipids. However, a peptide induced lipid segregation by antimicrobial peptides was also observed between two negatively charged lipids (101). The clustering ability was shown to increase with increasing peptide charge for peptides showing antimicrobial and cell penetrating properties (102).

Examples for antimicrobial peptides inducing lipid segregation is the naturally occurring helical peptide PGLa (103), the β -turn protegrin-1 (104) and HNP-2 (105) or the cyclic peptide polymyxin (106, 107). Also synthetic linear hexa- (108, 109) and nonapeptides (110) as well as cyclic hexapeptides (108) displayed a lipid clustering in mixed membranes.

Lipid clustering might also play a physiological role, e.g. in protein insertion and stabilisation or transduction of information. A study of Vanounou et al. (111) shows that PG and PE are segregated into different domains in an active bacteria cell. However, this is still a matter of research and will not be further discussed within this work.

For the role of lipid clustering in the antimicrobial activity of antimicrobial peptides two general mode of actions can be differentiated.

First, the clustering can be an initial step enabling the peptide to induce pore formation. Epanand et al. showed that short-chain derivatives of the cathelicidine LL-37, which is discussed to act as a pore forming peptide (see above), are incapable of pore formation but induce lipid segregation. Their respective antimicrobial activity was sustained against bacteria with high contents of zwitterionic lipid (*E. coli*), where the clustering has a more pronounced effect than for membranes with high content of negatively charged lipids (*S. aureus*) where the antimicrobial activity is contained (112). This shows that lipid segregation can already have antimicrobial effect without pore formation but it also indicates that lipid segregation might be a crucial intermediate state in pore formation as it is discussed for the antimicrobial peptide pleurocidin (113). This is supported by the finding that increased membrane tension leads to peptide insertion (90) and the accumulation of charges can lead to high local electric fields sufficient for transient pore formation (114). Also the aggregation of dermaseptin which led to the carpet model could be triggered by lipid clustering as clustering was observed for PC/PS mixed SUVs (93). Furthermore, antimicrobial specificity towards certain bacteria strains can result from the membrane composition, where clustering depends on the charge,

headgroup and alkyl chain distribution of the lipid species (112, 115-117). A similar result as for LL-37 derivatives was obtained for Magainin and respective derivatives including the highly charged MSI-78 (118). Moreover, these peptides even showed the capability of segregating two ionic lipids, DMPG and TOCL, from each other (101).

Second, the lipid-protein interplay is altered as a result of changes in lateral lipid organization influencing protein adsorption or insertion kinetics or inhibiting membrane protein functionality affecting cell homeostasis like cell division (119), metabolism, communication to the cell environment, structural integrity, taxis or growth.

Alteration in lipid miscibility can affect lipids with specific binding sites to protein structures. The activity of some membrane proteins has already been shown to be dependent on the presence of specific lipids (120-126). It has e.g. been shown that the ADP/ATP carrier (AAC) complex in yeast mitochondria dissociates upon depletion of cardiolipin (127, 128), whereas depletion of PE stabilizes AAC supercomplexes (129), both resulting in a reduced cytochrome *c* oxidase activity and a decreased membrane potential.

Moreover, the protein activity can also be distorted by changes in the physical state of the membrane affecting the lipid matrix or annular lipids surrounding the proteins (124, 125). Here, e.g. changes in distribution of charges over the membrane surface will affect binding of proteins and cofactors as well as ions which are necessary for protein functionality such as Ca^{2+} in close proximity to the protein. Also hydrophobic mismatch is crucial for protein functionality (5, 130-133) and can be altered by lipid clustering. Clustering might also affect protein functionality by changes in lipid phase state (133-135), in lipid free volume (125, 136, 137) or in critical packing parameter. As the resulting lipid phase is a sum of different forces acting on the lipids (29, 34, 138, 139), the cell membrane bilayer structure is maintained by containing non-bilayer forming lipids with low *c_{pp}* values. Changes in lateral pressure affects the protein functionality (140-142). Cytochrome *c* for example, induces a bilayer structure to cardiolipin, preferring an inverted hexagonal (H_{II}) phase (143).

Wenzel et al. (144) and Scheinpflug et al (145) reported examples for more complicated mechanisms of AMP action. They demonstrated recently how the cell homeostasis of *B. subtilis* is affected by the hexa-peptides RWRWRW-NH₂ (of which the cyclic analogue is part of this study) and the cyclic peptide c-RRRWW, respectively. They could show that the cytoplasmic membrane is the target of this trivalent cationic hexapeptide. As a result of RWRWRW-NH₂ addition they observed dissociation of cytochrome *c* from the outer membrane leaflet resulting in diminished intracellular ATP content and a breakdown of the membrane potential. The authors also reported a release of glutamine/glutamate and asparagine/aspartate by *B. subtilis* to the extracellular medium as response of osmotic stress. Lateral pressure as a result of osmotic stress leads to an increase in lipid area and thinning of the lipid membrane what can be sensed and regulated by mechanosensitive channels like MscL (146). This indicates that the binding of the short cationic hexapeptide induces lateral pressure,

e.g. by increasing the lipid area in the outside monolayer. A consecutive study with acyl chain modified derivatives indicate a similar mode of action as similar membrane proteins are up- or downregulated after peptide binding (147, 148).

Scheinflug et al. observed a lipid demixing accompanied with a delocalisation of membrane proteins upon addition of the cyclic peptide. In both studies MurG, a membrane protein involved in cell-wall biosynthesis, dissociated from the cytosolic membrane surface after addition of both hexapeptides, leading to an inhibition of cell-wall synthesis. Without cell wall lysis in the LysCDEF deficient strain, no membrane rupture upon the addition of c-RRRWFW was observed. This indicates that addition of c-RRRWFW disturbs the equilibrium of cell-wall synthesis and cell-wall lysis, which leads to the lipid membrane disruption. The authors linked the effect of lipid domain formation and protein delocalisation to the observed retardation in membrane fluidity. However, changes in membrane viscosity was shown to not largely effect the protein functionality as a dynamic phase boundary at the protein-lipid interphase exists (125, 149-151). This in result would mean that the protein delocalisation already leads to the inhibition of bacteria cell growth most likely due to constrains in protein-protein interactions or the inhibition of protein functionality is due to other changes in lipid membrane (see discussion above). In a simulation study binding of α -helical Ltc1 increases the PG domain size in a PG/PE 3:7 mixture resulting in slower diffusion times of the lipid domain and the single PG molecules (152). Therefore, the observed effects might result from changes in the lipid composition as a result of lipid domain formation. As the membrane state of the bacteria remains unresolved the universality of the observed effects and probable specificities related to AMP structures and membrane composition need to be further investigated in future studies.

1.2.3 Bacteria resistance strategies towards antimicrobial peptides

To understand the mechanism of antimicrobial action it is worthwhile investigating the mechanism bacteria developed during evolution to survive the presence of antimicrobial peptides. Furthermore, some understanding might come from a deeper investigation of AMPs that are produced by organisms to control growth of competitive organisms and therefore are target of antimicrobial peptides themselves, such as Gramicidin S produced by *Bacillus subtilis* (153).

Bacteria developed strategies like the active AMP export, proteolytic inactivation of AMPs (154) or inhibition by extracellular binding (155-158). As the peptides are active on the cell membrane or the inner cell and need to pass the outer murein layer, also the D-alanylation of teichoic acids increases the resistance by modification of the surface charge density or by increasing the cell wall density (159).

As the bacterial membrane plays a central role in antimicrobial action another mechanism to circumvent peptide binding are changes in membrane composition that prevents either a first binding or the further antimicrobial action (58). This can include modification of Lipid A like

phosphorylation, hydroxylation, addition of amino-sugars, phosphoethanolamine (160), glycine (156) or the change of O-Antigen length (157) as well as acylation and diacylation of fatty acids. However, different membrane lipid composition might be in conflict to bacteria growth potential such as fast cell proliferation (56).

Another strategy to induce antimicrobial peptide resistance by modifying the cell membrane is the aminoacylation of phosphatidylglycerols. The sn-3 position of the head group glycerol is esterified with either lysine, ornithine, arginine or alanine forming the respective aminoacid-PG. This modification is performed by the membrane protein multiple peptide resistance factor (MprF) and its homologues (161). This mechanism of resistance is explained as a possibility of bacteria to control the membrane net charge and therefore the binding affinity of antimicrobial peptides. Nevertheless, the conversion of PG to aminoacid-PG might change more physical membrane parameters that influence not only the binding but also the mode of antimicrobial action. It was shown that susceptibility towards MprF depletion only occurs for a number of AMPs (159). In a comparative study of the effect of different AMPs on MprF deficient *S. aureus* and model membranes consisting of PG and lysyl-PG, Andrae et al. (162) could show that the depth of peptide penetration and the formation of lipid clusters can play a certain role in peptide-membrane interactions leading to different resistance effects. Kilelee et al. (163) studied the reaction kinetics with Förster resonance energy transfer of a tryptophan containing cationic AMP on model membranes composed of different PG/lysyl-PG ratios labeled with an acceptor fluorophore. Their results show no major influence of lysyl-PG on the binding constant but a major impact on membrane leakage resistance within a lysyl-PG concentration range found in *S. aureus* clinical isolates. The authors also explain these effects by the occurrence of lipid clusters during peptide binding.

1.3 Aim of work

This study seeks to investigate the relation between lipid membrane composition and peptide structure on the clustering effect to unravel the key features responsible for peptide induced lipid segregation.

To mimic bacterial membranes, model membranes consisting of PG, PE and cardiolipin in binary and ternary mixtures are used. The physical properties of these different mixtures with respect to their mixing behaviour are described in Section 2 of this work.

These investigations are crucial to study the effect of different membrane properties, such as charge density, chain tilt or miscibility on the lipid-peptide interaction. Therefore, polyamines with three and four charges are studied in comparison to cyclic hexapeptides with three charges resulting from either arginine or lysine moieties. The charged amino acids are arranged with the hydrophobic amino

acids tryptophan and/or phenylalanine in different sequences with different resulting antimicrobial efficacy. Section 3 deals with this interaction with focus on understanding whether the lipid clustering correlates to the antimicrobial efficiency. Therefore, the efficiency of the different hexapeptides in inducing lipid cluster formation (f_c) in different model lipid membranes is compared to the antimicrobial efficacy. Furthermore, the variation in peptide structure should create an understanding on how changes in peptide amino acid sequence may alter lipid clustering. Furthermore, the occurrence of a threshold concentration (or a critical clustering ratio r_{cc}) at which clustering appears is investigated in dependence of peptide sequence and membrane composition. The aim is to propose a mechanism on how lipid-peptide interaction lead to lipid clustering and how this model can help to understand the antimicrobial efficacy and selectivity of antimicrobial peptides.

2

The phase behaviour of binary and ternary mixtures of DMPG, DMPE and TMCL

2.1 Introduction

Biological membranes contain at least three different types of phospholipid headgroups. Therefore, ternary mixtures are the simplest models to mimic the possible ongoing processes present in a biological membrane. To understand the effect of peptides (or any other molecule) on lipid membranes it is necessary to study the physical properties of the membrane itself. We focussed on the miscibility of the lipids in the membrane and the respective effect on the thermotropic lipid bilayer phase behaviour.

2.1.1 Ideal and non-ideal miscibility

The thermotropic phase behaviour of mixtures reveals information about the miscibility of the observed system. For example, upon heating, the lipids undergo a transition from gel to fluid phase. In each phase the free energy is described by:

$$\Delta G = \sum_i n_i \mu_i \quad (2.1)$$

where the chemical potential for each component in each phase is given by

$$\mu^{g,fl} = \mu^{\circ g,fl} + RT \ln x^{g,fl} \quad (2.2)$$

with μ° being the standard chemical potential and the mole fraction x of the lipid in the respective phase. In the gel to fluid phase transition of the lipid the equilibrium between both phases is described by $\mu^g = \mu^fl$ (g = gel phase, fl = fluid phase). The ratio of lipid mole fraction in the fluid and the gel phase is therefore

$$\frac{x^{fl}}{x^g} = e^{\left(\frac{\mu^{\circ fl} - \mu^{\circ g}}{RT}\right)} \quad (2.3)$$

With $\Delta\mu^o = \Delta H^o - T\Delta S^o$ and the entropy of the phase transition at T_m (the phase transition temperature) $\Delta S^o = \Delta H^o / T_m$, the equation of the ratio of lipid mole fraction in the fluid and the gel phase for one single component becomes

$$\frac{x^{fl}}{x^g} = e^{\left(-\frac{\Delta H^o}{R} \left(\frac{1}{T} - \frac{1}{T_m}\right)\right)} \quad (2.4)$$

In a binary lipid mixture, the mole fraction of both components (A and B) in each phase must add up to one.

$$x_A^{fl} + x_B^{fl} = 1 \quad (2.5)$$

$$x_A^g + x_B^g = 1 \quad (2.6)$$

Combining equation (2.4) with equation (2.5) and (2.6), the temperature dependence can be described as a function of phase transition temperature and enthalpy of the respective single component (4) which can easily be converted to the mole fraction dependence of the temperature.

$$T = \frac{\Delta H_A}{\frac{\Delta H_A}{T_{m,A}} - R \ln \left(\frac{x_A^{fl}}{x_A^g} \right)} \quad (2.7)$$

$$T = \frac{\Delta H_B}{\frac{\Delta H_B}{T_{m,B}} - R \ln \left(\frac{(1-x_A^{fl})}{(1-x_A^g)} \right)} \quad (2.8)$$

Figure 2-1-1 middle displays the solidus and liquidus curve (from equation (2.7) and (2.8)) of a mixture of two components with a phase transition temperature of 23°C (296.15 K) and 50°C (323.15 K) and a phase transition enthalpy of 7.2 kcal mol⁻¹ for both components. The graphs on the left and right display the solidus and liquidus curve for a mixture with the same transition temperatures, $T_{m,A}$ and $T_{m,B}$ but a transition enthalpy of 14.4 kcal mol⁻¹ for the higher melting component (left graph) and the lower melting component (right graph), respectively. The area between both graphs describes the phase coexistence regions.

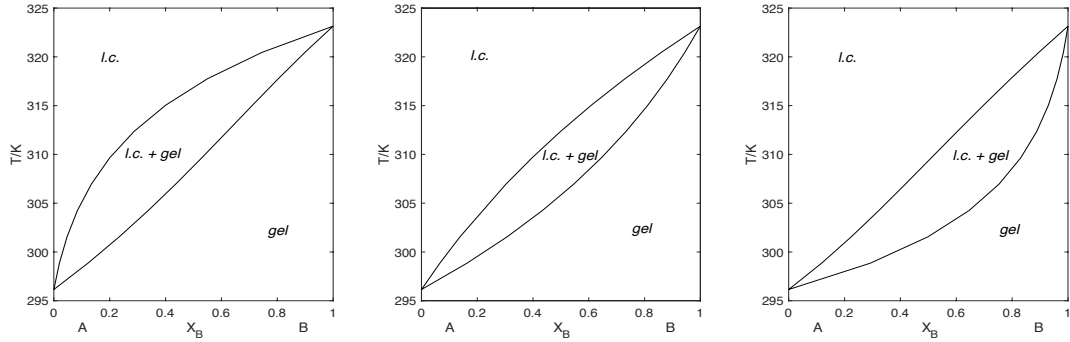


Figure 2-1-1 Phase diagrams of ideal mixtures. The solidus (x_B^g) and liquidus (x_B^l) are plotted versus temperature for two components with $T_{m,A} = 23\text{ }^\circ\text{C}$ (296.15 K), $T_{m,B} = 50\text{ }^\circ\text{C}$ (323.15 K) and different enthalpies: Left: $\Delta H_A = 7.2\text{ kcal mol}^{-1}$, $\Delta H_B = 14.4\text{ kcal mol}^{-1}$. Center: $\Delta H_A = 7.2\text{ kcal mol}^{-1}$, $\Delta H_B = 7.2\text{ kcal mol}^{-1}$. Right: $\Delta H_A = 14.4\text{ kcal mol}^{-1}$, $\Delta H_B = 7.2\text{ kcal mol}^{-1}$.

This phase behaviour describes an ideal mixture, i.e. each component is randomly distributed. The Gibbs free energy of mixing is a function of enthalpy and entropy of mixing, meaning the difference between the pure component and the component in the mixture.

$$\Delta G_{mix} = \Delta H_{mix} - T\Delta S_{mix} \quad (2.9)$$

The entropy contribution can be calculated from $\Delta G_{mix} = x_A\mu_A + x_B\mu_B$ (equation (2.1)) and equation

(2.2) and with $S = -\left(\frac{\partial G}{\partial T}\right)_{p,n}$ and (equation (2.6)) to be

$$\Delta S_{mix} = -R(x_B \ln x_B + (1 - x_B) \ln(1 - x_B)) \quad (2.10)$$

The maximum in ΔS_{mix} is reached at $x = 0.5$. A plot of ΔS_{mix} versus x is shown in the supplementary data S2-3-4. Here, the probability that the neighbouring molecule is of same kind or different is equal. This leads to the typical ‘‘cigar-shape’’ of the ideal phase diagram as shown in Figure 2-1-1 middle.

In the ideal solution no interaction between both molecules is regarded ($\Delta H_{mix} = 0$), meaning that

$$\Delta G_{mix}^{ideal} = RT(x_B \ln x_B + (1 - x_B) \ln(1 - x_B)) \quad (2.11)$$

In a regular solution, however, the enthalpic contribution (no additional entropy contribution, $\Delta S_{mix,excess} = 0$) between two like (A-A or B-B) and unlike (A-B) molecules are considered. Including this excess-enthalpy with $\Delta H_{mix}^E = \rho x_B(1 - x_B)$, the Gibbs free energy of mixing is described by

$$\Delta G_{mix} = \rho x_B(1-x_B) + RT(x_B \ln x_B + (1-x_B) \ln(1-x_B)), \quad (2.12)$$

where ρ is the non-ideality parameter or regular solution parameter for a symmetric mixture, which describes the deviation from ideal behaviour. It describes the energy needed to transform A-A or B-B to A-B pairs and can be calculated by

$$\rho = \frac{1}{c} \frac{(\varepsilon_{AB} - \frac{1}{2}(\varepsilon_{AA} + \varepsilon_{BB}))}{RT} \quad (2.13)$$

The mixing energy is a result of attractive or repulsive interactions between A and B which are denoted by ε with c being the coordination number (164). Here, ε is negative for attractive and positive for repulsive interactions.

This additional enthalpy adds to the chemical potential for each phase and each component like

$$\mu_A^f = \mu_A^{0,f} + RT \ln x_A^f + \rho^f (1-x_A^f)^2 \quad (2.14)$$

$$\mu_A^g = \mu_A^{0,g} + RT \ln x_A^g + \rho^g (1-x_A^g)^2 \quad (2.15)$$

$$\mu_B^f = \mu_B^{0,f} + RT \ln(1-x_A^f) + \rho^f (x_A^f)^2 \quad (2.16)$$

$$\mu_B^g = \mu_B^{0,g} + RT \ln(1-x_A^g) + \rho^g (x_A^g)^2 \quad (2.17)$$

For the thermodynamic equilibrium $\mu^g = \mu^f$ the equation combines to a relation of the temperature, enthalpy, mole fraction and non-ideality parameter, from which the phase diagrams can be calculated:

$$T = \frac{\Delta H_A + \rho^f (1-x_A^f)^2 - \rho^g (1-x_A^g)^2}{\frac{\Delta H_A}{T_{m,A}} - R \ln \left(\frac{x_A^f}{x_A^g} \right)} \quad (2.18)$$

$$T = \frac{\Delta H_B + \rho^f (x_A^f)^2 - \rho^g (x_A^g)^2}{\frac{\Delta H_B}{T_{m,B}} - R \ln \left(\frac{(1-x_A^f)}{(1-x_A^g)} \right)} \quad (2.19)$$

For a non-ideality parameter of 0 one obtains the equation describing the ideal mixture (equation (2.7) and (2.8), (4, 165)).

Figure 2-1-2 depicts exemplified topological features of phase diagrams determined from regular solution theory (166). Negative non-ideality parameters in both phases lead to a narrowing of the phase coexistence region of the “cigar-shape” phase diagram as depicted in the lower left corner in

Figure 2-1-2. A negative non-ideality parameter in the solid phase leads to an azeotropic maximum and a negative fluid phase non-ideality to an azeotropic minimum when the solid phase non-ideality parameter is 0. In case of small positive non-ideality parameters the coexistence phase is broadened but the “cigar shape” is maintained. When the non-ideality parameter reaches a critical value χ_{sp} , phase separation is observed.

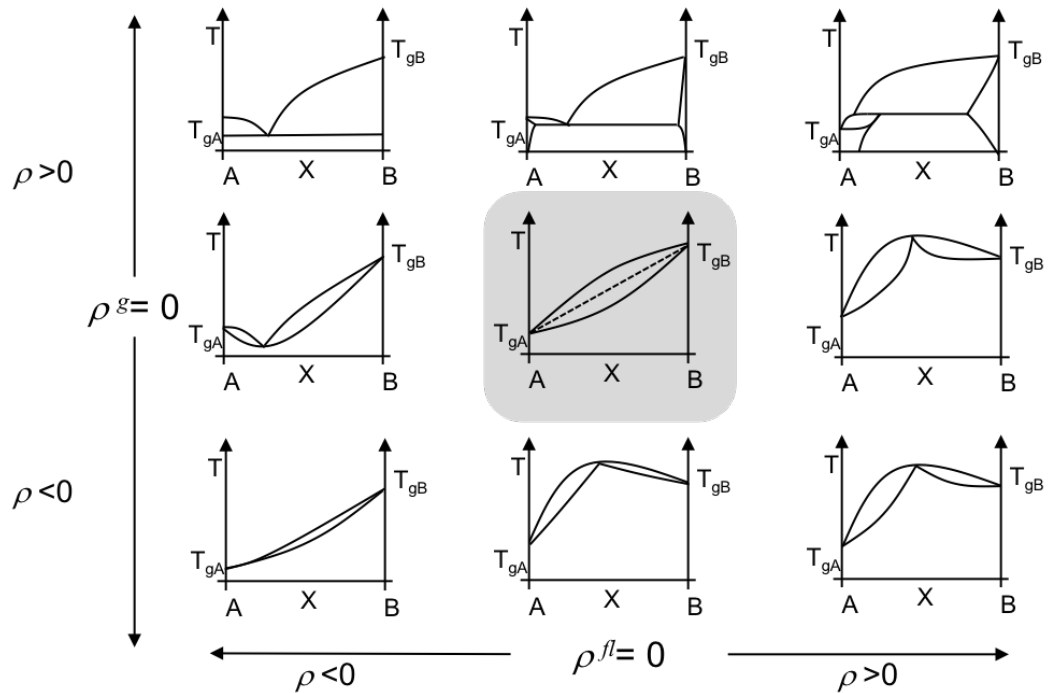


Figure 2-1-2 Topological features of phase diagrams determined from regular solution theory in dependence of the non-ideality parameter in the solid (y-axis) and fluid (x-axis) phase (adopted from (166)).

For positive non-ideality parameters ($\rho > \chi_{sp}$) in the solid phase, the mixture shows eutectic behaviour for negative or low fluid non-ideality parameters. In case of positive non-ideality parameters in the solid and liquid phase the mixture changes to a peritectic or monotectic behaviour. However, this is only a general rule of thumb valid for large positive and negative contributions.

2.1.2 Electrostatic interactions – general overview

About 10-40% of naturally occurring lipids are negatively charged (4). Examples are shown in Table 1-1 and Table 1-2. Therefore, electrostatic interactions as long-range interactions play an important role in biophysical processes, e.g. the interaction of positively charged peptides or proteins with negatively charged lipid vesicles. Charges especially impact the lipid membrane miscibility.

As like-charges repel and unlike-charges attract each other, charged lipids are not randomly distributed in solution. As they can counteract the lipid mixing or demixing tendency, they add to the free energy of a system.

For lipid membranes one can distinguish between 3 different effects of electrostatic interactions (167):

- i. nonspecific screening effects at the membrane surface that stabilise the charges by the formation of an ionic atmosphere.
- ii. shifts in the apparent pK due to the influence of surface charges and of the ionic strength on the ionization of surface groups
- iii. specific effects due to the binding of counterions. This is discussed in more detail in Chapter 3 for the binding of trivalent positively charged cyclic hexapeptides.

2.1.2.1 Gouy-Chapman

In a system containing a charged planar surface the cations of the solution will be repelled and the counterions will be attracted with closer distance to the surface. The charge density, i.e. the distribution of ions in the electric field, can be described by the Boltzmann relation:

$$\rho_{el} = \rho_{0,el} e^{\frac{-ze\Psi_0}{kT}} \quad (2.20)$$

where e is the elementary charge, Ψ_0 the electrical surface potential, k the Boltzmann constant and T the temperature. The charge density ρ is related to the electrostatic potential by the Poisson equation:

$$\frac{d^2\Psi}{dr^2} = -\frac{\rho_{el}}{\epsilon_0\epsilon} \quad (2.21)$$

where ϵ is the dielectric constant. The combination of equation (2.20) and (2.21) leads to the Poisson-Boltzmann equation

$$\frac{d^2\Psi}{dr^2} = -\frac{\rho_{0,el}}{\epsilon_0\epsilon} e^{\frac{-ze\Psi_0}{kT}} \quad (2.22)$$

For the charged planar surface the charge density σ plays an important role in the system characteristics. The total net charge of the solution will be equal and opposite to the surface charge.

$$\sigma = -\int_0^{\infty} \rho_{el}(r) dr \quad (2.23)$$

The so-called Grahame equation gives a relation between the surface charge density σ and the electrical surface potential Ψ_0 as a combination of equation (2.21), (2.22) and (2.23) by

$$\sigma = -\int_0^{\infty} \rho_{el}(r) dr = \epsilon_0 \epsilon \int_0^{\infty} \frac{d^2 \Psi(r)}{dr^2} dr = -\epsilon_0 \epsilon \left(\frac{d\Psi(r)}{dr} \right)_{r=0} = \left(\sqrt{8\epsilon_0 \epsilon kT} \sinh \left(\frac{e\Psi_0}{2kT} \right) \right) \quad (2.24)$$

or

$$\Psi_0 = \frac{2kT}{e} \sinh^{-1} \left(\sqrt{\frac{1}{8\epsilon_0 \epsilon kT} \frac{\sigma}{\sqrt{C}}} \right) \quad (2.25)$$

It can be seen that the surface potential Ψ_0 varies with the surface charge density σ and the reciprocal square root of the concentration c . The surface charge density is the number of charges per unit area in $C m^{-2}$, which, in case of lipids, can be determined by the mole fraction and the molecular area A_m of the charged lipid in the membrane:

$$\sigma = \frac{z_{lipid} e}{A_m} x_{Lipid} \quad (2.26)$$

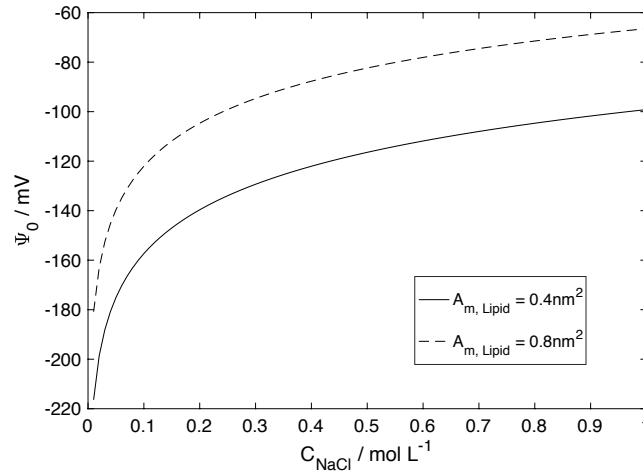


Figure 2-1-3 The dependence of the electrical surface potential Ψ_0 on 1:1 electrolyte concentration (here NaCl) for a lipid membrane with all-trans chains and a lipid containing fluid alkyl chains.

Figure 2-1-3 shows the dependence of the surface potential in mV for a negatively charged lipid membrane with two lipid A_m values on the electrolyte concentration of the surrounding medium, here a 1:1 electrolyte. It can be seen that the surface potential decreases most significantly within one phase state by adding a 1:1 electrolyte until a concentration of 100-150 mM is reached. In this concentration range the lipid phase transition leads to a change in surface potential by about 30-40 mV.

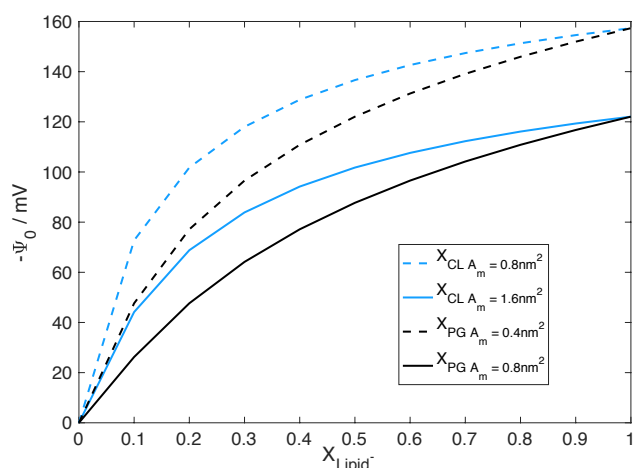


Figure 2-1-4 The dependence of the electrical surface potential Ψ_0 on the lipid mol fraction of a charged lipid in a mixture with a zwitterionic lipid at a given NaCl concentration of 100 mM. Displayed is the mole fraction dependence of the single charged lipid (here named PG) with two all-trans and two fluid alkyl chains and a divalent lipid (here named CL) with four all-trans and four fluid alkyl chains. The A_m for the zwitterionic lipid is 0.4 nm^2 for the gel and 0.8 nm^2 for the fluid phase, respectively.

The dependency of the surface potential on the molar fraction of a charged lipid with two A_m values in a mixed membrane is depicted in Figure 2-1-4. Here, the surface charge density was calculated for a single charged lipid containing two alkyl chains, e.g. PG, and a doubly charged lipid with four lipid alkyl chains like cardiolipin in a mixture with zwitterionic lipid with two alkyl chains, e.g. PE or PC. As the area A_m in equation (2.26) is also dependent on the mole fraction for mixtures of lipids with different areas, the surface potential of PG and cardiolipin in dependence of their respective molar fraction is not the same. The increase in surface potential with increasing molar fraction of charged lipid is much steeper for the doubly charged lipid with four lipid alkyl chains. For a 1:1 ($x = 0.5$) mixture of charged and zwitterionic lipid with same area the value in surface potential is the same as for the 1:2 mixture of a dimerised charged lipid with a zwitterionic lipid ($x = 0.33$). The largest differences in surface potential between both lipids of more than 20 mV occur in a molar fraction range of charged lipid of 0.15-0.35 in the gel and 0.1-0.3 in the fluid phase membrane.

2.1.3 The effect of electrostatic energy on lipid mixing behaviour

For mixtures containing charged lipids the influence of electrostatic free energy ΔG^{el} adds to the free energy of mixing and contributes for a 1:1 mixture of charged and uncharged molecules in a 100 mM salt solution with about 0.35 kcal mol⁻¹ (167).

$$\Delta G_{mix} = \Delta G_{mix}^{el} + \Delta G_{mix}^{ideal} + \Delta G_{mix}^{excess} = \Delta G_{mix}^{el}(x) + RT(x \ln x + (1-x) \ln(1-x)) + \rho x(1-x) \quad (2.27)$$

Gelbart and Bruinsma derived G^{el} from the Poisson-Boltzman equation for the limits of large and small interbilayer distances D , i.e. two bilayers in a distance much smaller and much larger than the Chapman length (168). The Chapman length, ξ , combines the Bjerrum length with the charge density σ with.

$$\xi = \frac{l}{l_B \sigma} \quad (2.28)$$

The electrostatic free energy of mixing can be calculated for large interbilayer distance by

$$G_{mix}^{el}(x) = A \left(2\sigma (\ln(2\pi l_B \sigma^2 v_0) - 1) + \frac{\pi}{4 l_B D} \right), D \gg \frac{1}{l_B \sigma} \quad (2.29)$$

and for small interbilayer distance by

$$G_{mix}^{el}(x) = A \left(2\sigma \ln\left(\frac{\sigma v_0}{D}\right) + 4\pi \sigma^2 l_B D \right), D \ll \frac{1}{l_B \sigma} \quad (2.30)$$

with A being the lipid area, σ the surface charge density, v_0 the counterion volume, D the interbilayer distance and l_B the Bjerrum length. As $G^{el}(x)$ for the pure component is $x G_{mix}^{el}$ with $x = 1$, the difference ΔG_{mix}^{el} of the charged component in the mixture (after mixing) and the pure component (before mixing) can be calculated by

$$\Delta G_{mix}^{el}(x) = G_{mix}^{el}(x=1) - x_{el} G_{mix}^{el}(x) \quad (2.31)$$

The contribution of ΔG_{mix}^{el} to ΔG_{mix} in equation (2.27) can be calculated for bilayers with large or small interbilayer distance by inserting equation (2.29) or (2.30) into equation (2.31), respectively. Figure 2-1-5 displays ΔG_{mix} for an uncharged mixture (left) and small (middle) or large interbilayer distance (right) of mixtures with one charged component, here x_B .

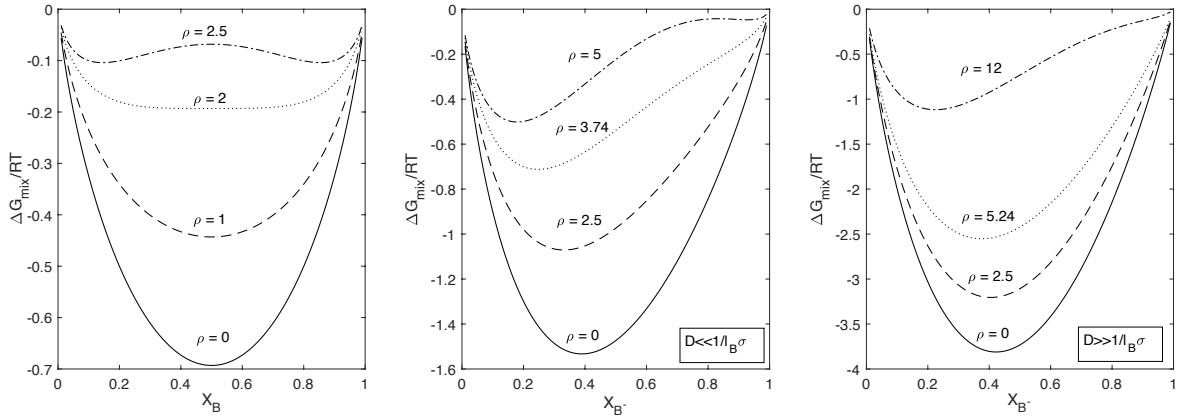


Figure 2-1-5 Plots of ΔG_{mix} for uncharged system (left) and mixtures with charged component B for small (middle) and large (right) interbilayer distances calculated from equation (2.27). The dotted line displays ΔG_{mix} for the non-ideality parameter $\rho = \chi_{sp}$.

For mixtures with one charged component ΔG_{mix} becomes more negative due to the mixing contributions of electrostatic repulsion. ΔG_{mix} is more negative for large interbilayer distance. Moreover, the minimum in ΔG_{mix} shifts to the lower mol fraction of the charge component.

Gelbart and Bruinsma also derived the spinodal equation for the two boundary conditions of small and large interbilayer distance (168). For a non-charged system the non-ideality parameter as a function of molar fraction is described by

$$\chi_{sp}(x) = \frac{(1/2)}{x(x-1)} \quad (2.32)$$

This equation predicts a minimum of $\chi_c = 2kT$ at $x = 0.5$, meaning that for $\chi > 2kT$ phase separation occurs (169).

For the approximation with interbilayer distance larger than the Chapman length ($D > 1/l_B\sigma$) equation (2.32) including charged lipids changes to

$$\chi_{sp}(x) = \frac{5/2 - 2x}{x(1-x)}, D \gg 1/l_B\sigma \quad (2.33)$$

For interbilayer distances far below the Chapman length the calculation of non-ideality parameter changes to

$$\chi_{sp}(x) = \frac{3/2 - x}{x(1-x)} + \frac{4\pi l_B D}{A_L}, D \ll 1/l_B\sigma \quad (2.34)$$

Where A_L is the area per lipid molecule. Figure 2-1-6 displays the dependence of χ_{sp} on the molar fraction calculated from equation (2.32), (2.33) and (2.34). As in Figure 2-1-5 it can be seen that the presence of charges leads to an increase in non-ideality parameter, i.e. a stabilisation of membrane miscibility, which is expected as the like-charges repel each other. However, with decreasing interbilayer distance the critical non-ideality parameter at which demixing occurs is significantly lowered. The minimum of the spinodal shifts to molar fraction with increasing charged lipid content. Therefore, a demixing of a charged membrane, i.e. when $\rho > \chi_{sp}$, is expected to occur at high molar ratios of the charged component.

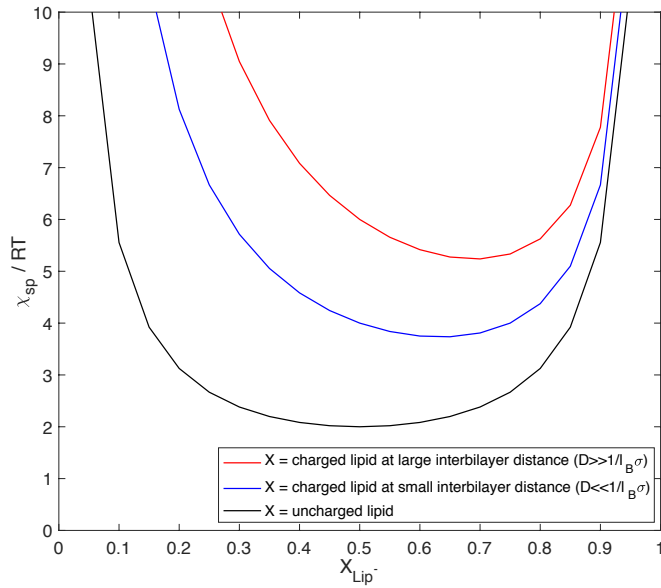


Figure 2-1-6 The dependence of the non-ideality parameter χ_{sp} on X_{Lip} for uncharged membranes and charged membranes with interbilayer distances above and below the chapman length (redrawn from Gelbart and Bruinsma (168)).

A similar shift to higher molar fractions and higher non-ideality parameter with decreasing counterion concentration was also reported by May et al. (170). More importantly, the authors calculated the effect of large counterions on the lipid membrane miscibility considering local changes in membrane composition. Here, the free energy of polyvalent counterions adsorbed to a lipid membrane is a sum of four terms:

$$G = G_{el}(x, \theta) + M_{\max}(\theta \ln \theta + (1 - \theta) \ln(1 - \theta)) + x \ln x + (1 - x) \ln(1 - x) + \rho x(1 - x) \quad (2.35)$$

The first term is the free energy of the contributions from electrostatic interactions, the second term includes the entropic contributions from the bound large polyvalent counterions where θ is the ratio of bound molecules, M , to the maximal possible bound molecules M_{\max} ($\theta = M/M_{\max}$), restricted by the surface area. The third term describes the neutral membrane with its entropic contribution and the fourth term the excess enthalpy of mixing contributions (see equation (2.12)). The authors used

the volume fraction ϕ instead of the molar fraction x which is also used for the next paragraph to enable the reader a fast tracking of the original publication.

Including the local change in membrane composition by binding of polyvalent macroions, the spinodal equation derived by the authors is

$$\chi_{sp} = \frac{1}{2\sqrt{\sigma_A} \Delta\phi\theta(1-\theta)} \frac{d\theta}{d\phi}. \quad (2.36)$$

Here, σ_A is the ratio of peptide to lipid area $\sigma_A = A_P/A_L$ which describes the covered membrane area in number of lipids. The difference in lipid composition between the covered membrane regions, the so called “clusters”, and the bare lipid membrane is described by $\Delta\phi = \phi_P - \phi_L$.

The resulting local compositions can be described by $\phi = \theta\phi_P + (1-\theta)\phi_L$. For the case that the adsorption of macroions is highly favourable, meaning that macroions adsorb until all charged lipids are bound, ϕ_L is 0 and θ equals ϕ/ϕ_P . Therefore, $\Delta\phi$ reduces to ϕ_P and $d\theta/d\phi$ is $1/\phi$. Assuming charge matching conditions, meaning that the macroion charge is perfectly screened by a respective number of lipids in the clustered area one can write

$$\phi_P = \frac{z_P}{\sigma_A}, \quad (2.37)$$

Where z_P is the number of macroion charge. Including these assumptions in equation (2.36) May et al. (170) calculated the critical minimal non-ideality parameter χ_c to be

$$\chi_c = \frac{2}{\phi_P^2 \sqrt{\sigma}} \quad (2.38)$$

which can be found at a critical molar fraction ϕ_c of

$$\phi_c = \frac{\phi_P}{2}. \quad (2.39)$$

In case of a macroion with a charge of $z = 10$ and an area ratio of $\sigma_A = 10$ resulting in ϕ_P of 1 binding to a charged lipid membrane the minimal critical non-ideality parameter χ_c of a charged membrane (~ 3.7 at large interbilayer distances) reduces to 0.63 at a molar fraction of 0.5, which is even below the critical non-ideality parameter of 2 for the neutral membrane.

Assuming an area of about 2 nm^2 for the cyclic peptides used in this study, the values for σ_A vary roughly between 2 to 5, depending on the lipid and its phase state. For a given z_P value of 3, ϕ_P varies between 1.5 and 0.6, respectively. The resulting values for χ_c therefore range from 0.6 for large to 2.5 for small lipid areas, meaning that charged induced demixing in the liquid crystalline phase is more likely than for membranes in gel phase. The respective critical mixtures ϕ_c range from 0.75 to 0.3. Figure 2-1-7 displays χ_{sp} as a function of ϕ for the given example, calculated from equation (2.36) with the given assumptions.

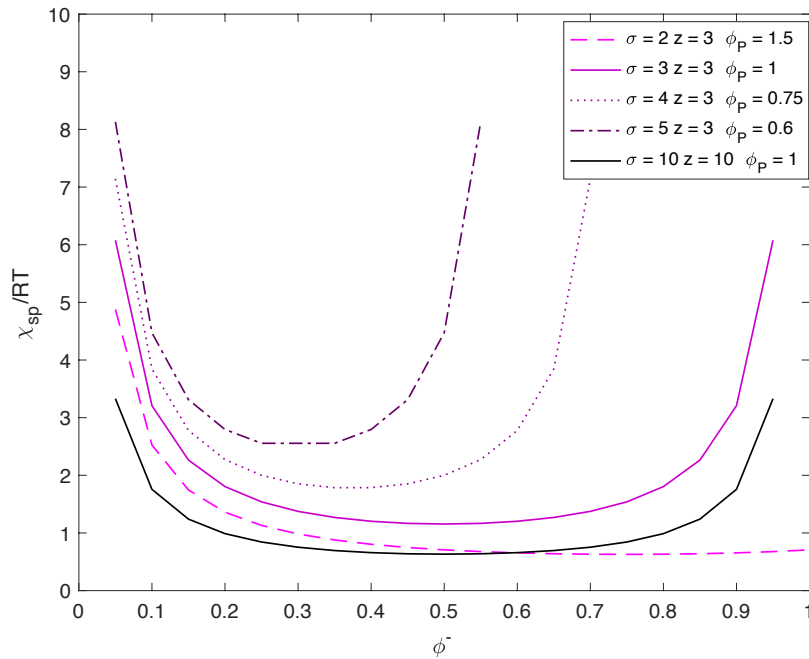


Figure 2-1-7 Examples for the influence of macroions on the non-ideality parameter of clustering charged lipid mixtures with ϕ representing the molar fraction of charged lipid.

It is apparent that for a given ϕ_P of 1, i.e. at charge matching conditions, the clustering ability, resulting from the decrease in non-ideality parameter, increases with increasing size and charge of the macroions. However, if charge matching is not fulfilled and ϕ_P is decreased the non-ideality parameter increases, which can be counterbalanced by changes in peptide-lipid area ratio σ_A . This can be achieved by decreasing peptide area, due to conformational changes or orientation towards the membrane or an increase in the electrostatically screened lipid area. The latter can for example be realized by change in lipid phase state or by (partially) insertion of the macroion into the lipid membrane.

Altogether, if the critical non-ideality parameter is reduced to energies sufficient for the chain non-ideality to overcome the translational entropy a clustering occurs. The addition of polyvalent counterions not only screens the lipid charges that counteract the lipid chain demixing tendency, it even reduces the critical non-ideality substantially below the non-ideality of a non-charged lipid membrane. One can assume that by adding macroions to a charged lipid membrane the reduction in non-ideality with increasing θ reaches the chain non-ideality. This is the critical lipid-peptide concentration ratio, or critical clustering ratio r_{cc} , which this study seeks to identify.

2.2 Single lipid components

2.2.1 DMPG and DMPE

The lipids DMPG and DMPE have been studied extensively during the past decades and will therefore only be reviewed here shortly. The DSC thermograms of both lipids are displayed in Figure 2-2-1.

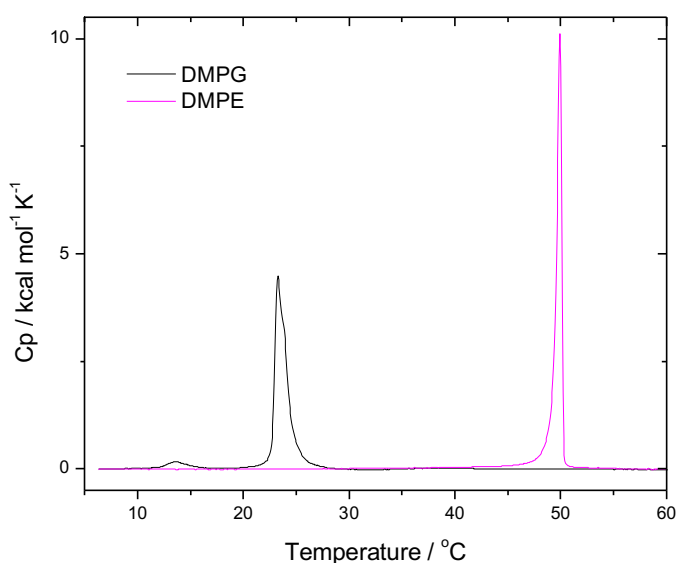


Figure 2-2-1 DSC thermograms of DMPG and DMPE multilamellar vesicles in Phosphate buffer at pH 7.2.

The apparent pK for the phosphate group in DMPG is 2.9 (171) in 100 mM NaCl solution. The protonated DMPG shows a main phase transition at ~ 40 °C which shifts upon deprotonation to lower temperatures. As can be seen in Figure 2-2-1, the phase transition at pH 7 is therefore ~ 24 °C (171) and comprises an enthalpy of ~ 6.7 kcal mol⁻¹ (172). For DPPG the phase transition temperature is shifted from 55° C to 40° C upon deprotonation of the phosphate group with a resulting enthalpy of ~ 10 kcal mol⁻¹. The hydrocarbon chains are untilted for the protonated DMPG and DPPG. Upon deprotonation, however, the headgroup area increases due to the negative charge which results in a gel phase tilt angle of 29° for DMPG and DPPG (171, 173-175).

Storage of DMPG at low temperature can induce a subgel or quasi-crystalline phase which is stable until ~ 40 °C where a subgel to liquid crystalline (L_{α}) phase transition takes place. The transition into the L_{α} phase shows a very high enthalpy of ~ 19 kcal mol⁻¹. The kinetics of this phase formation is dependent on the ionic strength (176, 177) and takes several days for a dispersion in 100mM NaCl solution (172, 178). Together with the FT-IR results it can be concluded that the lipid chains are

packed into an orthorhombic subcell lattice with the same tilt angle of 29° as observed for the gel phase (179, 180). The FT-IR results show additionally a shift of the carbonyl band to 1732 cm^{-1} , indicative for a change in the polar headgroup environment. The major reason for the dehydration is probably the formation of hydrogen bonds between hydroxy groups of the glycerol moiety and oxygens of the phosphodiester and carbonyl groups which substitute hydrogen bonds of water molecules. A reduction of the interbilayer distance observed by SAXS measurements also indicates a dehydration of the headgroup. Besides lipid bilayer stacks also bilayers forming cochleate cylinders are found in the subgel phase as a result of the dehydrated headgroups (172).

The effect of divalent cations on the phase behaviour was studied with various techniques by Garidel et al. (165, 181-184). The authors report an induction of a metastable subgel phase that transforms into a stable crystalline gel phase over time and thereby increases the phase transition temperature to $58\text{ }^\circ\text{C}$ by Sr^{2+} , $65\text{ }^\circ\text{C}$ by Mg^{2+} and $80\text{ }^\circ\text{C}$ by Ca^{2+} ions. The subgel phase induction is accompanied by a dehydration of the phosphate groups which is most pronounced for the calcium ions (182). Further cyclic heating showed a DMPG gel phase stabilisation for all divalent cations at various salt concentrations (181).

Phosphatidylethanolamines are zwitterionic at pH values between the pK value of the phosphate group at ~ 1.7 and the amine group at ~ 11.25 (185). The gel to liquid crystalline phase transition takes place at $50.4\text{ }^\circ\text{C}$, as shown in Figure 2-2-1, with a transition enthalpy of 6.0 kcal mol^{-1} for DMPE and $64.4\text{ }^\circ\text{C}$ with a transition enthalpy of 8.3 kcal mol^{-1} for DPPE (186). Due to the small headgroup to chain volume PEs undergo a lamellar (L_α) to inverted hexagonal (H_{II}) phase transition. Following the concept of Israelachvili the transition temperature decreases with increasing critical packing parameter (*cpp*), e.g. by unsaturation and increasing length of alkyl chains (185, 186). The temperature for this transition for DPPE is $123\text{ }^\circ\text{C}$ with a small transition enthalpy of 0.3 kcal mol^{-1} and increases with each additional CH_2 group by $0.06\text{ kcal mol}^{-1}$ (185).

The alkyl chain tilt angle observed in the gel phase varies between different publications. Some authors report no chain tilt for DMPE and DPPE (187, 188). Simulation studies report a tilt angle of 7° - 20° (189, 190). Also, monolayer studies report a chain tilt that decreases for DMPE and DPPE from 30° at low pressures to 0° at high pressures around 40 mN m^{-1} (191, 192). At the mono-bilayer equivalent pressure of 30 mN m^{-1} (193) a tilt angle of 9° for DMPE (194) and 13° - 18° for DPPE (192) was found using grazing incidence X-ray diffraction. These values are in good agreement with the tilt angle of 11° we determined for DMPE monolayer at 30 mN m^{-1} using IRRAS and measurements of multi bilayer stacks in the gel phase using ATR-IR (data not shown).

Annealing PEs at low temperatures can also lead to a subgel phase formation. In case of DMPE the subgel phase is stable until $56.4\text{ }^\circ\text{C}$ and shows a subgel to liquid crystalline transition enthalpy of $19.6\text{ kcal mol}^{-1}$ (186, 195). The subgel phase to liquid crystalline transition for DPPE takes place at $66\text{ }^\circ\text{C}$ and shows a transition enthalpy of $22.3\text{ kcal mol}^{-1}$ (186). The values, however, vary within different publications and might be due to different sample preparation and annealing time and

temperature (186, 196). The lamellar repeat distance for PEs shows a reduced water layer indicating a dehydrated headgroup (197, 198). The reduced headgroup hydration as well as the elevated transition temperatures when compared to PG or PC analogues are discussed to be due to hydrogen bonding between the nitrogen and the phosphate oxygens (199) which is further evidenced by simulation (189, 190).

2.2.2 Cardiolipin

Cardiolipin has only been studied more extensively in the recent years. Earlier studies focussed on the impact of chain length and salt dependence of cardiolipin main phase transition. Rainier et al. (200) compared the phase transition temperatures of cardiolipin and phosphatidylglycerols containing lauryl, myristoyl and palmitoyl chains. The presence of the second phosphate group and a connecting glycerol molecule in case of cardiolipin lead to phase transitions significantly below (>15K) the ones with a single phosphate group between the glycerol backbones. The slope of the phase transition temperature with increasing chain length of cardiolipin with ~7.5K per CH₂-group is comparable with the slope of T_m of monomeric phospholipids.

With the two phosphate groups the cardiolipin phase behaviour is sensitive to pH and ionic strength. Seddon et al. e.g. showed that in 0.1-1 M NaCl solution cardiolipin undergoes a H_{II} to L_α phase transition at pH 2.8 (201). This is due to a change in negative net charge by exceeding the pK of the phosphate group at this value. A simulation study by Dahlberg displays a different cardiolipin phase behaviour dependent on the chain number and headgroup charge (202).

In comparison to phosphatidylglycerol, the biochemical precursor, the headgroup glycerol motional freedom is reduced. NMR experiments of partially deuterated cardiolipin molecules showed a decrease in correlation times by a factor of 10 whereas the backbone glycerol orientation and segmental flexibility between both lipids is identical (203).

2.2.2.1 DSC

As not very many investigations on the thermotropic behaviour of Tetramyristoylcardiolipin (TMCL) have been reported, the next paragraph describes our results in more detail. The thermotropic phase behaviour of TMCL was described earlier by Lewis et al. using DSC, X-ray, P-NMR and IR-spectroscopy (197).

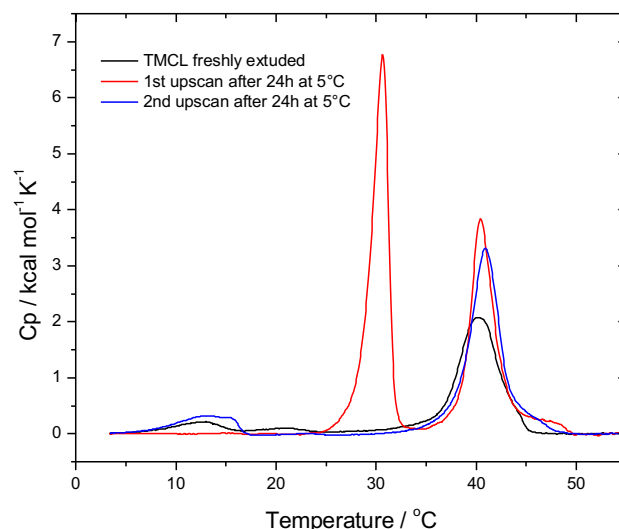


Figure 2-2-2 DSC thermograms of extruded TMCL vesicles in phosphate buffer freshly prepared and after 24 hours incubation time at 5 °C.

Freshly extruded vesicles show a L_{β} - L_{α} phase transition at 40.5 °C. Two additional transitions at 12 °C (1.3 kcal mol⁻¹) and 21 °C (0.6 kcal mol⁻¹) are observed (Figure 2-2-2). In the study by Lewis et al. the additional low temperature peaks occur at 14–18 °C and 25–30 °C, reflecting a subgel to gel phase transition (197). As the formation of the subgel phase depends on the nucleation event of gel phase lipids the kinetics of this event is most likely sensitive to differences in ionic strength and the cooperativity of transition. As the authors use phosphate buffer at pH 4 with 150 mM NaCl and multilamellar vesicles the difference in transition temperature might originate from the difference in sample preparation at higher ionic strength and higher pH. The enthalpies of these transitions are comparably low.

Storing the sample for 24 hours at 5 °C leads to a formation of a subgel phase that is stable until 30 °C and shows a high endothermic phase transition peak (~15 kcal mol⁻¹) from subgel to gel phase. The high endotherm is in a similar range as observed for the subgel to liquid-crystalline phase transition observed for pure DMPG (~19 kcal mol⁻¹). The L_{β} - L_{α} transition temperature remains unaltered. Reheating the sample immediately after cooling (60 K/h) leads again to a low temperature transition ~12 °C with comparably low transition enthalpy of 2.2 kcal mol⁻¹ and the L_{β} - L_{α} phase transition at 41 °C (see Figure 2-2-2).

The enthalpy of the L_{β} - L_{α} phase transition of freshly prepared vesicles is 11.3 kcal mol⁻¹. The L_{β} - L_{α} phase transition enthalpy of the samples stored for 24 hours at 5 °C is 13.6 kcal mol⁻¹. The transition enthalpy per myristoyl chain (~3.4 kcal mol⁻¹) is in good agreement with values for double-chain phospholipids (2.75 kcal mol⁻¹ for DMPG, 3.8 kcal mol⁻¹ for DMPE), indicating that also in cardiolipin bilayers the enthalpy of the L_{β} - L_{α} transition is mainly due to lipid chain melting. This value is also in good agreement with the values reported earlier for cardiolipin (197, 200).

The pH dependence of the main phase transition temperature of Tetramyristoylcardiolipin in 100 mM NaCl solution is shown in Figure 2-2-3. Two major effects can be observed: The phase transition temperature is downshifted with increasing pH from 44.1 °C at pH 4.4 to 39.8 °C at pH 9.9 and the cooperativity of the main phase transition increases in the same manner. The pK value of the second phosphate group can be derived from these measurements to 6.2.

A pK value for the second phosphate group in 50 mM KCl solution was reported by Kates et al. (204) and reviewed later again (205). The pK shifts among titration from 7.5 to 9.5 which, according to the authors, emphasises the biological role of cardiolipin as a proton trap for the ATPase functionality.

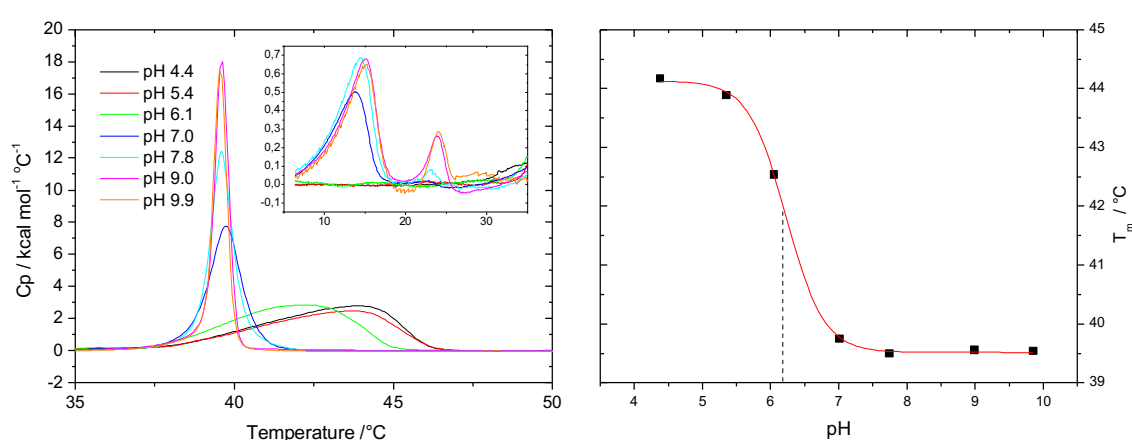


Figure 2-2-3 DSC thermograms of extruded TMCL vesicles at different pH in 100mM NaCl (left) and phase transition temperatures plotted versus pH (right).

This high and shifting pK value is discussed as a result from a hydrogen bond formation between a glycerol hydroxy group and phosphate oxygen, additionally supported by IR measurements from Hübner et al. (206). However, as our result shows that the second phosphate group of TMCL is already deprotonated at a pH of 7.2 the difference in result might be due to higher ionic strength. The second charge can be screened in the presence of Na⁺-ions which leads to the downshift in pK value in 100 mM NaCl compared to 50 mM KCl solution. The presence of the second charged phosphate group leads to increased phosphate group separation constrained by the glycerol moiety. The alkyl chain interactions are lowered by the increase in charge density, which can be seen by the downshift in phase transition temperature.

The downshift in phase transition temperature with increasing pH originates from reduced hydrocarbon chain interaction caused by the increased lipid headgroup charge due to deprotonation of the phosphate group and is reported for many lipids (207-214).

The increasing cooperativity of the phase transition with further headgroup deprotonation was also reported for PG (212, 215) and PC (216) in contrast to DMPA (207) and PS (213) where an increase in headgroup charge leads to a decrease in cooperativity. The difference in reported cooperativity might be a result of different sample preparation mainly influenced by the number of lamellae

formation. The effect observed here for cardiolipin results from the presence of a mixture of cardiolipin molecules in single and double charged states. The DSC curves for low pH values in Figure 2-2-3 left show an onset at 37 °C, indicating that at this pH already a certain number of doubly charged cardiolipin molecules are present which melt at low temperatures. The asymmetry of the peak at pH < 7.0 underlines this interpretation additionally. It is noteworthy that between the pH of 7.0 and 9.0 the cooperativity increases remarkably although the phase transition temperature does not change significantly and the symmetrical phase transition peak indicates a single melting event. However, in this case it seems more likely that at pH of 7.8 still some single charged cardiolipin molecules are remaining and the broader transition width is due to mixing of single and double negatively charged cardiolipin molecules. Prosnigg et al. observed a coexistence range of L_c and L_β phases at a pH of 7.4 and temperatures between 20-30 °C (217). It seems very likely that these phase coexistence results from differently charged TMCL moieties.

2.2.2.2 ATR-IR

The lipid chain melting can be monitored also by IR. The shift in wavenumber is observed from “ordered” to a more “unordered” state, i.e. an increase in *gauche*-conformers of lipid acyl chains. The asymmetric CH_2 stretching vibration shifts from 2918.5 cm^{-1} to 2922 cm^{-1} and the symmetric CH_2 stretching vibration from 2850.2 cm^{-1} to 2852.6 cm^{-1} at 40 °C (see Figure 2-2-4 left).

Furthermore, we could monitor the formation of the cardiolipin subgel phase. The wavenumber for the symmetric CH_2 -vibration decreases slightly from 2850.1 cm^{-1} to 2849.8 cm^{-1} , whereas the antisymmetrical vibration band decreases drastically from 2917.5 cm^{-1} to 2915.0 cm^{-1} upon heating from 2-12 °C. This effect is due to the time the probe was kept at low temperature and not to the effect of heating, because the lipid chains obtain an even more ordered structure.

As the methylene scissoring vibrational mode is split, due to a coupling between transition dipoles in ordered hydrocarbon chains that depends on the alkyl chain packing, further information about the chain packing can be gained (218). In the temperature interval of the subgel phase the CH_2 scissoring vibration is shifted to 1472 cm^{-1} with a shoulder at 1459 cm^{-1} , which can be attributed to the CH_3 antisymmetric bending vibration. The peak position at 1472 cm^{-1} is characteristic for a triclinic alkyl chain order. However, Lewis et al. determined by X-ray measurements an orthorhombic alkyl chain packing. Thus a splitting in scissoring vibration to the two bands at 1472 cm^{-1} and 1463 cm^{-1} would be expected (218). As this splitting is not observed in our measurements, the formation of a triclinic over an orthorhombic subgel phase with triclinic chain packing occurs. The reason for this might be due to little variations in lipid bilayer preparation. A splitting of the scissoring band is also shown for interdigitating monolayers, whereas the split in frequencies varies with the number of methylene groups involved in interdigitation (219, 220). However, as the X-ray measurements by Lewis et al. did not yield any indication of possible

interdigitating monolayers, this origin for the shift in scissoring band can be excluded. Also the simulation study by Dahlberg confirms a triclinic chain lattice formation (202).

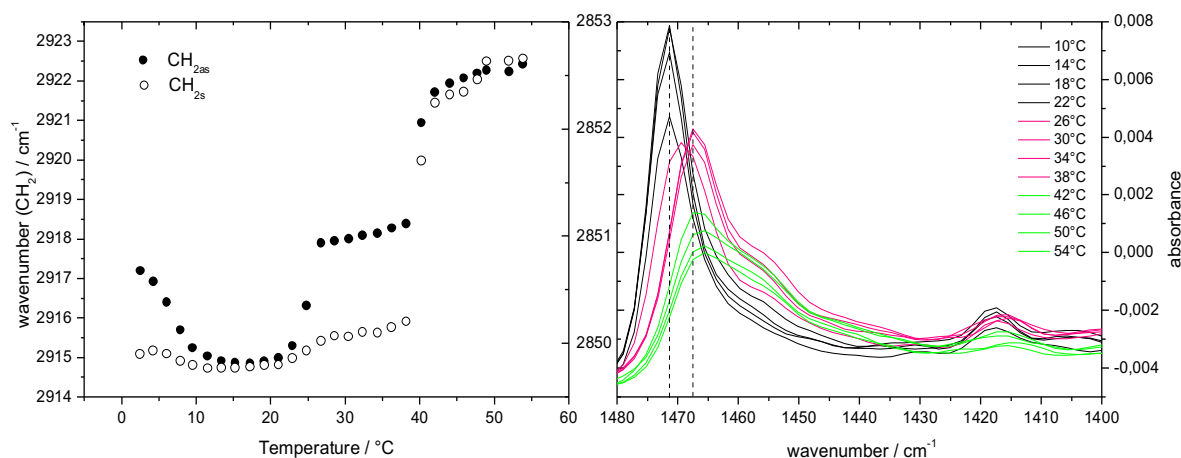


Figure 2-2-4 ATR-IR measurement of 1mM TMCL (100nm vesicles) in NaCl 100mM. *left*: Temperature dependence of the antisymmetric (filled circles) and symmetric (open circle) CH₂-vibration. *Right*: spectra showing the CH₂-scissoring vibration at different temperatures.

A shift in CH₂ stretching vibration wavenumber from 2915.1 cm⁻¹ to 2918.1 cm⁻¹ and the small change from 2849.9 cm⁻¹ to 2850.2 cm⁻¹, respectively, takes place at 25 °C and indicates the transition from subgel to gel phase. This is accompanied with a shift of the CH₂-scissoring band from 1472 cm⁻¹ to 1467 cm⁻¹, indicative for a hexagonal alkyl chain lattice (see Figure 2-2-4 right). Figure 2-2-5 displays the carbonyl band (left) and the PO₂⁻ antisymmetric and symmetric stretching vibration band (right) at selected temperatures. In the subgel phase, the carbonyl band maximum is shifted to 1734 cm⁻¹ indicative for a hydrogen bond formation between the carbonyl group (221) and ordered water molecules or OH-groups from the glycerol. This is supported by the slight upshift and increased intensity of the α-CH₂ vibration peak at 1418 cm⁻¹ (Figure 2-2-4 right) indicating that the lipid carbonyl group is immobilized in the subgel phase. However, the second peak occurring at 1425 cm⁻¹, as it was observed by Huebner at al. (206), cannot be detected. Also, the CH₂ scissoring vibration of the glycerol backbone appearing as a shoulder at 1457 cm⁻¹ increases during the subgel to gel phase transition indicative for a change in mobility of the neighbouring carbonyl vibration. Compared to DMPG, the band maxima of the C=O band at 1732 cm⁻¹ and the α-CH₂ scissoring band are similar (222), indicating that similar headgroup interactions in DMPG and TMCL lead to the subgel phase formation.

The antisymmetric and symmetric PO₂⁻ vibration band for phosphatidic acid at pH 6 is found at 1180 cm⁻¹ and 1075 cm⁻¹, respectively. For the PG headgroup these vibrational bands are located at 1200 cm⁻¹ and 1080 cm⁻¹ for the DMPG L_c phase (172) as a result of strong hydrogen bonding. In the L_{β'} phase the peak positions can be found at 1220 cm⁻¹ and 1072 cm⁻¹ (223), whereas the peak position shifts to 1240 cm⁻¹ and 1260 cm⁻¹ upon dehydration (206, 224). For TMCL, the antisymmetric PO₂⁻ vibration band is located at 1212 cm⁻¹ in the L_α and at 1208 cm⁻¹ in the L_β phase

(see Figure 2-2-5). This is in accordance to the values found by Huebner et al. (206) and is in-between the values found for the DMPG headgroup in the subgel and gel phase, indicating that only one of the two phosphate groups is affected by additional hydrogen bond interactions in the subgel phase, when compared to DMPG. The symmetric PO_2^- vibration band is located at 1076 cm^{-1} in the L_α and at 1073 cm^{-1} in the L_β' phase (see Figure 2-2-5) which is also in accordance to the values found for PA and PG. The peak at 1095 cm^{-1} , on top of the broader symmetric phosphate band is shifted to 1093 cm^{-1} in the liquid crystalline phase. This is attributed to the ester group vibration (CO-O-C). The glycerol-phosphate ether bond in the phosphatidyl headgroup displays a peak at 1050 cm^{-1} (223), which is also observed for TMCL in the L_α and the L_β' phase.

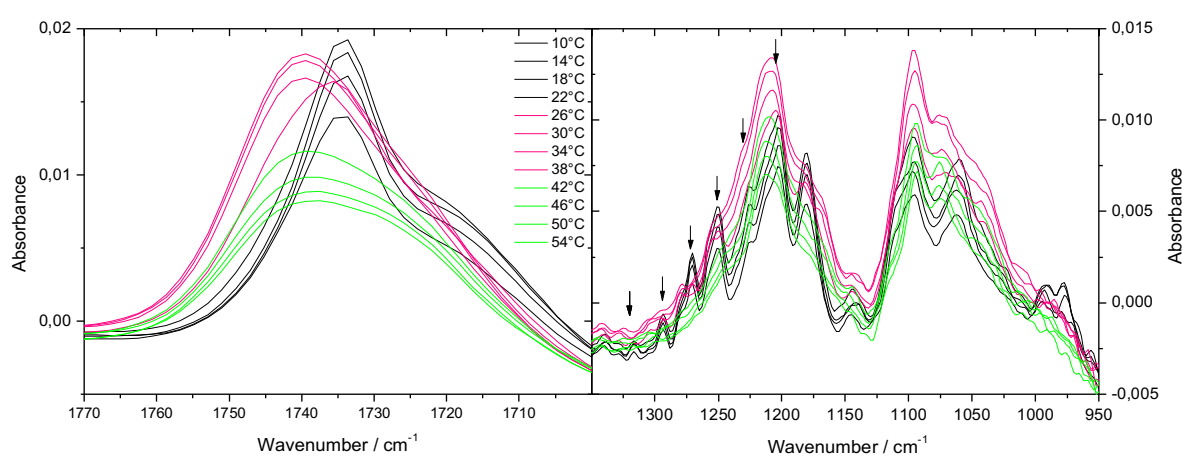


Figure 2-2-5 ATR-IR measurement of 1mM TMCL (100nm vesicles) in NaCl 100mM. *left*: spectra displaying the carbonyl vibration at different temperatures. *Right*: spectra displaying the antisymmetric and symmetric PO_2^- vibration at different temperatures. The wagging bands are marked with an arrow.

In spectra of the subgel phase, the equally spaced CH_2 wagging band progression, a series of equally spaced ($22 - 25\text{ cm}^{-1}$) narrow bands, occur as a result of non-localised vibrations, namely the coupling of wagging oscillations along the all-trans chain. For myristoyl chains, the wagging band progression reaches from 1325 cm^{-1} to 1205 cm^{-1} (223) and therefore overlap with the antisymmetric PO_2^- band which hinders the determination of the precise peak position. Wagging band progression also occurs in L_β phases, but in the subgel phase the bands are more pronounced due to the high alkyl chain order.

Altogether, the phosphate band region between $1300\text{-}1000\text{ cm}^{-1}$ shows significantly different peak positions for TMCL in the subgel phase than in the L_β' and the L_α phase, respectively. However, as many peaks overlap in this region a clear indication for a phosphate group interaction cannot be concluded. This result is in general agreement with the infrared data reported by Lewis et al. (197). The authors additionally report a reduced mobility of the phosphate group without any involvement in hydrogen bonding interactions in the subgel phase deduced from the ^{31}P -NMR spectra. The mobility increases in the gel phase and shows a phosphate mobility typical for phospholipids in the liquid crystalline phase. This is in line with our observation that the peak at 980 cm^{-1} , which is

indicative for the phosphoester bond to the glycerol backbone ($\text{P-O-C}_{\text{glycerol}}$), shows an increased intensity. A second peak at 990 cm^{-1} in the subgel phase indicating a cooperative C-O-P-O-C stretching vibration (223) is present. The intensity decreases in the gel phase and the two different peaks are no longer distinguishable. In the liquid crystalline phase, this peak is not observable. This peak also occurs in the DMPG subgel phase (172).

The formation of the triclinic subgel phase was argued by Lewis et al. to be a result of hydrogen bond formation between the lipid carbonyl group and water molecules. Huebner et al. hypothesised a hydrogen bond interaction between the lipid carbonyl group and the bridging glycerol OH group, which in cardiolipin is reduced in motional freedom (203). This indicates that for cardiolipin, a glycerol-carbonyl hydrogen bond will affect the chain mobility and induce the subgel phase formation.

The alkyl chain tilt angle for the gel phase was determined by Lewis et al. (197) to 0° . The alkyl chain tilt angle for a TMCL monolayer on 100 mM NaCl subphase at the monolayer-bilayer equivalent pressure of 30 mN m^{-1} determined by IRRAS was 13° (data not shown).

2.3 Binary mixtures

Cardiolipin is discussed in literature as an immiscible lipid or lipid with low miscibility (225). Not only in mixtures with negatively charged lipids a demixing was observed, also in TMCL/DPPC monolayer measurements a phase separation on a pure water subphase was identified (226). Moreover, lipid domains attributed to lipid segregation were detected with AFM techniques in POPE/CL mixtures whereas POPC/CL mixtures showed no lipid segregation (227). Another combined AFM and monolayer study reported a domain formation of unsaturated bovine cardiac cardiolipin when mixed in DPPE and DPPC mono- and supported bilayers (228). This low miscibility of cardiolipin is often discussed to act as a lipid template for membrane proteins (120, 127, 128, 229-235) and to play an important role in cell apoptosis (236, 237). However, the lack of data on cardiolipin miscibility does not yet lead to a comprehensive picture on the driving forces of cardiolipin miscibility. This is why the general reputation of an immiscible lipid is not justified. Mixtures of TMCL with DMPG and DMPE will be further discussed in Section 2.3.2 and 2.3.3, respectively.

2.3.1 DMPG/DMPE

Mixtures of lipids with PG and PE headgroups often serve as bacterial model membranes to study antimicrobial peptide lipid interaction. Therefore, different PG-PE-mixtures were analysed regarding their miscibility.

In the study by Garidel and Blume non-ideality parameters for the PG-PE mixtures in 100 mM NaCl solution were determined with respect to different chain length of saturated alkyl chains at pH 7 and 2, below the pK of the phosphate group, at which the PG molecule is uncharged (215). The mixtures also show a slight positive non-ideality at pH 7, but the parameters obtained are less positive than in the study of Lohner et al. (238). Lohner et al. described a phase diagram for two lipids with identical chain length (DPPG and DPPE) in 10mM Na-Phosphate buffer. At this low ionic strength the lipids show a peritectic mixing behaviour with a gel phase demixing at a PG content higher 60%. The non-ideality parameters are positive for the liquidus and solidus line, indicating a demixing of PG content higher 60% for the gel phase and higher 40% for the liquid crystalline phase. This is surprising as charges contribute to the free energy of mixing and the absence of screening of lipid charges should lead to lower non-ideality values at low counterion concentration and increased χ_c (see Sections 2.1.2 and 2.1.3). However, this is not observed. This shows that additional interactions in the headgroup region are present leading to the demixing in the gel phase. For the DMPG/DMPE mixture all non-ideality parameters are negative at high salt concentration indicating that the electrostatic repulsions between the PG molecules dominate and prevent a random distribution in

the bilayer plane. DMPG/DPPE mixtures show a peritectic mixing behaviour at high PG contents. Even POPG and POPE with unsaturated chains in a 20mM phosphate buffer in 130mM NaCl solution (and 50 vol% ethylene glycol to lower the freezing point of water) show a peritectic mixing behaviour at high POPG contents (239). Additionally, a study of pyrene labelled phospholipids indicates a demixing of PG and PE in *E. coli* and *B. subtilis* membrane (111).

2.3.1.1 DSC

In this study, the DSC analyses of DMPG/DMPE binary mixtures were performed in 20 mM sodium phosphate buffer and additional NaCl to achieve ionic strength of 100 mM (Figure 2-3-1 left). The phase diagram is displayed in Figure 2-3-1 (right) together with the calculation for ideal mixing behaviour (dotted line). The phase diagram indicates almost ideal mixing behaviour. Only the temperature onset of the mixture containing 25% DMPE is downshifted to a temperature similar to the T_m of pure DMPG. At a molar fraction of charged lipid of 0.6 to 0.7 the non-ideality parameter for spinodal decomposition χ_{sp} reaches a minimum (see Figure 2-1-5 (168)). Therefore, a miscibility gap would occur in this molar fraction range as the non-ideality of the mixture reaches the critical non-ideality parameter. However, the extruded vesicles show a similar DSC thermogram (see Figure 2-3-1 of the supplementary data) although a stabilisation of the mixture is expected with larger interbilayer distances (see chapter 2.1.3 (168)).

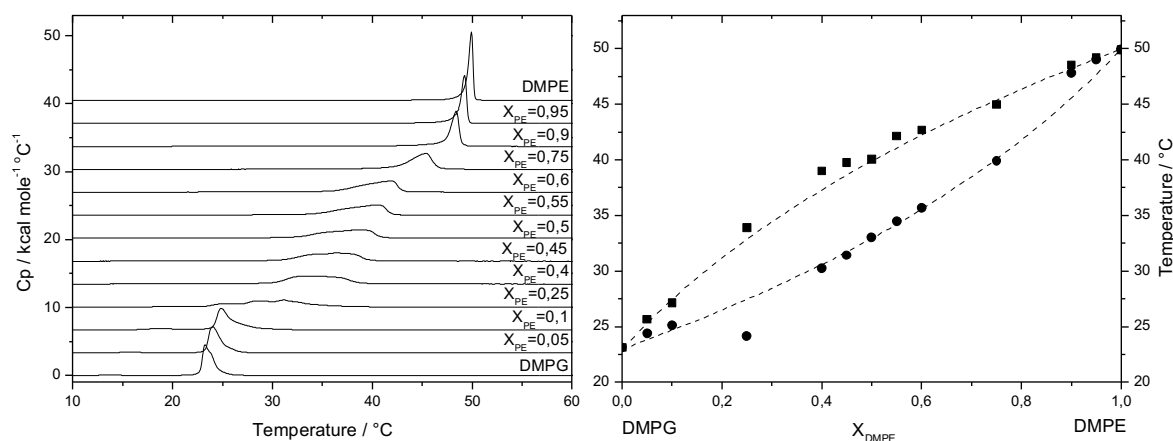


Figure 2-3-1 Left: DSC heating thermograms of DMPG/DMPE mixtures with varying molar ratios. Right: Temperature onset and end of the phase transition vs. molar ratio of the components. The dotted line is the calculated liquidus and solidus curve for ideal behaviour.

The reproducibility of this behaviour, together with the observations made from other authors for DPPG/DPPE, DMPG/DMPE and even POPG/POPE binary mixtures (239), lead to the conclusion that PG/PE mixtures in phosphate buffer seem to demix at a PG content around 60-70% which could even lead to the observed peritectic mixing behaviour with increasing lipid chain non-ideality and increasing ionic strength (170). As the critical non-ideality parameter is strongly influenced by the

ionic strength (χ_c varies between $2 kT$ at high to $3.7 kT$ at low ionic strength (170)) further investigations should be made to identify the demixing boundaries in dependence of ionic strength and lipid chain composition. For example, the comparison to mixtures with varying chain length, the tendency of gel and liquid phase demixing seems to be emphasized by additional hydrophobic mismatch caused by different acyl chain length (215, 240).

2.3.2 DMPG/TMCL

We also investigated the mixing behaviour of binary mixtures of negatively charged DMPG with doubly negatively charged TMCL. Both single lipids form a L_c phase which formation is dependent on annealing time and most likely also on buffer and preparation conditions. Therefore, we focussed within the miscibility studies on the L_β - L_α transition. This transition can be attributed to the lipid chain melting and is highly reversible, especially within the time frame of a calorimetric and IR-spectroscopy measurement. The complete thermotropic behaviour of DMPG and TMCL mixtures was investigated earlier by Benesch et al. (241). However, in their work they used 100 mM phosphate buffer plus additional 150 mM NaCl, so the buffer had a much higher ionic strength. This can influence the phase behaviour in these strongly charged systems. We therefore studied this system using our experimental conditions with 20 mM sodium phosphate buffer and additional NaCl to achieve an ionic strength of 100 mM.

2.3.2.1 DSC

The DSC thermograms of various DMPG/TMCL binary mixtures are shown in Figure 2-3-2 left. It can be seen that the main phase transition temperature only shifts up slightly by the addition of TMCL until a DMPG/TMCL 3:1 ratio is reached. Correspondingly, the transition width is barely affected by the addition of little amounts of TMCL. The pretransition of DMPG, indicating the ripple phase formation, is preserved by the addition of TMCL but shifted from 12 °C of pure DMPG to about 17 °C for the DMPG/TMCL 3:1 mixture. The DMPG/TMCL 3:2 mixture ($X = 0.4$) shows a very broad transition peak which shows a first temperature onset at around 24 °C, the phase transition temperature of DMPG. This could either indicate a gel phase demixing where the pure DMPG domains start melting at 24 °C or the pretransition of the mixture is shifted from 12 °C to 24 °C which seems unlikely. This temperature onset is also observed for the mixture up to a TMCL molar fraction of $X_{TMCL} = 0.45$ but is not observed for the 1:1 mixture and mixtures with larger amounts of TMCL. In these mixtures with $X_{TMCL} > 0.5$, however, the pretransition of TMCL at 12 °C is preserved and slightly downshifted to 10 °C with increasing amounts of DMPG.

The right side of the Figure 2-3-2 displays the onset and end of the main phase transition temperatures together with the ideal mixing behaviour calculated from the enthalpy and transition temperature of the pure components according to equation (2.7) and (2.8).

The two onsets for the phase transition of the mixture $X_{\text{TMCL}} = 0.4$ and $X_{\text{TMCL}} = 0.45$ are plotted twice. The triangles display only the onset of the large peak, assuming that the first onset belongs to a pretransition and not the main phase transition. The filled circles represent the temperature onset assuming that the lower temperature belongs to the melting of a DMPG-enriched gel phase domain. A magnification of the DSC curves for mixtures with $X_{\text{TMCL}} = 0.25$, $X_{\text{TMCL}} = 0.4$ and $X_{\text{TMCL}} = 0.45$ is shown in Figure S2-3-3 of the supplementary data.

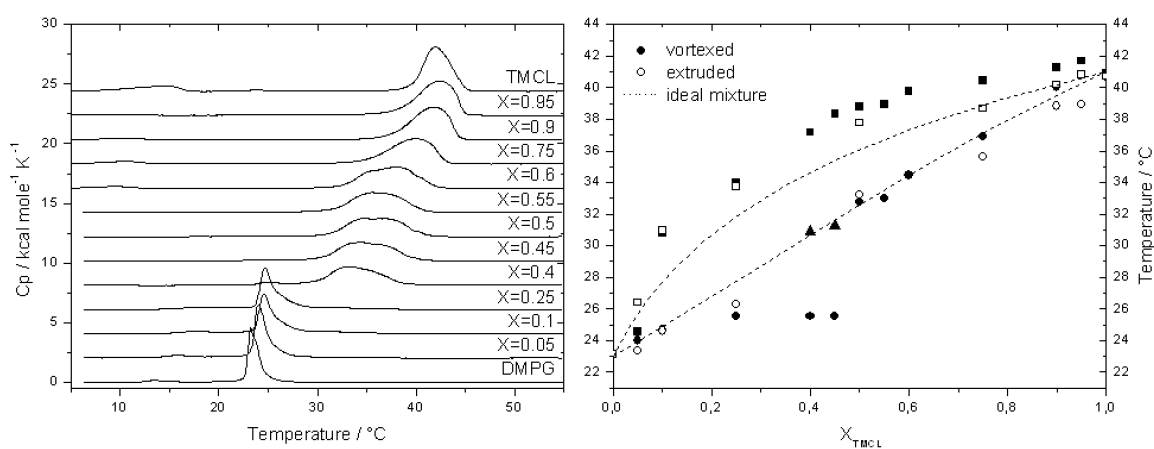


Figure 2-3-2 Left: DSC heating thermograms of DMPG/TMCL mixtures with varying molar ratios. Right: Temperature onset (circles) and end of the phase transition (squares) vs. molar ratio of the components. The triangles display the onset for the large peak in mixture $X_{\text{TMCL}} = 0.4$ and 0.45 . The dotted line is the calculated liquidus and solidus curve for ideal behaviour.

The main phase transition temperature taken from the peak maximum is similar when compared to the data acquired at higher ionic strength by Benesch et al. The phase transition width, however, is increased in our measurement at lower ionic strength for TMCL contents above $X_{\text{TMCL}} = 0.4$. At lower ionic strength the pretransition at higher TMCL contents which is attributed to the L_c - L_β phase transition is lower in enthalpy and occurs at lower temperatures. These differences might result from the different ionic strength as the screening of the headgroup charges will influence the subgel phase formation. As the formation of the gel phase also critically depends on the annealing time at low temperatures the slower scan rate of $10 \text{ }^\circ\text{C h}^{-1}$, when compared to $60 \text{ }^\circ\text{C h}^{-1}$, might give enough time for the subgel phase to form. For the mixtures containing high amount of DMPG ($X_{\text{TMCL}} < 0.2$) the observed phase transitions are very similar to the ones observed by Benesch et al. Above $X_{\text{TMCL}} = 0.2$, however, no pretransition is observed by the authors and the main phase transition region is shifted to higher temperatures than observed by our measurements. This supports the argumentation that the occurring low temperature peak at $X_{\text{TMCL}} = 0.4$ and $X_{\text{TMCL}} = 0.45$ belong to the main phase transition and indicate a gel phase demixing at lower ionic strength.

For some DMPG/TMCL mixtures also the transition onset and end of phase transition of the extruded vesicle is displayed (unfilled symbols). The original thermogram is displayed in Figure S2-3-2 of the supplementary data. The phase transition for extruded vesicles with high content in TMCL is shifted to slightly lower temperatures whereas the transition width is similar to the one observed for multilamellar vesicles. Unilamellar vesicles usually show a broader phase transition due to the reduced cooperative unit, resulting from vesicle curvature. Here, the 1:1 mixture displays even a reduced transition width for the unilamellar vesicles when compared the multilamellar vesicles. The unilamellar vesicle phase transition for the DMPG/TMCL 3:1 mixture starts at a similar temperature as for the multilamellar vesicles but the phase transition width is strongly increased and proceeds until 34 °C. As pure TMCL shows short interbilayer distances the addition of TMCL can lead to improved interbilayer coupling. Therefore, the extruded samples represent the unaltered transition temperature of the demixed bilayer. Prossnigg et al. found that with increasing TMCL content in DPPG/TMCL mixtures in 20 mM phosphate buffer and 130 mM NaCl at pH 7.4 multilamellar vesicles were formed. They argued that this formation is a consequence of a reduced surface charge density resulting from a proton trapped in the lipid headgroup by an interaction of the TMCL phosphate group with the hydroxy group of the bridging glycerol (217).

The comparison to the calculated ideal behaviour shows that in excess of TMCL the solidus line follows the ideal behaviour. Also, the onset of the large transition peak for the two mixtures at $X_{\text{TMCL}} = 0.4$ and $X_{\text{TMCL}} = 0.45$ fit well to the expected onset of the ideal behaviour.

However, the experimental values for the liquidus line are higher than expected for mixtures with ideal behaviour. This indicates a non-ideal mixing behaviour in the L_{α} phase with excess of TMCL. In excess of DMPG the gel phase seems to be demixed from a molar ratio of $X_{\text{TMCL}} = 0.25$ until $X_{\text{TMCL}} = 0.45$. This is further supported by our monolayer data, where fluorescence microscopy images showed that two different domain structures coexist in a DMPG/TMCL 3:1 mixture and our IRRAS data where two different tilt angles were found for DMPG and TMCL, respectively, in a DMPG- d_{54} /TMCL 3:1 mixture (data not shown). For the DPPG/TMCL mixture at higher ionic strength, Prossnigg et al. found a eutectic mixture at $X_{\text{TMCL}} = 0.2$ indicating that a gel phase demixing occurs. This is in contrast to the results from Benesch et al. who found higher temperature onsets in this composition range at higher ionic strength but, nevertheless, indicate a larger non-ideal behaviour. They also found two different gel phases, one DMPG governed below $X_{\text{TMCL}} = 0.1$ and a TMCL governed gel phase above $X_{\text{TMCL}} = 0.1$.

Altogether, we confirm the common finding by Benesch et al. and Prossnigg et al. that two different gel phases exist, one with high PG contents and one with high TMCL content. However, we further assume that between both gel phases a miscibility gap occurs around $X_{\text{TMCL}} = 0.33$ where both lipid alkyl chain are equally present. A non-ideal mixing in the gel phase and in the liquid crystalline phase in which the non-ideality parameters are slightly positive can lead to a peritectic mixing behaviour (166). The peritectic behaviour can be reconstructed from onset and end of the phase

transition as displayed in Figure 2-3-3. Here, the peritectic point is at 27 °C around $X_{\text{TMCL}} = 0.25$ and the gel phase is demixed between $X_{\text{TMCL}} = 0.25$ and $X_{\text{TMCL}} = 0.45$. However, to define exact phase boundaries and to understand the effect of ionic strength on these phase boundaries of this mixture, further experiments are necessary.

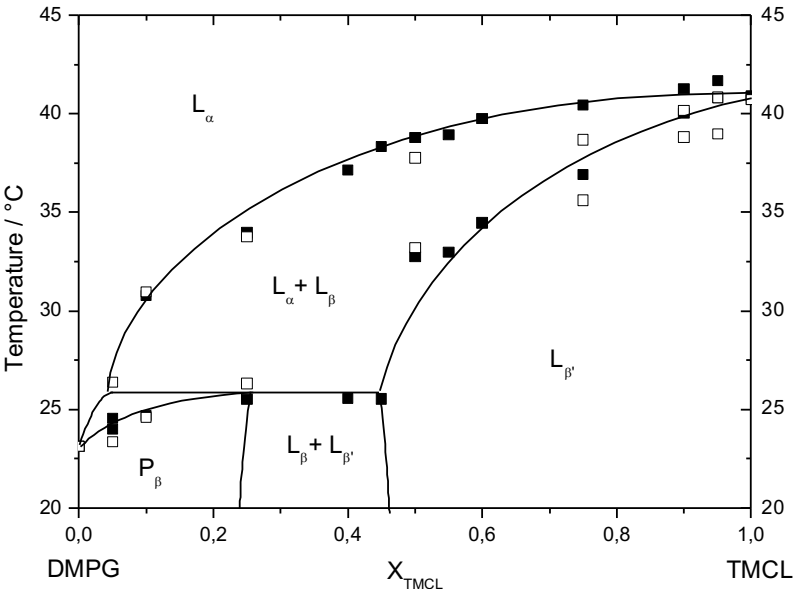


Figure 2-3-3 Temperature onset and end of the pre- and main phase transition of the different DMPG/TMCL mixtures are plotted with the assumed phase boundaries for the peritectic mixture.

2.3.3 DMPE/TMCL

Frias et al. investigated DMPE and TMCL mixtures in 100 mM phosphate buffer, 150 mM NaCl and 5 mM NaN_3 at pH 7.4 annealed at low temperature (242).

2.3.3.1 DSC

The temperature behaviour of the L_β - L_α main phase transition of various TMCL/DMPE mixtures is displayed in Figure 2-3-4. The left side displays the last heating scan of the different mixtures and the right side displays the onset and end of phase transition temperatures versus the molar fraction. In the resulting phase diagram, the narrow phase coexistence region of the measured results is in a similar temperature interval as the transition width calculated for ideal mixing behaviour.

Only in mixtures containing 90% and 95% DMPE a higher melting temperature than for the pure DMPE membrane is seen, indicating that the mixture possibly displays an azeotropic maximum for high DMPE contents. For comparison the expected calculated curve for ideal behaviour is plotted together with the lines displaying the presumed phase behaviour of a mixture displaying an azeotropic maximum.

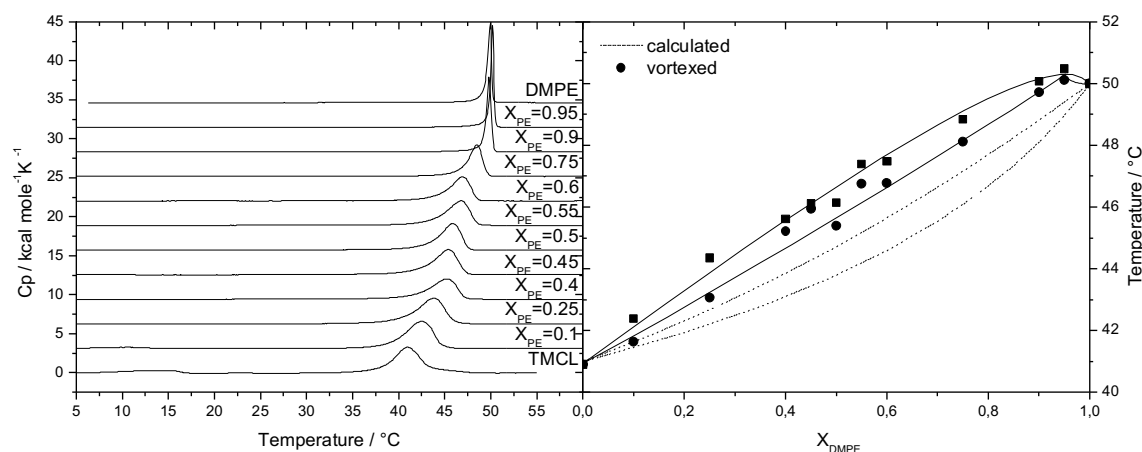


Figure 2-3-4 Left: DSC heating thermograms of TMCL/DMPE mixtures with varying molar ratios. Right: Temperature onset and end of the phase transition vs molar ratio of the components. The dotted line is the calculated liquidus and solidus curve for ideal behaviour and the solid line represents the assumed liquidus and solidus curve for a mixture with azeotropic maximum at high PE content.

From the phase diagram calculations from Pelton (166), as summarised in Figure 2-1-2, an azeotropic maximum results from a negative gel phase non-ideality parameter, i.e. a preferred interaction of unlike molecules, or a positive non-ideality parameter in the fluid phase, i.e. a preferred interaction of like molecules, or a combination of both.

In comparison to the observed L_β - L_α phase transition temperatures by Frias et al the phase transition is not largely affected by higher ionic strength and low temperature annealing. The transition width

at low ionic strength is slightly increased with increasing amount of TMCL when compared to the published data. Due to the annealing time the L_c phase is formed, displaying L_c - L_β phase transition for pure TMCL from 25-30 °C. The pretransition is observed for mixtures containing up to 90% DMPE. With increasing amounts of DMPE the pretransition temperature and enthalpy decreases. Without annealing at low temperatures, we observe a pretransition only for TMCL at 10-20 °C (see Section 2.2.2) and for the mixture containing 90% TMCL from 5 °C to 15 °C.

Frias et al. concluded from the FT-IR spectroscopic data that the non-ideal mixing behaviour results from a poor miscibility of both components suggesting a miscibility gap in the gel phase between an L_β and an L_c phase (242). This is in contrast to our interpretation of either poor miscibility in the liquid-crystalline phase or a preferred DMPE-TMCL interactions in the gel phase. However, the authors further concluded that the interpretation of poor miscibility can not directly be drawn from their measurements. Neither our FT-IR data of TMCL and DMPE- d_{54} mixtures without annealing at low temperature (Figure S2-3-5 and S2-3-6) nor our monolayer data (not shown) show any indication for a gel phase or liquid-condensed phase demixing.

2.4 Ternary mixtures of DMPG/DMPE/TMCL

Whereas the binary mixtures have been studied before, the mixing behaviour of the ternary mixture has not been investigated.

Figure 2-4-1 shows an overview of the compositions of the binary (Section 2.3) and ternary mixtures studied by DSC.

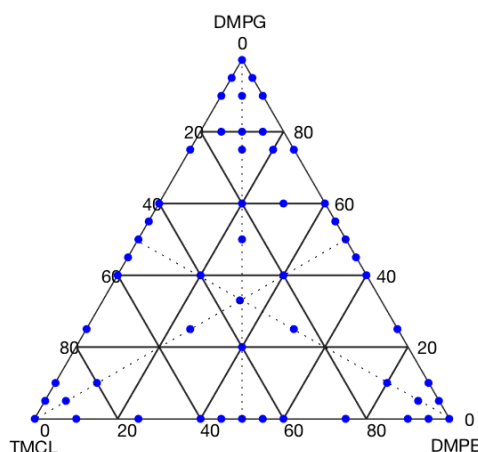


Figure 2-4-1 Ternary diagram of DMPG, DMPE and TMCL. The blue points indicate the composition of binary and ternary mixtures investigated by DSC. The dotted line represents the angle bisector along which two components display a 1:1 ratio.

2.4.1 DSC

The DSC results of ternary mixtures with increasing amounts of TMCL and a constant DMPG/DMPE 1:1 ratio are shown in Figure 2-4-2. The temperature maximum of the binary mixture and the pure TMCL only varies by 3°C. As seen already in Section 2.3, the transition width is increased in the binary mixture when compared to the pure lipid. However, the transition width and the end of melting temperature T_{end} increases further by adding TMCL until a ternary mixture with equal amounts of each component is reached. In excess of TMCL, the transition width decreases again and for the ternary mixtures of DMPG/DMPE/TMCL 10%/10%/80% and DMPG/DMPE/TMCL 5%/5%/90% a pretransition between 10-15°C, as observed for the pure TMCL, appears. This pretransition is not observed for the mixture containing 50% TMCL and 25% of TMCL and DMPE, respectively. In comparison to the binary mixtures where DMPE already suppressed the formation of the L_c phase at contents above 10% but DMPG was incorporated into the phase up to contents of 45%, this indicates the formation of the L_c phase in a ternary mixture is also suppressed by a DMPE content of more than 10%.

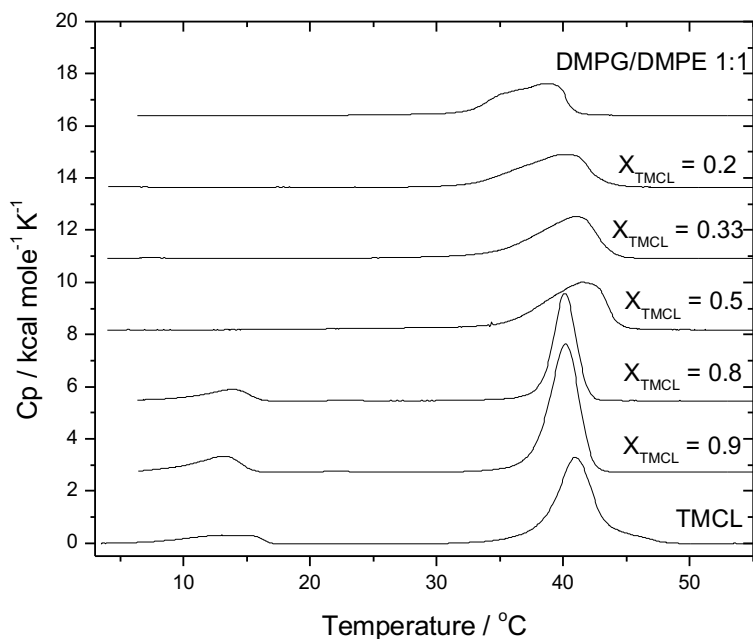


Figure 2-4-2 DSC thermograms of vesicles of ternary mixtures with increasing TMCL content in a DMPG/DMPE 1:1 mixture. For comparison the thermogram of the DMPG/DMPE 1:1 binary mixture and the pure TMCL is shown on top and bottom, respectively.

In Figure 2-4-3 the DSC thermograms of the ternary mixtures with increasing content of DMPE in a DMPG/TMCL mixture with a 1:1 ratio is displayed. The mixture with 33% of each component was already shown in Figure 2-4-2.

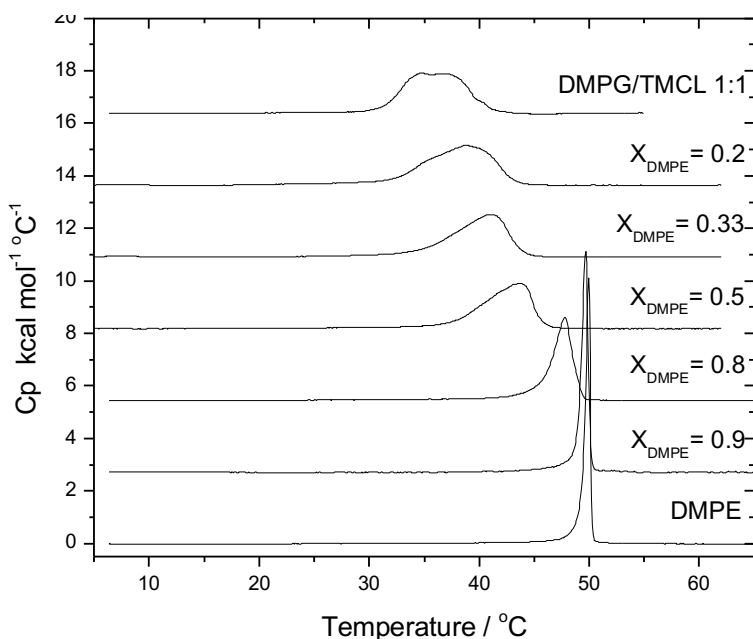


Figure 2-4-3 DSC thermograms of vesicles of ternary mixtures with increasing DMPE content in a DMPG/TMCL 1:1 mixture. For comparison the thermogram of the DMPG/TMCL 1:1 binary mixture and the pure DMPE is shown on top and bottom, respectively.

The transition temperature increases with increasing amount of DMPE as expected. No pretransition is seen in any of the mixtures. The transition width increases slightly with little amounts of DMPE and decreases strongly with higher content of DMPE. When compared to the DMPE/TMCL binary

mixture where an azeotropic maximum for $x_{\text{DMPE}} > 0.9$ was observed (see Figure 2-3-4), the ternary mixture for $x_{\text{DMPE}} = 0.9$ shows a downshift in transition temperature, meaning that the replacement of 50% of TMCL by DMPG inhibits the azeotropic behaviour.

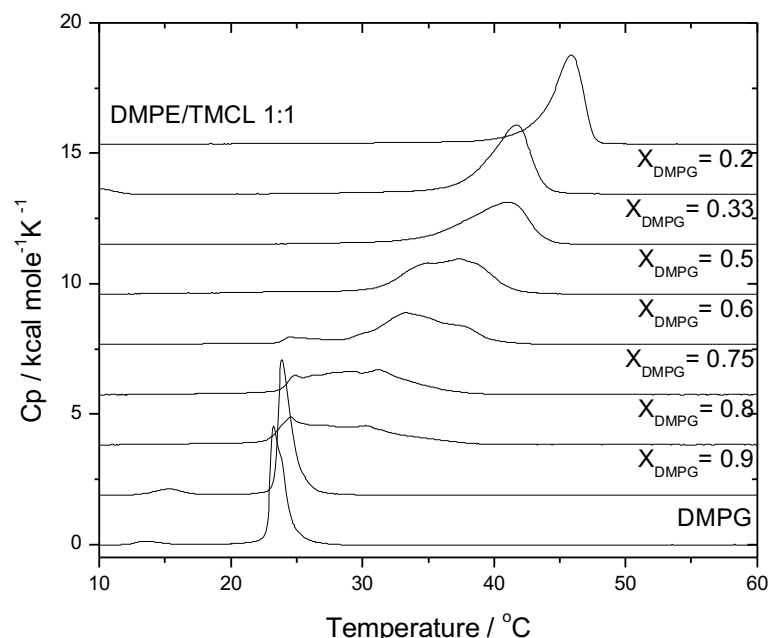


Figure 2-4-4 DSC thermograms of multilamellar vesicles of ternary mixtures with increasing DMPG content in a DMPE/TMCL 1:1 mixture. For comparison the thermogram of the DMPE/TMCL 1:1 binary mixture and the pure DMPG is shown on top and bottom, respectively.

The thermotropic behaviour of ternary mixtures with a DMPE/TMCL 1:1 ratio and increasing amounts of DMPG is displayed in Figure 2-4-4. The transition temperature decreases with increasing amounts of DMPG. Moreover, the transition width further increases with DMPG amounts higher 33% which is in contrast to an ideal behaviour. The transition width increases even more with a DMPG content higher 50%. This clearly shows that the non-ideal behaviour observed for the binary mixtures of DMPG with TMCL, is also observed for the ternary lipid mixtures.

A comparison of thermotropic behaviour of extruded and vortexed vesicles consisting of a ternary lipid mixture are shown in Figure S2-4-1, S2-4-2 and S2-4-3.

To investigate the temperature dependent phase behaviour of the ternary mixtures in more detail we additionally performed DSC measurements with high contents of DMPG and varying contents of DMPE and TMCL

The results are displayed in Figure 2-4-5 in comparison to the DMPE/TMCL 1:1 mixtures. The effect of transition temperature is, as expected, in the same range as observed for the ternary mixtures with DMPE/TMCL 1:1 ratio. However, the transition width decreases when the DMPE/TMCL ratio is varied. In case of the mixtures containing 50% DMPG and DMPE/TMCL by 40%/10% and 10%/40% the decrease in width is only marginal as both, the onset and offset of the transition, are shifted to higher temperatures. In the DMPG/DMPE/TMCL 60%/30%/10% mixture only the onset of the phase transition is shifted to higher temperatures whereas in the DMPG/DMPE/TMCL

75%/20%/5% mixture the transition onset is shifted to higher and the offset to lower temperatures. The transition onset of the mixture containing 80% DMPG and 15%/5% as well as 5%/15% of DMPE/TMCL are shifted to the higher temperatures but the offset is identical to the DMPE/TMCL 10%/10% mixture. The symmetry of the transition width of the mixtures varied in DMPE/TMCL content supports the finding that the DMPE/TMCL mixture has a nearly ideal mixing behaviour and non-ideality is induced by the addition of DMPG to the binary mixture.

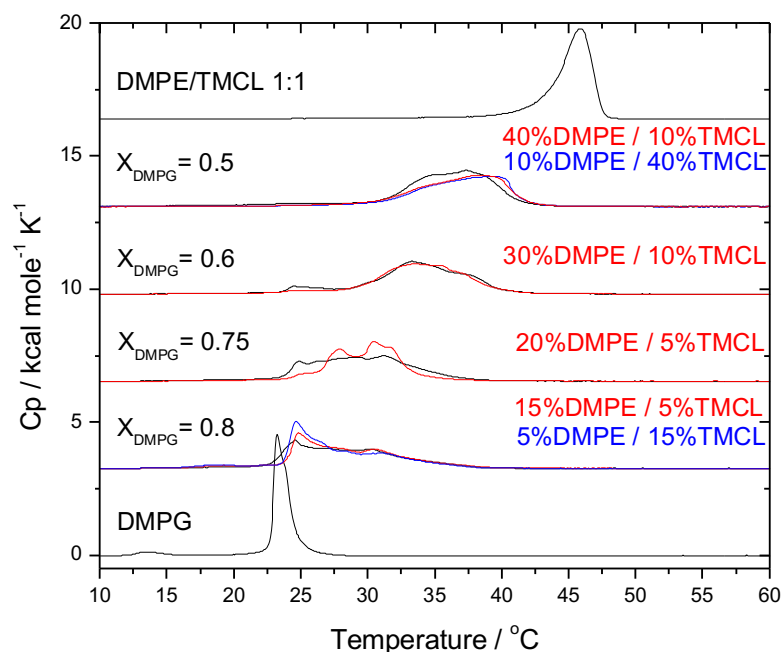


Figure 2-4-5 DSC thermograms of vesicles of ternary mixtures with increasing DMPG content in a DMPE/TMCL mixture with varying content of DMPE and TMCL. The black curves depict the DMPE/TMCL 1:1 mixture with the respective DMPG molar fraction for comparison as well as the thermogram of the DMPE/TMCL 1:1 binary mixture and the pure DMPG on top and bottom, respectively.

The phase behaviour of the ternary lipid mixture of DMPG, DMPE and TMCL shows gel-phase demixing with high contents of DMPG, although all components contain myristoyl chains. This means that gel phase demixing does not only occur from different chain non-ideality caused by hydrophobic mismatch of the different chain length (164) but also occurs as a result of different headgroup structure.

The ternary phase diagram is displayed in Figure 2-4-6 summarising the on- and offset temperatures of the measurements discussed above indicating a peritectic behaviour with a gel phase demixing at high DMPG content.

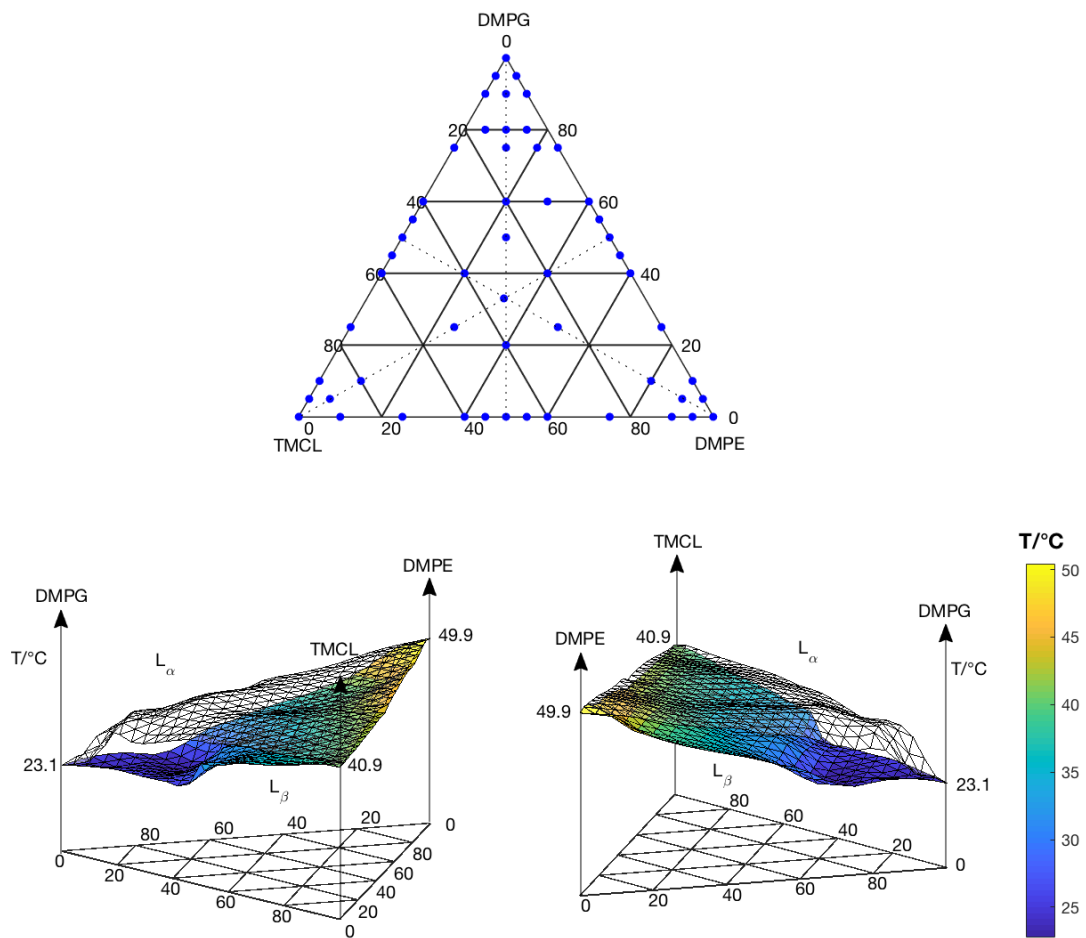


Figure 2-4-6 Ternary phase diagram of DMPG, DMPE and TMCL. Top: The blue points indicate the composition of the binary and ternary mixtures. Bottom: 3D plot of the solidus (coloured mesh) and liquidus (transparent mesh) area generated from the temperature on- and offsets. The two surfaces enclose the coexistence volume of the gel and liquid crystalline phase.

3

Interaction of cyclic antimicrobial hexapeptides with model lipid membranes

3.1 Introduction

The lipid-clustering model of antimicrobial action associates the specificity of antimicrobial peptides with the composition of lipid mixture of the bacterial target membrane. To understand in more detail the effect of the lipid clustering we studied the interaction of trivalent cationic cyclic hexapeptides possessing different amino acid compositions and antimicrobial activities with negatively charged PG and cardiolipin bilayers and binary mixtures with PE as well as ternary cardiolipin-PG/PE mixtures.

We determined the efficacy of the different peptides for inducing lipid clustering by analysing changes in the lipid phase transition temperature utilizing DSC (Chapter 3.2) and ATR-IR spectroscopy (Chapter 3.3). The binding properties were studied with ITC (Chapter 3.4).

Until now, peptide induced demixing has mostly been explained to be caused by charge interactions and, thus, to be mainly dependent on the number of charges (102). However, previous work already indicated that lipid clustering induced by cationic peptide binding is lipid specific, as mixtures of DPPG with DPPC did not show phase separation after peptide binding (108). Although an earlier article reported no effects of sequence variations on the lipid clustering efficacy (110), we show here that the amino acid sequence in trivalent cyclic hexapeptides has a major impact on the ability to induce lipid clusters.

3.1.1 Cyclic hexapeptides as antimicrobial peptides

Computational analyses and synthetic combinatorial libraries (45-47, 243-245) of natural occurring antimicrobial peptide structures have been successful in the prediction of sequences of small artificial model peptides with high antimicrobial potency. Some of them, for example pexiganan, a magainin 2 analogue with 22 amino acids, omiganan, a derivative of indolicidin, daptomycin or the cyclic polymyxin B found their way into clinical trials (48, 50).

The most common feature of antimicrobial peptides is their amphipathic structure, therefore, the synthesised small artificial peptides contain mostly the charged residues arginine, histidine or lysine and the hydrophobic amino acids tryptophan, leucine and phenylalanine (49).

The minimal inhibitory concentration (MIC) values of short peptides with three to six charged and hydrophobic amino acids against *E. coli* and *S. aureus* was investigated by Strøm et al. (246) showing that the highest antimicrobial effects were obtained by peptides with bulky hydrophobic residues such as tryptophan and tryptophan analogues. The most efficient motif consisted of three arginine and three tryptophan moieties besides two cysteine containing analogues (47, 243). Liu et al. (247) investigated the antimicrobial activity of linear $(RW)_n-NH_2$ structures with n being 1-5 against *E. coli* and *S. aureus* strains. The authors showed that $(RW)_3$ was the best choice in resolving the antimicrobial and haemolytic activity conflict. The hexapeptide $(RW)_3$ showed also the highest antiviral activity against vaccina virus (248) and showed promising results in contributing to the storage life of blood samples (249).

Dathe et al. showed in 2004 that the cyclisation of short peptide sequences shows up to a 62-fold higher antimicrobial activity and selectivity when compared to their linear analogues (250). Additionally, cyclisation results in a better stability towards trypsin (251), which makes cyclic antimicrobial peptides attractive for pharmaceutical usage.

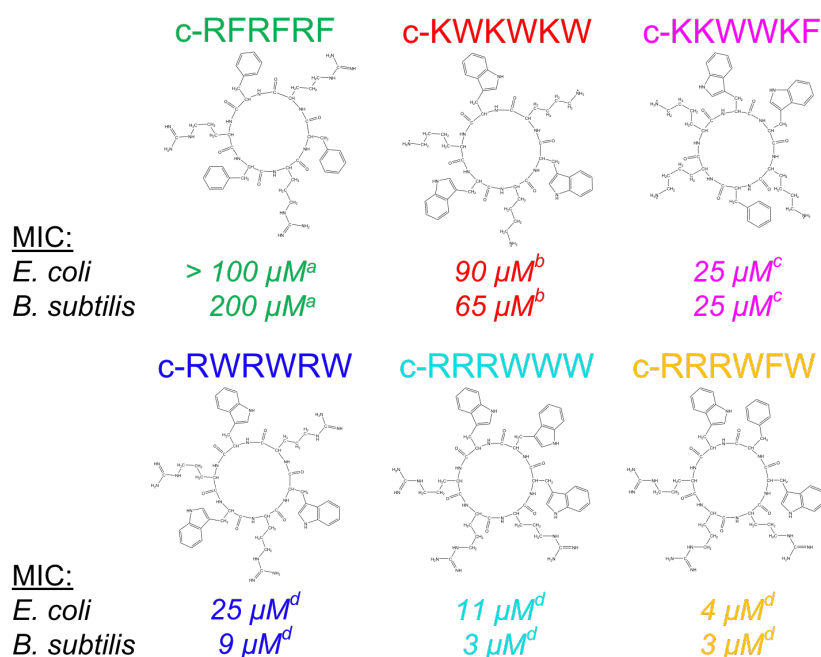


Figure 3-1-1 The cyclic trivalent hexapeptides used in this study with their respective minimal inhibitory concentration (MIC) taken from ^a(252), ^b(251), ^c(253), ^d(254). The colour coding used for the different peptides is the same as used for the presentation of data.

Figure 3-1-1 displays the structure of the cyclic peptides used in this study with their respective minimal inhibitory concentration (MIC values for c-RRRWWW and c-RRRWFW towards other bacterial strains can be taken from Speck et al. (255)). The cyclic peptides studied here are a result

of a combinatorial library study of lactoferricin in which the cyclic c-RRRWW was identified as the most potent candidate for antimicrobial action with a bactericidal effect at the minimal inhibitory concentration and a rapid killing kinetic (145, 245, 254).

To understand the effect of the primary amino acid sequence, the main focus of this study is the comparison of the alternating c-RWRWRW and the block-peptide analogue c-RRRWWW. Assuming the peptide backbone structure is similar for both peptides, c-RWRWRW is reduced in amphipathicity. Both show a high antimicrobial activity of which the block-peptide is still the more active antimicrobial peptide towards the investigated *E. coli* and *B. subtilis* strains. For further comparison, we also investigated the alternating c-KWKWKW with a significantly decreased antimicrobial activity and the alternating c-RFRFRF with the lowest antimicrobial activity of all studied peptides.

Additionally, the lysine analogue c-KKWWKF of the previously investigated arginine containing peptide c-RRWWRW (108, 109, 256) with a small block structure was included in this study. The antimicrobial activity of c-KKWWKF compared to c-RWRWRW is similar towards *E. coli* but still lower for *B. subtilis*.

Like a few other antimicrobial peptides (257) the cyclic peptides investigated here did not induce membrane leakage (119, 251). Therefore, their antimicrobial action must depend on other effects resulting from the interaction with bacteria membranes.

3.1.2 Cyclic peptide secondary structure

Secondary structures of protein and peptide backbones can be defined by the sequence of dihedral angles of the N-C α and C α -C bond called *phi* (φ) and *psi* (ψ), respectively, as defined by Ramachandran et al. (258). For the amide bond, only *cis*- or *trans*- isomers for the C=O and N-H group need to be characterized as it has a partial double-bond character and is, therefore, restricted in rotation (259). The common backbone structures like α -helices, β -strands, turns and loops result from distinctive rotations of these bonds stabilised by N-H to C=O hydrogen bonding. As the protein and peptide backbone are chemically equivalent, the determination of the secondary structure, i.e. the dihedral angle of each amino acid, is determined by the primary amino acid sequence, which is known as the “Anfinsen concept” (260). However, the driving forces behind these folding processes are still under discussion and a matter of current research (261, 262)¹. Within the protein or peptide folding mechanisms, turns and loops play a key role as they can reverse the overall chain direction (263, 264). About 50% of residues are involved in repetitive sequences with about one-third in α -helices and one-fifth in β -strands (265).

¹The interested reader is advised to the cited reviews

The common motifs to reverse a chain direction are turns and loops. Here, cyclic peptides play a key role in the study of detailed structures. Turns are classified by the number of amino acids involved in the turn structure of a hydrogen bond formed between the i th and the $i+n$ th position in the peptide chain. The turns are denoted π -turn, α -turn, β -turn and γ -turn with n being 5, 4, 3 and 2, respectively, and where the β -turns build up 45 % of the coil structures (266).

The β -turn has a characteristic distance of up to $\sim 7 \text{ \AA}$ between amino acids in the i th and the $i+3$ rd position (266), which can be a result of a hydrogen bond formation (also named a $1\leftarrow 4$ hydrogen bond). The two amino acids forming the turn can adopt different torsion angles and, therefore, lead to different turn structures. A turn is regarded as different when 3 of the angles deviate by $\pm 30^\circ$, whereas the fourth can deviate by $\pm 45^\circ$.

A turn comprising only one amino acid in which a hydrogen bond is formed between the amino acid in the i th and $i+2$ nd position (a $1\leftarrow 3$ hydrogen bond) is called γ -turn. The occurrence is only about 3% of the turn structures when compared to β -turns. Two structures, the classic γ -turn and the inverse γ -turn, can be distinguished by their respective dihedral angle (267). Table S3-1-1 gives a brief overview of the various β -turn and γ -turn structures identified in proteins.

The cyclic hexapeptides used in this study can be unstructured or adopt a β - or γ -turn structure or combinations thereof with mono- or bifurcated hydrogen bonds (please note that an α -turn would be considered as a single γ -turn). The different amino acid sequence allows different combinations of turn structures. The three peptides with alternating sequences can only form a $1\leftarrow 4$ hydrogen bond between a charged and a hydrophobic residue in a β -turn structure, leaving one charged and one hydrophobic residue on each $i+1$ st and $i+2$ nd position in the β -turn, respectively. Also for the block-peptide c-RRRWWW and c-RRRWWF the $1\leftarrow 4$ hydrogen bond can only be formed between a charged and a hydrophobic residue resulting in two possible structures. One possible structure leaves one charged and one hydrophobic residue on each $i+1$ st and $i+2$ nd position, whereas the amino acids in i th and $i+3$ rd position are exchanged when compared to the alternating sequence. The second possible structure leaves two charged and two hydrophobic amino acids in each turn. In two of three possible β -turn structures of the semi-block-peptide c-KKWWKF, a $1\leftarrow 4$ hydrogen bond can either be formed between two charged or two hydrophobic residues. In these cases one turn comprises a charged and a hydrophobic amino acid and the other turn either both charged or hydrophobic residues, as shown for c-RRWWRF (268). In a third possible structure, the $1\leftarrow 4$ hydrogen bond is formed between a charged and a hydrophobic amino acid that leaves a charged residue in $i+1$ st and a hydrophobic residue in $i+2$ nd position for each turn. The possibility of variations in structure formation, i.e. changes in distance between hydrophilic and hydrophobic residues, influences the amphipathicity of the peptides which might play a role in membrane binding.

Previous NMR studies, supported by MD simulations, resolved a β -turn structure (268-270) for two hexapeptides c-RRWRF and c-RRRWF (270). The c-RRWRF forms a 1 \leftarrow 4 hydrogen bond between tryptophan in the third place (W3) and the phenylalanine (F6) with two arginines forming a type I and the tryptophan and arginine forming a type II' β -turn. The same principle structure was found for c-KKWWKF with two lysines forming a type I and the lysine-tryptophan moieties forming a type II' β -turn (269). In c-RRRWF, the hydrogen bond is formed between the middle arginine (R2) and phenylalanine (F5), as depicted in Figure 3-1-2, leaving one arginine in the $i+1$ st and one tryptophan in the $i+2$ nd position of one turn and one tryptophan in the $i+1$ st and one arginine in the $i+2$ nd position of the other turn. This results in a hydrophilic and hydrophobic side perpendicular to the hydrogen bonds. However, the β -turn is rather flexible and contributes to bifurcated hydrogen bonding with amine groups of the peptide backbone, as well as the sidechain guanidinium groups (see 2OTQ in PDB database for details). No γ -turn structure was found in the NMR experiments.

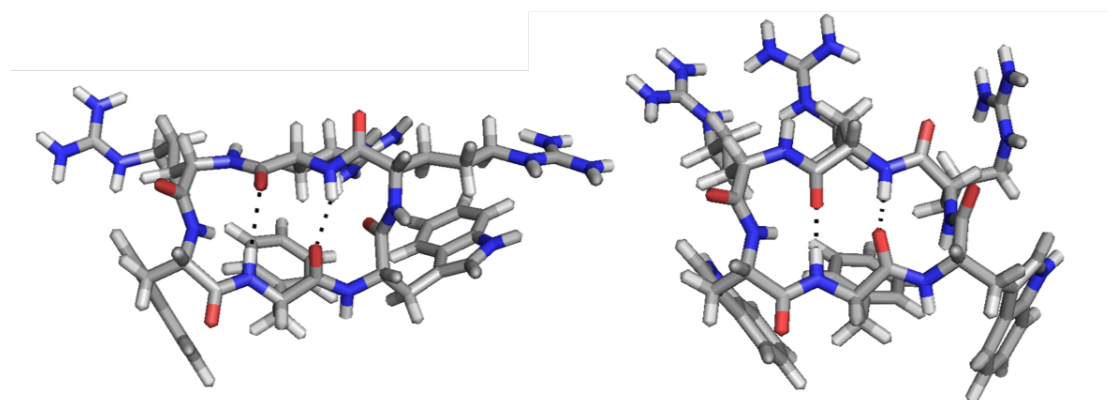


Figure 3-1-2 Two top views of the structures of c-RRRWF bound to DPC micelles showing the β -turn backbone structure from Appelt et al. (268). Bifurcated amide H-bonds including the N-H group in the β -turn were also observed within these structures (PDB database: 2OTQ).

Since proteins and peptides show characteristic infrared absorption bands, the respective structural relations are a matter of research (218). Typical absorbance peaks from peptides and proteins are the amide A and amide B bands at 3300 cm^{-1} and 3100 cm^{-1} , respectively (more than 95% N-H stretching vibration) and the combined vibrational modes, such as amide I at $1600\text{-}1700\text{ cm}^{-1}$ (76% C=O stretch, 14% C-N stretch, 10% C-C-N deformation vibration), amide II at $1510\text{-}1580\text{ cm}^{-1}$ (43% N-H in-plane bending, 29% C-N stretch, 11% C=O in-plane bending, 9% C-C stretch and 8% N-C stretch vibration), amide III at $1200\text{-}1400\text{ cm}^{-1}$ (55% N-H in-plane bending, 19% C-C stretch, 15% and 11% C=O in-plane bending vibration) and amide V at $610\text{-}710\text{ cm}^{-1}$ (66% C-N torsion and 34% N-H out-of-plane bending vibration) (271).

The amide I absorption band is the most widely used to determine secondary structures. The β -turn absorbance bands occur at $1690\text{-}1660\text{ cm}^{-1}$ and a second peak between $1645\text{-}1635\text{ cm}^{-1}$ (272). The absorption band at $1645\text{-}1635\text{ cm}^{-1}$ can be attributed to intramolecular hydrogen bonded carbonyl moieties, the 1 \leftarrow 4 hydrogen bond, whereas the absorption band at $1690\text{-}1660\text{ cm}^{-1}$ results from the

bond vibration of “free” solvent exposed carbonyl groups, i.e. weakly solvated or non-acceptor carbonyls. Although the precise amide I wavenumbers of all conducting sub-bands vary with different studied peptides (273), the attribution of low and high wavenumbers to intramolecular bound and free amide carbonyls, respectively, is a common finding (274-276) among cyclic peptides like tetrapeptides (277, 278) and cyclic surfactin (279). Also studies with time resolved IR-measurements (280) concluded the same attribution of free and bound carbonyls in amide I vibration. The band ratio of high to low wavenumber in the observed β -turns is therefore $\sim 2:1$ or $3:2$, whereas β -sheet ratios are $\sim 1:10$ (273, 281)

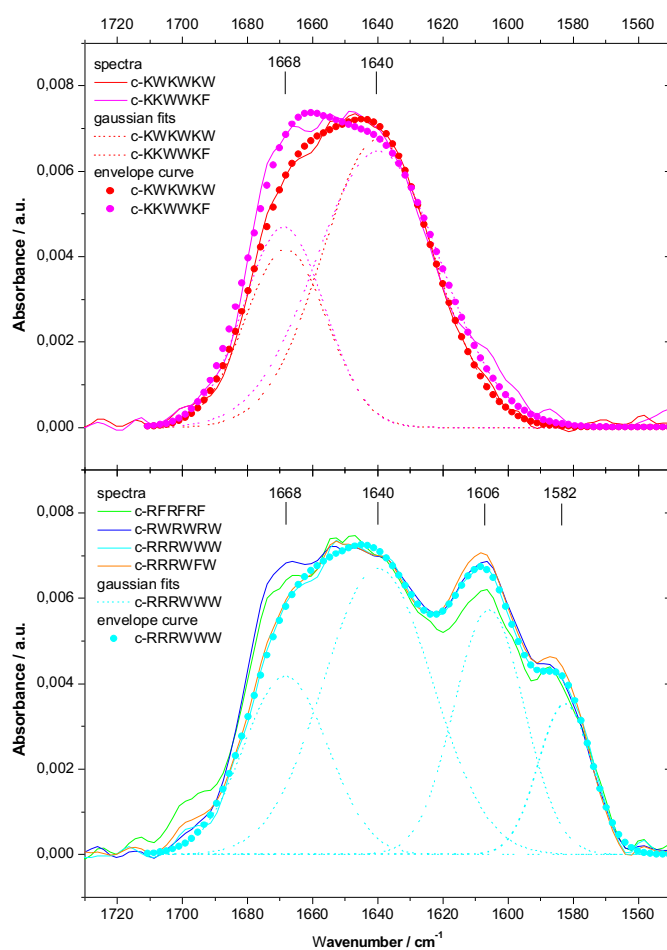


Figure 3-1-3 Top: Amide I bands of the lysine containing peptides at 10°C in 100mM NaCl (in D₂O, pH 6.8) recorded using ATR-IR spectroscopy (lines). Bottom: Amide I and guanidinium bands of the arginine containing peptides. The curves were fitted with sub-bands at 1668 cm⁻¹ (1670 cm⁻¹), 1640cm⁻¹, 1606 cm⁻¹ and 1582 cm⁻¹ (dashed lines – exemplified for c-KWKWKW, c-KKWWKF and c-RRRWWW). The resulting fitted curve is plotted in dots. The spectra have been normalized to achieve 7.5 milliabsorbance at 1640 cm⁻¹.

Figure 3-1-3 shows the amide I and guanidinium bands recorded for the different hexapeptides in NaCl-D₂O solution with the respective fits. As the arginine containing peptides show two additional guanidinium vibrational bands at 1606 cm⁻¹ and 1582 cm⁻¹ overlapping with the amide I band, the amide I fit was first performed with the lysine containing peptides. The fit resulted in two amide I sub-bands at 1668 cm⁻¹ (or 1670 cm⁻¹) and 1640 cm⁻¹ with a band area ratio of $\sim 1:2$. The small

absorption bands at 1607 cm^{-1} and 1596 cm^{-1} for c-KKWWKF and c-RRRWWF belong to the absorption of the phenylalanine moiety in D_2O (282). The fits of the arginine containing peptides yield similar results for the amide I band with additional guanidinium vibrational bands, as displayed for c-RRRWWW. The overall band shape is very similar among all observed cyclic peptides. Only c-RFRFRF, c-RWRWRW and c-KKWWKF show a more pronounced shoulder at 1670 cm^{-1} .

Many attempts have been made to identify the different β -turns by their infrared absorption pattern (267, 283-285). However, the more comprehensive review of Vass et al. shows that no general rules apply to the assignment of vibrational bands or vibrational band patterns to respective β -turn structures, although some tendencies within cyclic peptides can be observed (273). Here, the influence of the amino acid side chains seems to have a significant contribution to the amide I frequency. Bour et al. could show with DFT calculations that the amide C=O stretching mode varies between 1630 cm^{-1} and 1705 cm^{-1} for different amino acid side chains (286). In addition to the effect on the backbone vibration, the side chain could affect the backbone accessibility for solvent molecules, which might mostly affect the solvent exposed C=O group vibration at $1660\text{-}1690\text{ cm}^{-1}$. According to Mantsch et al. (281) a band area ratio for a β -turn motif would be expected to be 3:2 or 2:1 (4:2) for the solvent exposed C=O band at higher wavenumbers to the band at lower wavenumbers, attributed to the C=O groups forming intramolecular hydrogen bonds which is not observed in our measurements. However, the relative band ratio or band area ratio of cyclic peptides cannot be interpreted quantitatively since hydrogen bonded and non-acceptor carbonyls have different dipole moments and, therefore, different molar extinction coefficients (273).

Some publications on β -sheet vibrational frequencies of single stranded peptides support a more complex interpretation of the amide I band frequencies (287, 288) where the splitting of the amide I band is mainly influenced by interstrand coupling and the extinction coefficient depends on structural contributions. The *ab initio* based simulation by Kubelka and Keiderling (288) found that the splitting and intensity of the amide I band in β -sheets is mostly influenced by the phase of the respective vibrational mode. Twisted and pleated strands show the lowest splitting and highest intensity due to reduced interstrand coupling. Therefore, variations in the backbone twist might as well be a cause for the unexpected band area ratio.

As the peptides show a similar amide I band, we conclude that these peptides have a rather flexible β -turn structure that forms bifurcated hydrogen bonds within the backbone and in combination with amino acid side groups.

Besides the vibrational frequencies belonging to the lipid and the peptide backbone, additional information about molecular interactions can be attained from the arginine and tryptophan side group vibrations.

The charged guanidinium group ($\text{pK} = 11.2$) shows characteristic IR vibrational bands, such as the band at 1608 cm^{-1} and 1586 cm^{-1} (282) in D_2O or 1673 cm^{-1} and 1633 cm^{-1} in H_2O , respectively

(218, 289, 290). Both vibrational bands correspond to a combination of C-N and N-H guanidinium vibrations often referred to as symmetric and antisymmetric vibrational bands. The pure symmetric planar guanidinium with a 3-fold symmetry shows a single symmetric vibrational peak at $\sim 1600\text{ cm}^{-1}$ when solvated in D_2O ($\epsilon = 868\text{ M}^{-1}\text{ cm}^{-1}$ (291)) resulting from the C-N antisymmetric stretch combined with NH_2 scissoring motions. However, 2-D spectroscopy revealed that as a result of solvent interactions this vibrational peak already consists of two underlying degenerated vibrational modes, located slightly above and below 1600 cm^{-1} (291).

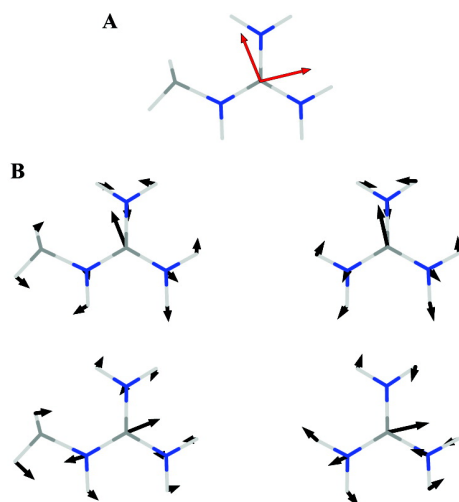


Figure 3-1-4 (A) Transition dipole directions of the degenerated modes of methyl guanidinium. (B) Comparison of the degenerated modes of methyl guanidinium (left) and guanidinium (right) for the guanidinium vibration at wavenumbers $< 1600\text{ cm}^{-1}$ (top) and $> 1600\text{ cm}^{-1}$ (bottom). The atomic displacements are indicated with black arrows. Taken from Ghosh et al. (292).

The difference in split frequency is further increased by the binding of residual groups to the guanidinium group, which influences the vibrational mode, as in methyl-, ethylguanidinium and arginine (292, 293). The resulting transition modes corresponding to the two vibrational frequencies are shown in Figure 3-1-4. The angle between the two transition dipoles changes from 90° in guanidinium to 99° for methylguanidinium and was calculated to be shifted to 114° for arginine in a dipeptide (292). The guanidinium band, therefore, can be influenced by the peptide backbone vibration depending on the secondary structure (292, 294). On one hand, the position of the guanidinium bands are sensitive to solvent and counter ion interaction (292, 294-298). On the other hand, a change in guanidinium band intensity ratio might also occur as a result of changes in the extinction coefficient of both contributing modes due to changes in dipole moment. Hydrogen bond formation of the guanidinium group or counterion interaction, for example, affect the dipole moment leading to changes in guanidinium band ratio (296-301).

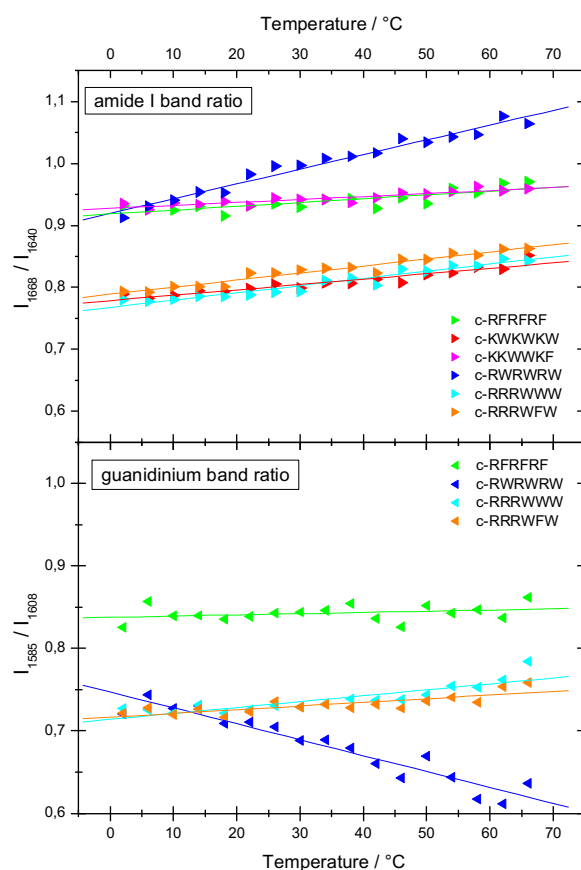


Figure 3-1-5 Temperature dependence of the amide I (I_{1668}/I_{1640}) and guanidinium (I_{1585}/I_{1608}) band ratio of the different peptides in 100 mM NaCl (in D_2O , pH 6.8) recorded using ATR-IR spectroscopy with their respective linear fit.

Figure 3-1-5 top displays the temperature dependence of the amide I band ratio (I_{1668}/I_{1640}) of the different peptides in solution. One example for an original spectra for c-RWRWRW at 2°C and 60°C is shown in Figure S3-1-2 of the supplementary data. The positive slope is according to the expectation that increasing temperature leads to a decreased amount of hydrogen bonds for the benefit of “free” carbonyls. The absolute value should not be over-interpreted as the underlying water vapour signal might be a source of errors.

However, the comparison of the slope yields information about the temperature stability of the peptide bond. The slope varies between $0.5 \times 10^{-3} \text{ } ^\circ\text{C}^{-1}$ to $0.8 \times 10^{-3} \text{ } ^\circ\text{C}^{-1}$ for both lysine-containing peptides and c-RFRFRF, whereas the slope for the arginine-tryptophan containing block-peptides c-RRRWWW and c-RRRWFW is $1.2 \times 10^{-3} \text{ } ^\circ\text{C}^{-1}$ and $1.1 \times 10^{-3} \text{ } ^\circ\text{C}^{-1}$, respectively. The temperature stability of the amide bond is significantly decreased for c-RWRWRW, yielding a slope of $2.3 \times 10^{-3} \text{ } ^\circ\text{C}^{-1}$.

Figure 3-4-1 bottom displays the guanidinium band ratio I_{1585}/I_{1608} of the arginine containing peptides in solution as a function of temperature. With increasing temperature the guanidinium peaks decay in intensity but the ratio remains almost constant for c-RFRFRF, c-RRRWWW and c-RRRWFW. The alternating RW-peptide, however, shows a negative guanidinium band ratio. This

could be a result of additional bifurcated hydrogen bonds or γ -turn formation at the expense of a 1 \leftarrow 4 hydrogen bond leading to an additional infrared absorption around 1608 cm^{-1} (the original spectra at 2 $^{\circ}\text{C}$ and 60 $^{\circ}\text{C}$ can be found in the supplementary data). These data show that the combination of arginine and tryptophan in an alternating sequence has a major impact on the peptide bond stability.

Regarding the tryptophan indole vibrational frequencies, Fabian et al. (302) could identify a characteristic tryptophan band occurring at 1334 cm^{-1} . This band can be attributed to a combinatorial vibration of mainly benzene and pyrrol-C-C stretching vibration (303) potentially accompanied by benzene C-H deformation vibration (289, 304-306). This band is sensitive to environmental changes, such as pH (305) and hydrophobicity (307) and expected to change upon hydrogen bonding and π -interactions. Therefore, a correlation of temperature dependent changes in guanidinium ratio or frequency and indole vibrational peak position is expected for guanidinium-indole interaction of arginine-tryptophan-containing peptides and will be discussed in Section 3.3.

3.1.3 Specific lipid-peptide interactions

In this section we discuss the different driving forces and possible interactions resulting from different primary peptide sequence causing a different antimicrobial and clustering efficiency.

The electrostatic interaction between the positively charged peptides and the negatively charged lipids of many bacterial cell membranes (see Section 1.3) is the main driving force of antimicrobial peptide-lipid interaction. The binding constant of counter ions interacting with negatively charged membranes has been shown by de Kruijff to increase tenfold with each additional charge (308, 309), resulting in a change of ΔG by $-1.34 \text{ kcal mol}^{-1}$ at $20 \text{ }^\circ\text{C}$. The observed binding constant values for trivalent molecules, such as R_3 , K_3 (310) and spermidine (311, 312) binding to a PG membrane, were in the order of 10^3 M^{-1} ($\Delta G = -4.01 \text{ kcal mol}^{-1}$), which is in accordance to the finding by de Kruijff (308).

Additionally to the electrostatic contributions hydrophobic contributions can be observed. Ladokhin and White probed the additivity of free energy arising from hydrophobic and electrostatic interaction (313). The observed ΔG value for indolicin and phenylalanine, leucine and tyrosine variants thereof, binding to pure POPC and POPG membranes, was measured by equilibrium dialysis and plotted versus hydrophobic free energies $\Delta G_{H\Phi}$ calculated from the Wimley and White hydrophobicity scale (314). The resulting slope for peptides binding to POPC was one, which is in good agreement with the assumption that the binding constant increases with increasing hydrophobicity in the case of non-electrostatic binding $\Delta G = \Delta G_{H\Phi}$ and supports the determined values of free energy in the hydrophobicity scale. In the case of peptide binding to POPG, the observed absolute ΔG values were remarkably increased (by ~ -2 to -8 kcal mol^{-1}), but the slope was reduced to 0.3. This means that the resulting ΔG cannot be simply calculated by the addition of the hydrophobic and electrostatic contribution $\Delta G = \Delta G_{H\Phi} + \Delta G_{ES}$ with

$$\Delta G_{H\Phi} = -\sigma_{NP} A_{NP} \quad (3.1)$$

and

$$\Delta G_{ES} = -zF\Phi \quad (3.2)$$

where σ_{NP} and A_{NP} are the solvation parameter of non-polar groups and the non-polar surface exposed to the solvent, respectively, z is the number of charges, F the Faraday constant and Φ the surface potential (computed from Gouy-Chapman theory - see Section 1.3). Moreover, the authors found that the effective charge of the peptide z_{eff} reduces by 20 % for each additional increase of 3 kcal mol^{-1} in hydrophobic free energy.

Besides these general aspects, many additional contributions to the free energy of binding, like conformational changes, π -stacking or changes in hydrogen bonding, can be expected.

In a combined study of DSC, ITC, fluorescence and NMR spectroscopy, Jing et al. found an upshift in phase transition temperature of pure DPPG of the linear analogue Ac-RRWWRF-NH₂, combined with a penetration of the hydrophobic amino acids in the lipid chains of SDS and DPC micelles (315) which was further confirmed by a blue shift in fluorescence absorption of the tryptophan emission band. The identified binding constant to POPG at 30 °C was $5 \times 10^6 \text{ M}^{-1}$.

The NMR study by Appelt et al. (269) on the cyclic peptides c-RRWWRF, c-KKWWKF, c-RRYYRF and a β -(2-naphthyl)-L-alanine analogue supported the finding of alkyl chain penetration by hydrophobic amino acid residues also for the cyclic analogues. Using Nuclear Overhauser Enhancement Spectroscopy (NOESY) the authors could identify interaction sides of the lipid-peptide interactions. For SDS micelles the c-RRWWRF β -turn structure was found parallel to the detergent surface with the arginine guanidinium groups interacting with the detergent headgroup and the arginine side chains buried in the hydrophobic core. The peptide backbone was tilted in the case of c-RRWWRF and c-KKWWKF interacting with DPC micelles. The two neighbouring arginine side groups of the type I β -turn and the phenylalanine interacted with the detergent headgroup. The third arginine was buried with the tryptophan in the hydrophobic membrane region, showing an interaction of the arginine CH₂-groups with the surfactant alkyl chain. A similar structure was found for c-KKWWKF.

In an MD-simulation of the cyclic peptides interacting with DPPC membranes in different lipid-peptide ratios performed by Appelt et al. (270), the resulting tilt of the peptide backbone was found to be $15\text{-}20 \pm 8^\circ$ for the peptide, supporting the NMR finding for DPC micelles. The penetration of the peptide into the lipid chain region was found to extend over the first eight to nine methylene groups. The area increase per monolayer for peptide insertion is expected to be 18 % for simple area addition in a 12:128 peptide-lipid mixture but was shown to be only 5 %. This was due to the fact that the lipid chains compress, i.e. the chain order increases in the first eight to nine CH₂-groups where the peptide side chains inserted into the membrane. The resulting decrease in area per lipid molecule was about 14 % from 0.64 nm^2 to 0.55 nm^2 , assuming a constant peptide area of 1.4 nm^2 . The simulation further showed an increase in water penetration of the bilayer due to peptide insertion. The water density along the penetration depth of the peptide was reduced, but the overall penetration depth by water molecules was increased for the $\sim 10:1$ lipid-peptide ratio. In particular, this led to a decrease in free energy barrier width for water molecules making the trespassing of water through the membrane more likely. This might contribute to the antimicrobial effect as the proton gradient of the bilayer decreases.

Appelt et al. further showed that a distinct lipid-peptide interaction between DPPC and c-RRWWRF occurred. Up to eight lipids were bound by one peptide molecule in the 128:2 lipid-peptide ratio simulation. Each lipid headgroup formed hydrogen bonds with the ester carbonyl or the phosphate oxygen to the guanidinium moiety of the arginine side chain. Increasing peptide concentration led

to a dehydration of the lipid headgroup accompanied by a decrease in hydrogen bonding to the lipid carbonyl group. The lipid-peptide complex formation led to a significant decrease of the lipid diffusion coefficient of about one-third. This could serve as a seed crystal in a crystallisation process. The ability of complex formation with lipid headgroups was discussed as the reason for increased antimicrobial activity observed for arginine containing peptides when compared to lysine containing analogues, e.g. c-KKWWKF and c-RRWRF. Arginine showed up to five hydrogen donors, whereas lysine could only form up to three possible hydrogen bonds.

3.1.3.1 Lipid interaction with lysine and arginine

In a systematic simulation study Li et al. (316) reported a different interaction of lysine and arginine with the lipid phosphate group. The formation of monodentate hydrogen bonds between lipid-phosphate-oxygen and lysine-ammonium makes up 98 % of lipid-phosphate-peptide interaction but only 38 % for the guanidinium group binding to a lipid-phosphate-oxygen (see also (317)). Multidentate hydrogen bonds were found in 41 % of phosphate-methylguanidinium clusters. Various combinations of arginine binding to the lipid headgroup are possible. In 52 % of these multidentate clusters one arginine binds to two phosphate groups. In 7 % of these guanidinium-phosphate 1:2 clusters an “arginine-fork” structure was observed. The “arginine-fork” describes the binding of one guanidinium group by four H-bonds with two oxygens of two phosphate groups (318). Additionally also a “2:1 guanidinium-phosphate complex” (319) or an “arginine-claw” (320) binding have been reported, each resulting in a different stoichiometry of lipid-arginine binding.

Also (ion-mediated) arginine-arginine interactions (321, 322) and structures including water in a cyclic water-phosphate-guanidinium binding has been shown in MD simulations (323).

Since arginine and lysine containing peptides show different antimicrobial and cell penetrating properties, a variety of studies focussing on structural transformations of lipid bilayers or peptide secondary structures have been performed. Schwieger and Blume studied the different behaviour of poly-arginine and poly-lysine with PG and PG-PC mixed membranes (324, 325). The authors reported the ability of both cationic peptides to demix a PG-PC membrane. The effect was more pronounced for poly-lysine, showing a gel phase demixing for PC-PG membranes consisting of less than 50 % PG lipids. It was shown that poly-arginine binds in a β -sheet and poly-lysine in an α -helical conformation to DPPG gel phase membranes. Both peptides adopt an α -helical conformation when bound to the mixed membrane in the gel state. Upon the phase transition, the peptides adopt a random coil structure indicating that the peptide secondary structure is dependent on the charge density (326).

Another difference between lysine and arginine is their respective effect on membrane curvature. Wu et al. reported positive and negative curvature induction by arginine and lysine, respectively,

seen in coarse grained simulations (327). They identified hydrogen bonds formed with the lipid carbonyl group as the critical parameter for the resulting lipid phase. Carbonyl hydrogen bonds with arginine were formed with a 70 % probability, whereas the occurrence of carbonyl-lysine hydrogen bonds was less than 10 %. Binding to the lipid carbonyl leads to a peptide insertion into the lipid chain region and induces a positive curvature whereas the binding to lipid headgroup phosphates only screen the lipid charges and induce a negative curvature. This model of curvature induction is in accordance with the model for antimicrobial action of Bechinger and Lohner (97, 98) (see Section 1.1.3).

This finding is further supported by the “saddle splay curvature selection rule” which states that the loss of curvature induction with decreasing arginine content can be compensated by an increase in lysine and hydrophobic residues. The authors could show that the ratio of lysine to arginine residues of 1080 different antimicrobial peptides correlated to the hydrophobicity in an exponential manner (328).

3.1.3.2 Lipid interaction with hydrophobic amino acid residues

According to the Wimley-White hydrophobicity scale (314) the Gibbs free energy for the transfer of phenylalanine and tryptophan from the aqueous to the membrane phase is $-1.13 \text{ kcal mol}^{-1}$ and $-1.85 \text{ kcal mol}^{-1}$, respectively, whereas the molecular volume of phenylalanine makes only about 83 % of the tryptophan volume (329, 330). The main contributions for the indole group to the free energy are enthalpy-driven bilayer interactions and only minor entropy-driven contributions from the “hydrophobic effect” were observed (60). This observation is often referred to as the “non-classical hydrophobic effect”.

The main difference of the interaction of phenylalanine and tryptophan with lipid membranes is their respective localisation in the lipid bilayer. In contrast to phenylalanine, which preferably locates in the lipid bilayer (331-333), the tryptophan indole group is located at the hydrocarbon-water interface (331). About ~25 % of the indole surface is buried in the hydrophobic chain region (60). The lipid chain order, therefore, increases near the interface and decreases slightly in the hydrocarbon core (334).

The localisation of the indole group at the hydrophilic-hydrophobic interface was also reported by different authors using neutron scattering (335), fluorescence spectroscopy (60, 336, 337), NMR spectroscopy (334) and MD simulations (333, 338, 339). The orientation of tryptophan with respect to the membrane normal was determined by NMR to be $64-67^\circ$ for gramicidin A (340) and 58° for the WALP peptide (341). Several reasons for the preferred tryptophan location at the lipid-water interface, such as non-specific electrostatic effects, dipolar and quadrupolar interactions, cation- π -interaction, hydrogen bond formation and lipophobic effects, are reported in the literature (333, 334):

- I. **Hydrogen bond formation** of the indole N-H (340) to the lipid headgroup (342), lipid carbonyl (333, 338) or water molecules (339) is discussed as the origin of the preference of the tryptophan location. Chaudhuri et al. (343) showed the importance of tryptophan hydrogen bonding for the gramicidin channel formation. However, the possible lipid carbonyl-indole hydrogen bond was shown not to be the decisive parameter for the indole position within the membrane as van der Wel et al. (344) and Yau et al. (334) found the same membrane localisation for the indole analogues indene and N-methyl indole which are incapable of forming hydrogen bonds (see also Esbjörner et al. (345) and Persson et al. (346)).
- II. **Intermolecular π -stacking between lipid and peptide**, more precisely of charged lipid headgroup residues with the indole ring is another reason leading to the observed tryptophan localisation, which is discussed in literature. The important role of π -interactions in biophysical interactions related to their quadrupole moment was proposed earlier (347-349). Tryptophan has a preferred membrane interface localisation when compared to phenylalanine because cation- π interactions are usually stronger with indole than benzene, as determined in the gas phase (350). The occurrence of choline-indole π -interactions was shown in simulations (333) for PC and, even more pronounced, for PE lipids (339). A combined simulation and NMR ROESY study on small amino acid analogues interacting with diacetylphosphocholin (DAPC) supported the finding of H-bonding and π -stacking (351). However, in the NMR NOESY experiments by Yau et al. no specific lipid headgroup interactions were observed (334).
- III. **Intra- and intermolecular π -stacking of peptides** as an important interaction for antimicrobial efficiency was emphasised by Chan et al. and Khandelia et al. (352, 353). The effect of the arginine-tryptophan π -stacking on lipid membranes was observed in simulations by Aliste et al (354). In these simulation studies different interpeptide bonding mechanisms occurred for the Wimley-White peptide Ac-WL-X-LL, with X being R or K. The arginine-tryptophan interaction led to a deeper penetration of the peptides into the hydrophobic bilayer centre. However, salt bridge formation between R and K to the peptides' C-terminus influenced the partitioning coefficient of the peptides, as the guanidinium-indole π -stacking competed with the salt bridge formation. In the case of peptide backbone cyclisation, no C-terminus salt bridge formation is possible, what might be one reason for the observed increased antimicrobial activity upon cyclisation (250). Additionally, Aliste showed (354) that the percentage of hydrogen bonds of arginine to headgroup water is reduced from 42 % to 32 % by the additional possibility to interact with the tryptophan indole ring (348, 355-357). The binding energies for the different π -interactions were determined by another simulation study (358). In water (with the dielectric

permeability $\epsilon = 80.4$ at $20\text{ }^\circ\text{C}$) only negative Gibbs free energy values were observed for arginine-phenylalanine and arginine-tryptophan interactions of $-1.68\text{ kcal mol}^{-1}$ and $-2.18\text{ kcal mol}^{-1}$, respectively. In a low dielectric permeability environment such as chloroform ($\epsilon = 4.8$) the Gibbs free energy values were $-3.5\text{ kcal mol}^{-1}$ for arginine-phenylalanine and $-5.5\text{ kcal mol}^{-1}$ for arginine-tryptophan interactions.

The different symmetries of the peptides would also allow different complex formations via π -stacking of peptide side groups (350, 359-362) with possible contributions of the peptide backbone (363-365) which could occur with charged lipid headgroups, peptide side groups or counter ions (366). Here, the size of the complexed group contributes significantly to the free energy of the complex formation.

- IV. **The lipophobic effect** is described by Yau et al. as a cohesive repulsion of the lipid chains that expels the flat and rigid indole from the hydrocarbon core into the interfacial region (334) as an entropic effect that circumvents the induced lipid chain order. Additionally, the fluorescence data of Schibli et al. (336) indicate that the penetration depth of the indole group results from a given peptide structure and is enhanced by consecutive hydrophobic amino acids. In a comparative NMR and fluorescence spectroscopy study, they observed that the antimicrobial peptide tritrypticidin with three tryptophans in the $i+2$ to $i+4$ position of type VI β -turn (367) shows a restricted movement when compared to other peptides without this consecutive sequence, indicating a deeper insertion into the membrane bilayer.
- V. **The dipole moment** of tryptophan was calculated to be 1.9 D for indole and 2.1 D for N-methyl indole, respectively, with a direction parallel to the N-H bond (346). The dielectric constant of the medium drops from 80.4 for water to 2 in the inner hydrocarbon chain region. In the region 12-18 Å from the bilayer centre the dielectric constant increases to 3-4 (368). The biggest difference in dielectric constant occurs at the interface to the lipid headgroup. As a result of their simulations, some authors report values of the dielectric constant in the lipid headgroup above the one of bulk water, caused by the zwitterionic dipole of choline and phosphate groups of the investigated PC molecules (369, 370). The dielectric tryptophan, therefore, localises in the interfacial area as a result of the difference in the dielectric constant (333, 371, 372). Marrink et al. (373) performed a simulation study focusing on the permeability of the lipid membrane towards molecules of different hydrophobicity, size and shape. They reported that the lipid tail region at the interface is the main barrier for the penetration of polar molecules, showing increasing positive free energy values with increasing dipole moment. For elongated polar molecules, they additionally predicted a lower Gibbs free energy than for spherical molecules in the interfacial lipid chain area, because the higher density of lipid chains in this area leads to free volume with anisotropic behaviour. This means that the tryptophan with its “hydrophilic character” (335)

could reduce the surface energy at the hydrophobic-hydrophilic interface which would additionally lead to a deeper penetration of water molecules.

We used ATR-IR spectroscopy method to identify a possible correlation of these interaction to the antimicrobial or clustering efficiency of the respective peptides. Therefore we investigated the temperature dependent behaviour of the wavenumbers and intensities of the lipid carbonyl and the peptide amide I as well as the guanidium and indole vibrational bands (Section 3.3).

3.2 Differential Scanning Calorimetry (DSC)

To quantify the effect of the binding of cyclic hexapeptides on lipid demixing we studied the influence of different peptide to lipid ratios on the phase transition behaviour of the pure lipid components as well as various binary and ternary lipid mixtures by DSC.

3.2.1 The impact of cyclic hexapeptides on the phase transition of pure lipid membranes

The impact of trivalent cyclic and linear hexapeptide binding on the phase transition of PEs was already the subject of earlier investigations (108, 109). The effects were negligible due to weak binding to the zwitterionic PE; therefore no further attention was paid to this interaction in this work. The cationic peptides bind much stronger to negatively charged lipids. The effect of different hexapeptides on the DPPG and DMPG main phase transition is shown in Figure 3-2-1. Despite much higher binding constants, the overall effect of the binding of the peptides on the phase transition of pure DPPG and DMPG vesicles is small.

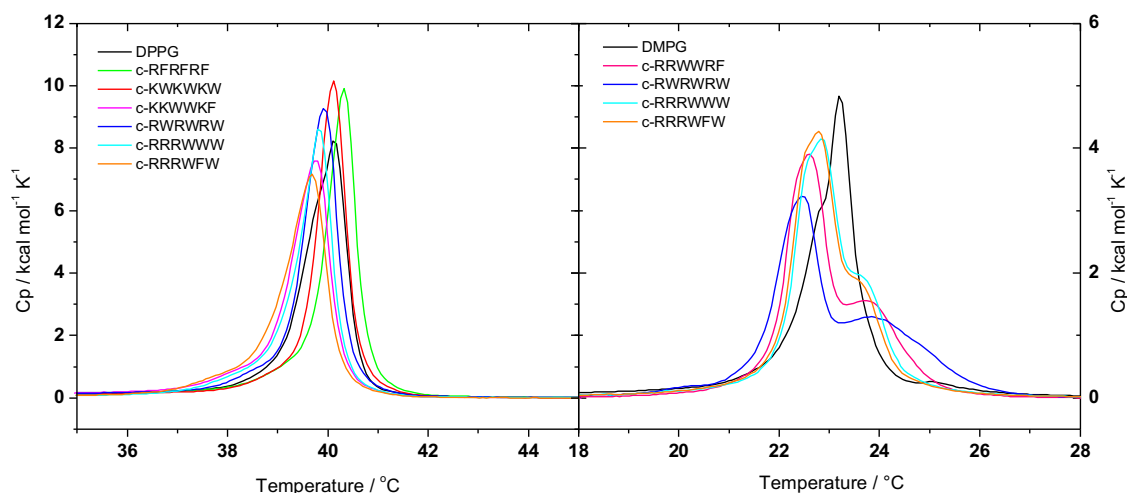


Figure 3-2-1 DSC thermograms of vesicles of PG (black) and PG after addition of the cyclic hexapeptides at a lipid-peptide ratio of 20:1 for DPPG (left) and 100:1 for DMPG (right).

The effect of the cyclic hexapeptide binding on the main phase transition is shown in Figure 3-2-1 for DPPG (right) and DMPG (left). The investigated lipid-peptide ratio for DPPG is 50:1 (not shown) and 20:1. As no significant temperature differences in dependence on lipid-peptide ratio were observed, the effect of peptide binding to DMPG membrane was only investigated at 100:1 lipid-peptide ratio.

The transition temperature of DPPG vesicles interacting with the peptides varies from 39.7°C to 40.3 °C with a transition of the pure lipid at 40.1 °C, respectively. Also, the transition enthalpy of 10 kcal mol⁻¹ for DPPG varies only slightly by about -0.9 kcal mol⁻¹ for DPPG interacting with c-RRRWFW and by +0.9 kcal mol⁻¹ for DPPG interacting with c-RWRWRW. The binding of the

peptide with the alternating sequence containing arginine and phenylalanine (c-RFRFRF) leads to a slight increase of the phase transition temperature of DPPG indicating a gel phase stabilisation, whereas the peptide containing lysine and tryptophan in an alternating sequence (c-KWKWKW) does not affect the phase transition temperature at all. The remaining peptides shift the phase transition temperature to slightly lower temperature for DPPG and DMPG.

The downshift in phase transition temperature is slightly increased for DMPG compared to DPPG. Both amino acid analogue peptides c-RRWRF and c-RRRWF shift the main phase transition by $-0.4\text{ }^{\circ}\text{C}$, the amino acid analogues c-RWRWRW and c-RRRWWW by $-0.6\text{ }^{\circ}\text{C}$ and $-0.8\text{ }^{\circ}\text{C}$, respectively. The transition enthalpy of 6.8 kcal mol^{-1} of extruded DMPG varies between -0.3 kcal per mol for c-RRWRF and $+0.2\text{ kcal per mol}$ for c-RRRWWW.

The phase transition of DMPG mixed with cyclic hexapeptides in a 100:1 lipid-peptide ratio shows a clear shoulder, in contrast to the transition of DPPG (108, 109). The origin of a second apparent phase transition in a lipid vesicle consisting of only one lipid component was observed earlier, mostly occurring for interactions including opposing charges. For example negatively charged membranes interacting with oligovalent molecules like polyamines (312, 374) or positively charged oligo- (375-377) and polypeptides (325) as well as other antimicrobial peptides (378) like PGLa (103, 379), cathelicidine (380), the linear peptide analogue Ac-RRWRF (315) or generally membrane-active peptides (381) lead to two discriminable phase transition peaks.

Different explanations are given in literature for the occurrence of the second transition peak. A decoupling of the transition of the bilayer leaflets is discussed (382) where the phase transition of the peptide bound outer monolayer and inner monolayer is separated.

As additional phase transitions are also observed for pure DMPG at low ionic strength an occurrence of a sponge phase (383, 384) or a holey phase (385, 386), a bilayer phase with holes formed by high positive curvature could be the reason for the second transition (for further details see also the publications by Riske et al. (387-389)).

The most likely reason for the occurrence of the second transition peak is, however, the lateral phase separation into a lipid phase with no or few bound peptides and a peptide enriched domain (103, 325, 375, 380). As a result of the lipid-peptide interaction the enriched domain might be shifted to higher or lower phase transition temperatures.

Many authors argue that domain formation is a result of amine groups interacting with the lipid headgroup. However, as guanidinium and indole group containing peptides are also capable of inducing a second phase transition peak in a DMPG bilayer the different capabilities of amine and guanidinium groups for hydrogen bonding with the lipid headgroup (see section 3.1.3.1) can therefore not explain the observed phase transition behaviour.

The DSC measurements of pure PG membranes interacting with the different cyclic hexapeptides show that the cationic peptides compensate the anionic lipid charges. But the effect on lipid phase transition is only marginal, indicating that counteracting effects like charge compensation,

headgroup hydration and dehydration as well as frustration of lipid alkyl chain interaction by penetration of the hydrophobic side chain residues into the hydrophobic bilayer region (324, 376) and the effect of different charge distances play a role (312). An explanation could be π -stacking, e.g. between guanidinium and indole groups, a reduced surface tension caused by the dipole moment of tryptophan, the lipophobic effect (see section 3.1.3.2) or a combination thereof.

The impact of selected peptides on the phase behaviour of TMCL is shown in Figure 3-2-2. Depicted are the first and the last upscans at lipid-peptide ratios of 20:1 and 5:1 of the alternating peptides and c-RRRWWW or c-RRRWFW, respectively (the 2nd upscan is shown Figure S3-2-1).

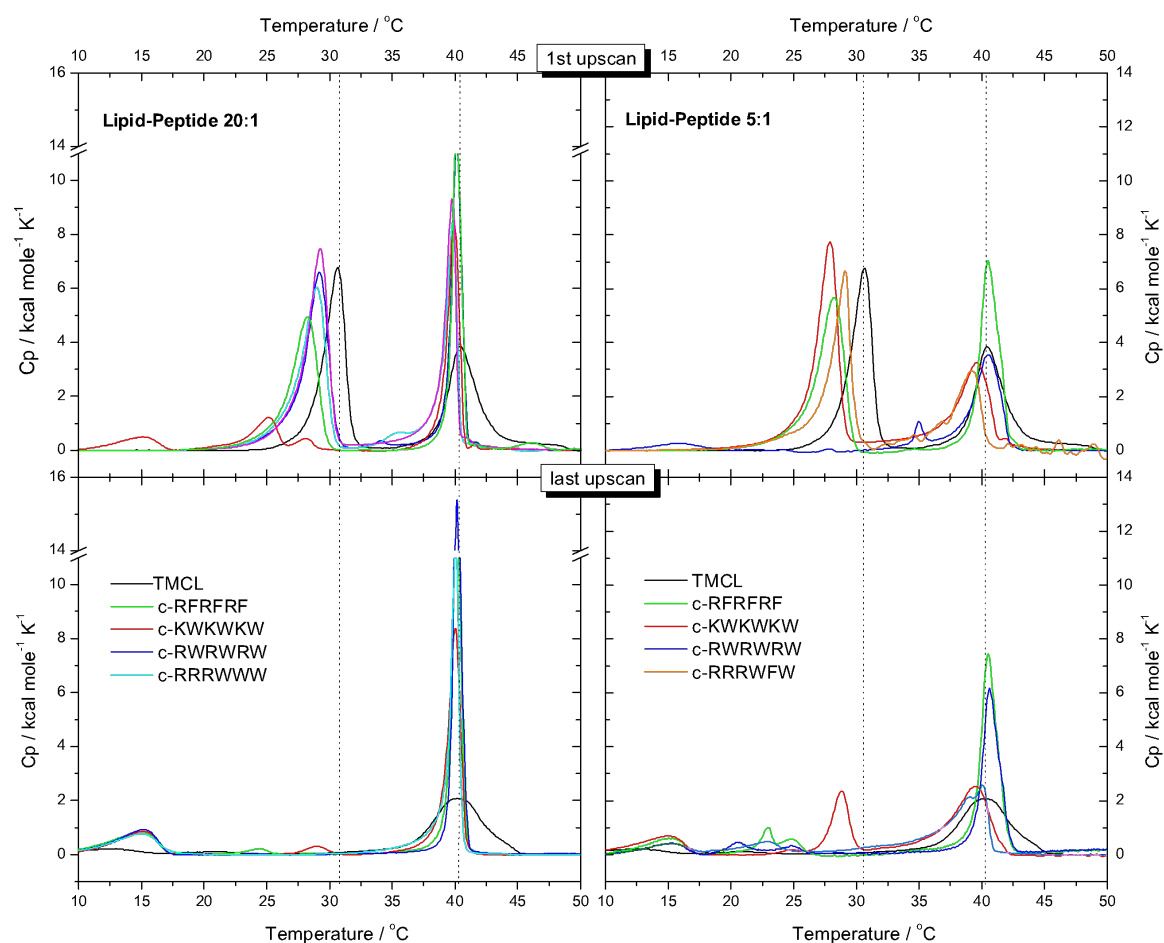


Figure 3-2-2 DSC thermograms of vesicles of TMCL (black) and TMCL after addition of the cyclic hexapeptides at a lipid-peptide ratio of 20:1 (left) and 5:1 (right). The first (up) and last (bottom) upscan is shown. The dotted black line at the phase transition temperatures of pure TMCL should guide the eye.

The main phase transition temperature is only slightly affected by the addition of the cyclic hexapeptides. The cooperativity of the main phase transition increases by the addition of cyclic hexapeptides at lower peptide concentration (lipid-peptide ratio 20:1), most pronounced for c-RWRWRW. This effect is also observed for the TMCL phase transition with increasing pH (see Figure 2-2-3). Therefore, the higher cooperativity might be a result of the downshift of the apparent pK due to trivalent peptide binding resulting from a redistribution of ions and protons at the interface

(390). The shift of the apparent pK of negatively charged lipids to lower values with increasing ionic strength was also observed for the second pK value in PA membranes (210, 391).

The first upscans show that the highly endothermic subgel to gel transition at 31 °C is preserved after addition of the peptides and is shifted to lower temperatures. The cases where no transition is observed were the first samples measured after the preparation of the lipid vesicles. Therefore, we assume that in these cases the subgel phase was not formed until the peptide was added. A pronounced subgel to gel phase transition around 30 °C can still be observed for the 5:1 TMCL-c-KWKWKW ratio even after a couple of temperature cycles, which might be a result of lysine interaction with the cardiolipin headgroup. Cardiolipin interacting with the other arginine containing peptides observed, shows the two L_c - L_β transition around 15 °C and 20 °C which are increased in enthalpy and a slightly upshifted in temperature when compared to the pure TMCL. This L_c phase stabilisation can also be discussed as a result of screened charges and a shift in the pK value by the addition of peptides.

The effect of the cyclic hexapeptides on the main phase transition temperature of PG and TMCL for the 20:1 lipid-peptide mixture is in both cases only marginal. However, the cooperativity of the phase transition increases for TMCL, whereas DMPG shows two distinguishable transition peaks. The difference is explained by the formation of peptide enriched clusters for DMPG. As the second pK value for TMCL is with 6.8 closer to the pH of 7.2 of the phosphate buffer, the observed cooperativity increase is discussed as a result in pK downshift of the second phosphate moiety due to peptide binding.

Although the observed binding constants for the cyclic hexapeptides is increased by about one order of magnitude for binding to TMCL when compared to PG (see Table 3-4-2 and 3-4-3) the difference in bound peptides is negligible at high lipid-peptide ratios.

3.2.2 Peptide interaction with PG/PE mixed membranes

The influence of the cyclic hexapeptide c-RRWWRWF on demixing DPPG/DPPE membranes has been reported by Arouri et al. (108).

Over the recent years the lipid demixing became a more recognized model for antimicrobial interaction (392). To provide further proof the viability of this model, a better understanding of the driving forces leading to a peptide-induced lipid segregation is necessary. Therefore, we tried to quantify the amount of lipids clustered by trivalent cyclic hexapeptides with different amino acid sequences to identify parameters like peptide sequence, charge distance, hydrophobicity, amphipathicity as well as lipid chain length, membrane composition, charge density and the non-ideality parameter of mixing. The phase behaviour of binary mixtures of PG and PE is discussed in chapter 2.2 and the given references therein.

3.2.2.1 Spermine binding to DMPG/DMPE bilayers

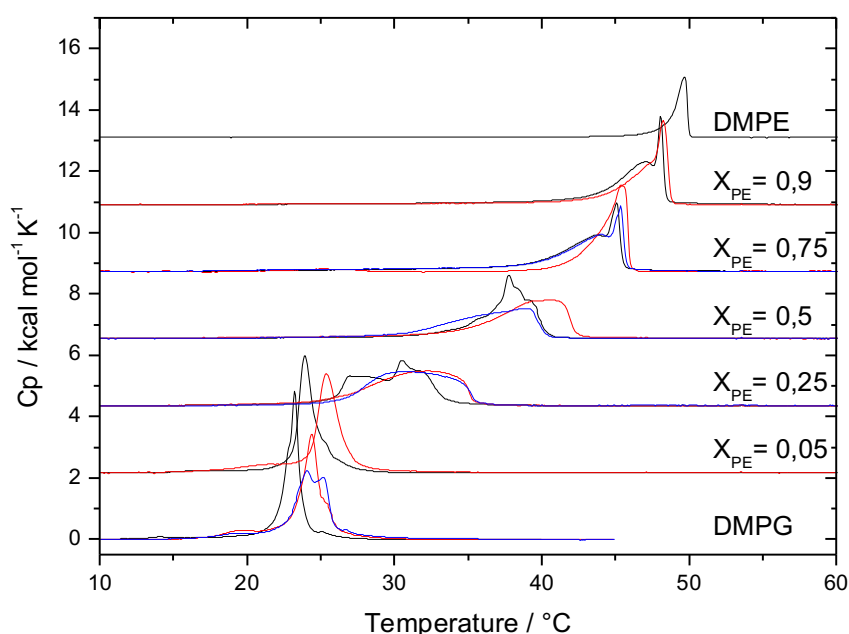


Figure 3-2-3 DSC thermogram of various mixtures of DMPG/DMPE and the pure lipids interacting with spermine at a charge ratio $R_c=1$ (blue line) and $R_c=20$ (red line).

Undoubtedly, charge interactions play a major role in antimicrobial peptide-lipid membrane interaction. As the amphipathic character is an important feature of antimicrobial peptides we wanted to understand to which extend hydrophobic contributions add up to the demixing capability. As a first step, we tried to induce lipid clustering by the addition of simple organic macro ions, such as polyamines, where the charges are located in the backbone of the molecule. Polyamines bind only superficially on the membrane surface of pure PG bilayers as we have shown before (312). To test whether the binding of oligovalent counter ions is sufficient to demix a lipid mixture consisting of

negatively charged and zwitterionic lipids, we investigated the effect of polyamines binding to a DMPG/DMPE membrane of different lipid ratios.

Figure 3-2-3 displays the effect of spermine, a tetravalent oligoamine. In this molecule, the two central amine groups are separated by a $-(\text{CH}_2)_4-$ spacer and the terminal amines by two- $(\text{CH}_2)_3-$ spacers. The tetravalent polyamine was chosen for comparison, as the binding constant is close to the ones observed for the trivalent hexapeptides. Here, the charge ratio is displayed. The charge ratio gives the concentration ratio of positively charged macroion and negatively charged lipids multiplied by the number of charges of both components

$$R_c = \frac{C_{\text{macroion}^+} z_{\text{macroion}^+}}{C_{\text{Lipid}^-} z_{\text{Lipid}^-}} \quad (3.3)$$

At a polyamine-lipid charge ratio $R_c = 1$ and in excess of positively charged molecules $R_c > 1$, no demixing was observed. Binding of spermine to the bilayers led in all mixed lipid vesicles and for pure DMPG as well to gel phase stabilisation, i.e. the transition temperature T_m was slightly shifted upward. This indicates that spermine binds superficially to the lipid head group region and counterbalances the lipid charges, hence the lipid chain interaction is increased leading to the observed increase in T_m . In case of higher charge densities the effect of charge distance plays an important role on the stabilising effect of the gel phase as reported in earlier studies of polyamines interacting with PG membranes (311, 312, 374).

3.2.2.2 PG/PE mixtures –chain length dependence

The effect of various concentrations of cyclic hexapeptides varying in amino acid sequences (Figure 3-1-1) on the phase transition of a DPPG/DPPE mixture is shown in Figure 3-2-4. The lipid to peptide ratio was varied from 75:1 to 10:1. All six cyclic peptides were able to induce a phase separation in DPPG/DPPE mixtures even at very low concentration, i.e. a high lipid to peptide ratio. This is evident from the appearance of a transition peak at a lower temperature around 40 °C corresponding to the phase transition of almost pure DPPG clustered by the binding of the peptides. This temperature remains unchanged with increasing peptide concentration, except for the two peptides c-RRRWWW and c-RRRWFW at high peptide concentration, i.e. low lipid-peptide ratio (10:1). It is also evident from the DSC curves that the enthalpy of the lower transition increases with increasing peptide concentration, supporting the assumption that the amount of clustered DPPG is related to the amount of bound peptide. The temperature of the second transition peak, corresponding to the transition of the remaining DPPE, still mixed with some DPPG, increases with increasing peptide concentration, because the mixture is reduced in the lower melting component DPPG, due to the clustering of DPPG induced by the peptides.

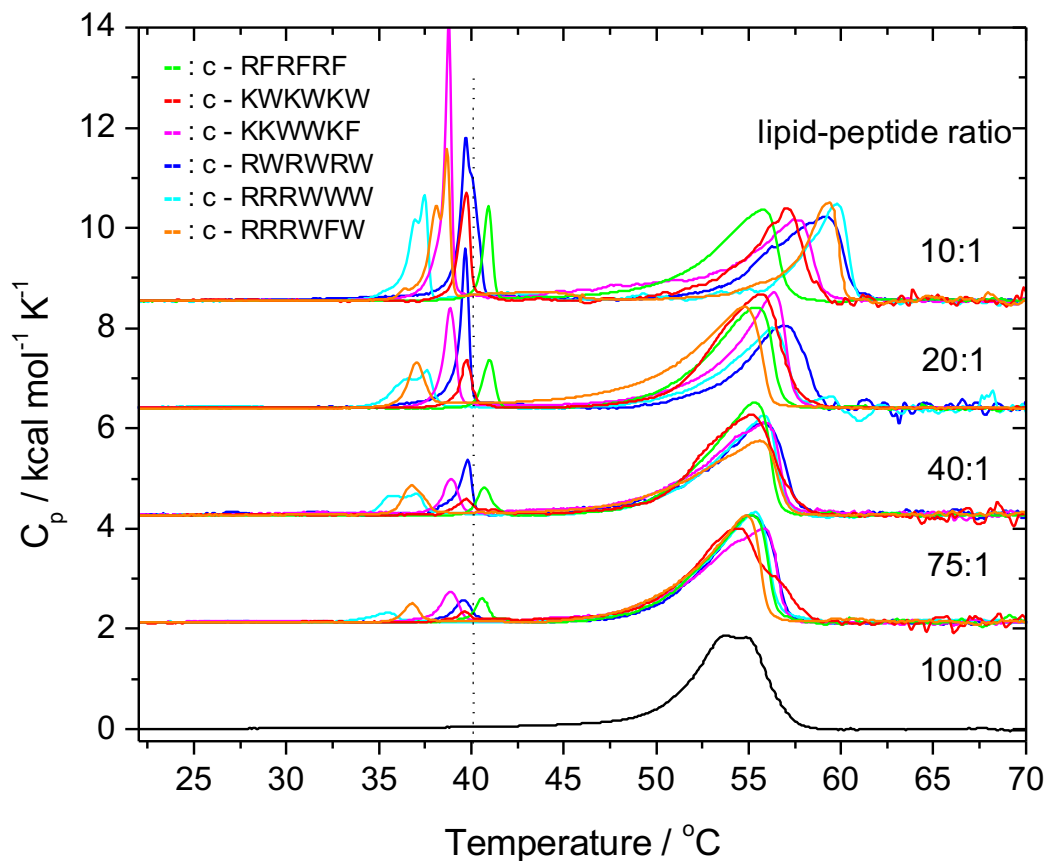


Figure 3-2-4 DSC thermograms of vesicles of DPPG/DPPE 1:1 (black) and DPPG/DPPE 1:1 after addition of the cyclic hexapeptides (lipid-peptide ratios are indicated). The dotted black line indicates the phase transition temperature of pure DPPG.

This means that below 40 °C clustered domains coexist with mixed lipid membranes, both in the gel phase. Between 40 °C and the respective upper phase transition temperature fluid PG-clustered domains coexist with the gel phase of the PG-depleted lipid mixture, therefore named the “molten cluster state”. Above the second phase transition temperature the whole mixture is in the fluid state. If the clusters are still present in this state cannot be deduced from these measurements.

The phase transition temperature of the clustered DPPG domains in the mixed DPPG/DPPE bilayers varies much stronger (from 35.4°C for the DPPG-c-RRRWWW cluster to 40.9°C for the DPPG interacting with c-RFRFRF) than for pure DPPG interacting with the different peptides (see Figure 3-2-1). For all peptides, except c-RFRFRF, a downshift of the transition temperature of the clustered DPPG domains can be observed, similar to the observation made for pure DPPG. Only for the binding of c-RFRFRF the phase transition temperature of the clustered DPPG is shifted to slightly higher temperatures compared to the pure DPPG interacting with c-RFRFRF. The temperature difference is most pronounced in cases of interaction with the most amphipathic hexapeptides c-RRRWWW ($\Delta T = -4.3$ °C), c-RRRWFW ($\Delta T = -3.0$ °C) and c-KKWWKF ($\Delta T = -0.9$ °C). This indicates that the penetration of the cyclic peptides into the hydrophobic membrane region induces a perturbation of the lipid chain packing. The perturbation of the bilayer packing induced by c-

RRRWFW and c-RRRWWW correlates with their high effective hydrophobicity and amphipathicity as determined by reversed phase HPLC (251, 393). This means that either the penetration is more pronounced in the domain inside a mixed membrane compared to the pure PG membrane, or the effect of this penetration on the phase transition temperature is more pronounced in the mixed membrane, e.g. due to changes in curvature energy.

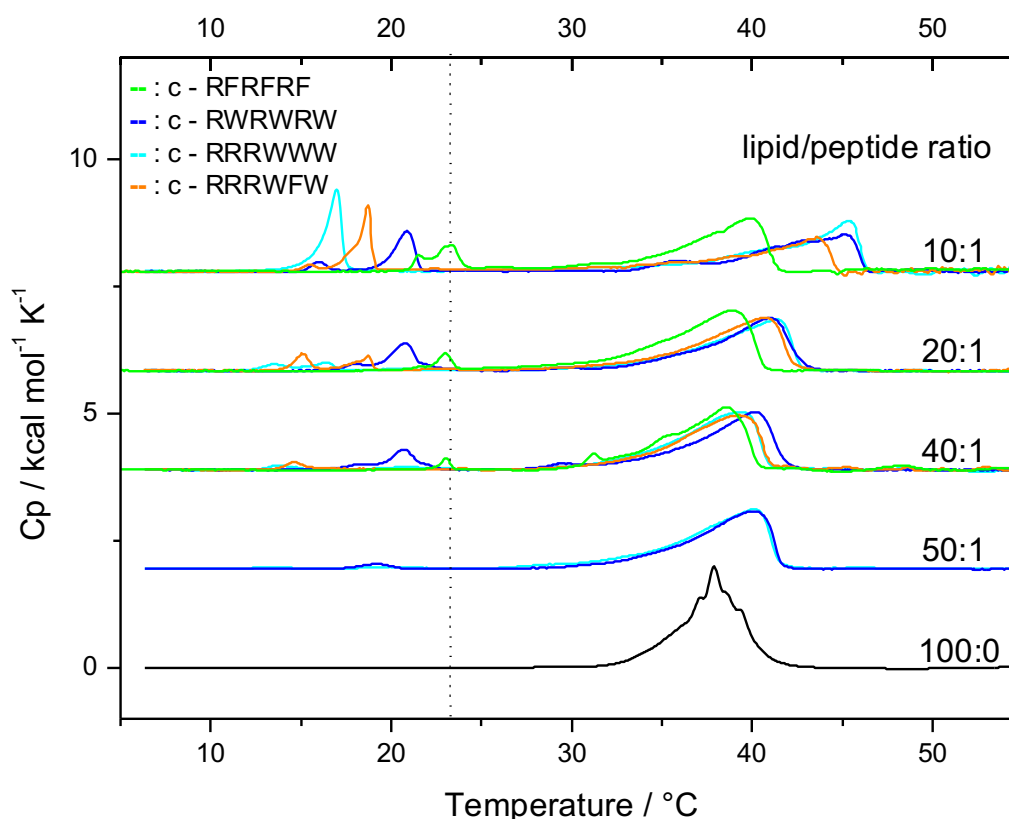


Figure 3-2-5 DSC thermograms of vesicles of DMPG/DMPE (1:1) (black) and DMPG/DMPE (1:1) after addition of the cyclic hexapeptides (lipid-peptide ratios are indicated). The dotted black line indicates the phase transition temperature of pure DMPG.

A similar phenomenon as in DPPG/DPPE 1:1 mixtures interacting with the cyclic peptides can be observed for arginine-containing peptides with DMPG/DMPE 1:1 mixtures, shown in Figure 3-2-5. An additional phase transition peak around the phase transition temperature of pure DMPG occurs upon the addition of the peptides, which increases in intensity with increasing peptide concentration. In the same manner the phase transition temperature of the DMPG-depleted remaining mixture is shifted to higher temperatures. For all observed lipid-peptide ratios, the T_m values for the clustered DMPG domains with the bound peptides is downshifted compared to the T_m value of pure DMPG, again except for c-RFRFRF.

Binding of c-RFRFRF induces no shift in transition temperature compared to pure DMPG. Only in case of a 10:1 ratio, i.e. at higher peptide concentration, a second peak at lower transition temperature occurs ($\Delta T = -1.8^{\circ}\text{C}$). The downshift of the transition temperature for the clustered DMPG containing domain is more pronounced for the respective peptides interacting with DMPG/DMPE

1:1 when compared to the DPPG/DPPE 1:1 mixture, namely $-6.3\text{ }^{\circ}\text{C}$ for c-RRRWWW, $-4.6\text{ }^{\circ}\text{C}$ c-RRRWFW and $-2.6\text{ }^{\circ}\text{C}$ c-RWRWRW. This indicates that the alkyl chain perturbation is more pronounced when these peptides interact with short chain lipids due to decreased van der Waals interactions between the shorter chains.

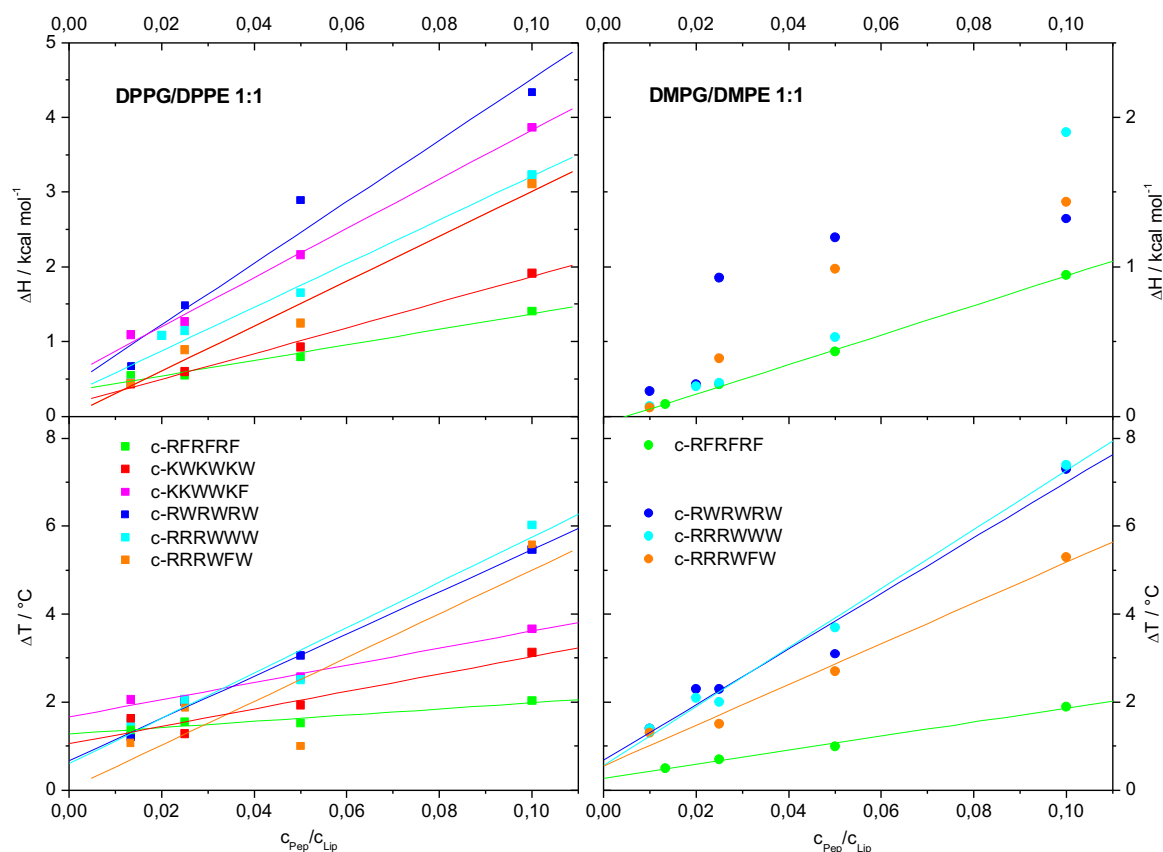


Figure 3-2-6 Top: Transition enthalpy ΔH of the low temperature peak. Bottom: Difference ΔT in phase transition temperature (peak value) of the PG/PE 1:1 mixture and the upper phase transition peak of thermograms of PG/PE 1:1 mixture interacting with cyclic peptides. Left: DPPG/DPPE 1:1 mixture. Right: DMPG/DMPE 1:1 mixture.

Figure 3-2-6 shows a comparison of the phase transition enthalpy of the low temperature peak (top) and the difference in upper phase transition temperature compared to the respective phase transition temperature of the pure lipid mixture (bottom) as a function of lipid-peptide ratio between the DPPG/DPPE 1:1 (left) and the DMPG/DMPE 1:1 mixture (right).

A priori, a linearity between ΔH and the peptide to lipid ratio cannot be expected over the whole peptide concentration range. Instead, a saturation behaviour at high peptide content should be seen. However, the DSC-experiments shown in Figure 3-2-4 and 3-2-5 were performed only up to a lipid-peptide ratio of 10, i.e. saturation of binding was not reached. This would occur at a ratio of 6 (PG-peptide ratio of 3), if only electrostatic effects were considered. However, for peptides with lower binding affinity, saturation will occur at even lower lipid-peptide ratios (higher peptide-lipid ratios). Thus, the curves appear almost linear at low peptide concentrations.

If the influence of peptides on the phase transition enthalpy of PG is only marginal and no other heat contributions occur, e.g. mixing enthalpy, the amount of clustered PG induced by the binding of the peptides can be estimated from the enthalpy plot. Based on the low temperature peak assigned to the PG transition the percentage of DPPG content ($\Delta H_{\text{DPPG}} = 10 \text{ kcal mol}^{-1}$) clustered into a lipid-peptide domain at a 10:1 lipid-peptide ratio, is about 30 % for c-RFRFRF, 40 % for c-KWKWKW but around 80 % for c-RWRWRW (see also Figure 3-2-9). For mixtures with c-RFRFRF and c-KWKWKW, the temperature of the phase transition maximum of the resulting DPPG-depleted domains with a composition of 59 mol% DPPE (c-RFRFRF) and 62.5 mol% DPPE (c-KWKWKW) is in good agreement for c-RFRFRF and c-KWKWKW with the expected values assuming that no peptide is bound to the DPPE-rich domains. For the DPPG/DPPE-c-RWRWRW 10:1 mixture the phase transition maximum at 59 °C for the remaining DPPE enriched domains containing 83 mol% DPPE is only slightly below the expected 62 °C for a pure DPPG/DPPE mixture with the same composition (215). This deviation is probably within the precision of the experiments.

This conformity in both effects of increasing enthalpy and increasing phase transition temperature of the depleted mixture also shows that the fluid domains are stable within the gel phase matrix of the resulting lipid mixture in the timeframe of the measurement.

For the DMPG/DMPE vesicles composed of lipids with shorter chains, the melting enthalpy of the clustered DMPG domain is much lower. This could be either due to less efficient clustering or to perturbations of chain packing in the PG-rich clusters. As mentioned above, the T_m -values for the lower peak indicate lipid chain perturbations. For vesicles of DMPG/DMPE, the change in transition enthalpy assigned to the clustered DMPG seems to be linear only for mixtures containing c-RFRFRF. The apparent linearity observed for the binding of c-RFRFRF is therefore due to the low binding affinity of this peptide, saturation thus being achieved only at much higher peptide/lipid ratios. For mixtures with c-RWRWRW, c-RRRWWW and c-RRRWFW the change in enthalpy is definitely non-linear, indicating that the binding affinity is higher. The higher transition enthalpies observed for the low temperature peak in these mixtures supports this finding. Due to the perturbation of chain packing in the DMPG-enriched domains, an analysis of the transition enthalpy of the peak due to DMPG-rich domains in terms of amount of clustered DMPG is not possible.

When the shift of the maximum of the DSC peak at higher temperature is analysed, it is linear with increasing peptide-lipid ratio for both lipid mixtures, except DPPG interacting with c-RRRWFW (Figure 3-2-6, bottom panels). This shift is the result of the depletion of the remaining lipid mixture by the peptide induced clustering of the PG component. Assuming that the peptide would have no effect on the phase transition enthalpy of the PG cluster, this temperature shift should correlate with the transition enthalpy of the clustered PG domains, i.e. higher phase transition enthalpies at low temperature due to the clustered PG domains should lead to larger temperature shifts of the high temperature peak. This is observed only for DPPG/DPPE bilayers interacting with c-RFRFRF, c-KWKWKW and c-RWRWRW. As not all mixtures show this behaviour, we conclude that the

hydrophobic peptide residues perturb the alkyl chain interaction in the clustered PG domains leading to lower transition enthalpies. This effect is even more pronounced for the DMPG/DMPE bilayers (Figure 3-2-6, right panels), where the plots of the transition enthalpy vs. peptide-lipid ratio are mostly non-linear, but can also be observed for the more amphipathic peptides c-KKWWKF, c-RRRWWW and c-RRRWFW interacting with the DPPG/DPPE mixture.

For example, for the DMPG/DMPE 1:1 mixture interacting with c-RWRWRW in a 10:1 lipid-peptide ratio the enthalpy of the lower peak indicates that about 30% of DMPG is clustered in the domain (Figure 3-2-6 upper right and 3-2-9 right). At this lipid-peptide ratio, the transition temperature of the peak at higher temperatures is at $\sim 45^{\circ}\text{C}$, i.e. the phase transition temperature maximum of a DMPG/DMPE 1:3 mixture (Figure S3-2-2). This, however, would mean that 67% of the DMPG is clustered by c-RWRWRW at the lipid-peptide ratio of 10:1. This is close to the amount of clustered PG in a DPPG/DPPE 1:1 mixture, where both analyses are in line (see discussion above). From the different dependencies of the enthalpy and the transition temperature upshift on the peptide-lipid ratio it is evident that these analyses of clustered PG also leads to varying results for DPPG/DPPE mixtures. For example, for the DPPG/DPPE 1:1 mixture in a lipid-c-RWRWRW ratio of 20:1, the enthalpy analysis indicates an amount of clustered DPPG of about 70% (Figure 3-2-3 upper left and Figure 3-2-9) but the remaining lipid mixture displays a transition temperature of $\sim 57^{\circ}\text{C}$, i.e. a transition temperature comparable to a DPPG/DPPE 2:3 mixture. This would mean that only 33% of DPPG is clustered. Although the temperature upshift of the high temperature peak seems to be a more reliable indicator for the clustering efficiency of a given peptide due to the alterations in transition temperature and enthalpy observed for the DSC peak at lower temperatures, the transition temperature of the remaining mixture might also be altered. Alterations might be due to peptides bound to the remaining mixture that could be both, stabilising or destabilising the gel phase of the remaining mixture in the molten cluster state. Moreover, during melting of the clustered domain, PG molecules might also dissolve in the remaining lipid mixture leading to a downshift in the respective transition temperature. In these cases where the analysis of the enthalpy of the lower temperature transition with the analysis of the temperature upshift of the higher melting peak is not in line, it is difficult to quantify the clustering efficiency. However, tendencies can still be compared. For DPPG/DPPE mixtures, the highest temperature upshift is induced by the amphipathic peptides c-RRRWWW, c-RWRWRW and c-RRRWFW, respectively (Figure 3-2-6, bottom left). We therefore conclude that the amount of clustered DPPG is the highest for these three peptides. For DMPG/DMPE mixtures, the situation is only slightly different. Here the two peptides c-RRRWWW and c-RWRWRW also induce the highest temperature upshift, but the effect of c-RRRWFW is slightly less.

3.2.2.3 PG/PE mixtures –dependence on chain length difference

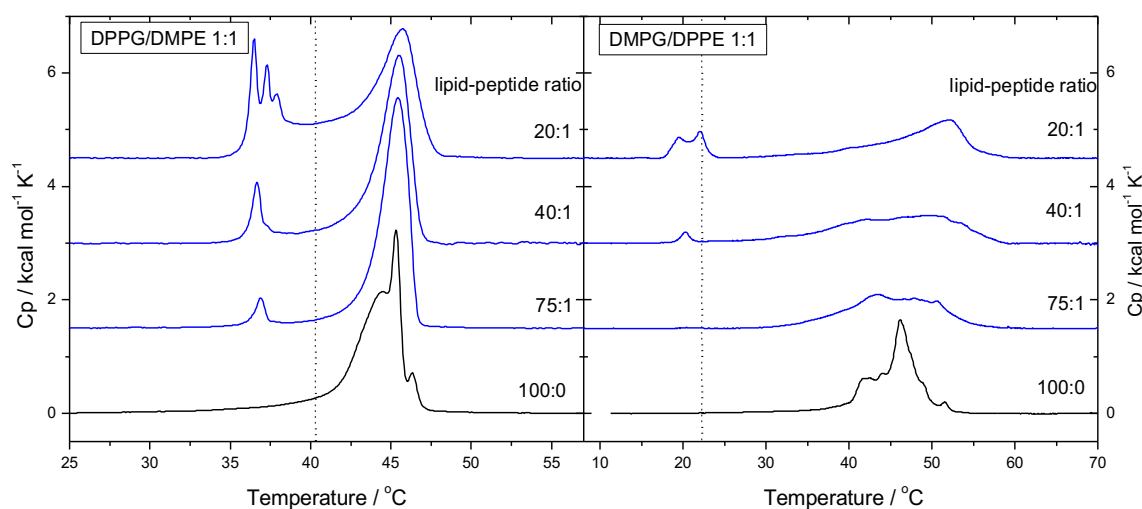


Figure 3-2-7 DSC thermograms of vesicles of DPPG/DMPE 1:1 (left) and DMPG/DPPE 1:1 (right) after addition of c-RWRWRW (lipid-peptide ratios are indicated). The dotted black line indicates the phase transition temperature of the respective pure PG component.

To investigate the effect of non-ideality of the lipid mixture, we studied the binding of c-RWRWRW on the phase behaviour of PG/PE mixtures with different chain length and varying peptide-lipid ratios (Figure 3-2-7). For PG/PE mixtures with the same chain length, the non-ideality parameters are all negative for 1:1 mixtures (-400 to -800 cal mol⁻¹) indicating that the electrostatic repulsions between the PG molecules prevent a random distribution in the bilayer plane (215). For PG/PE mixtures where the chain lengths have a difference of two CH₂ groups, analysis of DPPG/DMPE mixtures showed that the non-ideality parameters were again negative for both phases. However, for DMPG/DPPE mixtures, an indication for a eutectic phase behaviour was observed at high DMPG content. This would indicate a change to positive non-ideality parameters for the gel phase leading to demixing in the gel phase due to the large difference in phase transition temperature between the two compounds (215). For both mixtures, DPPG/DMPE and DMPG/DPPE, a clustering of the charged PG component could be observed after peptide addition. In case of DPPG/DMPE mixtures, the transition temperature of the clustered DPPG domains is significantly lower (-3.4°C) (Figure 3-2-7, left panel) when compared to the T_m -value of the clustered DPPG domains in DPPG/DPPE mixtures (Figure 3-2-4) or the T_m -value of pure DPPG vesicles after addition of c-RWRWRW (Figure 3-2-1, left panel). This indicates a much higher perturbation of the chain packing in the clustered DPPG domain, probably due to a higher degree of binding. For the PE-enriched domains, no significant shift in the transition temperature is seen, as the T_m -values of the pure lipid component are close together.

The T_m -value for the DMPG-rich domains in the DMPG/DPPE mixture is also shifted again compared to the T_m values of pure DMPG with bound peptide, but the shift is almost the same as observed in DMPG/DMPE mixtures. For the DMPG/DPPE mixture at a 20:1 lipid-peptide ratio a

splitting of the low temperature peak is seen (Figure 3-2-7, right panel), very similar to the splitting observed for pure DMPG after peptide binding (Figure 3-2-1, right panel). For this mixture, a clear upshift of the T_m -value for the PE-enriched domain is observed. The position of the maximum for a lipid-peptide ratio of 20:1 indicates that the PE-enriched domains contain still ca. 40 mol% DMPG.

3.2.2.4 PG/PE mixtures –dependence on lipid mixing ratio

We now wondered, whether a variation of the mixing ratio in binary DPPG/DPPE mixtures would have an effect on the demixing induced by the peptides. We therefore investigated DPPG/DPPE mixtures with different mixing ratios as shown in Figure 3-2-8. The DSC peak for a DPPG/DPPE 1:1 mixture is located at ca. 54 °C. For a DPPG/DPPE 1:3 mixture, the peak maximum is shifted to 59 °C as expected. After addition of the three most efficient peptides similar peak splittings are observed as for the 1:1 mixtures. A low temperature peak corresponding to the melting of the DPPG-peptide clusters occurs and the transition temperature of the remaining PG-depleted lipid mixture is shifted to higher temperatures. Both, the enthalpy and the difference in phase transition temperature, increase with increasing peptide concentration.

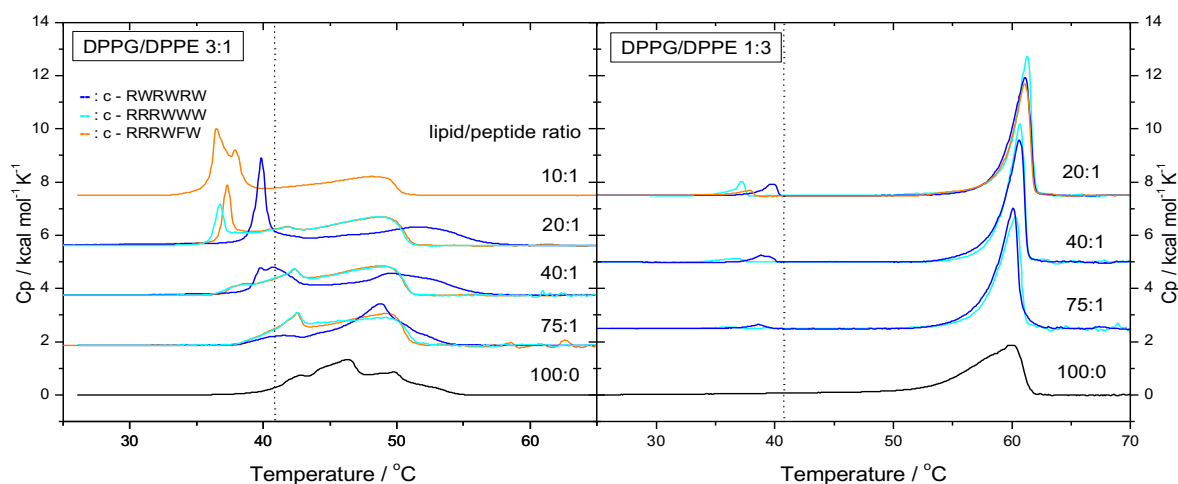


Figure 3-2-8 DSC thermograms of vesicles of DPPG/DPPE 3:1 (left) and DPPG/DPPE 1:3 (right) after addition of cyclic hexapeptides (lipid-peptide ratios are indicated). The dotted black line indicates the phase transition temperature of pure DPPG.

The DSC peak observed for the pure DPPG/DPPE 3:1 mixture is shifted to lower temperature compared to the 1:1 mixture due to the higher DPPG content. The cyclic peptides induce different effects on the transition behaviour. When c-RWRWRW is bound, the height of the transition peak of the lower melting domain increases with increasing peptide concentration and the maximum of the DSC peak for the remaining lipid mixture shifts again to higher temperatures. At a lipid-peptide ratio of 20:1, i.e. a lipid-peptide charge ratio of 15:3, the peak temperature indicates that the PE-enriched domains have a composition close to 3:2 DPPG/DPPE, i.e. ca. 50% of the DPPG is

clustered by the peptide (Figure S3-2-3). That means that even in the clustered domains there is no charge compensation. The charge ratio is ca. 7.5:3 and therefore below saturation.

The effects of c-RRRWWW and c-RRRWFW binding on the phase behaviour of a DPPG/DPPE 3:1 mixture are clearly different from the effects induced by c-RWRWRW. At low peptide concentrations, a peak occurs at the temperature of pure DPPG at 41.5°C. At a lipid-peptide ratio of 40:1, an additional peak at even lower temperature appears and increases with increasing peptide concentration on the cost of the peak at 41.5°C.

For the block-peptides the peak maximum of the upper transition is not shifted to higher temperatures with increasing peptide concentration but stays constant and the DSC peak is very asymmetric. The end of the transition occurs even at lower temperature than for the mixture without peptide. The DSC peaks can therefore not be analysed in the usual way presented above. The peculiar different thermotropic behaviour of the 3:1 DPPG/DPPE mixture interacting with block-peptide c-RRRWWW and c-RRRWFW compared to the alternating RW-peptide implies a more profound change in phase behaviour of the binary lipid mixture upon the interaction with the block-peptides. It seems likely that the low transition temperature of the upper DSC peak is due to the binding of the peptide also to PG in the PE-enriched clusters, thus perturbing the chains due to partial insertion into the hydrophobic chain region and therefore reducing T_m .

Lohner et al. determined the phase diagram for DPPG and DPPE in 10 mM Na-Phosphate buffer, i.e. under low salt conditions. The lipids show peritectic mixing behaviour with a gel phase demixing at a PG content higher 60% (238). Although in low salt conditions, where one would expect that, due to less screening of charges, electrostatic repulsion between PG molecules are increased resulting in a tendency for better mixing, the opposite effect is seen which is probably due to more specific effects such as H-bonding between headgroups. From this data one can conclude that PG/PE mixtures seem to be close to the critical non-ideality for demixing, strongly dependent on counterion concentration. The binding of the block-peptides might therefore also lead to non-idealities above the spinodal decomposition. This might lead to mono-, eu- or peritectic mixing behaviour with a mono- eu- or peritectic PG-enriched lipid-mixture with bound peptides melting at low temperatures and a remaining PE-enriched lipid mixture with or without bound peptides. Most likely the peptide-enriched domain melting at lower temperatures dissolves after melting. Therefore, the second phase transition peak is not upshifted in temperature because the DPPG dissolves in the remaining lipid matrix, but is downshifted when compared to the pure lipid mixture as the bound peptides insert into the hydrophobic chain region.

However, independent of the phase behaviour of the DPPG/DPPE mixture the differences on the effect of binding between block-peptides and alternating peptides is due to a deeper penetration of block-peptides into the lipid chain lattice.

3.2.2.5 Comparison of clustering efficacy of c-RWRWRW and c-RRRWWW

To compare the effect of the clustering efficiency of c-RRRWWW and c-RWRWRW in different PG/PE lipid mixtures, the transition enthalpy of the domains melting at lower temperature ΔH_{clus} was evaluated and then scaled by the expected transition enthalpy ΔH_{PG} of the respective pure PG in the mixture (Figure 3-2-9). The change in $\Delta H_{clus}/\Delta H_{PG}$ with increasing peptide concentration is non-linear in almost all cases.

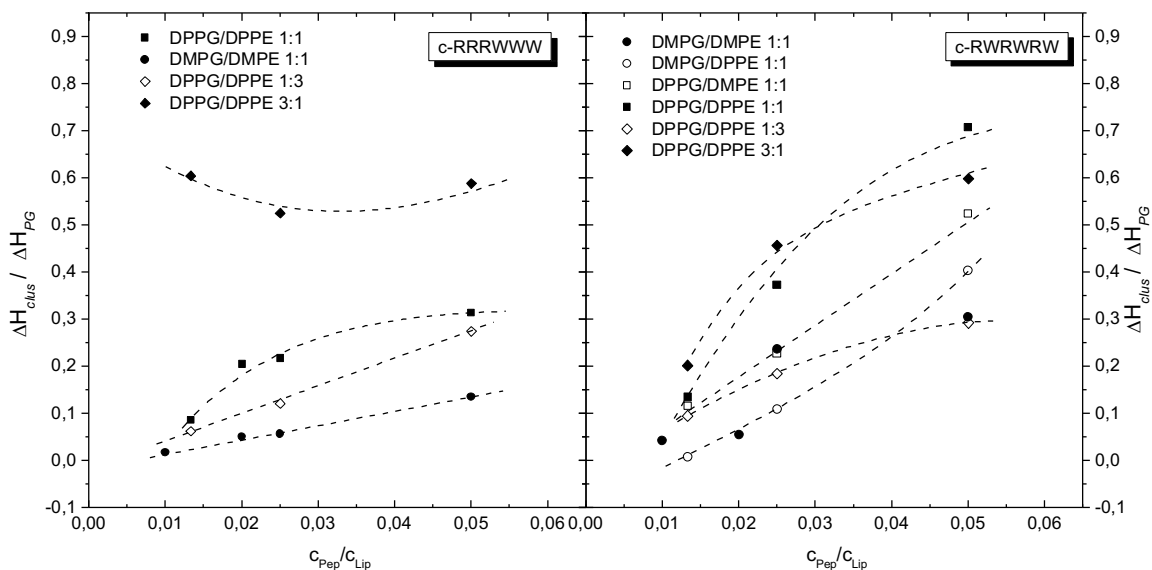


Figure 3-2-9 Ratio $\Delta H_{clus}/\Delta H_{PG}$ of the transition enthalpy of the peak at lower temperature over the molar transition enthalpy of the pure respective lipid component. Left: c-RRRWWW. Right: c-RWRWRW. Dashed lines were drawn to guide the eye.

For c-RRRWWW, the change in $\Delta H_{clus}/\Delta H_{PG}$ with increasing peptide concentration is similar for all lipid mixtures except for the DPPG/DPPE 3:1 mixture (Figure 3-2-9). Here, $\Delta H_{clus}/\Delta H_{PG}$ seems to be constant for all peptide-lipid ratios, possibly due to the higher charge density of the vesicles. For the 3:1 mixture, $\Delta H_{clus}/\Delta H_{PG}$ is always between 0.5 and 0.6, i.e. 50-60 % of all DPPG molecules are clustered. This indicates that the DPPE-rich domains still contain residual DPPG, the mixing ratio in this domain being now ca. 3:2. For the 1:1 mixtures, the ratio is smaller and dependent on the peptide-lipid ratio. A maximal value of 0.3 at a peptide-lipid ratio of 0.05 is observed for DPPG/DPPE 1:1, i.e. only 30 % of the DPPG is clustered. The remaining PE enriched clusters have then a composition of ca. 2:3. For the DPPG/DPPE 1:3 mixture, the maximal ratio $\Delta H_{clus}/\Delta H_{PG}$ is ca. 0.25. The PE-rich domains still contain ca. 19 mol% PG. For DMPG/DMPE, the ratio is even lower with maximal 0.1, i.e. much less PG is clustered.

The alternating c-RWRWRW has generally a higher effect, i.e. a higher clustering ability. The ratio $\Delta H_{clus}/\Delta H_{PG}$ at a peptide-lipid ratio of 0.05 varies between 0.3 for the DMPG/DMPE 1:1 and DMPG/DMPE 1:3 mixture and 0.7 for the DPPG/DPPE 1:1 mixture.

For the 1:1 mixtures the charge density and therefore electrostatic potential remains the same, so no major changes in binding constant of peptide bound vesicles are expected. Changes in PG content alters the surface potential as shown in Figure 2-1-4. At a peptide-lipid ratio of 0.05, the charge ratio R_c (peptide/lipid) for the 1:1 mixture would be 0.3, for 3:1 mixtures 0.2, and for 1:3 mixtures 0.6, respectively. If charge compensation alone would be responsible for the clustering of PG containing domains, then one would expect $\Delta H_{clus}/\Delta H_{PG}$ -values of the same value, i.e. the clustering should be more efficient in mixtures containing less PG. For instance, for a 1:1 mixture one would expect that in all cases, 30% of the PG molecules are clustered and thus charge compensated. The $\Delta H_{clus}/\Delta H_{PG}$ -values, however, are between 0.3 and 0.7 for the binding of c-RWRWRW and thus higher than expected. For DMPG/DMPE 1:1 charge compensation seems to occur ($R_c = 0.3$, $\Delta H_{clus}/\Delta H_{PG} = 0.3$), whereas for DPPG/DPPE 1:1 the PG molecules in the cluster are not charge compensated ($R_c = 0.3$, $\Delta H_{clus}/\Delta H_{PG} = 0.7$). The situation is different for the DPPG/DPPE 1:3 mixture. Here, $R_c = 0.6$, but $\Delta H_{clus}/\Delta H_{PG} = 0.3$. This means that less PG is clustered than expected assuming charge compensation alone to determine the clustering effect. For the DPPG/DPPE 3:1 mixture, $R_c = 0.2$ and $\Delta H_{clus}/\Delta H_{PG} = 0.6$. Thus the opposite effect is seen, the clusters are not charge compensated and contain more PG than expected. These differences clearly show that the electrostatic binding is not the only driving force for clustering, but that the lipid composition and the chemical structure of the peptide interacting with the bilayer interface is important.

The estimations of the clustering efficacy presented above rely on the assumption that the bound peptides have no significant influence on the transition enthalpy of the lower melting domains. However, the plots of $\Delta H_{clus}/\Delta H_{PG}$ vs. peptide-lipid ratio are non-linear in most cases. This again indicates that perturbation of chain packing in the PG-rich clusters can occur, so that the analyses presented above are only an estimate. The shift in phase transition temperature T_m of the upper domain could in principle be a better indicator to judge the clustering ability of the peptides. However, the change in T_m -value is not necessarily linear with decreasing PG-content of the PE-rich clusters, as the phase diagrams indicate (see Section 2.3 and (215)). Therefore, only trends can be compared.

Garidel and Blume (215) investigated the mixing behaviour of the pure PG/PE mixtures with same and varying acyl chain lengths. The non-ideality parameter ρ describing the asymmetry of mixing for either gel or liquid-crystalline phase can be written as $\rho = \rho_1 + \rho_2(2x + 1)$, with $\rho_1 = \rho$ being the non-ideality parameter for an equimolar mixture (x is the molar fraction) and ρ_2 describing the asymmetry of mixing. For DPPG/DPPE, the ρ_1 values are negative for both phases and the ρ_2 values are relatively small. Nevertheless, it can be seen that for PG-rich mixtures ρ is less negative for the gel phase enhancing the tendency for demixing (215). Also the critical value for spinodal decomposition χ_c is lowest for PG-rich mixtures which additionally enhances the tendency for demixing (see Section 2.1.3). The values of $\Delta H_{clus}/\Delta H_{PG}$ for c-RWRWRW and a peptide/lipid ratio

of 0.025 are in the order DPPG/DPPE (3:1) > DPPG/DPPE (1:1) > DPPG/DPPE (1:3). For a peptide-lipid ratio of 0.05 (lipid-peptide ratio 20:1), the first two are reversed. This shows that DPPG-rich mixtures are more prone to demixing after peptide binding.

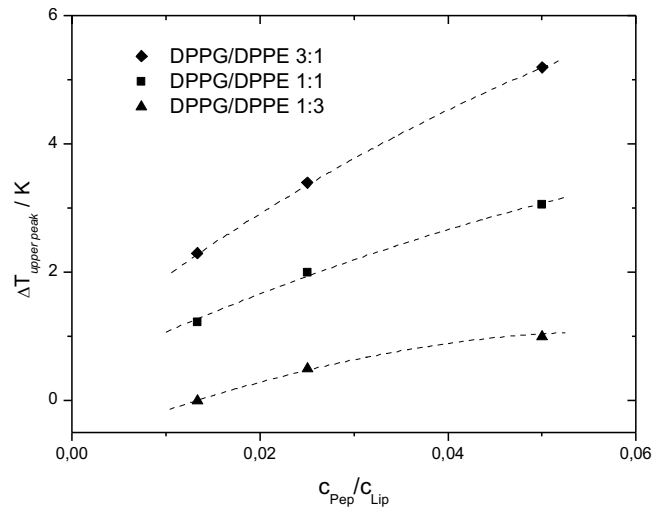


Figure 3-2-10 Change of transition temperature of the upper peak in the DSC-curves for DPPG/DPPE mixtures after binding of c-RWRWRW vs. the peptide-lipid ratio.

Figure 3-2-10 shows the shift of the upper peak corresponding to the melting of the PE-rich domains after peptide binding. Here, the same trend is seen, i.e. the change in T_m is largest for the PG-rich mixtures and lowest for the PE-rich mixture. A quantification of the effect is difficult, as the phase diagram is such that T_m of the mixtures does not change linearly with the mole fraction, the change in T_m becoming smaller at high PE content demixing (215).

A direct comparison of the upper melting peak of the clustered mixture with the respective DPPG/DPPE mixture is displayed in Figure S3-2-3. Here, the upper peak of the DPPG/DPPE 3:1 bilayer interacting with c-RWRWRW in a 20:1 lipid-peptide ratio shows a peak position similar to a DPPG/DPPE 3:2 mixture as discussed above. For the DPPG/DPPE 1:1 mixture the upper peak position of the remaining mixture is comparable to a DPPG/DPPE 2:3 mixture and for the DPPG/DPPE 1:3 mixture the upper peak can be compared to a DPPG/DPPE 1:4 mixture. This means that for the DPPG/DPPE 3:1 mixture 50%, for the DPPG/DPPE 1:1 mixture 33% and for the DPPG/DPPE 1:3 mixture 25% of PG is clustered. Here, the percentage of clustered PG calculated from the T_m shift for the upper peak for the DPPG/DPPE 3:1 and 1:3 mixture is with 50% compared to 60% and with 33% compared to 30% in good agreement with the calculation of the enthalpy analysis. However, the 1:1 mixture deviates strongly between the analysis in enthalpy and the T_m shift for the upper peak which was already discussed above. Nevertheless, both, the $\Delta H_{clus} / \Delta H_{PG}$ -values and the shift in T_m for the upper peak observed after peptide binding point in the same direction, namely that the extent of clustering depends on the mixing ratio of PG and PE.

For c-RRRWWW this analysis of the shift in T_m fails, because this peptide seems to perturb the lipid packing much more than c-RWRWRW (see above).

3.2.3 Peptide interaction with Cardiolipin/PE mixed membranes

By exchanging the PG component in the PG/PE mixture by cardiolipin two counterbalancing effects might influence the peptide clustering efficacy. The surface potential is decreased for a Cardiolipin/PE 1:1 mixture when compared to PG/PE 1:1 mixture (see Figure 2-1-4), resulting in an increased amount of sodium ions in close proximity to surface. Additionally, as cardiolipin contains four lipid chains, the entropy losses are smaller when TMCL is demixed compared to PG. If demixing is driven by release of counter ions due to electrostatic binding, an increase in clustering efficacy should be observed. This expectation would be underlined by the increased binding constant of the peptides to cardiolipin compared to PG (see chapter 3.4.1). But the miscibility of a cardiolipin and PE is increased compared to the PG and PE. This could lead to a reduced clustering efficiency f_c , i.e. the amount of clustered lipid per peptide is lowered, or an increase in critical clustering peptide-lipid ratio r_{cc} , which means that more peptides need to bind to the membrane surface until a demixing takes place or both.

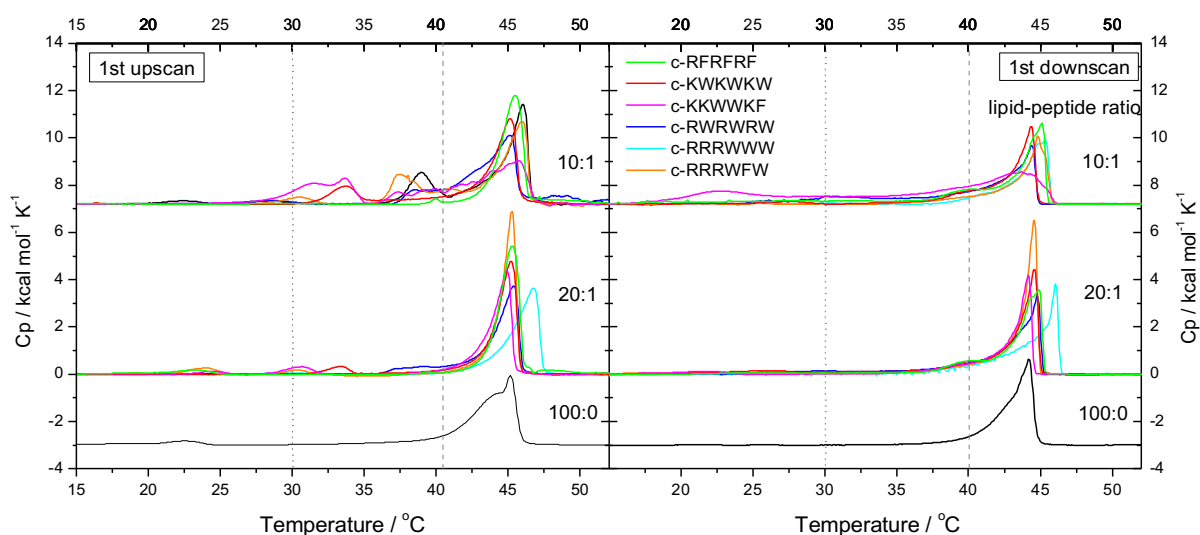


Figure 3-2-11 DSC thermograms of TMCL/DMPE 1:1 vesicles pure (black) and after addition of cyclic peptides (lipid-peptide ratios are indicated). The first upscan (left) and first downscan (right) are depicted. The dotted grey lines indicate the subgel to gel and the main phase transition temperatures of the pure TMCL component, respectively (see Figure 3-2-2 top). Downscans are inverted for better comparison.

Figure 3-2-11 displays the first up- and downscan of a pure TMCL/DMPE 1:1 mixture and after addition of the cyclic peptides. The addition of the cyclic peptides in a 10:1 lipid-peptide ratio leads to an additional phase transition up to 3 °C below T_m of TMCL at 40 °C for all observed peptides. A peak at 40 °C is maintained for the 1st downscan, but the transition extends down to 25 °C for all peptides, except c-KKWWKF, which shows an additional transition peak at 21 °C. After binding of c-KWKWKW, c-KKWWKF and c-RRRWFW an additional transition at 31 °C or above is seen, in the same temperature range as the highly endothermic transition temperature observed for the subgel to gel phase transition in pure TMCL. The thermogram of TMCL/DMPE mixture interacting with

c-RWRWRW shows a small peak below 31°C at a lipid-peptide ratio of 10:1. This indicates that cyclic peptides also cluster membranes consisting of TMCL and DMPE.

Equilibrium was achieved after two upscans and the measured thermograms were reproducible. Figure 3-2-12 shows the last DSC scan of the TMCL/DMPE 1:1 lipid mixture with the respective peptides in a 20:1 and 10:1 lipid-peptide ratio.

In all cases a lower temperature transition peak that increases with increasing peptide concentration and an upshift of the high temperature transition peak, corresponding to the main phase transition of the remaining lipid mixture can be observed.

Although the finding is similar to the observation made for PG/PE mixtures, the lower temperature transition does not occur at the main phase transition temperature region of pure TMCL, besides the broad shoulder at 40 °C occurring in the 10:1 lipid-c-RWRWRW mixture.

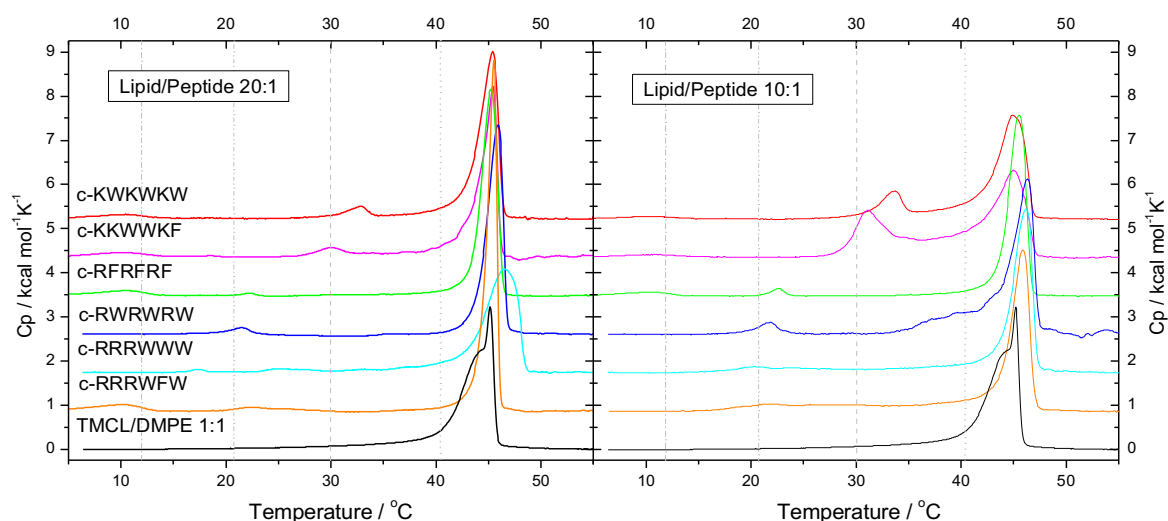


Figure 3-2-12 DSC thermograms of the last upscan of pure TMCL/DMPE 1:1 vesicles (black) and after addition of cyclic peptides in a 20:1 (left) and a 10:1 (right) lipid-peptide ratio. The dotted black lines indicate the pretransition, subgel to gel and main phase transition temperatures occurring for pure TMCL (see Figure 2-1-2).

The thermograms of TMCL interacting with both lysine containing peptides c-KWKWKW and c-KKWWKF show a low temperature transition in the transition temperature regime of the subgel to gel phase transition of pure cardiolipin at 30 °C. This might indicate that these clusters consist of TMCL in a triclinic chain lattice (see Section 2.2 and 2.3). However, the phase transition temperature of the main peak remains almost constant. This either means that the clustered domains dissociate in the remaining lipid matrix after melting or the observed transition is a pretransition, e.g. a L_c - L_β transition or L_β - P_β transition, of the overall lipid mixture, stabilised by the lysine containing peptides. In both cases an increased heat capacity between both transition peaks would be expected as can be seen in Figure 3-2-12.

The two alternating arginine peptides c-RWRWRW and c-RFRFRF induce a clustered domain that melts at 22 °C and 24 °C, respectively. The block-peptides c-RRRWFW and c-RRRWWW show

both a small transition peak below 20 °C in the 20:1 lipid-peptide mixture and a broad pretransition starting at 24 °C that merges into the main phase transition.

The broad and smeared pretransition starts below 20 °C for both block-peptides at a 10:1 lipid-peptide ratio. This indicates that a clustering takes place, but the cooperativity is reduced and therefore no single transition peak can be detected. In contrast, the cooperativity for the main phase transition is drastically increased for c-RRRWWF in the 20:1 lipid-peptide ratio, whereas the main phase transition cooperativity remains the same as for the pure lipid mixture by addition of c-RRRWWW. The peptides c-RFRFRF, c-RWRWRW and c-RRRWWF show a peak in the same temperature interval when bound to pure TMCL in the 5:1 lipid-peptide mixture (see Figure 3-2-2), which is the same TMCL-peptide ratio as for TMCL/DMPE 1:1 mixture in a 10:1 lipid-peptide mixture. As none of the pure TMCL/DMPE mixtures show a pretransition (see Figure 2-3-5 left), the additional low temperature transitions can be attributed to demixed TMCL interacting with the respective peptides. The reason why no main phase transition peak of pure TMCL with bound peptide occurs at ~39°C for c-RRRWWW and c-RRRWWF might be due to the fact that the clusters dissolve after melting, which would also explain the smeared low temperature transition.

All arginine-containing peptides show a slight upshift in the phase transition temperature of the main peak, indicating that the clusters are preserved at least until the melting of the remaining lipid mixture. As the difference in temperature of the pure components is only 8°C, the upshift of the remaining lipid mixture compared to the reference is also comparatively small. Therefore, only an evaluation of the transition enthalpy of the melting peak at lower temperatures can be used for further interpretations of clustering abilities.

A comparison of the normalized enthalpies of the clustered phase transition, i.e. the enthalpy of the lower transition temperature domain divided by the content weighed enthalpy of the negatively charged lipid component of PG and Cardiolipin in their respective 1:1 PE mixtures with the same chain length is depicted for c-RWRWRW and c-KWKWKW in Figure 3-2-13. For the lipid mixture interacting with c-RWRWRW the lowest increase in enthalpy of the phase transition of the clustered domain is seen for the TMCL/DMPE 1:1 mixture and increases for the DMPG/DMPE 1:1 mixture and further for the DPPG/DPPE 1:1 mixture. The increase in enthalpy of the clustered domain for c-KWKWKW interacting with DPPG/DPPE is similar to the increase observed for DMPE/TMCL. This underlines the interpretation that c-KWKWKW binds superficially to the membrane and shows no perturbation of lipid chains because the increase in enthalpy of the clustered domain is not dependent on the lipid chain length.

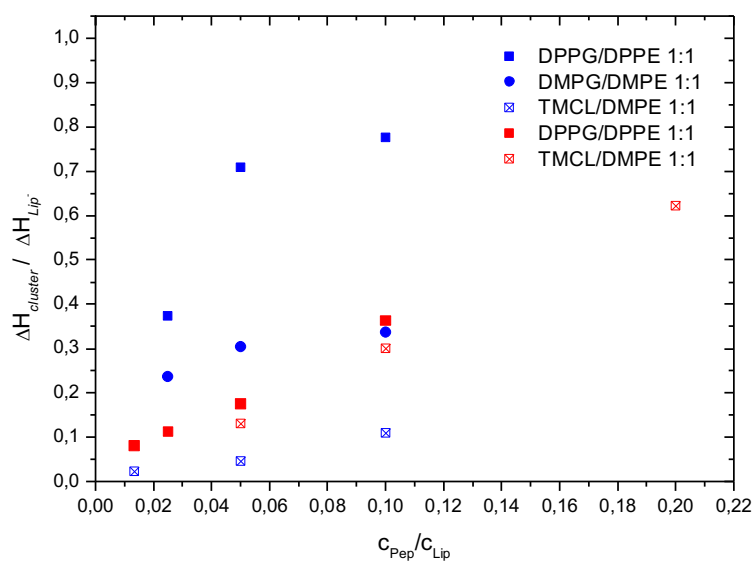


Figure 3-2-13 Ratio of the transition enthalpy of the peak at lower temperature over the molar transition enthalpy of the pure respective lipid component for c-RWRWRW (blue) and c-KWKWKW (red) interacting with different lipid mixtures as indicated.

Nevertheless, the enthalpies of the clustered lipid domain in the TMCL/DMPE mixture are for both peptides below the enthalpies observed for the DMPG/DMPE mixture. Therefore, we assume that the amount of clustered lipids per peptide is similar for both mixtures, but the critical threshold ratio at which the clustering occurs (r_{cc}) is significantly different.

3.2.4 Peptide interaction with the ternary lipid mixtures

As the ability to cluster negatively charged lipids by trivalent cyclic hexapeptides is fundamentally different for the binary mixture PG/PE and TMCL/PE, we studied the effect of adding the respective third component to the binary mixture on the clustering efficacy of the peptides.

Figure 3-2-14 shows DSC curves of ternary mixtures with DMPG/DMPE 1:1 ratio with increasing TMCL content for a 40:1 lipid-peptide ratio with c-RWRWRW and c-RRRWWW. Although the charge density increases by the addition of cardiolipin, the peak height characteristic for the clustered domains induced by binding of c-RWRWRW decreases slightly with respect to the peak observed for the binary DMPG/DMPE mixture.

The mixture containing 20 % and 33% TMCL with bound c-RRRWWW shows two distinguishable phase transition peaks around 14°C and 22°C, indicating that two clustered domains of different lipid content are present. The lipid mixture consisting of 50 % TMCL shows a broad phase transition starting at 20 °C. This was similarly observed for the binary DMPE/TMCL membrane containing 50% TMCL with bound c-RRRWWW in a 10:1 lipid- peptide ratio (see Figure 3-2-12 or Figure 3-2-15). When compared to the ternary mixture, where half of the DMPE is replaced by DMPG, a pretransition around 10°C is present, indicative for a clustered domain of TMCL or a TMCL enriched binary or ternary mixture.

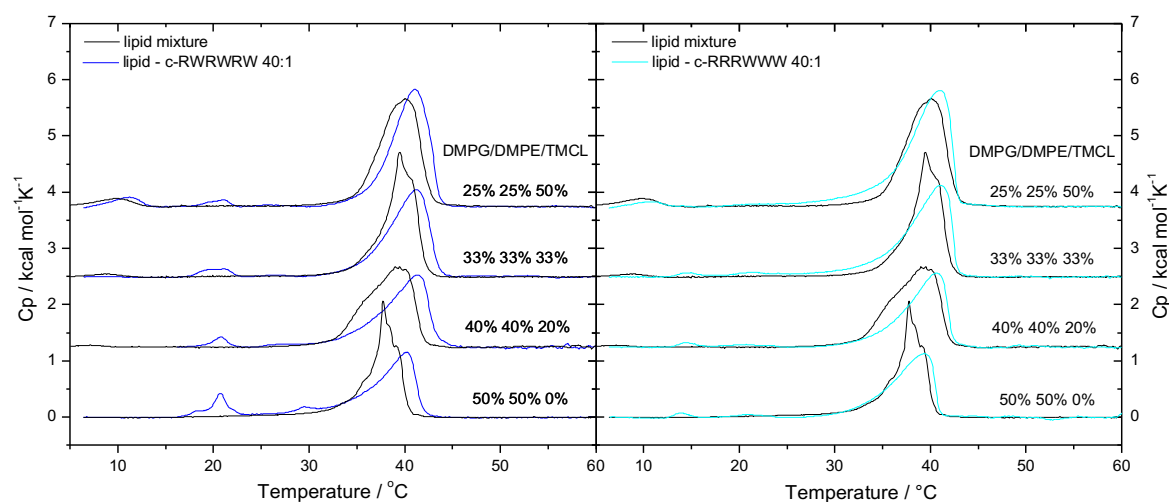


Figure 3-2-14 DSC thermograms of the last upscan of pure DMPG/DMPE and DMPG/DMPE/TMCL vesicles of different composition as indicated (black) and after addition of c-RWRWRW (left) and c-RRRWWW (right) in a 40:1 lipid-peptide ratio.

To eliminate the effect of different net charges of the ternary mixtures on the clustering behaviour we investigated the effect of c-RWRWRW and c-RRRWWW on ternary mixtures containing the same net charge. Figure 3-2-15 displays the effect of c-RWRWRW (left) and c-RRRWWW on TMCL/DMPE 1:1 mixtures with increasing DMPG content maintaining the same net charge but displaying increasing charge densities (see Figure 2-1-4).

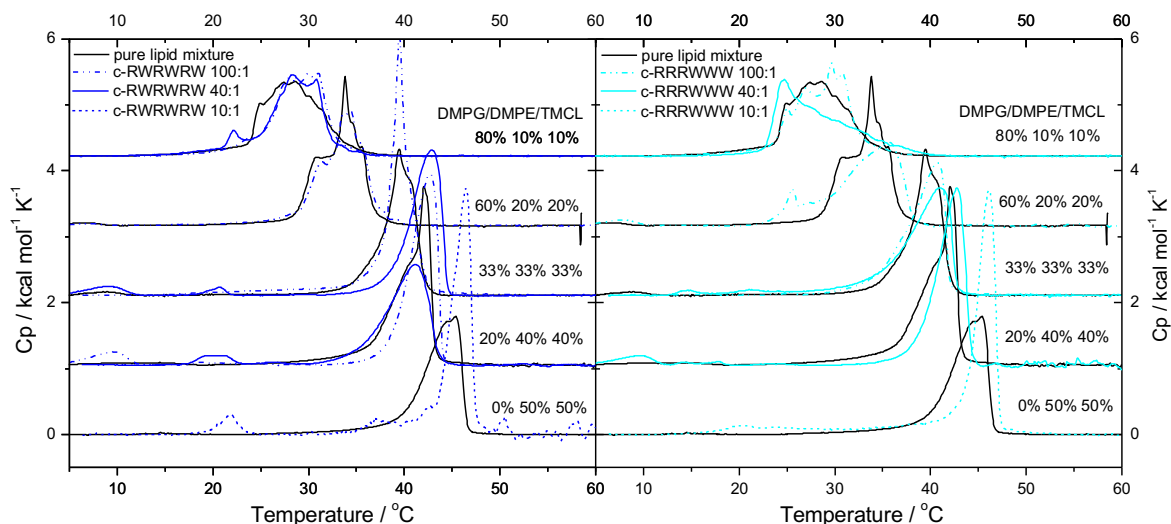


Figure 3-2-15 DSC thermograms of the last upscan of pure DMPE/TMCL and DMPG/DMPE/TMCL vesicles of different composition as indicated (black) and after addition of c-RWRWRW (left) and c-RRRWWW (right) in a 100:1 (dotted and dashed line), 40:1 (solid line) and a 10:1 (dotted line) lipid-peptide ratio.

From the comparison of the 10:1 lipid-peptide ratio of the binary TMCL/DMPE mixture and the 40:1 lipid-peptide ratio of ternary mixtures it is evident that low peptide concentrations are sufficient for the ternary mixture to induce a phase transition of the clustered domain of comparable transition enthalpy. Already at low DMPG content of 20% a 100:1 lipid-c-RWRWRW ratio is sufficient to cluster TMCL or TMCL enriched domains as it can be deduced from the low pretransition peak at around 10 °C. For the ternary mixture with 60% DMPG, i.e. a content slightly lower than DMPG contents where demixing is observed (see Figure 2-4-6), c-RWRWRW shows almost no effect on the phase behaviour. For 100:1 lipid-c-RRRWWW ratio at the same lipid-composition peak at 24°C occurs, that can be attributed to a DMPG-enriched cluster. For the ternary mixture with 80% DMPG content c-RWRWRW induces a cluster that displays a phase transition temperature of 22°C below the onset of the ternary phase transition temperature and similar to transition temperature found for the cluster of the binary DMPG/DMPE and TMCL/DMPE mixture. The ternary DMPG/DMPE/TMCL 80%/10%/10% mixture interacting with c-RRRWWW, however, displays a peak at 24°C, i.e. the melting temperature of the pure DMPG component, which is decreased for the 100:1 and increased for the 40:1 lipid-peptide ratio when compared to the pure lipid mixture. For the binary DMPG/DMPE 1:1 mixture interacting with c-RRRWWW the melting temperature of the cluster was decreased to ~17 °C (see Figure 3-2-5). This indicates that for the block-peptide c-RRRWWW interacting with a demixed ternary mixture a more profound change in phase behaviour is expected as it was similarly observed and discussed for the DPPG/DPPE 3:1 mixture (Figure 3-2-8). This is supported by the effect of c-RRRWWW on the ternary mixture containing 60% DMPG in a 100:1 lipid-peptide ratio. Here, the non-ideality of the mixture is already close to the spinodal decomposition and therefore small amounts of block-peptide can already induce a demixing.

Altogether, these findings show that independent of the membrane net charge, the addition of DMPG destabilises the TMCL/DMPE binary mixture with respect to the peptide induced clustering efficacy because lower amounts of peptide can lead to a demixing. The occurrence of a low temperature transition peak below 10 °C additionally supports the finding that cardiolipin is part of the clustered domain.

A possible reason for the increased clustering efficacy can be the increased charge density of the ternary mixture compared to the binary TMCL/DMPE mixture that leads to an increased number of bound peptides.

3.2.5 Summary

The binding of cyclic peptides to mixed PG/PE lipid bilayer membranes leads to phase separation or clustering of PG-rich domains with bound peptide. However, the different peptide sequences have an influence on the amount of clustered PG at the same peptide concentration. Specifically, we could show that the ability to demix PG/PE membranes depends on the sequence of the peptides and the nature of their amino acids. The order of the ability to cluster DPPG in a DPPG/DPPE mixed membrane, deduced from the slope of the fitted lines and the temperature upshift of the high temperature phase transition at a 10:1 lipid-peptide ratio (Figure 3-2-6 bottom left) is c-RRRWWW > c-RRRWFW > c-RWRWRW > c-KKWWKF > c-KWKWKW > c-RFRFRF which resembles with good agreement the different antimicrobial activities of the peptides towards *B. subtilis* (see Figure 3-1-1). Although, the ability to induce clustering of PG in different amounts does not correlate for every mixture and peptide concentration with the respective antimicrobial activity the highest activity of block-peptides is observable. The amount of clustered lipids increases with increasing amphipathicity indicating that the observed lipid alkyl chain penetration plays an important role in the driving force of lipid clustering.

Furthermore, we could show that for PG/PE membranes containing 1:1 molar ratios but lipids with equal or unequal chain lengths, the amount of clustered PG depended slightly on the chain length of the two lipids and on the chain length difference between PG and PE. However, much larger differences were observed when the mixing ratio between PG and PE was changed. In mixtures of DPPG/DPPE with high PG content, both methods of analysis, the evaluation of the enthalpy increase of the lower temperature peak and the analysis of the higher temperature peak shift, show that the amount of clustered PG per added peptide was much higher than in PE-rich mixtures. This indicated a defined influence of the mixing properties on peptide induced clustering. PG/PE mixtures show negative non-ideality parameters indicating the preferential formation of mixed PG/PE pairs (215). However, this tendency for mixed PG/PE pair formation is less likely in PG-rich bilayers, as the phase diagram shows an asymmetric behaviour regarding the non-ideality. Therefore, PG-rich PG/PE bilayers are more prone to demixing, as also the results of a study of DPPG/DPPE mixed

vesicles in aqueous solutions having low ionic strength show (238). In our case, the addition of peptides obviously induces the formation of demixed PG clusters.

For TMCL/PE lipid bilayer membranes also two distinguishable phase transition peaks occur that indicate a phase separation of pure cardiolipin or cardiolipin enriched domains. However, the interaction differs from the observations made for the PG/PE mixtures. Difference in temperature of the clustered domain occur in dependence of the peptide structure of the interacting peptide. This more complex behaviour is most likely due to the more complex phase behaviour observed for pure cardiolipin but also mixed with PE or PG as discussed in Section 2.2.2, 2.3.2 and 2.3.3. As the complex phase behaviour is attributed to cardiolipin headgroup interaction and these interactions of the doubly charged headgroup also show a strong pH and ionic strength dependence, the different effects observed for different peptide structure can be attributed to different amphipathic character and charge distances. Nevertheless, the results clearly show that clusters occur at smaller lipid-peptide ratios (higher peptide concentration) indicating that the efficiency is reduced for the TMCL/DMPE mixture. This can be explained by the different phase behaviour of the TMCL/DMPE mixture which shows an azeotropic maximum indicating negative non-ideality parameters for the gel phase resulting from the preferential formation of mixed TMCL/DMPE pairs most likely due to headgroup hydrogen bonding (Section 2.3.3). These interactions can be perturbed by peptide interaction leading to an increase in lipid non-ideality.

Clustering is also observed for the ternary mixtures interacting with the cyclic hexapeptides. When compared to the binary mixtures the clustering efficiency of the peptides is comparable to PG/PE membranes. This indicates that the non-ideality is increased by the addition of DMPG to the TMCL/DMPE mixture and therefore the clustering efficacy of the peptides increases as well.

Generally, the demixing phenomenon takes place at high lipid-peptide ratios which indicates that non-specific peptide-lipid interactions lead to clustering. The observed lipid alkyl chain penetration plays a crucial role in the driving force of clustering efficiency as discussed above. This is additionally underlined by the finding that the superficially bound tetravalent polyamine does, even in excess, not lead to a demixing of a PG/PE membrane.

The demixing tendency and penetration depth is abetted by the presence of tryptophan and arginine residues and therefore due to distinct interaction accompanied with these amino acids as discussed in Section 3.1.3. In case of tryptophan this is due to increased hydrophobicity of the side chain favouring interactions with the lipid acyl chains and the increased molecular volume when compared to phenylalanine, which makes only about 83% of the tryptophan volume (329, 330). This additionally means that the induction of curvature by the tryptophan containing peptides is increased (327, 328). Additionally, the high dipole moment of tryptophan, together with the preferred location at the hydrophilic-hydrophobic interface might decrease the surface energy of the lipid bilayer and lead therefore to a deeper penetration (373). In case of c-RRRWWW and c-RRRWFW the lipid

chain penetration is enhanced as it was observed for other peptides with consecutive hydrophobic amino acid sequences (336, 367).

In the case of arginine, it is well known that the charge is more delocalized in the guanidinium moiety compared to lysine where the cationic charge is localized in the NH_3^+ group. Lysin was reported in several simulation studies to form hydrogen bonds with the lipid phosphate group (316, 317, 327). Thus the arginine side chain is more hydrophobic than the lysine side chain and can be more easily incorporated into a hydrophobic environment which was also observed by NOESY experiments of c-RRWWRF interacting with DPC and SDS micelles (269). A deeper insertion of the arginine sidegroup might also result from the guanidinium group interaction like the formation of π -stacks between with the tryptophan indole residues (354) or the formation of hydrogen bonds with the lipid carbonyl group.

Moreover, the negative non-ideality parameters in PG/PE mixtures indicate a preferential formation of mixed PG/PE pairs (215). This pair formation is probably driven by headgroup interactions via hydrogen bonds which is also discussed for cardiolipin/PE interaction. Arginine side chains might also replace hydrogen bonds to the PG or cardiolipin headgroup, respectively, previously donated by the PE headgroups thus increasing the non-ideality parameter and creating an additional driving force for PG clustering after peptide binding.

3.3 Attenuated Total Reflection Infrared (ATR-IR) Spectroscopy

We used ATR-IR spectroscopy to investigate structural changes which are related to the transitions observed in DSC measurements. Therefore, we utilised the Bio-ATR device from Bruker where only small volumes of lipid suspension and peptide solution are required (Section 6.2.3). Within this chapter, we mainly want to answer the question if the clustered domains indeed consist solely of charged molecules. Additionally, we want to investigate structural changes in peptides (see Section 3.1.2) and lipids upon their respective interaction as well as identify if specific interactions are responsible for the peptide-induced lipid clustering, as they were discussed in Section 3.1.3.

Above the peptide-lipid charge ratio R_c of 1 no further clustering is observed (see Section 3.4). For the ATR-IR measurements, we chose a lipid-peptide ratio of 2:1, i.e. excess of peptide charges for the mixed lipid membranes ($R_c > 1$), to ensure observable effects of lipid clustering on the lipid band intensities and vibration wavenumber but also to judge on the peptide inherent bands of bound peptides versus unbound peptides. However, for pure TMCL membranes interacting with cyclic peptides (Section 3.3.1.2) R_c is only 0.75.

3.3.1 Peptide interaction with pure lipid membranes

3.3.1.1 Peptide interaction with pure DMPG membrane

3.3.1.1.1 Analysis of CH₂ vibrational bands

Figure 3-3-1 shows the impact of the different cyclic peptides on the phase transition of DMPG, followed by the shift in wavenumber due to the lipid chain “melting”. It can be seen that all peptides shift the phase transition to lower temperatures compared to pure DMPG.

A downshift in phase transition temperature was also observed in DSC measurements but the temperature difference compared to pure DMPG is much higher in ATR-IR measurements which can be a result of the decreased lipid-peptide ratio. The cooperativity of the transition increases compared to pure DMPG in ATR-IR measurements, whereas the DSC results show a second transition peak. All these differences might be due to the increased peptide concentration or the different reaction time to the applied heat of each lipid-peptide mixture as the heating scan rate is much lower in ATR-IR experiments.

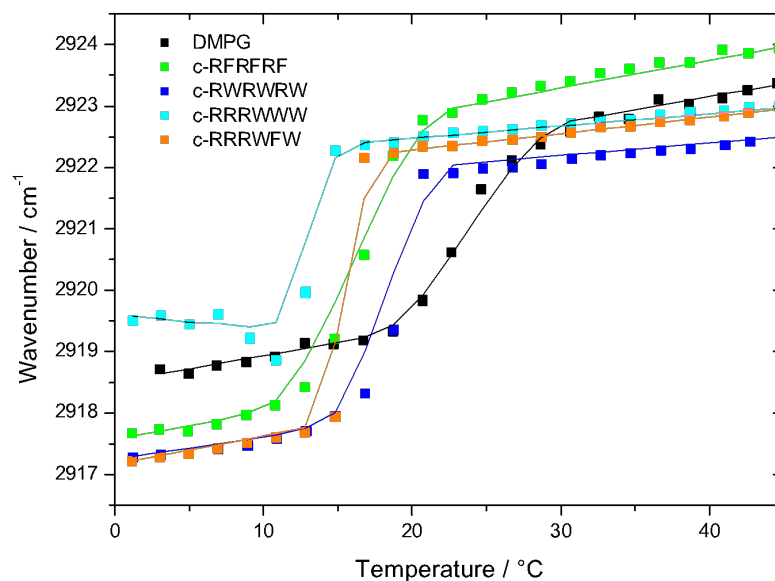


Figure 3-3-1 Temperature dependence of the wavenumber of the antisymmetric CH₂ stretching band of DMPG (black) and DMPG interacting with the respective peptides. The lipid-peptide ratio was 2:1.

For all peptides, except c-RRRWWW, a downshift in wavenumber is seen at low temperature for bilayers in the gel phase and, except for c-RFRFRF, also for the fluid phase. The upshift in wavenumber in the gel phase for c-RRRWWW supports the finding that the peptide penetrates deeper into the membrane and therefore alters the lipid chain order. When the peptide's hydrophobic moieties only partially penetrate the lipid chain area water molecules from the lipid headgroup and the hydrophobic-hydrophilic interphase are expelled. This leads, together with the screening of the repelling headgroup charges, to a higher order of lipid chains as it can be seen for c-RFRFRF, c-RWRWRW and c-RRRWFW.

The higher chain order in the liquid crystalline phase for c-RRRWWW, c-RWRWRW and c-RRRWFW results from the insertion of hydrophobic sidegroups into the lipid chain area as it was demonstrated with MD simulations by Appelt et al. (270). This indicates that during the lipid phase transition c-RWRWRW and c-RRRWFW insert deeper into the membrane. The insertion of the tryptophan indole ring leads to an increase of the order parameter *S* within the first eight to nine CH₂ groups of the lipid acyl chain in the fluid phase (see Section 3.1.3) whereas the remaining CH₂ groups need to compensate for the increasing lipid area (270). Therefore, the downshift in phase transition temperature might be due to reduced interaction between the alkyl chains, hindered by the penetrating sidegroups. The alkyl chain interaction with the hydrophobic peptide residue does not stabilise the gel phase. This might have geometrical origins occurring from the flat and rigid indole structure (334) or might be due to the high dipole moment of the tryptophan indole (346).

3.3.1.1.2 Analysis of lipid carbonyl and peptide amide I bands

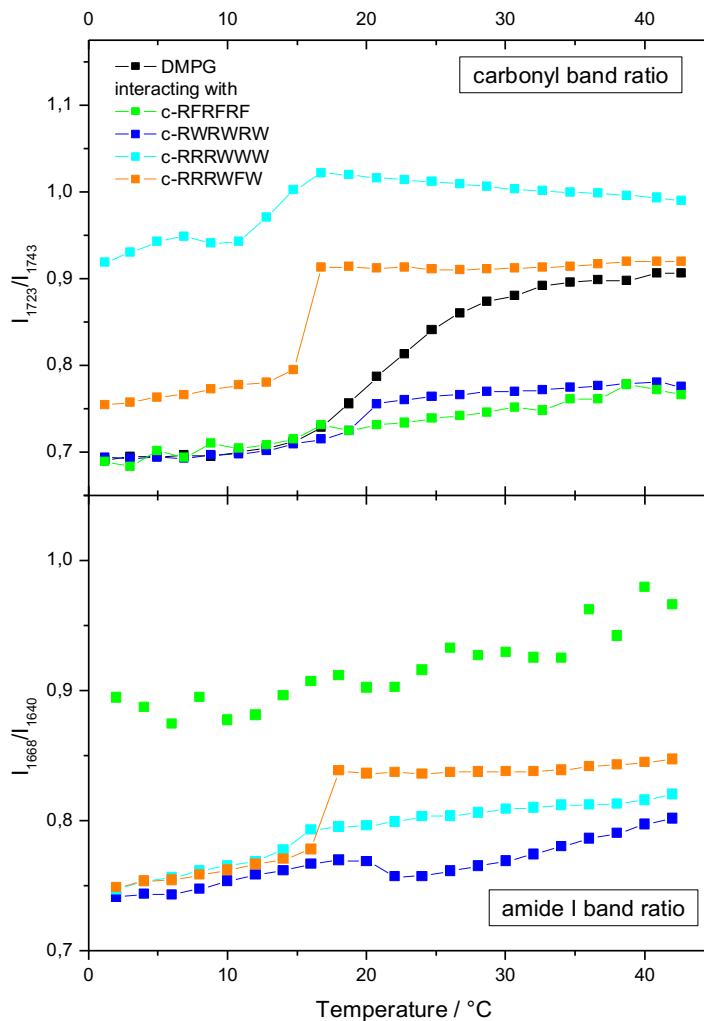


Figure 3-3-2 Top: Temperature dependence of the DMPG carbonyl band intensity ratio (I_{1723}/I_{1740}) of the pure lipid (black) and interacting with the various peptides. Bottom: Temperature dependence of the amide I band intensity ratio (I_{1668}/I_{1640}) of the different peptides interacting with DMPG membranes. The solution was 100 mM NaCl (in D_2O , pH 6.8).

Figure 3-3-2 (top) shows the intensity ratio of the lipid carbonyl band at 1723 cm^{-1} and 1742 cm^{-1} (I_{1723}/I_{1742}) of DMPG with and without bound peptides. The ratio yields information about the respective hydration state of the C=O groups as the formation of hydrogen bonds to the lipid carbonyl groups lead to a downshift in wavenumber from 1742 cm^{-1} to 1730 cm^{-1} and 1723 cm^{-1} (221). For the pure lipid a sigmoidal increase is seen, i.e. an increased headgroup hydration, when the lipid is heated from the gel to the liquid-crystalline phase. The binding of peptides leads to a reduced change in hydration when the lipid is heated above the phase transition. The addition of c-RRRWWW leads to a headgroup hydration in both phases, but stronger pronounced in the gel phase which is in line with the observed decrease in chain order due to the penetration of peptide sidegroups. In the case of c-RRRWFW, the headgroup hydration in the gel phase is increased supporting that the peptide inserts into the hydrophilic-hydrophobic interphase region. In the

liquid-crystalline phase the carbonyl band ratio is comparable to the pure DMPG membrane. When compared to c-RRRWWW, this difference in hydration effect is due to the replacement of one tryptophan by phenylalanine, leading to a reduced disturbance in lipid chain packing and therefore reduced amount of additional water molecules in the hydrophilic-hydrophobic interphase.

The two alternating and arginine-containing peptides c-RFRFRF and c-RWRWRW show almost no changes in headgroup hydration upon the lipid phase transition and remain close to the headgroup hydration observed for the pure DMPG gel phase. This indicates that either the change in lipid area upon the phase transition is reduced and therefore fewer water molecules can access the lipid carbonyl groups or the peptides occupy the difference in area and block the water molecules away from the carbonyl groups, e.g. by forming lipid-peptide hydrogen bonds with the lipid carbonyl bonds. The latter supports the interpretation that the alternating peptides insert deeper into the membrane during the lipid phase transition. Moreover, this also indicates that the binding of the alternating peptides is parallel to the membrane plane in the lipid headgroup to tail interface and, therefore, has a bigger impact on the carbonyl hydration.

Figure 3-3-2 (bottom) shows the temperature dependence of amide I band ratio of the intensity at 1668 cm^{-1} and 1640 cm^{-1} of the different peptides interacting with DMPG.

The block-peptide c-RRRWWW shows a slight stepwise increase in amide I band ratio upon the phase transition. The change in amide I frequency indicates an opening of the peptide β -turn structure. This increase is more pronounced for c-RRRWWF. This supports the finding that c-RRRWWF inserts deeper into the membrane only upon the lipid phase transition which is accompanied by more profound changes in β -turn structure upon insertion into the membrane when compared to c-RRRWWW. As the slope in gel and liquid-crystalline phase is comparable to the slope observed for the pure peptides in solution (see Figure 3-1-5), no further changes in peptide structure are observed. For c-RWRWRW, which was also discussed to insert deeper into the membrane above the lipid phase transition, the amide I band ratio decreases slightly upon the phase transition. This could either be a result of lipid-carbonyl with peptide-amide interaction or mean that the number of β -turn structures increase when c-RWRWRW is bound to the liquid crystalline phase. In both cases this could be a result of the deeper membrane penetration.

3.3.1.1.3 Analysis of lipid guanidinium and indole bands

The temperature dependence of the guanidinium band intensity ratio (I_{1584}/I_{1605}) and the peak maximum of the indole vibration peak of the different peptides interacting with DMPG are shown in Figure 3-3-3. All data have been averaged to reduce the noise and display tendencies in temperature dependence using the Savitzky-Golay 5-point-averaging method implemented in the Origin software. The signal-to-noise ratio of the guanidinium peak of c-RFRFRF was too low to give a clear temperature dependency. The guanidinium band intensity ratio of the low to high

wavenumber peak of arginine is reported to be 0.9 (282) and 0.75 in an arginine dipeptide (292). Both values are in line with the values measured for the pure peptides c-RFRFRF, c-RRRWWW (see Figure 3-1-5) and the arginine containing peptides interacting with the DMPG membrane.

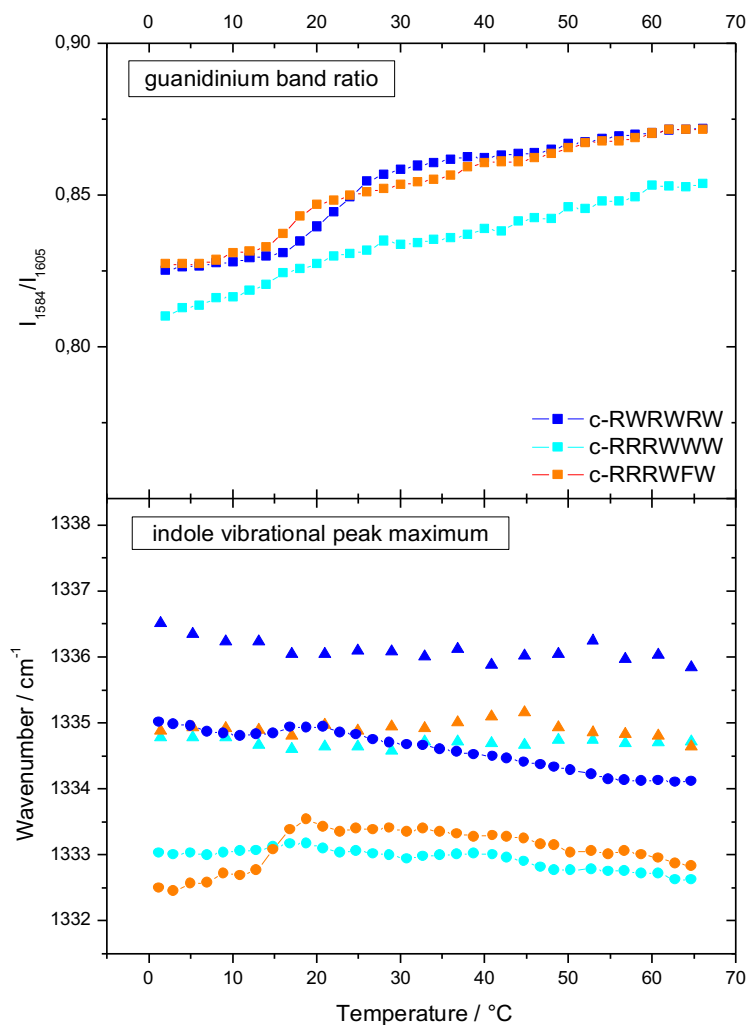


Figure 3-3-3 Top: Temperature dependence of the guanidinium band intensity ratio (I_{1584}/I_{1605}) of the three arginine-tryptophan containing peptides bound to DMPG membranes. Bottom: Temperature dependence of the indole vibrational peak position of the different tryptophan containing pure peptides (triangles) and bound to DMPG membranes (circles). The solution was 100 mM NaCl (in D_2O , pH 6.8).

A comparison to the values observed for the pure peptides in solution (Figure 3-1-5) show that, upon interaction with the DMPG membrane, the guanidinium band ratio is shifted to higher values. The original spectra in Figure S3-1-1 and S3-3-1 already show that both guanidinium bands change in position and intensity upon membrane interaction. The difference in the guanidinium band intensity ratio over the whole temperature range is similar for all three peptides. However, for c-RRRWWW the ratio is shifted to lower absolute values and changes only slightly upon the lipid phase transition. This means that no major changes that are accompanied by the lipid phase transition affect the guanidinium interaction. In the case of c-RWRWRW and c-RRRWFV, the guanidinium band intensity ratio shows a stepwise increase at the phase transition temperature, meaning that the

guanidinium interaction is different in the gel and in the liquid-crystalline phase. This difference in guanidinium interaction between c-RRRWWW and c-RRRWFW or c-RWRWRW, respectively, might result from the different hydration of the lipid headgroup as it was observed earlier (see Figure 3-3-2). Additional water molecules compete with the guanidinium and lipid hydrogen bond formation and, in turn, contribute to shielding the lipid and peptide charges.

The temperature dependence of the indole vibrational peak maximum of the peptide in solution and interacting with DMPG membrane is shown in Figure 3-3-3 bottom. The peptides display a downshift in wavenumber of ~ 1.5 to 2 cm^{-1} when bound to the DMPG membrane. This indicates changes in indole environment, most likely due to the reduced water exposure by insertion into the hydrophobic membrane region. This is more pronounced for the block-peptides which again supports the finding of deeper membrane penetration by these peptides.

The minor changes observed for c-RRRWWW support the finding that the peptide does not change significantly upon the lipid phase transition as no changes in amide I and guanidinium band is observed. This also means that a guanidinium-indole interaction over the whole temperature range cannot be excluded for this peptide.

However, the impact of the lipid phase transition on the indole vibration of c-RRRWFW is more pronounced. This supports the conclusion drawn from the changes in carbonyl and amide I vibration bands, that c-RRRWFW, in contrast to c-RRRWWW, displays structural changes upon the lipid phase transition that could lead to a reorientation of the peptide. This difference in positioning of the block-peptides in the lipid membrane seems to be due to the replacement of one tryptophan by a phenylalanine because the phenylalanine does not have a preferential localisation in the membrane as observed for tryptophan, as discussed in Section 3.1.3.2 (331-333). As c-RRRWFW displays changes of guanidinium and indole vibration at the lipid phase transition temperature this could be an effect attributed to changes occurring during the lipid phase transition, e.g. change in hydration, or a result of arginine-tryptophan interactions like π -stacking of the indole and guanidinium groups. The alternating c-RWRWRW, however, shows also minor changes in indole vibration but more pronounced changes in guanidinium band intensity ratio at the lipid phase transition temperature. Therefore, a guanidinium-indole interaction can be excluded.

3.3.1.2 Peptide interaction with pure TMCL membrane

3.3.1.2.1 Analysis of the CH₂ vibrational bands

The effect of the different peptides on the phase transition of TMCL is depicted in Figure 3-3-4. The pure TMCL was shown in Figure 2-2-4, where the subgel formation and subgel to gel phase transition at 25°C was already discussed.

All peptides shift the phase transition to lower temperatures in the case of TMCL, as already observed for DMPG. However, all arginine containing peptides show two different steps in transition from gel to fluid phase, most pronounced for c-RFRFRF, indicating the presence of two domains or two different phases with each a distinguishable phase transition peak. The temperature regime from 15 °C to 25 °C for the first transition of the arginine containing peptides corresponds well to the low melting peaks observed in the last DSC upscans of the 5:1 lipid-peptide mixtures (see Figure 3-2-2). The three arginine- and tryptophan-containing peptides show the same transition temperature of 17 °C.

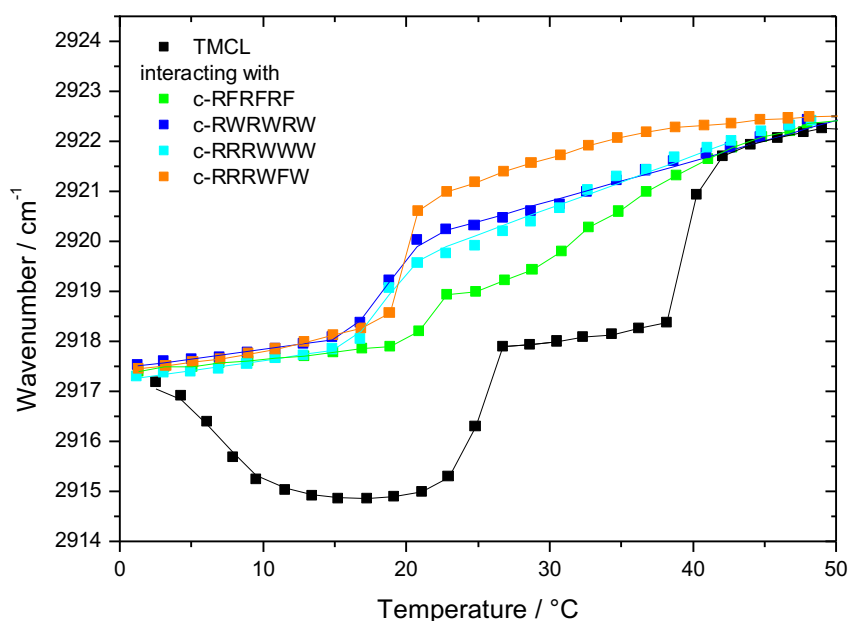


Figure 3-3-4 Temperature dependence of the wavenumber of the antisymmetric CH₂ stretching band vibration of TMCL (black) and TMCL interacting with the respective peptides in D₂O. The lipid-peptide ratio was 2:1.

The main phase transition of TMCL interacting with the cyclic peptides is not distinguishable as a second upshift in the ATR-IR measurement as it occurs in DSC at 41 °C. Here, it is smeared across the low melting temperature transition and the main phase transition temperature (please note that the alternating and the block c-RW peptides show a similar behaviour). The difference to the DSC results might be an effect of lower pH of 6.8. The pure lipid membrane at this pH consists of a mixture of mono- and divalent TMCL molecules that lead to the broad transitions already observed in the pH dependent study shown in Figure 2-2-3. The observed decrease in melting temperature by addition of peptides can again be interpreted as a penetration of the hydrophobic peptide fragments into the lipid chain area.

However, the lipid alkyl chain order of TMCL in the gel and liquid crystalline phase is the same for the pure and peptide bound membrane. This means no shift to lower wavenumbers, indicating the subgel phase formation, as observed for the pure TMCL, is observed with peptides bound to the membrane. Therefore, the attribution of the transition at 30 °C to a subgel to gel phase transition, as discussed in the DSC chapter, seems unlikely. The fact that the CH₂ wavenumber of TMCL in the

lipid gel and liquid-crystalline phase is not largely altered by the interaction with the arginine containing peptides might result from the smaller TMCL headgroup size when compared to DMPG. This means that the peptides have more space by insertion in the bilayer interphase and do not alter the chain packing by inducing lipid curvature.

3.3.1.2.2 Analysis of lipid carbonyl and peptide amide I bands

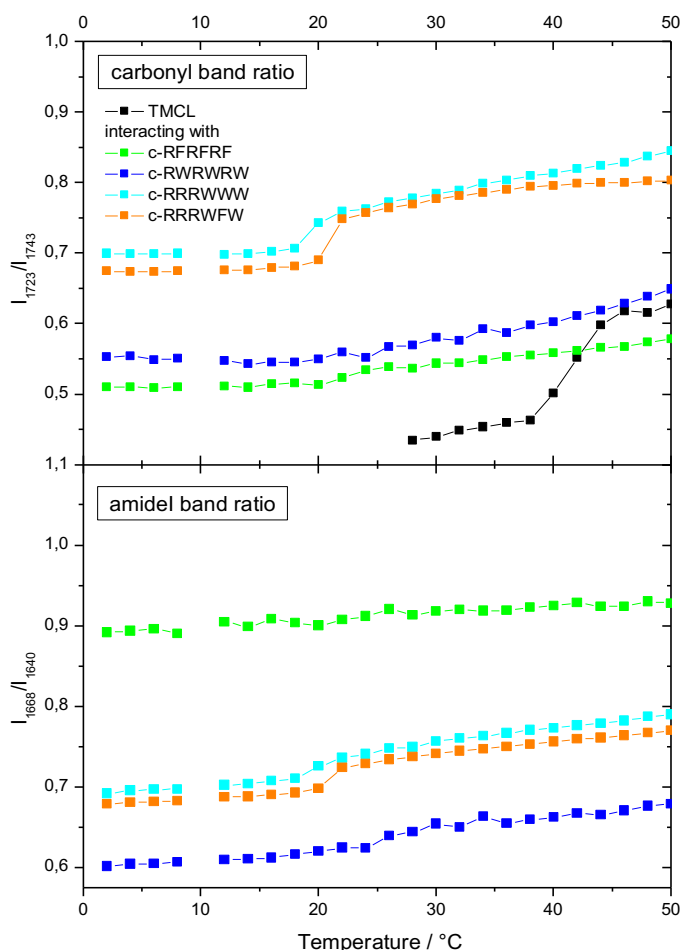


Figure 3-3-5 Top: Temperature dependence of the TMCL carbonyl band intensity ratio (I_{1723}/I_{1740}) of the pure lipid (black) and interacting with the various peptides. Bottom: Temperature dependence of the amide I (I_{1668}/I_{1640}) band intensity ratio of the different peptides interacting with TMCL membranes. The solution was 100 mM NaCl (in D_2O , pH 6.8).

Figure 3-3-5 top shows the temperature dependence of the TMCL carbonyl band ratio. As the carbonyl band of pure TMCL is largely affected by the subgel phase formation (see Section 2.2.2.2) a direct comparison can only be performed above 28 °C. When compared to DMPG the absolute value for the carbonyl band ratio is decreased which might be a result of TMCL headgroup interactions resulting in a reduction of interfacial water molecules. The change in carbonyl band ratio from gel to liquid-crystalline phase is comparable between TMCL and DMPG.

Both alternating peptides increase the gel phase hydration of TMCL but show only a small upshift upon the phase transition around 20° C where the shift in alkyl chain vibration is observed.

Due to the deeper penetration of the block-peptides c-RRRWWW and c-RRRWFV the hydration of TMCL is strongly increased for both phases. Also, the shift in carbonyl band ratio at the phase transition temperature around 20 °C is more pronounced for the block-peptides.

However, the shift in carbonyl band ratio is decreased for the peptide bound membrane when compared to the pure TMCL hydration change which might be due to the fact that the hydration state is already increased by the bound peptides.

The amide I band intensity ratio shifts slightly upon the lipid phase transition to higher numbers for the three arginine-tryptophan containing peptides indicating an opening of the β -sheet structure. The absolute values are comparable to those observed for the peptides interacting with DMPG in gel phase and slightly reduced for the liquid-crystalline phase.

3.3.1.2.3 Analysis of guanidinium and indole bands

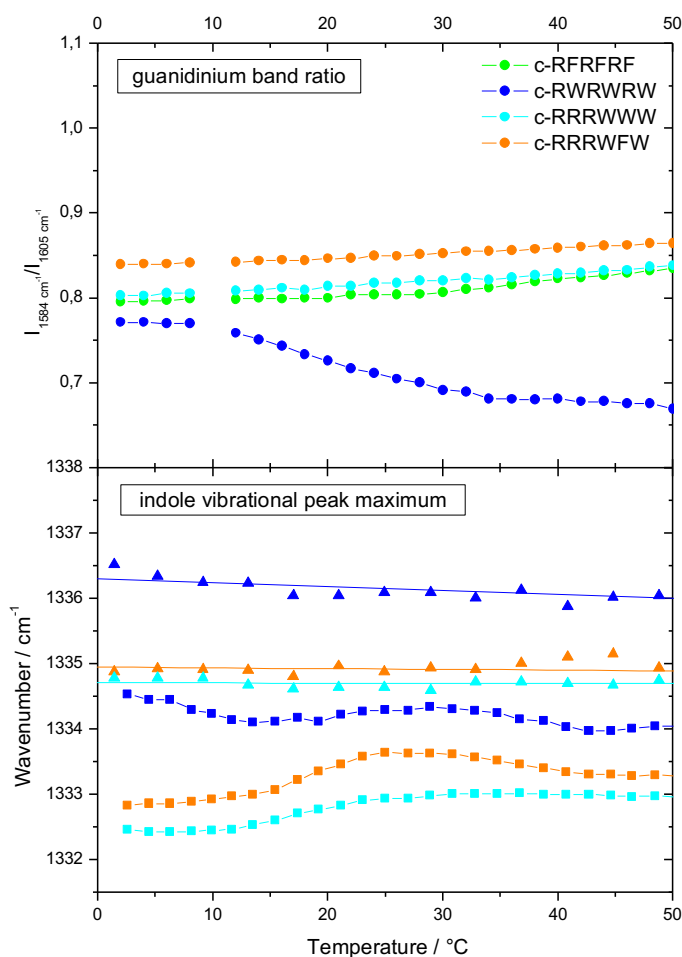


Figure 3-3-6 Top: Temperature dependence of the guanidinium band intensity ratio (I_{1585}/I_{1605}) of the four arginine-containing peptides bound to TMCL membrane. Bottom: Temperature dependence of the indole vibrational peak position of the different tryptophan-containing pure peptides (triangles with their respective linear fits) and bound to TMCL membrane (squares). The solution was 100 mM NaCl (in D_2O , pH 6.8).

Figure 3-3-6 top shows the temperature dependence of the guanidinium band intensity ratio of the four arginine-containing peptides when bound to TMCL. For TMCL no shift in guanidinium band

intensity ratio is observed, meaning that the guanidinium remains unaffected of the changes occurring during lipid phase transition. The absolute values of c-RRRWWW in the gel phase are the same for TMCL as for DMPG, whereas for c-RRRWWF the absolute values of the liquid-crystalline phase are comparable. Also, the slope of c-RFRFRF, c-RRRWWF, c-RRRWWW and between 10°C to 34°C for c-RWRWRW is comparable to the slope observed for the block-peptides in solution. As the temperature stability of the guanidinium interaction is similar to the unbound peptides in solution the guanidinium group might not be strongly interacting with the lipid headgroup. The slight changes in guanidinium ratio when compared to the peptide in solution might therefore be due to slight changes in hydration when located at the membrane interphase.

The indole vibrational peak maximum is shifted to lower wavenumbers after binding to TMCL membranes, as displayed in Figure 3-3-6 (bottom). The temperature dependent measurement displays a shift in the indole peak maximum at the phase transition temperature for c-RRRWWW and most pronounced for c-RRRWWF. This indicates again that c-RRRWWF reorients upon the lipid phase transition as already discussed for the DMPG membrane. As the signal is an average of two tryptophan moieties in case of c-RRRWWF and an average of three tryptophan moieties in case of c-RRRWWW, the observed differences might also be a result of different penetration depth of the central hydrophobic amino acid (394) leading to a further downshift and reduced changes upon the phase transition of the indole vibrational peak maximum.

However, for c-RRRWWW bound to the TMCL membrane the indole peak maximum is shifted to lower wavenumbers in the lipid gel phase when compared to DMPG. This might be a result of less hydrated membrane interphase where the tryptophan moieties are located.

The indole vibrational maximum of c-RWRWRW bound to TMCL undulates around a constant value in the temperature dependent measurement. This value is slightly below the one observed for the DMPG membrane which might also indicate a better shielding of the indole groups from water molecules when the alternating peptide is bound to the TMCL membrane.

3.3.1.3 Comparison of peptide interaction with pure DMPG and pure TMCL membrane

For both lipid membranes the block-peptide seem to orient more parallel and the alternating peptide more perpendicular to the membrane normal. This can be deduced from the increased lipid carbonyl hydration of the block-peptides observed for DMPG (Figure 3-3-2) and TMCL (Figure 3-3-5) where similar tendencies are observed. Also the changes in carbonyl band ratio upon the lipid phase transition are decreased for the two alternating peptides bound to both lipid membranes. This can be explained by a better compensation of the increase in lipid area by the superficially bound peptides. Furthermore, the lower indole vibration wavenumbers for the block-peptides when compared to the alternating c-RWRWRW observed for the peptides bound to both membranes indicate that the block-peptides insert deeper into the membrane. However, the reorientation of c-RRRWWF seems

to be of larger scale for the DMPG phase transition where a larger shift in the amide I band intensity ratio, guanidinium band intensity ratio and indole vibrational peak maximum is observed than for c-RRRWWF bound to TMCL.

Another major difference is that peptide binding has a higher impact on lipid chain order for the DMPG membrane than for the TMCL membrane. This means that TMCL can better compensate for the occupied peptide volume which might be a result of the reduced headgroup area. The headgroup area per lipid chain is smaller for TMCL when compared to DMPG (and even when compared to DMPA) and the headgroup hydration is reduced when compared to DMPG (compare absolute values in Figure 3-3-2 and 3-3-5), the free area per peptide located in the lipid headgroup is therefore larger. This additionally explains why almost no changes in guanidinium and amide I band ratio is observed for the peptides bound to TMCL.

3.3.2 PG/PE mixtures

To investigate the structural effects occurring during lipid clustering, we performed ATR-IR measurements of DMPG and TMCL in membranes mixed with DMPE. To confirm the interpretation of lipid clusters that mainly consist of charged lipid moieties, we studied the lipid chain melting of each lipid component with ATR-IR spectroscopy. Upon the lipid phase transition, the wavenumber of the CH₂ vibration shifts to higher wavenumbers due to decreasing alkyl chain order. To distinguish between the phase transitions of the single components, we use DMPE with deuterated lipid chains (DMPE-d₅₄). Furthermore, the effect of the additional interaction partner DMPE is discussed in light of the previous results of pure lipid membranes.

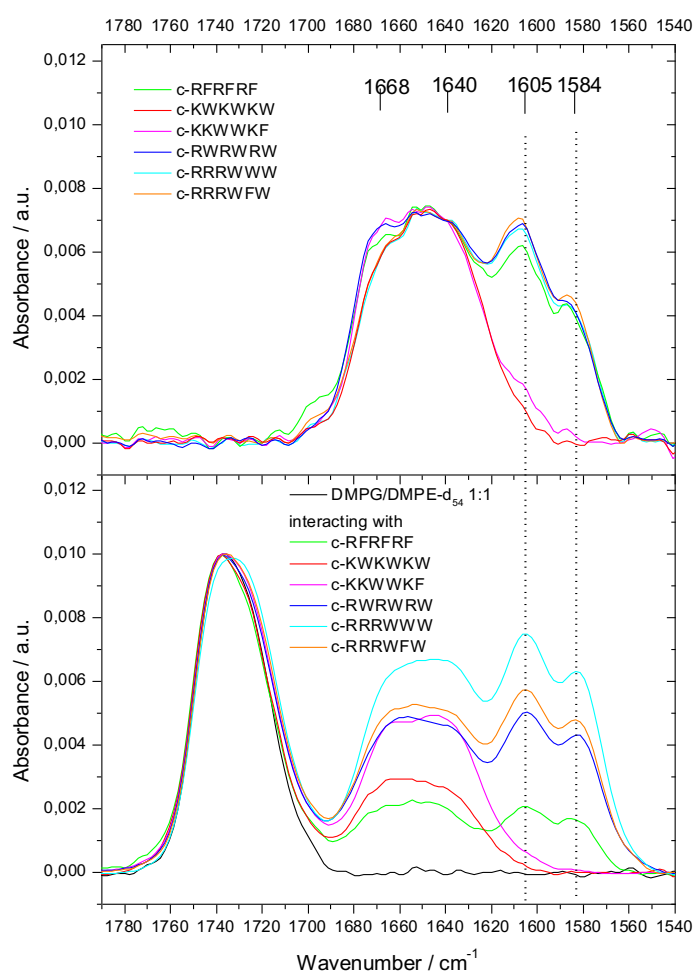


Figure 3-3-7 Top: Amide I and guanidinium band of the pure peptides in D₂O at 10 °C (100 mM NaCl) from Figure 3-1-3. Spectra are normalized at 1640 cm⁻¹. Bottom: Lipid carbonyl, amide I and guanidinium band of the different peptides bound to vesicles consisting of a DMPG/DMPE-d₅₄ 1:1 mixture in D₂O at a lipid-peptide ratio of 2:1 at 10 °C (100 mM NaCl and pH 6.8). Spectra are normalized to the same intensity at 1742 cm⁻¹.

Figure 3-3-7 shows a comparison of the amide I and guanidinium bands of the different peptides in solution with the different peptides bound to DMPG/DMPE-d₅₄ 1:1 mixed vesicles. Normalizing the spectra to the lipid carbonyl band intensity shows that the intensities of the peptide bands vary in the

following order: c-RFRFRF < c-KWKWKW < c-KKWKWF = c-RWRWRW < c-RRRWFW < c-RRRWWW. Assuming that the extinction coefficient is the same for all peptides, this finding means that different concentrations of peptides are in the measurement path. As the lipid vesicles precipitate on the crystal surface after peptide addition, one can either deduce that the density of the precipitating aggregates is higher within the more amphipathic block-peptides or that the amount of peptides bound within these aggregates varies in the afore mentioned order. The latter one is more likely and supported by ITC results (Figure 3-4-8 (252)).

The guanidinium bands are shifted to lower wavenumbers and the ratio also changes upon peptide binding to the membrane (compare top to bottom) indicating inter- or intramolecular interactions with peptide backbone, side groups or the lipid headgroup (see discussion below).

Upon binding to lipid vesicles, only minor changes in amide I band are observed. The amide I band intensity ratio at 1668 cm⁻¹ to 1640 cm⁻¹ is displayed for all different temperatures in Figure S3-3-2 and Figure 3-3-10 and will be discussed later. It should be noted that the ethanolamine lipid headgroup vibration (218) shows only minor contributions to the peptide amide band.

3.3.2.1 Analysis of the CH₂, CD₂ and lipid carbonyl vibrational band

Figure 3-3-8 shows the effect of different cyclic peptides on the phase transition temperature of a 1:1 mixed DMPG/DMPE-d₅₄ membrane. Upon addition of cyclic peptides, an additional phase transition is seen at low temperature for the non-deuterated DMPG (Figure 3-3-8 top) but not for the deuterated DMPE (Figure 3-3-8 middle), meaning that the clustered domains consist solely of DMPG molecules.

An impact on the phase transition temperature of the DMPE molecules can be observed for the block-peptide c-RRRWWW and a little less pronounced for c-RRRWFW. They show the highest effect on the phase transition downshift of DMPG and DMPE-d₅₄ in the remaining mixed phase (upper temperature). The lipid chain order for DMPE-d₅₄ in the gel phase of the mixed membrane interacting with the peptides is slightly increased for the arginine and tryptophan containing peptides. The fluid phase order of DMPE does not change significantly by peptide interaction.

This finding is in contrast to the phase transition temperature upshift for the resulting PG depleted lipid mixture observed with DSC measurements for various PG/PE mixtures (see Section 3.2.2).

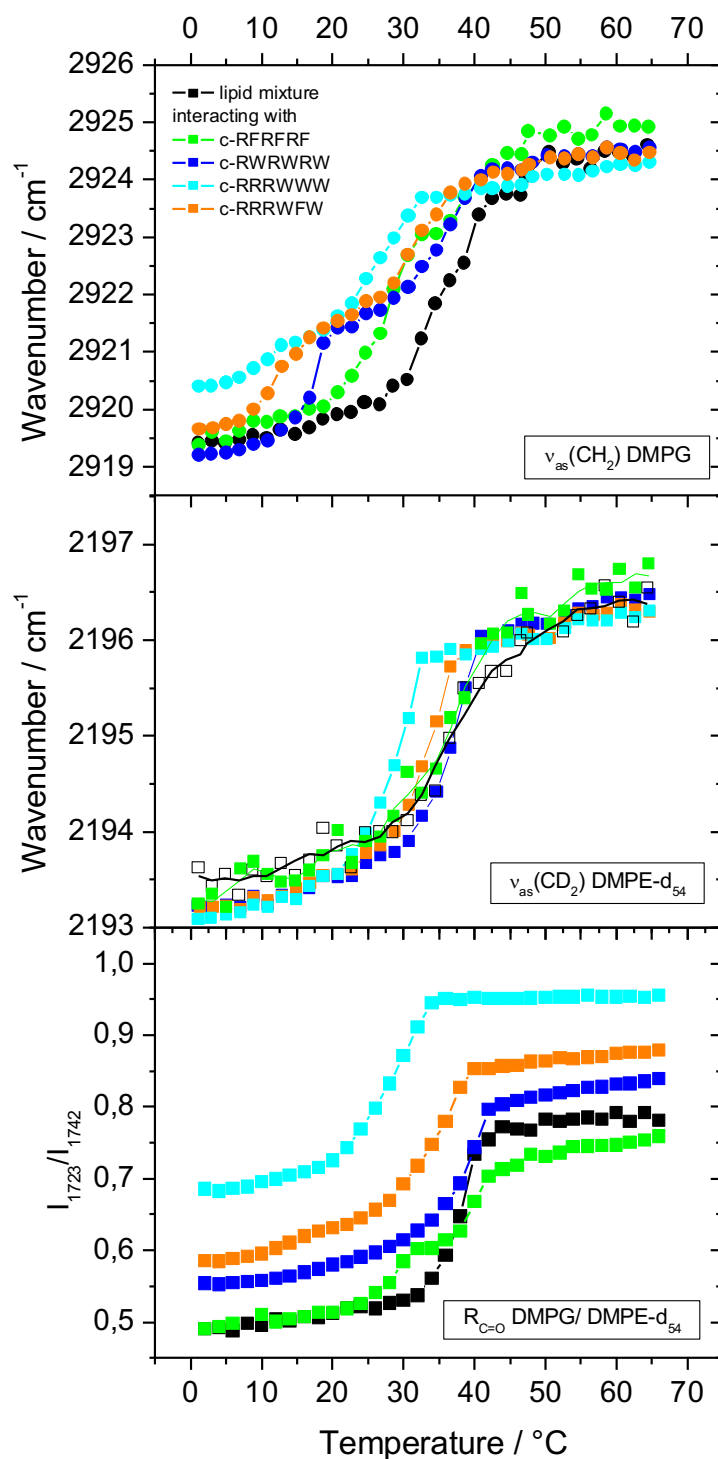


Figure 3-3-8 ATR-IR temperature dependent measurements of DMPG/DMPE-d₅₄ 1:1 mixture pure and interacting with the tryptophan containing hexapeptides. Top: Temperature dependence of the maximum of the antisymmetric CH₂ stretching band of DMPG. Middle: Temperature dependence of the antisymmetric CD₂ stretching band of DMPE-d₅₄. Bottom: The intensity ratio of the C=O stretching band at I₁₇₂₃/I₁₇₄₂. The lipid-peptide ratio was 2:1.

The increased peptide-lipid ratio used in ATR-IR compared to DSC measurements might have this effect when more peptides accumulate in the mixed membrane, which shifts the phase transition temperature down due to the insertion of peptide sidegroups into the lipid chain lattice. This might occur especially when the addition of peptide does not lead to additional clusters, which is assumed

to occur at a lipid-peptide charge ratio of one (see Section 3.4.2 for details). Here, the measurements are performed in excess of peptide charges with a peptide-lipid charge ratio of 3 to ensure that enough lipid clusters are formed, which can be determined by ATR-IR measurements.

For DMPG in the mixed membrane, c-RRRWWW induces a significantly higher chain disorder in the gel phase deduced from the upshift in wavenumber. This indicates a higher penetration of these peptides into the lipid chain region. Also, increasing headgroup size caused by sufficiently high charge distances or additional headgroup hydration might influence the lipid chain order accordingly. Melting of the clustered DMPG moiety around 20 °C leads to similar wavenumber for the antisymmetric CH₂ band of the DMPG molecules, irrespective of the interacting peptides, except for c-RFRFRF. This indicates that the chain order of the molten clusters in the gel phase matrix of the depleted mixture is similar in the interaction with the respective peptides. It furthermore means that the change in lipid chain order from gel phase DMPG to the molten cluster state DMPG is the lowest for c-RRRWWW and increases to c-RRRWFW and again to c-RWRWRW. Either the lipid chain order in the gel phase varies with the bound peptides, or the amount of clustered lipid varies with the respective peptide or, a combination of both, which is most likely.

In the liquid-crystalline phase, the lipid chains of DMPG molecules show a higher order compared to the pure lipid mixture for the three peptides with highest antimicrobial activity c-RRRWWW, c-RRRWFW and c-RWRWRW. This is in accordance with the MD simulations performed by Appelt et al. (270), which predicted an increase of the order parameter S within the first eight CH₂ groups of the lipid acyl chain in the fluid phase due to the insertion of the tryptophan indole ring. This higher order in the liquid-crystalline phase is pronounced for the peptides that show the deepest penetration. Comparing the wavenumber of DMPG in pure (Figure 3-3-1) and DMPG/DMPE-d₅₄ mixed membranes interacting with the different peptides, the induction of lipid chain order is reduced in the clustered lipid mixture. Therefore, the insertion of “bulky” hydrophobic groups such as the indole group could indeed be an additional driving force contributing entropically to the lipid demixing, similar to the lipophobic effect (334), as proposed earlier by Appelt et al. (270). The increased chain order was also shown with WPR measurements for magainin binding to lipid membranes containing of a PC/PG mixture (395) and in simulation binding to DPPC membranes (90).

Figure 3-3-8 (bottom) shows the intensity ratio of the carbonyl band at 1723 cm⁻¹ and 1742 cm⁻¹ (I_{1723}/I_{1742}) for the pure lipid component and interacting with the respective peptides. The interaction with c-RFRFRF has no effect on the lipid hydration in the gel phase and shows a slight lipid dehydration in the liquid-crystalline phase. Here, two transitions are clearly distinguishable by the shift in headgroup hydration.

All arginine-tryptophan containing peptides increase the hydration of the mixed membrane. The highest upshift is shown by the amphipathic block peptide c-RRRWWW that results in a hydration level of the gel phase that is comparable to the fluid phase hydration of the pure DMPG membrane.

The upshift in gel phase hydration is slightly lower for c-RRRWW. The alternating c-RWRWRW shows the smallest increase in headgroup hydration when compared to both block-peptides. The tryptophan-arginine peptides show only a slight stepwise increase in hydration at about 20 °C, the melting temperature of the lipid cluster, which is most reduced for c-RRRWWW. This reduction in hydration upon the lipid phase transition of the cluster indicates that the clusters contain most bound peptides. Therefore, the accessibility of the carbonyl group to water molecules is hindered by the peptides bound to the clustered DMPG.

3.3.2.2 Analysis of the guanidinium and indole bands

Figure 3-3-9 top displays the temperature dependence of a guanidinium intensity ratio (I_{1584}/I_{1605}) of the three arginine-tryptophan containing peptides bound to DMPG/DMPE-d54 1:1 mixed membrane and to the pure DMPG membrane for comparison (see Figure 3-3-3). The guanidinium intensity ratio (I_{1584}/I_{1605}) increases at temperatures corresponding to the lipid main phase transition (Figure 3-3-8). A comparison to the pure values and c-RFRFRF is shown in Figure S3-3-3. When the peptides are bound to the mixed membrane, the difference in guanidinium ratio between the lipid gel and liquid-crystalline phase is increased when compared to the pure DMPG membrane, indicating that either additional guanidinium interaction changes occur or that the temperature-induced changes affect more peptides when bound to the mixed membrane.

As discussed earlier, the difference in guanidinium band intensity ratio from the lipid gel to the liquid-crystalline phase is similar for all three peptides bound to pure DMPG membrane. The values of c-RRRWWW bound to the mixed membrane are similar to those observed for the peptide bound to the pure DMPG membrane. The guanidinium band intensity ratio, however, is shifted to lower absolute values for c-RRRWW and c-RWRWRW. Moreover, both peptides also show a stepwise change in guanidinium band intensity ratio at the main phase transition temperature as it was observed for the pure DMPG membrane. This indicates that also for the mixed membrane the increased hydration by c-RRRWWW (see Figure 3-3-8) leads to a competition of water molecules and the guanidinium group to interact with lipid headgroup moieties.

The temperature dependence of the indole vibrational peak maximum of the three arginine-tryptophan containing peptides bound to the DMPG/DMPE-d₅₄ 1:1 lipid mixture is shown in Figure 3-3-9 (bottom) in comparison to the indole vibrational peak maximum of the pure peptides in solution. In Figure S3-3-4 of the supplementary data the original spectra show the band at 1333 cm⁻¹ of the different tryptophan-containing peptides in solution and bound to DMPG and DMPG/DMPE mixed membranes, respectively (c-RFRFRF is shown for comparison). The highest wavenumber of the tryptophan band position is shown by c-RWRWRW emphasising the different behaviour of the pure peptide in solution as already discussed for the amide I and guanidinium band ratios when compared to the other peptides (see Chapter 3.1.2)

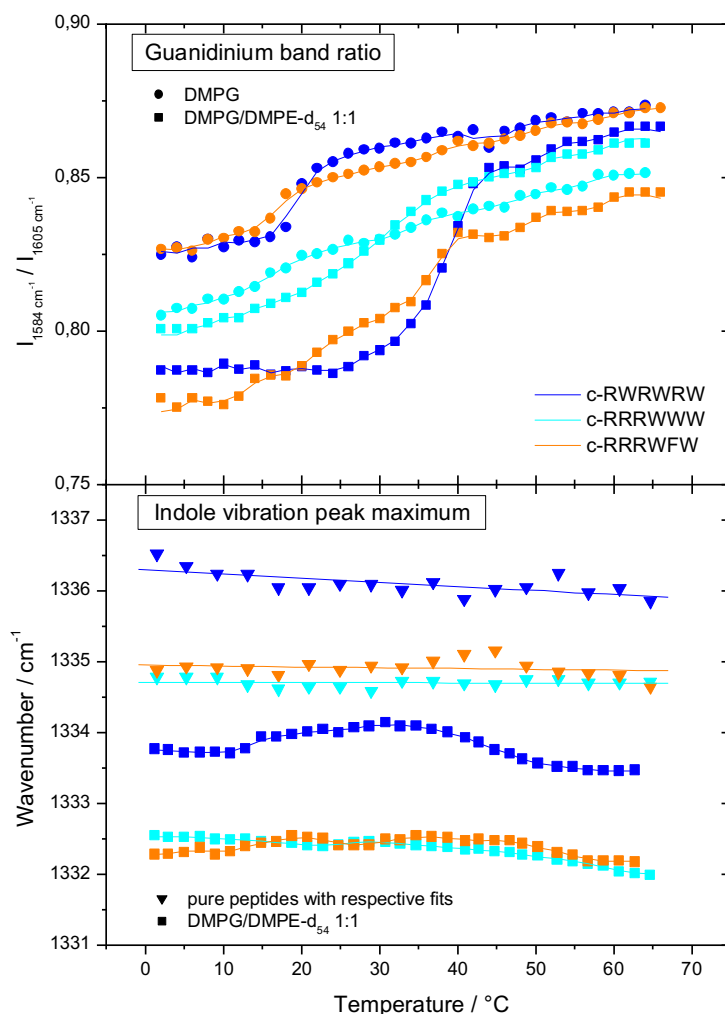


Figure 3-3-9 Top: Temperature dependence of the guanidinium band intensity ratio (I_{1584}/I_{1605}) of c-RWRWRW, c-RRRWWW and c-RRRWFW bound to DMPG (circles) and DMPG/DMPE-d₅₄ 1:1 mixture (squares). Bottom: Temperature dependence of the indole vibrational peak position of c-RWRWRW, c-RRRWWW and c-RRRWFW pure (triangles) and bound to DMPG/DMPE-d₅₄ 1:1 mixed membrane (squares). The solution was 100 mM NaCl (in D₂O, pH 6.8). The lipid-peptide ratio was 2:1. The lines are plotted to guide the eye.

Binding to the mixed lipid membrane leads to a decrease in wavenumber of the indole vibrational peak, as it was already observed for the pure lipid membranes. However, the downshift is further increased for all peptides meaning that the peptides insert deeper into the mixed membrane than into the pure DMPG as a result of reduced headgroup size and charge density. As observed for the pure membrane c-RRRWWW shows no changes in indole vibration within the observed temperature interval supporting the finding that the location of the peptide is not altered upon changes in lipid phase state. Unlike the observation for the pure DMPG membrane, c-RRRWFW shows no changes in indole vibration upon lipid melting when bound the mixed membrane, neither for the melting of the lipid cluster nor the remaining lipid mixture. The value for the indole peak maximum of c-RWRWRW increases slightly upon the transition from gel phase to the molten cluster state as it was observed for pure DMPG and decreases again to lower wavenumbers upon the melting of the remaining lipid mixture. This indicates that the indole group is more exposed to water in the molten

cluster state. This indicates that c-RWRWRW changes in peptide structure, orientation or location within this state.

3.3.2.3 Comparison of relative changes in CH₂, CD₂, amide I and guanidinium bands

To compare the relative molecular changes of lipid and peptide moieties like shifts in lipid alkyl chain and carbonyl vibrational band position, as well as amide I and guanidinium band intensity ratios, Figure 3-3-10 shows the respective lipid and peptide transitions plotted for the arginine-tryptophan-containing peptides scaled from 0 to 1.

The absolute values for the amide I band intensity ratios for each peptide in solution, bound to DMPG and to the DMPG/DMPE-d₅₄ mixture, are shown in Figure S3-3-2 of the supplementary data. Here, it can, additionally, be seen that the most pronounced change in amide I band intensity ratio occurs for the three arginine-tryptophan-containing peptides when bound to the mixed membrane.

The scaling of the wavenumbers for the antisymmetric CH₂ vibration band relates the relative number of changes in lipid order to the structural changes in peptides and allows to identify a correlation more quantitative and, thus, possible interaction partners. From the scaled plot in Figure 3-3-10 it is evident that for c-RRRWF_W the melting of the clusters around 20 °C correlates to an upshift in amide band ratio (I_{1668}/I_{1640}). The c-RRRWF_W amide I band intensity ratio remains constant for a short temperature range in the molten cluster state where the fluid clusters coexist with the gel phase of the remaining mixture. This effect is less pronounced for c-RRRWW_W where changes in amide I band intensity ratio are seen at lower temperature. For c-RRRWW_W the amide I band intensity ratio does not remain constant after melting of the lipid cluster. However, for c-RWRWR_W and c-RRRWW_W different slopes in amide I band intensity ratio change can be observed for the different phases indicating that the lipid phase state influences the opening of the 1←4 β-sheet hydrogen bond of the turn structure. This can be a result of increasing lipid headgroup area and/or intermolecular hydrogen bonds, e.g. with the lipid headgroup moieties like phosphate, glycerol or ethanolamine, upon the melting of the lipid chains.

The guanidinium band intensity ratio (I_{1584}/I_{1605}) is found to increase for the block-peptide c-RRRWW_W and c-RRRWF_W upon melting of the lipid cluster. Before the melting of PE occurs, these peptides already show more than 50 % of the overall guanidinium band intensity ratio change occurring during the entire lipid melting.

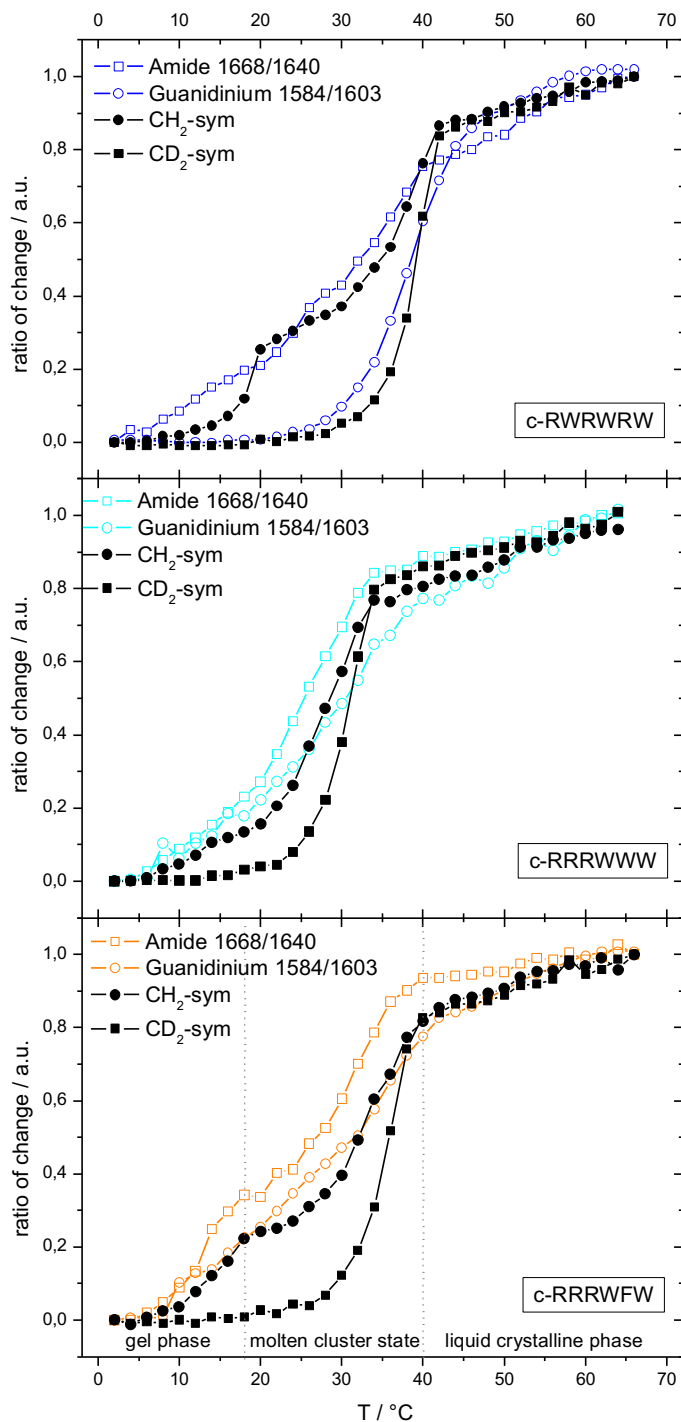


Figure 3-3-10 ATR-IR temperature dependent measurements. Scaled plot of the ratio of change vs. temperature of the CH_2 , CD_2 , amide I band, carbonyl band and guanidinium band intensity ratios for c-RWRWRW (top), c-RRRWWW (middle) and c-RRRWFV (bottom). The lipid-peptide ratio was 2:1.

However, c-RWRWRW shows a completely different behaviour. The guanidinium band intensity ratio is clearly not affected by the melting of the lipid cluster. It increases with DMPE melting of the remaining lipid mixture. This clearly illustrates again the different interaction of c-RWRWRW and c-RRRWWW which might most likely result from different orientation. The perpendicular orientation might allow the alternating peptide to maintain a guanidinium-headgroup interaction

upon the melting of the cluster whereas the orientation parallel to the membrane normal of the amphipathic block-peptides leads to changes in guanidinium interaction upon the increase in lipid headgroup distance during the melting of the cluster. The overall reduced hydration of the c-RWRWRW bound membrane, combined with the reduced hydration of the cluster upon the phase transition, might also not affect the guanidinium vibration when the moieties are buried in the membrane core. However, an interaction with the tryptophan moieties of c-RWRWRW in the lipid cluster can be excluded, as the indole vibrational peak maximum shows a clear upshift upon the melting of the cluster (Figure 3-3-9).

Although different interactions occur between the alternating and block-peptides, in both cases lipid demixing is observed. This means that this specific lipid-peptide interaction cannot be the decisive parameter for the clustering.

3.3.3 TMCL/DMPE mixtures

When DMPG is replaced by TMCL in a 1:1 mixture with DMPE, the peptide induced demixing is observed at lower lipid-peptide ratios as a result of better lipid miscibility, as discussed in Section 3.2.3. The structural effects occurring in this lipid mixture are discussed within the following section in comparison to the previous observation for the DMPG/DMPE-d₅₄ mixture. Of particular interest is the composition of the domains observed for the TMCL/DMPE clusters, as the phase transition temperature occurring after peptide addition is different from the main phase transition of the pure TMCL.

3.3.3.1 Analysis of the CH₂, CD₂ and lipid carbonyl vibrational band

The lipid-specific vibrational bands for TMCL and deuterated DMPE-d₅₄ of the TMCL/DMPE-d₅₄ 1:1 mixture interacting with the two alternating peptides c-RFRFRF and c-RWRWRW, and the block-peptide c-RRRWWW in a 2:1 lipid-peptide ratio, are shown in Figure 3-3-11.

TMCL shows two distinguishable phase transition peaks when peptides are bound to the mixed membrane (Figure 3-3-11, top). For DMPE only one transition, the transition of the mixed membrane, can be observed (Figure 3-3-11, middle).

Some differences emerge when comparing the results of TMCL in the mixed membrane with the ones from the pure membrane interacting with the different peptides. For the pure lipid, no shift in gel phase and fluid phase order upon peptide binding was observed (see Figure 3-3-4). In the mixed membrane, however, the alternating peptides c-RWRWRW and c-RFRFRF shift the wavenumbers in the fluid phase and c-RFRFRF also the wavenumbers in the gel phase to values about 1 cm⁻¹ above the ones of the pure lipid in the lipid mixture. The block-peptide c-RRRWWW seems to decrease the fluid phase order of TMCL slightly. Therefore, the fluid phase order is influenced differently by

block-peptide or alternating peptides. As an outcome, the shift in wavenumber from an ordered TMCL gel phase to a disordered fluid phase is decreased by c-RFRFRF and c-RRRWWW when compared to TMCL in the pure membrane.

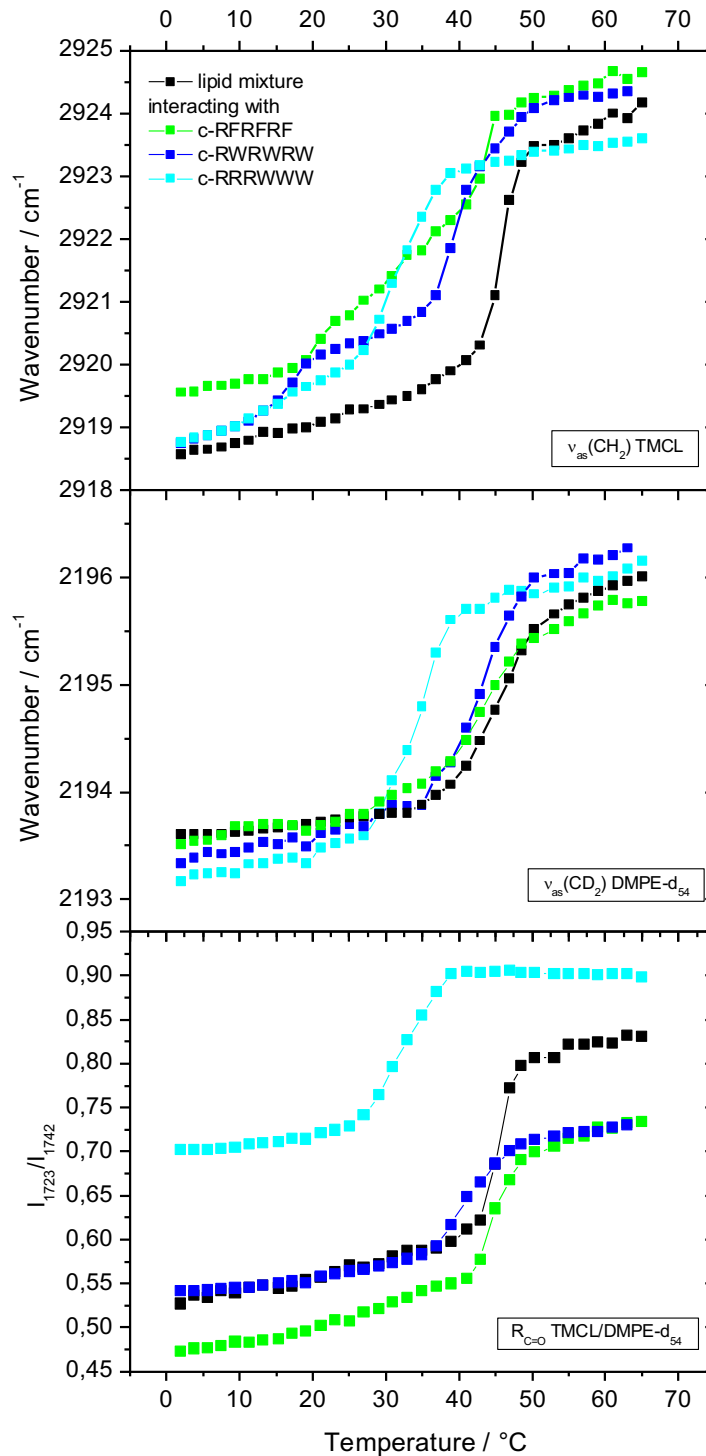


Figure 3-3-11 ATR-IR temperature dependent measurements. Top: Effect of peptides on the wavenumber of the maximum of the antisymmetric CH_2 stretching band of TMCL. Middle: Antisymmetric CD_2 stretching band of DMPE- d_{54} in a TMCL/DMPE- d_{54} 1:1 mixture (black). Bottom: The intensity ratio of the C=O stretching band I_{1723}/I_{1742} . The lipid-peptide ratio was 2:1.

When compared to the fluid phase order of DMPG in the DMPG/DMPE-d₅₄ mixture a similar tendency, but not as pronounced for c-RWRWRW, is observed. For the gel phase order in DMPG/DMPE-d₅₄ 1:1 membranes, however, no impact of c-RFRFRF binding is observed and c-RRRWWW induces the highest gel phase disorder of DMPG.

The wavenumber of the charged TMCL after the first transition in the molten cluster state varies in dependence of the bound peptide. This is also in contrast to the DMPG/DMPE-d₅₄ mixture where the DMPG wavenumbers for all peptides is ~2921 cm⁻¹ except for c-RFRFRF (see Figure 3-3-8).

For both mixtures, the peptide impact on DMPE acyl chains is similar. The phenylalanine-containing c-RFRFRF has no impact on the gel phase acyl chain order, whereas c-RWRWRW and c-RRRWWW increase the lipid chain order slightly. However, the lipid chain order of DMPE in the fluid phase is somewhat decreased by c-RFRFRF and marginally increased by c-RWRWRW and c-RRRWWW. This means that the change in lipid chain order from gel to fluid phase is increased by c-RWRWRW and c-RRRWWW and decreased by c-RFRFRF when compared to the DMPE in the pure lipid mixture.

The effect of peptide binding on the lipid carbonyl band of the TMCL/DMPE-d₅₄ mixture is displayed in Figure 3-3-11 (bottom). The highest impact on headgroup hydration of both lipids is shown by c-RRRWWW, as observed for the DMPG/DMPE-d₅₄ mixture. However, the binding of c-RFRFRF decreases the headgroup hydration in both states and not only the fluid phase, as observed for DMPG/DMPE-d₅₄. The alternating c-RWRWRW has no impact on the headgroup hydration in the gel phase but decreases the fluid phase headgroup hydration to the same extent as c-RFRFRF does when compared to the pure lipid mixture.

The difference in fluid to gel phase hydration is slightly decreased for the other peptides in the order c-RRRWWW < c-RFRFRF < c-RWRWRW when compared to the pure lipid mixture. This is a remarkable difference to the peptide effect on DMPG/DMPE-d₅₄ lipid hydration where the arginine-tryptophan-containing peptides show only little to no effects on the difference of lipid gel to liquid-crystalline phase hydration when compared to the pure mixture. This indicates that arginine-containing peptide-lipid interactions take place in the lipid chain region in the case of DMPG/DMPE-d₅₄ 1:1 mixtures and are more pronounced in the headgroup region for TMCL/DMPE-d₅₄ 1:1 mixtures.

Another remarkable difference of c-RWRWRW and c-RRRWWW bound to the TMCL/DMPE-d₅₄ mixture compared to the DMPG/DMPE-d₅₄ mixture is that the hydration correlates to the melting temperature of DMPE-d₅₄ and does not increase as significantly with the melting of the lipid clusters, as observed when DMPG is clustered. However, as the effect of headgroup hydration is reduced for clustered DMPG, as it can be seen in Figure 3-3-10, a reduced amount of clustered TMCL together with minor changes in critical packing parameter might lead to this observation.

3.3.3.2 Analysis of the amide I, guanidinium and indole bands

The temperature dependence of the amide I and the guanidinium band of c-RFRFRF, c-RWRWRW and c-RRRWWW bound to the TMCL/DMPE-d₅₄ 1:1 mixed membrane is displayed in Figure 3-3-12. Whereas c-RFRFRF displays a constant positive slope in the temperature dependence of the amide I ratio, as observed for the pure peptides, c-RWRWRW and c-RRRWWW display a stepwise increase at temperatures of the respective main phase transition. This increase indicates an opening of the β -turn upon the phase transition of the remaining mixture. For the DMPG/DMPE-d₅₄ mixture, an additional shift of the amide I band was observed upon the melting of the clustered lipid (Figure 3-3-10) which is absent when the peptides are bound to the TMCL/DMPE-d₅₄ 1:1 mixed membrane. This means that either no peptide is bound to the lipid clusters or the cardiolipin does not induce a hydrogen bond opening as a result of different peptide orientation, alternative binding partners or change in lipid area. As the amount of clustered lipid is reduced for the TMCL/DMPE mixture (see Section 3.2.3) when compared to the DMPG/DMPE mixture also the number of bound peptides to the cluster might be reduced and therefore the impact of these peptide transition is not sufficient to change the overall amide I ratio of the peptide band.

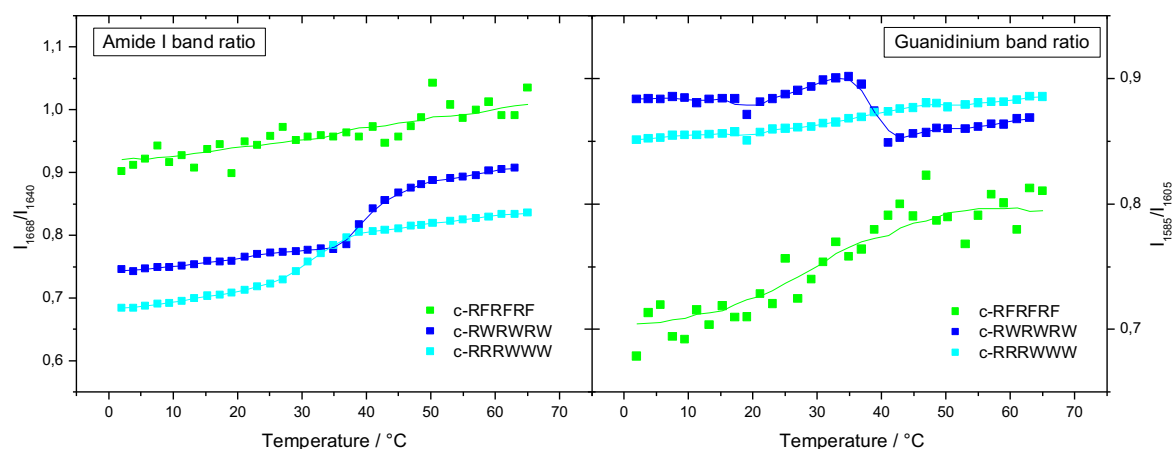


Figure 3-3-12 ATR-IR temperature dependent measurement of the amide I band intensity ratio I_{1668}/I_{1640} (left) and the guanidinium band intensity ratio at I_{1584}/I_{1603} (right) of the different peptides interacting with the TMCL/DMPE-d₅₄ 1:1 mixture. The lipid-peptide ratio was 2:1. The lines are averaged data points to guide the eye.

The effect of peptide binding on the temperature behaviour of the guanidinium band ratio is shown in Figure 3-3-12 (right). Here, c-RFRFRF again shows a steady increase in band ratio with increasing temperature. The guanidinium band ratio for c-RRRWWW remains unaffected in the observed temperature range including the phase transition temperatures. This was already observed for the interaction with pure TMCL (Figure 3-3-6) indicating a guanidinium interaction that is independent of the lipid phase changes. The guanidinium band intensity ratio of c-RWRWRW bound to TMCL/DMPE-d₅₄ 1:1 mixed membrane shifts to lower wavenumbers at ~40 °C where the mixed

lipids undergo a phase transition. For c-RWRWRW interacting with the pure TMCL membrane a negative slope for the temperature dependent guanidinium band ratio was observed (Figure 3-3-6) but a downshift in guanidinium band intensity ratio was not observed for the DMPG containing mixture. This indicates that c-RWRWRW can form guanidinium interactions with the TMCL headgroup with increasing temperature. In case of the TMCL/DMPE-d₅₄ membrane the lipid phase transition leads to a decrease in headgroup interactions between TMCL and DMPE-d₅₄ which enables the interaction of both lipid headgroups with the guanidinium group of c-RWRWRW leading to the observed downshift.

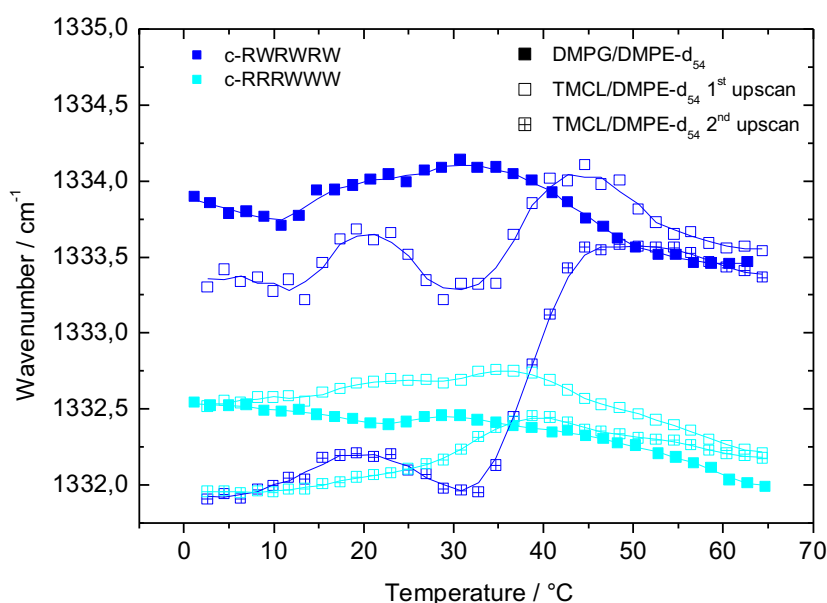


Figure 3-3-13 Temperature dependence of the tryptophan-indole peak-maximum of c-RWRWRW and c-RRRWWW bound to DMPG/DMPE-d₅₄ 1:1 and TMCL/DMPE-d₅₄ 1:1 mixtures. For the TMCL/DMPE-d₅₄ 1:1 mixture the first and second upscan is depicted. The lipid-peptide ratio was 2:1. The lines are plotted to guide the eye.

Figure 3-3-13 shows a comparison of the tryptophan peak position of the first and second temperature upscan of c-RWRWRW and c-RRRWWW bound to TMCL/DMPE-d₅₄ 1:1 mixture (the DMPG/DMPE-d₅₄ mixture is also displayed for comparison).

In equilibrium, i.e. in the second upscan, the indole vibrational peak maximum at low temperatures is downshifted to 1332 cm⁻¹ for c-RWRWRW and c-RRRWWW, indicating that the tryptophan interaction is similar for both peptides in the clustered gel phase of the TMCL/DMPE-d₅₄ mixture. This low value could be the result of a specific indole interaction or a dehydration of the indole group, indicating that the indole group is buried deeper in the membrane.

During melting of the lipid clusters, a slight upshift in wavenumbers is observed, which is more pronounced for c-RWRWRW. This indicates a hydration of the peptides bound to the melting cluster. For c-RWRWRW, however, the wavenumber decreases again upon further heating which

hints towards a reorientation of the peptide or a redistribution of the peptide between the clustered TMCL liquid crystalline phase and the gel phase of the remaining lipid mixture.

Upon melting of the remaining mixture at 40 °C, the indole vibrational peak of c-RWRWRW shifts by 1.5 cm⁻¹ to higher wavenumbers, resulting in a similar wavenumber as observed for the peptide bound to the DMPG/DMPE-d₅₄ fluid phase membrane. For c-RRRWWW, this shift in indole vibration upon the phase transition of the remaining mixture is only 0.5 cm⁻¹ but also results in a similar wavenumber as observed for the peptide bound to the DMPG/DMPE-d₅₄ fluid phase membrane.

This means that the state of tryptophan in the gel phase is similar for both peptides bound to the TMCL/DMPE-d₅₄ 1:1 mixed membrane. In the liquid-crystalline phase it is different for each peptide but similar for both binary lipid mixtures. In the case of c-RWRWRW also a downshift in guanidinium ratio was observed (Figure 3-3-12) upon the phase transition of the remaining mixture. This indicates that the reorientation of c-RWRWRW from the molten cluster to the liquid-crystalline phase of the TMCL/DMPE-d₅₄ 1:1 membrane might be a result of guanidinium interaction with the lipid headgroup that become accessible during lipid melting or a result of an arginine-tryptophan interaction like hydrogen bonding or π -stacking. The arginine-tryptophan interaction are unlikely for the clustered phase because changes in tryptophan are observed with melting of the lipid clusters, whereas the guanidinium band intensity ratio remains constant in this temperature interval below 20 °C (see Figure 3-3-13).

3.3.3.3 Changes in lipid and peptide band frequencies and intensities from first to second upscan

As TMCL shows a more complicated thermotropic behaviour as pure lipid membrane (Section 2.2.2), in lipid mixtures (Section 2.3.2 and 2.3.3) and interacting with the cyclic peptides (Section 3.2.3) we investigated the effect of c-RRRWWW and c-RWRWRW on the TMCL/DMPE-d₅₄ 1:1 membrane with ATR-IR spectroscopy for also the first upscan. The DSC results of the different peptides interacting with the TMCL/DMPE-d₅₄ 1:1 mixture, are shown in Figure 3-2-11. They show a difference between the first upscan where the peptide is bound to the membrane in the gel phase and following upscans where, due to cycles through the phase transition, an equilibrium is reached (see Section 3.2.3). The CH₂ antisymmetric vibrational band, however, does not show a major change in acyl chain vibration from the first to the second scan as displayed in Figure S3-3-5. Also, only minor variations in lipid carbonyl vibration (not shown) as well as amide I and guanidinium vibration (Figure S3-3-6) are observed from first to second upscan.

The peak position of the indole vibration, however, shifts downwards after the first heating cycle as displayed in Figure 3-3-13. This effect is more pronounced for c-RWRWRW than for c-RRRWWW. The indole vibrational peak maximum after first binding of c-RWRWRW and c-RRRWWW to the TMCL/DMPE-d₅₄ membrane is in similar range as the peak position observed for the peptides binding to the DMPG/DMPE-d₅₄ membrane. As observed in the second upscan an upshift in indole

vibration wavenumber is observed upon melting of the lipid cluster that decreases again to the same value upon further heating.

The fact that the DSC and ATR-IR measurements display differences between the first and the second heating cycle support the interpretation that DMPE and TMCL in the gel phase form headgroup interactions as discussed in Section 2.3.3 leading to the observed gel phase stabilisation. These headgroup interactions hinder the tryptophan moieties to penetrate the lipid chains as it is observed for the first upscan. The transition to the liquid crystalline phase leads to an opening of the headgroup H-bonds and therefore the tryptophan moieties can insert into the lipid gel phase bilayer during the second cooling and heating cycle.

3.3.3.4 Effect of lipid mixture on the peptide indole vibrational peak maximum

A comprehensive comparison of the temperature-dependent indole vibration peaks of the tryptophan-containing peptides bound to different lipid membranes is presented in Figure 3-3-14.

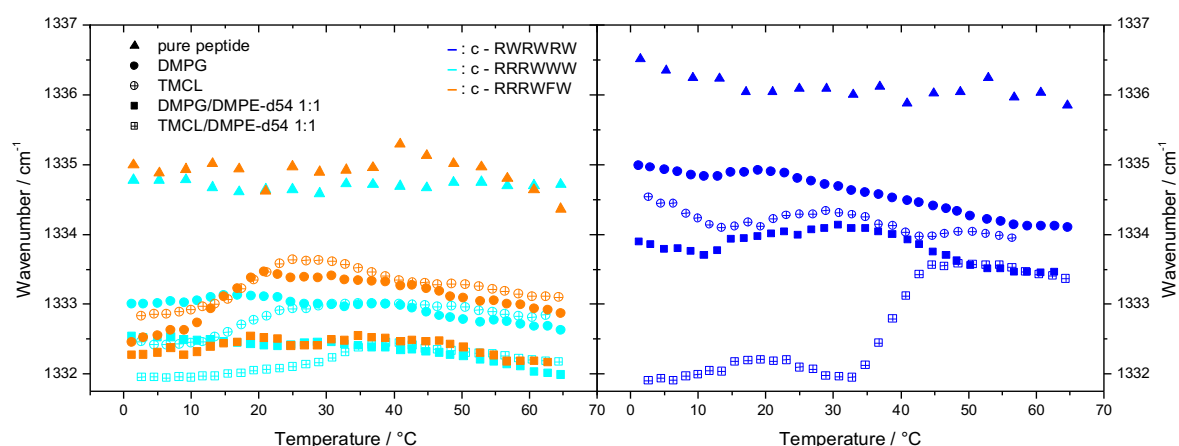


Figure 3-3-14 Temperature dependence of the tryptophan-indole peak-maximum for c-RRRWWW and c-RRRWFW (left) and c-RWRWRW (right) in solution and bound to the different lipid membranes. The lipid-peptide ratio was 2:1.

All arginine containing peptides display a similar value in downshift of the wavenumber of the characteristic tryptophan band maximum upon membrane interaction, as shown in Figure 3-3-14. The largest shift is seen for the peptides bound to the mixed membrane, especially the TMCL/DMPE-d₅₄ 1:1 mixed membrane in the gel phase. This indicates that in presence of DMPE the tryptophan groups are better shielded from water molecules due to a deeper membrane penetration which might simply be an effect of reduced headgroup area and decreased critical packing parameter of DMPE.

The block-peptide c-RRRWWW shows no temperature dependence of the indole vibration peak maximum in solution and bound to pure DMPG or DMPG/DMPE-d₅₄ mixed membranes indicating that no conformational peptide transitions or reorientation takes place. The value of the

c-RRRWWW indole vibration peak maximum in the liquid crystalline phase is comparable between both pure lipid membranes and both mixed membranes. The indole vibration peak maximum for c-RRRWWW bound to the TMCL and TMCL/DMPE-d₅₄ gel phase membrane, however, shifts to lower wavenumbers. This might be a result of increased chain packing and stronger dehydration of the TMCL containing membrane interphase.

The absolute values of the peak maximum for c-RRRWWW are comparable to those observed for c-RRRWWW. However, when bound to the pure lipid membrane, DMPG or TMCL, the indole vibration shifts to higher wavenumber upon the lipid phase transition. This is due to the conformational or orientational changes of the c-RRRWWW block-peptide resulting from the lipid phase transition as already discussed above.

The wavenumbers of the indole vibrational peak of the alternating c-RWRWRW show higher absolute values when compared to the indole groups of the block-peptides which supports the finding that the alternating peptide is bound more superficially to the membrane and therefore the indole moiety is exposed to more water molecules. The highest downshift in indole vibrational wavenumber when compared to the peptide in solution is displayed by c-RWRWRW bound to the TMCL/DMPE-d₅₄ 1:1 mixture in the lipid gel phase. This indicates that the insertion depth of the alternating and the block-peptide is comparable when bound to the TMCL/DMPE-d₅₄ mixture in the gel phase which might be a result of guanidinium-tryptophan interactions.

3.3.4 Ternary DMPG/DMPE/TMCL mixtures

DSC experiments revealed a phase transition temperature of the clustered domain at 24 °C for the ternary lipid mixtures interacting with c-RWRWRW, as shown in Figures 3-2-14 and 3-2-15. As both negatively charged lipids show a transition temperature of the lipid-peptide cluster at 24 °C for their respective binary mixtures with DMPE, it remained unclear if only one or both negatively charged lipids are clustered in the domain.

We performed ATR-IR experiments of ternary mixtures composed of DMPG/DMPE/TMCL in a 20%/40%/40% mixture with one of the negatively charged lipids identifiable, i.e. with deuterated or undeuterated chains. Please note that the surface charge remains constant with increasing DMPG content in a DMPE/TMCL 1:1 mixture.

Figure 3-3-15 (left) displays the effect of c-RWRWRW on the antisymmetric CH₂-vibrational band of TMCL in the respective ternary mixture when DMPG and DMPE both have completely deuterated chains. In Figure 3-3-17 (right) the effect is displayed for the same mixture with only DMPG-d₅₄ as the deuterated lipid, compared to the respective lipid in the ternary mixture without peptide. In both cases, two transitions can be observed meaning that both charged lipids are present in the clustered domain.

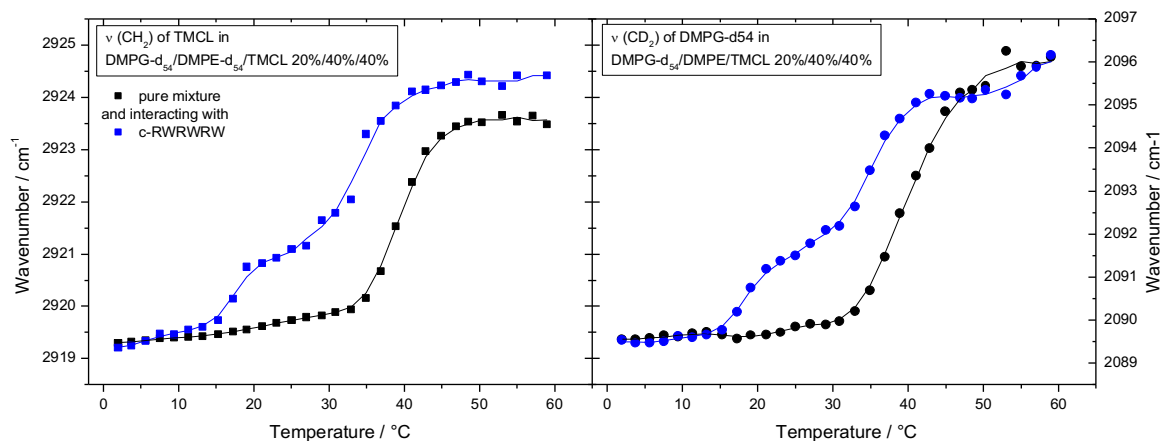


Figure 3-3-15 ATR-IR temperature dependent measurements. Effect of c-RWRWRW on the wavenumber of the maximum of the antisymmetric CH₂ stretching band of TMCL in a DMPG-d₅₄/DMPE-d₅₄/TMCL 20%/40%/40% mixture compared to TMCL in the pure lipid mixture (left). Effect of c-RWRWRW on the wavenumber of the maximum of the symmetric CD₂ stretching band of DMPG-d₅₄ in a DMPG-d₅₄/DMPE/TMCL 20%/40%/40% mixture compared to DMPG-d₅₄ in the respective pure lipid mixture (right). The lipid-peptide ratio was 2:1. The lines are averaged data points to guide the eye.

The order of both lipids remains unaltered by peptide binding in the gel phase whereas the fluid phase disorder also remains the same for DMPG-d₅₄ but is increased for TMCL after peptide binding when compared to the lipid in the pure ternary mixture.

3.3.5 Summary

The ATR-IR measurements clearly prove the assumption from the DSC results (Section 3.2) that the clustered lipids consist solely of the charged lipid component (Figure 3-3-8 and 3-3-11). For the studied lipid-peptide ratio, the clustered domain in the ternary DMPG/TMCL/DMPE mixture consists of both charged lipid components DMPG and TMCL (Figure 3-3-17).

The ATR-IR results further support the finding from the DSC results that the penetration depth varies among the different peptides interacting with lipid membranes. The block-peptide c-RRRWWW shows the highest impact on the headgroup hydration of all four investigated lipid membranes (Figures 3-3-2, 3-3-5, 3-3-8 and 3-3-11) and the lowest indole vibrational peak wavenumbers (Figure 3-3-13 and Figure 3-3-14) as a result of a deeper membrane penetration.

The alternating c-RWRWRW (and for some lipid mixtures also the block-peptides) display structural changes that follow the phase transitions of the lipid membrane. These changes most likely originate from a relocation or reorientation of the peptide where the alternating peptide is discussed to be oriented more perpendicular and the block-peptides more parallel to the membrane normal.

The differences in location and orientation also affects the inter- and intramolecular interaction of the peptide. For example, when c-RWRWRW is bound to the DMPG/DMPE mixture no change in guanidinium band intensity ratio was observed upon melting of the lipid cluster, whereas the block-peptides showed a clear dependency (Figure 3-3-10).

Also in dependence of the lipid membrane, e.g. for the change from DMPG/DMPE to TMCL/DMPE, different lipid-peptide interactions are observed. For the DMPG/DMPE-d₅₄ 1:1 mixture the melting of the DMPG clusters induces changes in the amide I band intensity ratio of all arginine-tryptophan containing peptides, whereas no changes in amide I band intensity ratio are observable upon the melting of TMCL clusters.

In both mixed lipid systems the melting of the lipid clusters does not lead to the expected increase in carbonyl hydration. This might be a common effect in both lipid mixtures as the peptides accumulate in the clusters and the increase in lipid area is not compensated for by water molecules but by changes in peptide structure, orientation or concentration.

Altogether, although the lipid-peptide interaction is influenced by the peptide structure and the membrane composition, none of the observed structural effects correlate to the clustering efficacy and antimicrobial efficiency. Therefore, specific lipid-peptide interactions are not the origin of the observed clustering efficacy of the different peptides. In fact, the peptide structures and the membrane composition define the orientation of the molecules and thus, lead to a different penetration depth of the peptide side chains which correlates to the observed clustering.

Another model of antimicrobial action of cyclic peptides occurs from the observation made for cyclic peptides consisting of alternating L- and D-amino acids which have shown the ability to form tube-like aggregates (396-398). Therefore, a pore mechanism of antimicrobial action similar to the barrel stave or toroidal pore mechanism, in which these tube structures span the membrane and lead to leakage, is discussed for cyclic peptides. The assembly of the peptides to tube-like structures can be followed by the appearance of an IR band at 3281 cm⁻¹ and 1688 cm⁻¹ (399, 400), corresponding to an intermolecular hydrogen bonded β -sheet network by the cyclic peptide backbone. However, as these bands do not appear in any of the recorded spectra, the amide I band frequencies show no further splitting upon membrane interaction and also no membrane permeabilization was observed (119, 254, 401) we tend to neglect the possibility of peptide aggregation and this model of antimicrobial action.

3.4 Isothermal Titration Calorimetry

Isothermal titration calorimetry (ITC) can be used to determine stoichiometry, enthalpy (ΔH°) and the binding constant K of ligands binding to model membranes. The relation $\Delta G^\circ = \Delta H^\circ - T\Delta S^\circ$ gives the free energy of binding (ΔG°) and with $\Delta G^\circ = \Delta H^\circ - T\Delta S^\circ$ the respective entropy can be calculated. Isothermal Titration Calorimetry allows a detailed thermodynamic characterisation giving insights into the initial peptide binding at low peptide concentration than it could be realised by DSC or ATR measurements.

To verify the findings of the DSC results and to investigate whether the clustering of lipids occurs after the first peptides have been added or after reaching a certain threshold peptide to lipid concentration ratio (r_{cc}), we performed ITC measurements with different peptides and lipid mixtures. Many authors reported thermodynamic parameters on antimicrobial peptide binding to lipid model membranes. A short, non-comprehensive, overview is given in table S3-4-1. Although the observed binding parameters vary greatly, a common finding among the publications is that the degree of peptide binding increases significantly when additional electrostatic interactions occur in charged lipid membranes compared to membranes only composed of zwitterionic lipids (see also (402)).

3.4.1 Pure lipid-peptide interaction

3.4.1.1 Peptide interaction with DPPG

Figure 3-4-1 displays the titration of DPPG vesicle suspension into solution of the alternating peptide c-RFRFRF, c-KWKWKW and c-RWRWRW at 20°C. Two separate processes are identifiable. A first process shows a lipid to peptide stoichiometry of ca. 3, i.e. at a lipid-peptide charge ratio of 1, followed by a slightly endothermic processes with roughly twice the stoichiometric value. The first process is endothermic for c-KWKWKW and c-RFRFRF but exothermic for c-RWRWRW. In the liquid crystalline state of the lipid the binding processes of all three peptides are exothermic as can be seen in Figure 3-4-2, 3-4-3 and in Figure S3-4-2 and S3-4-3 of the supplementary data. The comparison shows that the combination of arginine and tryptophan leads to a different heat of binding profile indicating a different lipid-peptide interaction. As the heat of binding for the second process seems to be similar among all three peptides, we believe that the second process is of electrostatic origin and is connected to adhesion and dissociation of vesicles, whereas the first stoichiometry factor is accountable for the lipid-peptide interaction.

A negative enthalpy of binding was also observed for polyarginine and polylysine binding to POPG membranes with a value of $-1.2 \text{ kcal mol}^{-1}$ and $-0.2 \text{ kcal mol}^{-1}$ at 20 °C, respectively (326). The enthalpy value for pentyllysine binding to a 1:3 POPG/POPC mixture at 27 °C also showed a slightly

negative enthalpy of $-0.1 \text{ kcal mol}^{-1}$ (403) and the binding to a DMPG membrane showed a negative value of $-2.5 \text{ kcal mol}^{-1}$ in the liquid crystalline phase at $30 \text{ }^\circ\text{C}$ (unpublished data from Andreas Erbe). Also, some antimicrobial peptides show a negative enthalpy of binding to different membranes at certain temperatures as depicted in Table 3-4-1.

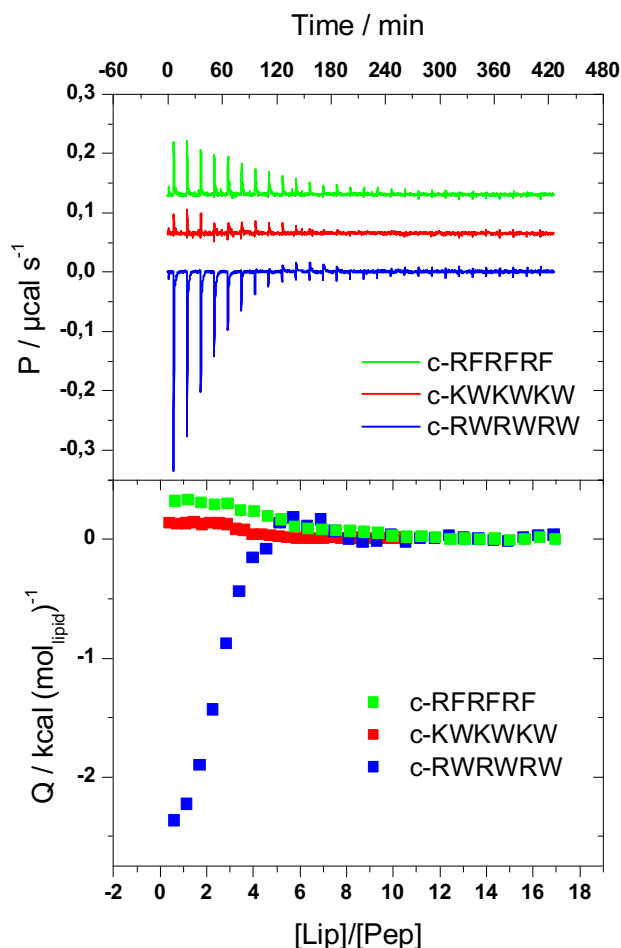


Figure 3-4-1 Top: ITC titration curves at $20 \text{ }^\circ\text{C}$. 1.6 mM DPPG vesicle suspension titrated into $20 \text{ } \mu\text{M}$ c-RFRFRF. 1 mM DPPG titrated into in $20 \text{ } \mu\text{M}$ c-KWKWKW and 0.8 mM DPPG titrated into $10 \text{ } \mu\text{M}$ c-RWRWRW. All solutions contained 20 mM phosphate buffer (pH 7.2) with 100 mM NaCl. Bottom: Heat of binding Q in kcal mol^{-1} of lipid vs. lipid-peptide ratio.

Therefore, the negative enthalpy contribution for the binding of c-RWRWRW to DPPG membranes seems to have a different origin than the dehydration of amino acids or lipid alkyl chains. One reason for this negative enthalpy contribution could be the formation of additional inter- or intramolecular peptide-peptide, lipid-lipid or lipid-peptide hydrogen bonds upon the lipid-peptide interaction, e.g. conformational changes of peptides upon membrane binding (325, 326, 404). As the ATR-IR experiments showed that the amide band ratio of 1668 cm^{-1} to 1640 cm^{-1} decreases for c-RWRWRW, remains static for c-RFRFRF and increases slightly for c-KWKWKW when bound to lipid membranes, as shown in Figure S3-3-2, it is likely that the negative enthalpy contribution results from a β -turn formation of c-RWRWRW upon membrane binding. As the guanidinium and indole

vibrational bands show a different temperature behaviour (Figure 3-3-3), a contribution to the negative enthalpy from arginine-tryptophan interactions seems unlikely.

Another difference between c-RFRFRF, c-KWKWKW and the arginine-tryptophan containing peptides is their lipid membrane penetration depth as discussed in the previous chapters. The contribution to the negative enthalpy observed for c-RWRWRW could therefore also originate from the hydrophobic interactions known as the “non-classical hydrophobic effect”. These negative enthalpic contributions are discussed to appear as a result of van-der-Waals interactions between non-polar molecule parts, here from the peptide sidegroups, and the membrane hydrocarbon core (59). Additionally, the induction of increased lipid chain order (405) as seen in the simulation of cyclic hexapeptide c-RRWWRW binding to DPPC membranes (270) would contribute to the observed negative enthalpy.

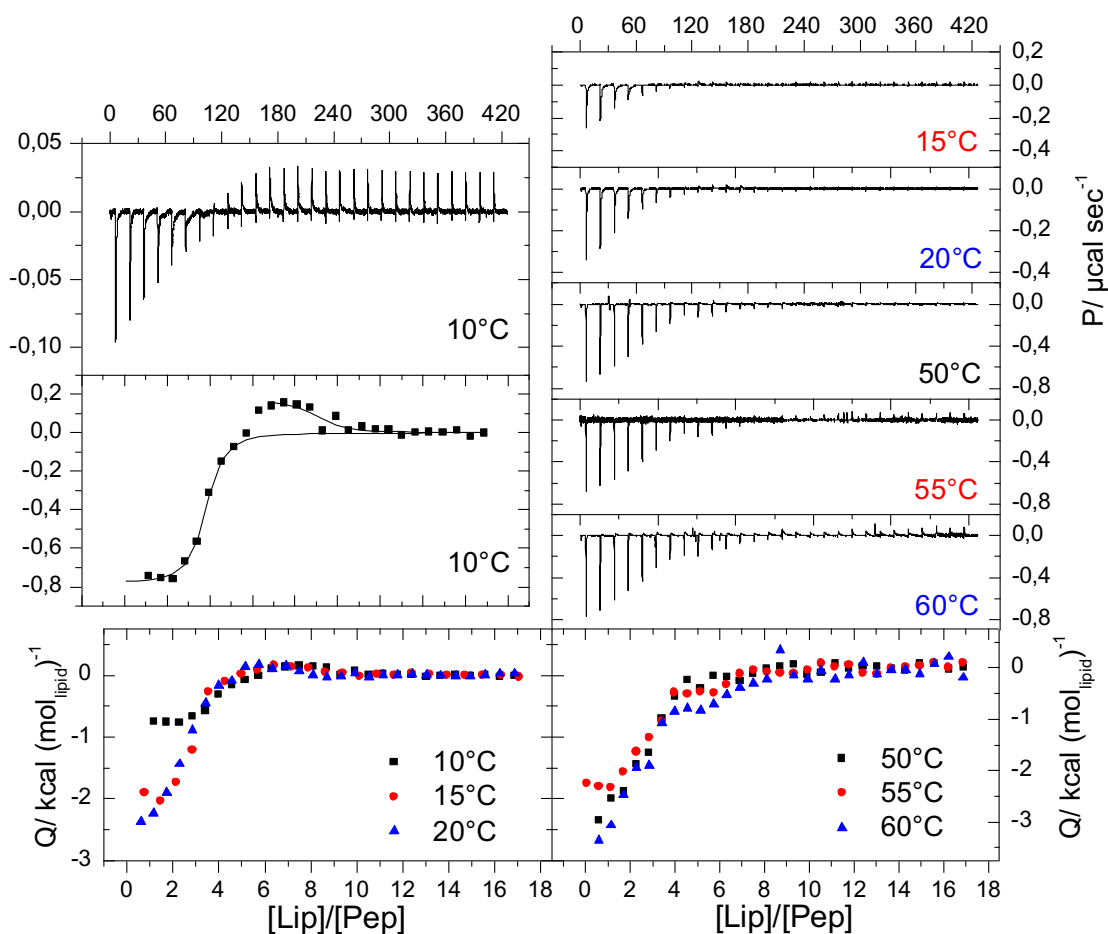


Figure 3-4-2 Top left inset: ITC titration curves of 0.8 mM DPPG into 10 μ M c-RWRWRW at 10 $^{\circ}$ C (top) and heat of binding (bottom) vs. lipid-peptide ratio (square) and a fit of two binding processes (line). Top right: ITC titration curves of 1 mM DPPG at 15 $^{\circ}$ C into 10 μ M c-RWRWRW and 0.8 mM DPPG at 20 $^{\circ}$ C, 50 $^{\circ}$ C, 55 $^{\circ}$ C and 60 $^{\circ}$ C. All solutions contained 20 mM phosphate buffer (pH 7.2) with 100 mM NaCl. Bottom left: Heat of binding vs. lipid-peptide ratio at 10 $^{\circ}$ C-20 $^{\circ}$ C. Bottom right: Heat of binding vs. lipid-peptide ratio at 50 $^{\circ}$ C-60 $^{\circ}$ C.

Figure 3-4-2 displays the titration curve of DPPG into c-RWRWRW solution at different temperatures. The inset displays the experiment at 10 $^{\circ}$ C where the two processes are clearly

distinguishable. The first process is exothermic at temperatures below and above the lipid phase transition temperature, whereas the process with a higher stoichiometry is endothermic in the gel phase and exothermic in the liquid-crystalline phase. The first process shows a negative temperature dependence, i.e. a negative Δ_{RC_P} , in both lipid phases, meaning that with increasing temperature the measured heat of binding becomes more exothermic.

As the ITC data is sensitive to the ionic strength (109), vesicle size and vesicle size distribution we included the peptide c-RRWRF in our ITC studies for direct comparison. The complete dataset of titration curves at various temperatures is displayed in Figure S3-4-1 of the supplementary data. From the direct comparison to c-RWRWRW in Figure S3-4-4 of the supplementary data it is evident that the more amphipathic small-block cyclic hexapeptide c-RRWRF, which was investigated in earlier studies (108, 109, 256, 406), shows a similar binding enthalpy but a lower binding stoichiometry for both observed processes. The stoichiometry of binding is about half of the value observed for the alternating peptides.

However, this finding is in contrast to the stoichiometry values found earlier where the stoichiometry of c-RRWRF binding to DPPG at 25 °C was determined to be about 1:3 (109). This can mainly be explained by the use of a buffer system with higher ionic strength (154 mM NaCl solution and 10 mM Tris buffer) and different vesicle preparation. In the present study LUV were prepared by extrusion to yield a narrow size distribution around 100 nm. The LUVs in the previous study were prepared by sonication, which leads to a broader size distribution. The different sizes lead to different curvature energies that impact the lipid-peptide interaction, especially when different charge distances might play a crucial role, as it was shown for polyamines (312).

The reason for the reduced stoichiometry factor observed for the block-peptide can be that either only outside binding occurs or that the orientation is different when compare to the alternating peptide. For the alternating peptide it is likely that it follows a charge stoichiometry when bound parallel to the surface. For the block-peptides the binding stoichiometry could be lowered when the peptides orient perpendicularly to the membrane surface because the charge density is higher and the charges are screened more efficiently.

The thermodynamic parameters ΔG° , ΔH° and $T\Delta S^\circ$ of the different PG-peptide interactions for both processes observed at the stoichiometry parameter N_1 and N_2 are summarised in Table 3-4-2. The binding enthalpy of the first process for the different peptides is displayed in Figure 3-4-3 (ΔG° , ΔH° and $T\Delta S^\circ$ are shown in Figure S3-4-5).

In case of c-KWKWKW an effect of temperature on the binding enthalpy but no systematic behaviour is observed in the particular temperature range. This might be a result of compensation of heat effects arising from the different underlying processes. The heat of binding of c-RFRFRF to DPPG membranes is comparably small. This confirms the finding of DSC and ATR-IR measurements where c-RFRFRF shows charge compensation effect but no major impact on the PG

phase transition temperature and the lipid chain order, which means that no processes with large heat contributions takes place.

Peptide	T/°C	N ₁ ; N ₂	K/M ⁻¹ (N ₁ ; N ₂)	ΔG°/kcal mol ⁻¹ (N ₁ ; N ₂)	ΔH°/kcal mol ⁻¹ (N ₁ ; N ₂)	TΔS°/kcal mol ⁻¹ (N ₁ ; N ₂)	
c-RFRFRF	10	3.7; 9.6	2.7·10 ⁵ ; 3.3·10 ⁵	-7.1; -7.1	0.44; 0.10	7.5; 7.2	
	15	3.3; 6.0	1.1·10 ⁵ ; 1.2·10 ⁵	-6.6; -6.7	0.62; 0.27	7.2; 7.0	
	20	4.5; 9.3	1.6·10 ⁵ ; 6.1·10 ⁵	-7.0; -7.8	0.35; 0.09	7.3; 7.9	
	50	No heat signals detectable					
	55	4.4; 7.7	7.3·10 ⁴ ; 2.0·10 ⁵	-7.2; -7.9	-0.74; -0.23	6.5; 7.7	
	60	4.1; 8.3	1.3·10 ⁵ ; 1.1·10 ⁶	-7.7; -7.9	-0.74; -0.15	7.0; 9.1	
c-KWKWKW	10	2.3; 5.3	5.4·10 ⁵ ; 7.3·10 ⁵	-6.4; -6.6	0.4; 0.14	6.8; 6.7	
	15	2.2; 4.7	1.0·10 ⁵ ; 1.3·10 ⁵	-5.7; -5.9	0.7; 0.24	6.4; 6.1	
	20	3.4; 4.8	4.9·10 ⁵ ; 3.4·10 ⁶	-7.3; -7.7	0.14; 0.04	7.4; 7.7	
	50	1.5; 4.6	4.5·10 ⁵ ; 3.2·10 ⁵	-7.6; -7.2	-1.6; -0.21	6.0; 7.0	
	55	1.3; 4.1	4.9·10 ⁵ ; 5.9·10 ⁵	-8.7; -8.7	-1.7; -0.26	7.0; 8.4	
	60	1.3; 4.1	1.5·10 ⁶ ; 1.1·10 ⁶	-8.5; -8.2	-1.6; 0.29	6.9; 8.5	
c-RWRWRW	10	3.6; 8.1	2.0·10 ⁶ ; 2.0·10 ⁶	-8.2; -8.2	-0.78; 0.17	7.4; 8.35	
	15	2.7; 7.9	3.9·10 ⁶ ; 2.8·10 ⁶	-8.7; -8.5	-2.0; 0.18	6.7; 8.7	
	20	2.3; 7	8.2·10 ⁵ ; 3.0·10 ⁶	-7.9; -8.6	-2.5; 0.17	5.4; 8.8	
	50	2.7; 7.1	5.0·10 ⁵ ; 5.0·10 ⁶	-8.4; -9.9	-3.1; -0.26	5.3; 9.6	
	55	3; 6.3	3.5·10 ⁵ ; 7.7·10 ⁶	-8.2; -10.3	-2.5; -0.51	5.7; 9.8	
	60	2.7; 6.4	3.3·10 ⁵ ; 3.3·10 ⁵	-8.4; -8.4	-3.6; -1.1	4.8; 7.3	
c-RRWRF	10	0.7; 2.6	2.7·10 ⁵ ; 1.8·10 ⁵	-7.0; -6.8	-1.2; 0.2	5.8; 7.0	
	15	1.0; 2.1	2.4·10 ⁶ ; 5.7·10 ⁵	-8.4; -7.6	-1.5; 0.16	6.9; 7.8	
	20	1.0; 3.2	1.9·10 ⁶ ; 1.2·10 ⁶	-8.5; -8.1	-2.2; 0.06	6.3; 8.2	
	50	1.0; 3.0	1.0·10 ⁶ ; 1.0·10 ⁶	-8.8; -8.9	-2.7; -0.25	6.1; 8.6	
	55	0.8; 1.8	4.7·10 ⁵ ; 7.5·10 ⁵	-8.5; -8.9	-3.1; -0.66	5.4; 8.2	
	60	0.9; 2.7	4.6·10 ⁵ ; 1.1·10 ⁵	-8.6; -7.7	-4.0; -0.79	4.6; 6.9	

Table 3-4-2 Thermodynamic parameters of different cyclic antimicrobial hexapeptides interacting with DPPG membranes determined by ITC measurements.

For c-RWRWRW temperature dependence of the enthalpy, $\Delta_R C_P$, is $-170 \text{ cal mol}^{-1} \text{ K}^{-1}$ in the lipid gel phase and $-50 \text{ cal mol}^{-1} \text{ K}^{-1}$ in the liquid crystalline phase. The determined value for c-RRWRF is $-100 \text{ cal mol}^{-1} \text{ K}^{-1}$ in the lipid gel and $-130 \text{ cal mol}^{-1} \text{ K}^{-1}$ in the liquid crystalline phase. For other peptidic counter ions the $\Delta_R C_P$ values are in a similar range. The value per amino acid residue for polyarginine binding to POPG membranes in the liquid crystalline phase is $-17.7 \text{ cal mol}^{-1} \text{ K}^{-1}$ and for polylysine $-15 \text{ cal mol}^{-1} \text{ K}^{-1}$ (326). Generally, the $\Delta_R C_P$ value, yields information about the hydration or dehydration of the lipid headgroup and lipid chain region. For the dehydration of the

headgroup a Δ_{RC_P} value of approximately $+10 \text{ cal mol}^{-1}\text{K}^{-1}$ (181) was determined by adding glycerol-1-phosphoglycerol to divalent cation solution. The dehydration of a methylene group gives a Δ_{RC_P} value of ca. $-15 \text{ cal mol}^{-1} \text{K}^{-1}$ (407) resulting from changes in hydrogen bond length and angle and the number of the perturbed hydrogen bonds in the first hydration shell around the aliphatic chains (408). For the dehydration of the peptide bond, Makhatadze and Privalov calculated a Δ_{RC_P} value of $+14 \text{ cal mol}^{-1} \text{K}^{-1}$. The Δ_{RC_P} value of the amino acid residue including the methyl group of the peptide chain is $-72 \text{ cal mol}^{-1} \text{K}^{-1}$ for tryptophan, $-60,1 \text{ cal mol}^{-1} \text{K}^{-1}$ for phenylalanine and $-40 \text{ cal mol}^{-1} \text{K}^{-1}$ for arginine and lysine (409).

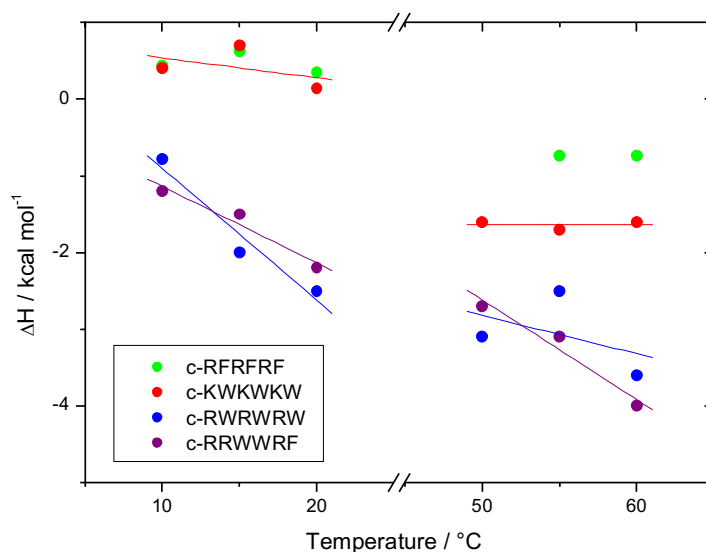


Figure 3-4-3 Temperature dependence of ΔG , $-\Delta S$ and ΔH of c-RFRFRF, c-KWKWKW, c-RWRWRW and c-RRWWRW for the processes with the stoichiometry value N1.

For c-RFRFRF and c-KWKWKW the superposition of hydrophilic and hydrophobic contributions seems to compensate whereas the fact that both arginine-tryptophan containing peptides show a decreased Δ_{RC_P} supports the finding from DSC and ATR measurements that these peptides insert deeper into the lipid membrane. Therefore, the negative contributions to the heat capacity change by the dehydration of lipid chains and amino acid side chains are increased.

However, this rough overview of Δ_{RC_P} contributions does not consider concurrent changes in lipid area and chain packing. For the binding of the earth cations Mg^{2+} , Sr^{2+} and Ca^{2+} to DMPG bilayers, a negative temperature dependence of $-2.9 \text{ cal mol}^{-1} \text{K}^{-1}$, $-3.6 \text{ cal mol}^{-1} \text{K}^{-1}$ and $-14.1 \text{ cal mol}^{-1} \text{K}^{-1}$ is found, respectively (181) because the headgroup charge compensation leads to a better chain interaction and a reduced water content in the hydrophobic bilayer region. For divalent polyamines the Δ_{RC_P} values increase with increasing CH_2 -spacer length from $-5.8 \text{ cal mol}^{-1} \text{K}^{-1}$ for ethylenediamine to $-2.7 \text{ cal mol}^{-1} \text{K}^{-1}$ for propylenediamine to $+0.5 \text{ cal mol}^{-1} \text{K}^{-1}$ for butenediamine (putrescine) when binding to DPPG vesicles (see supplementary data S3-4-8). This is in general agreement with the finding from Garidel and Blume (181), as the longer polyamine spacer leads on

the one hand to an increased dehydration of the headgroup and on the other hand the increasing charge distance deteriorates the lipid chain interaction as demonstrated by DSC and monolayer experiments (312).

The determined binding constants of the alternating peptides bound to DPPG at 20 °C are $1.6 \cdot 10^5 \text{ M}^{-1}$ for c-RFRFRF, $1.6 \cdot 10^6 \text{ M}^{-1}$ for c-KWKWKW and $8 \cdot 10^5 \text{ M}^{-1}$ for c-RWRWRW (see Table 3-4-2). These values are in the same range as observed for the linear analogue Ac-RRWWRF-NH₂ ($4.8 \cdot 10^6 \text{ M}^{-1}$ and $1.5 \cdot 10^5 \text{ M}^{-1}$ when bound to POPG and POPC vesicles at 30 °C, respectively (315)) and are two orders of magnitude higher than expected for trivalent cations (see Section 3.1.3). This already indicates that the hydrophobic residues also contribute as a driving force for binding to lipid vesicle membranes. The Gibbs free energy change ($\Delta_R G^\circ$) is similar for all arginine containing peptides in both lipid phases and is $\sim -7.2 \text{ kcal mol}^{-1}$ for c-RFRFRF and $-8.3 \text{ kcal mol}^{-1}$ for c-RWRWRW and c-RRWWRF. For c-KWKWKW binding to DPPG membranes $\Delta_R G^\circ$ is $-7.2 \text{ kcal mol}^{-1}$ in the lipid gel and $-8.8 \text{ kcal mol}^{-1}$ in the liquid crystalline phase. For all peptides the entropy is the main contributor to the Gibbs free energy. However, for c-RWRWRW and c-RRWWRF in both phases and for c-KWKWKW in the liquid crystalline phase the negative enthalpy also contributes to the Gibbs free energy.

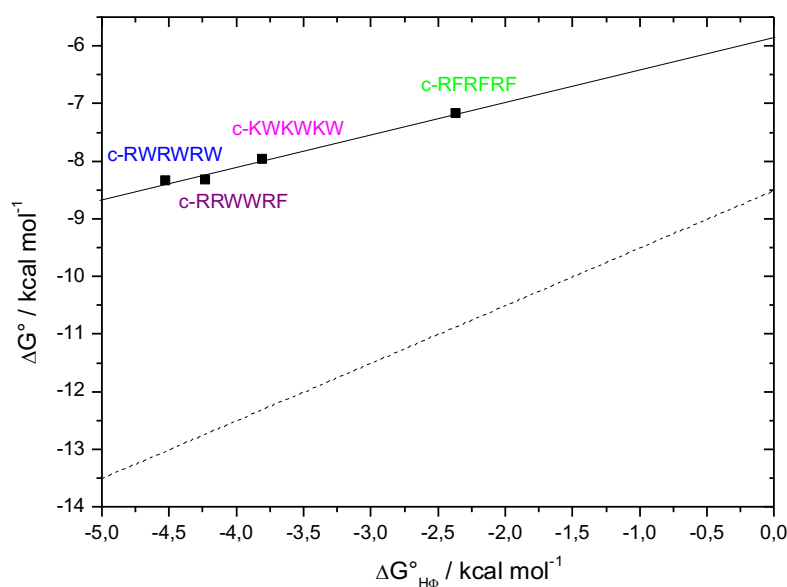


Figure 3-4-4: ΔG° calculated from the K-values determined by ITC for cyclic peptides plotted against hydrophobic free energies $\Delta G^\circ_{\text{H}\Phi}$ which were calculated using the Wimley-White interfacial hydrophobicity scale. The dotted line displays the theoretical values for a simple electrostatic and hydrophobic binding additivity.

To understand the influence of hydrophobic and electrostatic interactions on the measured ΔG° , a plot versus the theoretical $\Delta G^\circ_{\text{H}\Phi}$, calculated from the hydrophobic free energies for each amino acid and the peptide backbone is shown in Figure 3-4-4. The values were taken from the Wimley-White hydrophobicity scale (314). In case of pure additivity of electrostatic and hydrophobic interactions,

a shifted straight line with a slope of one would be expected (see Section 3.1.3 and (313)). The expected ΔG° resulting from pure electrostatic interactions, calculated from equation (3.2), is -8.5 kcal mol⁻¹ for a trivalent peptide interacting with a pure DPPG membrane comprising an electrical surface potential of 122 mV. The observed ΔG° values are shifted to less negative values. This means that a simple additivity does not hold.

All data points are on a straight line with a slope of 0.57. However, the value for the slope is below one, which again means that hydrophobic and electrostatic interactions do not simply sum up. The electrostatic interaction is decreased by hydrophobic interactions, as it was described earlier for different indolicidin derivatives by Ladokinh et al. (313). The authors report a reduction of the slope to a value of 0.3 with a reduction in effective valence (z_{eff}) (410) of 6-7% for each additional increase in hydrophobic free energy of 1 kcal mol⁻¹. As our value is significantly above the reported value we believe that additional contributions to the free energy take place in case of cyclic peptide binding to DPPG membranes. For indolicidin, the formation of secondary structure upon peptide to vesicle binding could be excluded. For cyclic peptides, the ATR-IR experiments show that the additional β -sheet formation upon c-RWRWRW binding to DPPG membranes in both phases takes place. A decrease in amount of β -sheets is observed upon vesicle binding of c-RFRFRF in the liquid crystalline phase and for c-KWKWKW in both phases (see Figure S3-3-2 of the supplementary data) as it was discussed above. The enthalpic contributions from the formation or opening of β -sheet forming H-bonds might cause the difference in $\Delta_R G^\circ$.

3.4.1.2 Peptide interaction with TMCL

3.4.1.2.1 The alternating peptide c-RWRWRW interacting with TMCL

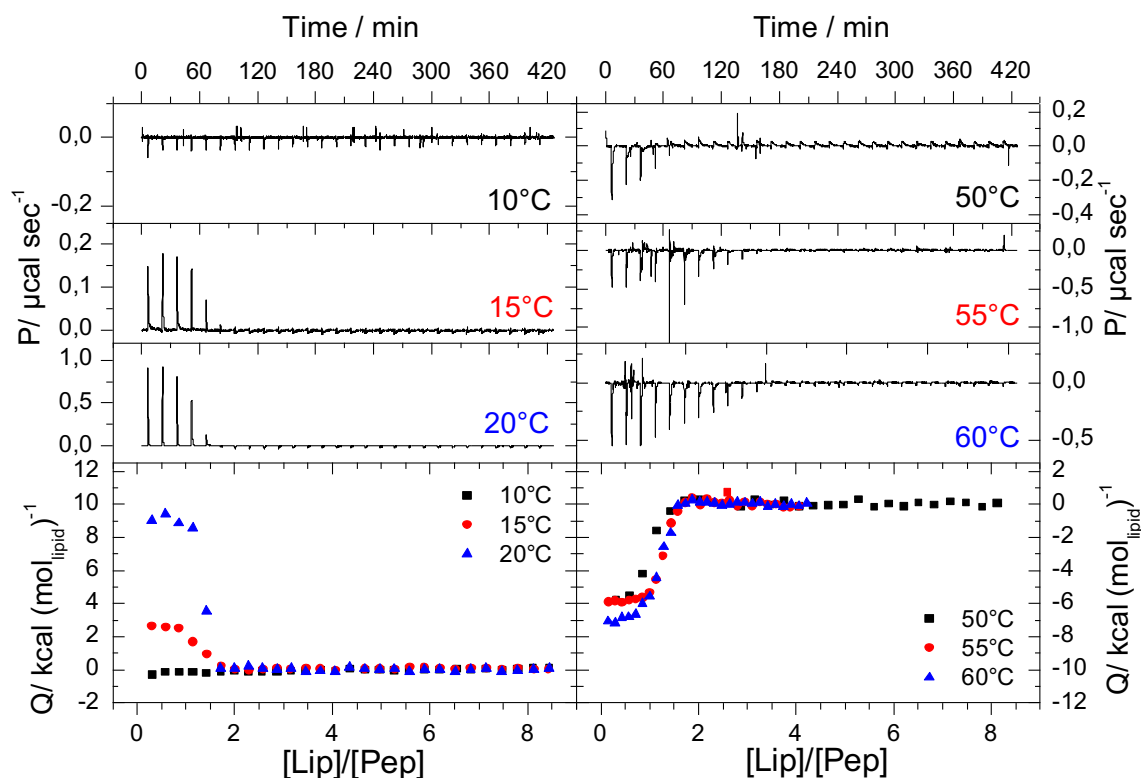


Figure 3-4-5 400 μM TMCL suspension (100 nm vesicles in phosphate buffer pH 7.2) titrated into 10 μM c-RWRWRW solution at 10 $^{\circ}\text{C}$, 15 $^{\circ}\text{C}$, 20 $^{\circ}\text{C}$ and 50 $^{\circ}\text{C}$ and 20 μM c-RWRWRW solution at 55 $^{\circ}\text{C}$ and 60 $^{\circ}\text{C}$. Top three left and right: Titration curves. Bottom left: Heat of binding vs. lipid-peptide ratio at 10 $^{\circ}\text{C}$ -20 $^{\circ}\text{C}$. Bottom right: Heat of binding vs. lipid-peptide ratio at 50 $^{\circ}\text{C}$ -60 $^{\circ}\text{C}$.

Figure 3-4-5 shows the titration of 400 μM pure TMCL vesicle suspension into 10 μM and 20 μM c-RWRWRW solutions at different temperatures below and above the lipid phase transition. For TMCL interacting with cyclic peptides, only one heat effect and one binding stoichiometry is observed at all temperatures (besides c-KWKWKW at 20 $^{\circ}\text{C}$, see Figure S2-4-5 of the supplementary data).

At 15 $^{\circ}\text{C}$ and 20 $^{\circ}\text{C}$ an endothermic heat of reaction is observed which strongly increases with increasing temperature. In the liquid-crystalline phase of TMCL, the peptide binding is exothermic and becomes slightly more negative from 50 $^{\circ}\text{C}$ to 60 $^{\circ}\text{C}$ indicating a negative $\Delta_{\text{R}}C_{\text{p}}$. The average stoichiometry of 1.4 is close to the expected value of 1.5 where charge equilibrium is reached. This means that also the inner lipid monolayer is accessible for peptide binding.

3.4.1.2.2 The block-peptide c-RRRWWW interacting with TMCL

The interaction of c-RRRWWW with pure TMCL membranes is shown in Figure 3-4-6. Similarly to the alternating peptide, the heat of binding is endothermic and shows a large positive $\Delta_R C_P$ value for TMCL in the gel phase. For c-RRRWWW $\Delta_R H^\circ$ for binding to the liquid crystalline phase is also negative.

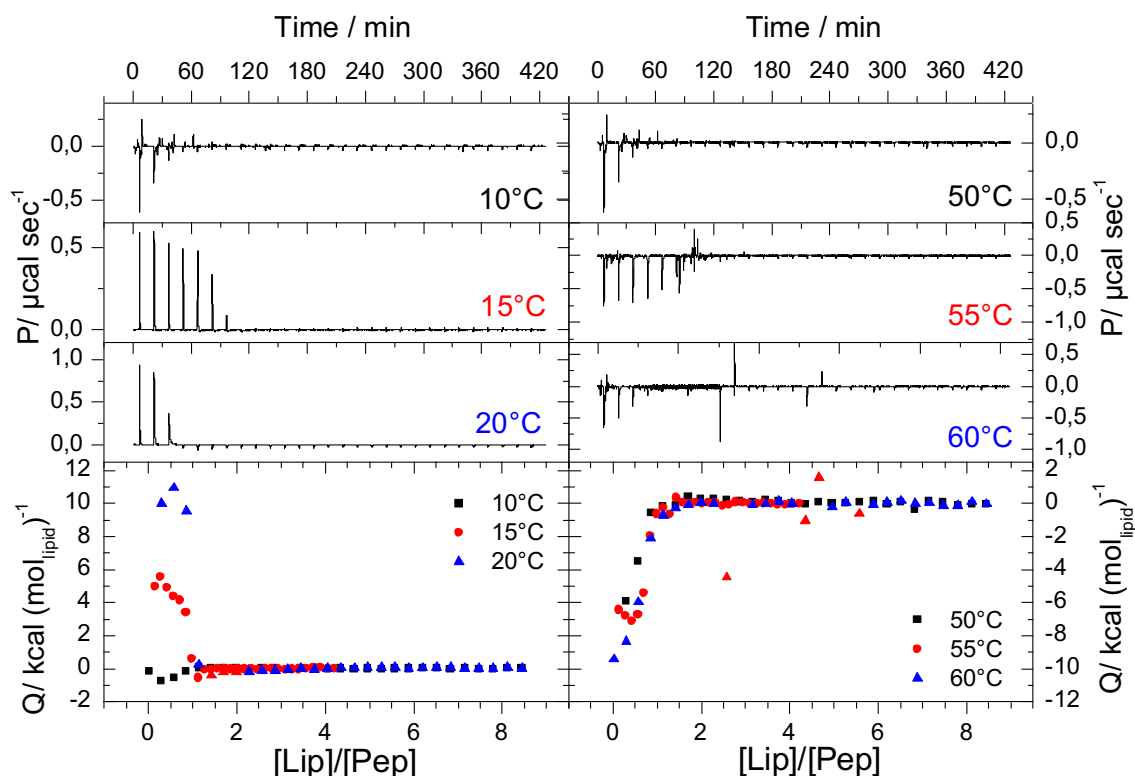


Figure 3-4-6 400 μM TMCL suspension (100 nm vesicles in phosphate buffer pH 7.2) titrated into 10 μM c-RRRWWW solution at 10 $^\circ\text{C}$, 20 $^\circ\text{C}$, 50 $^\circ\text{C}$ and 60 $^\circ\text{C}$ and 20 μM c-RRRWWW solution at 15 $^\circ\text{C}$ and 55 $^\circ\text{C}$. Top three left and right: Titration curves. Bottom left: Heat of binding vs. lipid-peptide ratio at 10 $^\circ\text{C}$ -20 $^\circ\text{C}$. Bottom right: Heat of binding vs. lipid-peptide ratio at 50 $^\circ\text{C}$ -60 $^\circ\text{C}$.

The average stoichiometry of the block-peptide binding to a TMCL membrane, however, is with 0.6 only, about half the value observed for the alternating peptide. This was similarly observed for c-RRWWRF and c-RWRWRW binding to DPPG membranes (Figure 3-4-4). This means that the stoichiometry of binding of alternating peptides to lipid membranes is governed by charge interactions, whereas for the block-peptides the lipid-peptide stoichiometry is lowered. As the other thermodynamic values are comparable between the block-peptide and alternating peptides, the heat-contributing effects like bond-formations, hydrophilic and hydrophobic interactions are similar. However, the difference in stoichiometry could be explained that mainly outside binding occurs for the block peptides whereas the alternating peptide binds to the inner monolayer. Another possibility is that the orientation of the peptide to the lipid bilayer might cause the difference in stoichiometry as the block-peptides might screen the lipid charges more efficiently.

The different interaction for the cyclic peptides in the lipid gel phase of DPPG and TMCL might be due to a formation of the subgel phase in case of TMCL during the temperature equilibration time of the ITC instrument. The DSC results show that the peptide decreases the subgel transition temperature, indicating that the peptides insert into the lipid chain lattice (Section 3.2.1). The lipid chain order is strongly increased in the subgel phase with its triclinic structure (see Section 2.2.2). It undergoes an endothermic transition into a hexagonal chain lattice of the gel phase with reduced chain interactions. The insertion of peptide side groups and the partial transformation of a triclinic into a hexagonal structure might lead to the observed positive $\Delta_R H^\circ$ values and a $\Delta_R C_P$ value of about 1 kcal mol⁻¹ K⁻¹.

For the liquid-crystalline phase, the value for $\Delta_R H^\circ$ is about double negative when compared to the one observed for the arginine-tryptophan containing peptides binding to the liquid-crystalline phase of DPPG. The determined $\Delta_R C_P$ value of c-RRRWWW binding to TMCL is -360 cal mol⁻¹ K⁻¹. This value is about two to three times more negative than observed for c-RWRWRW and c-RRWWRF interacting with DPPG. As the binding constant is increased for the peptide binding to TMCL, the increased amount of binding peptides might also cause an increased dehydration of the lipid chains leading to the observed decrease in $\Delta_R C_P$.

Peptide	T/°C	N	K/M ⁻¹	ΔG° /kcal mol ⁻¹	ΔH° /kcal mol ⁻¹	T ΔS° /kcal mol ⁻¹
c-RWRWRW	15	1.2	4.5x10 ⁶	-8,7	2.7	11.4
	20	1.2	4.5x10 ⁷	-10,3	9.1	19.4
	50	0.9	6.8x10 ⁶	-10,1	-5.9	4.2
	55	1.2	8.3x10 ⁶	-10,4	-5.9	4.5
	60	1.2	3.9x10 ⁶	-10,0	-7.0	3.0
c-RRRWWW	15	0.8	2.9x10 ⁷	-9,8	4.9	14.7
	20	0.8	5.0x10 ⁸	-11,6	10.5	22.1
	50	0.5	8.3x10 ⁶	-10,2	-6.3	3.9
	55	0.7	1.0 x10 ⁷	-10,5	-6.9	3.6
	60	0.6	2.6x10 ⁶	-9,8	-9.9	-0.1

Table 3-4-3 Thermodynamic parameters of c-RWRWRW and c-RRRWWW interacting with TMCL membranes determined by ITC measurements.

The titration of TMCL membranes to c-RFRFRF and c-KWKWKW solution is shown in Figure S3-4-6 and S3-4-7 of the supplementary data, respectively. Table 3-4-3 summarises the thermodynamic parameters for c-RWRWRW and c-RRRWWW binding to TMCL membrane at different temperature.

The average binding constant of $1.4 \cdot 10^7$ M⁻¹ for c-RWRWRW binding to TMCL is about one order of magnitude higher than the binding constants observed for binding to DPPG. The observed binding

constant of c-RRRWWW with an average value of $9.3 \cdot 10^7 \text{ M}^{-1}$ is even higher. As the vesicle surface charge density, i.e. is the number of charges per surface area, does not change between DPPG and TMCL (see Section 1.3.2), the binding constant should be in a similar range. However, as the localisation of charges seems to play a role, describing the membrane surface with a certain potential of smeared charges is not sufficient. The $\Delta_R G^\circ$ for the binding of c-RWRWRW to the lipid gel phase is $-9.5 \text{ kcal mol}^{-1}$ (only the value at 15°C and 20°C were averaged) and $-10.2 \text{ kcal mol}^{-1}$ for binding to the liquid crystalline phase. For c-RRRWWW binding to TMCL in both phases $\Delta_R G^\circ$ is $-10.2 \text{ kcal mol}^{-1}$. This value is closer to the expected value of $-13 \text{ kcal mol}^{-1}$ in case of pure additivity of hydrophobic and electrostatic interactions. This means that z_{eff} is much closer to z for the trivalent peptides binding to TMCL membranes. One reason for the more effective binding could be the decreased sterically hinderance of the peptides when they approach the membrane surface. In case of PG, each charged phosphate group is bound to a glycerol moiety, whereas in cardiolipin two phosphate groups share one glycerol molecule. This means that most likely the hydrophobic contribution to the binding is increased for the peptide interacting with TMCL when compared to DPPG.

3.4.2 PG/PE mixtures

The DSC and ATR experiments (Section 3.2.2 and 3.3.2) clearly show that binding of the different cyclic peptides always lead to phase separation in a PG/PE mixture with almost pure DPPG separating with bound peptides from the rest of the lipids.

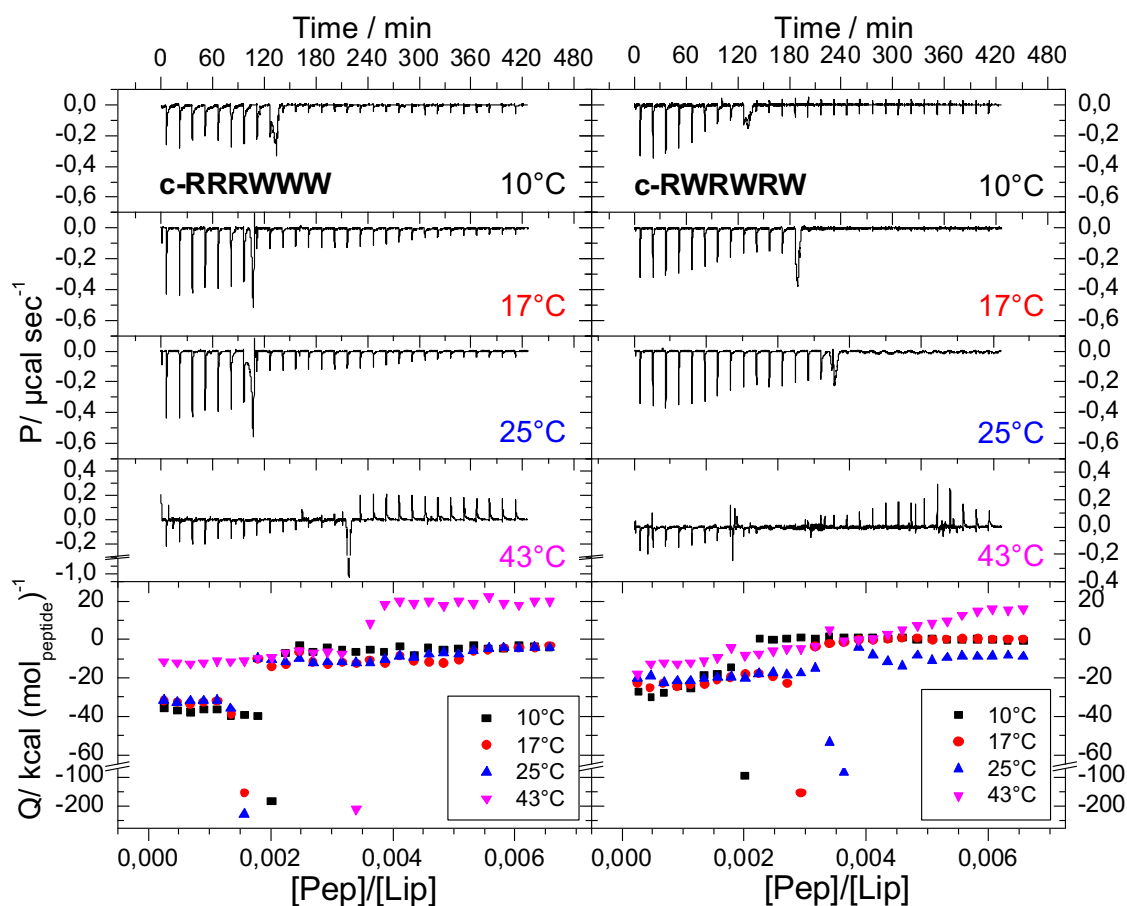


Figure 3-4-7 *top*: ITC titration curves (heating power vs. time) of 62 μM c-RRRWWW (left) and c-RWRWRW (right) titrated into a 2 mM DPPG/DPPE (1:1) vesicle suspension at the indicated temperatures. *bottom*: integrated heats per mol injected peptide vs. peptide-lipid ratio of the respective titration curve at 10 $^{\circ}\text{C}$ (square), 17 $^{\circ}\text{C}$ (circle), 25 $^{\circ}\text{C}$ (triangle) and 43 $^{\circ}\text{C}$ (inverse triangle).

To further quantify the effect of demixing after peptide binding we investigated the induction of lipid domains at constant temperature by titrating either peptides to lipid vesicles or *vice versa* using ITC. Of particular interest was the question whether demixing takes place immediately with the first bound peptides or whether a critical clustering ratio r_{cc} is needed. The heats of reaction in titrations of the peptide c-RRRWWW and c-RWRWRW to DPPG/DPPE 1:1 mixed vesicles at different temperatures are shown in Figure 3-4-7. At 43 $^{\circ}\text{C}$ the pure DPPG/DPPE mixture is still in the gel state whereas the DPPG/DPPE mixture in presence of the cyclic peptides is in the molten cluster state. After injection of the peptide solution exothermic peaks indicating binding can be observed. The exothermic binding peaks persist until a lipid-peptide threshold ratio of $\sim 500:1$ (peptide-lipid = 0.002) is reached and then a much larger exothermic peak is seen. Titrating additional peptide to the

vesicles leads to the appearance of endothermic peaks. This is obviously due now to a formation of lipid-peptide clusters that have to undergo a P_{β} - L_{α} phase transition in the molten cluster state, i.e. at 43 °C part of the vesicles membranes is now in the liquid-crystalline state as shown by the DSC curves in Figure 3-2-2. This identifies the existence of a critical clustering ratio r_{cc} .

Similar threshold ratios can be observed for the other peptides c-RFRFRF and c-KWKWKW as well as c-KKWWKF and c-RRRWWF as can be seen in Figures S3-4-9 and S3-4-10, respectively, of the supplementary data. This indicates that the critical clustering ratio is independent of the temperature within a given lipid phase and the peptide amino acid sequence within the variations investigated here.

Below a temperature of 43°C. i.e. in the lipid gel phase, only exothermic heats of binding are observed. The enthalpies above the critical clustering ratio are less negative than the enthalpies of initial binding for all investigated peptides. The $\Delta_R H^\circ$ above r_{cc} includes peptide binding to the pure DPPG in the lipid domain and to the remaining mixed membrane and might as well include an aggregation enthalpy contribution (411, 412).

The larger exothermic peaks occur at certain thresholds ratios (r_{cc}) between 1000:1 and 250:1 for c-RRRWWW, c-RRRWWF and c-RWRWRW also at lower temperatures in the pure gel phase and can be interpreted by the contemporaneity of events when the critical clustering ratio is reached. As the membrane is restructured it is more likely that the heat is a sum of contributions occurring from changes in lipid membrane, which means that the molar heat is about 200-500 times lower, when attributed to the lipid concentration. For example, if the initial binding increases the hydrophobic area in contact with water the lipid aggregation into clusters could circumvent this unfavoured interaction leading to an aggregation which contributes exothermically to the observed heat of reaction (see discussion below). The gel to liquid-crystalline phase transition enthalpies are about 0.5 kcal mol⁻¹ per CH₂ group but with dipole-dipole interactions ranging up to 5 kcal mol⁻¹ (60). Also, the release of curvature stress leading to morphological changes (256) induced by the initial binding of peptides to the outer monolayer could be a process contributing to the large exothermic reaction heat. Assuming, for example, that at these peptide-lipid ratios permeabilization of the vesicles takes place, so that inside binding can also occur, the high exothermic reaction heat is then due to the cumulative heat of these effects resulting from peptides binding to the inside of the vesicles. Moreover, as the binding of cationic peptides leads to a downshift in the energetic barrier of the non-ideality parameter (170, 413), the release of the mixing enthalpy is part of the highly exothermic peak occurring at the critical clustering ratio.

Additionally, lipid-peptide binding energies occurring during the lipid domain formation can contribute to this exothermic event. For example, the complex formation of guanidinium-phosphate hydrogen bonds was simulated to be around -100 kcal mol⁻¹ (316).

Comparison of the binding properties of different cyclo-peptides leads to the following observation. The exothermic reaction heats observed for the different peptides seem to be correlated with their ability to induce lipid-peptide clusters as seen by DSC. The peptides c-RRRWWW and c-RRRWFW showed the strongest exothermic events whereas c-RWRWRW and c-KKWWKF showed only a moderate exothermic reaction peak. In these cases, the highest peak was observed at 10 °C with $-30 \text{ kcal mol}^{-1}$ for c-RWRWRW and $-15 \text{ kcal mol}^{-1}$ for c-KKWWKF, respectively. Almost no exothermic heat events were observed at any temperature for c-RFRFRF and c-KWKWKW.

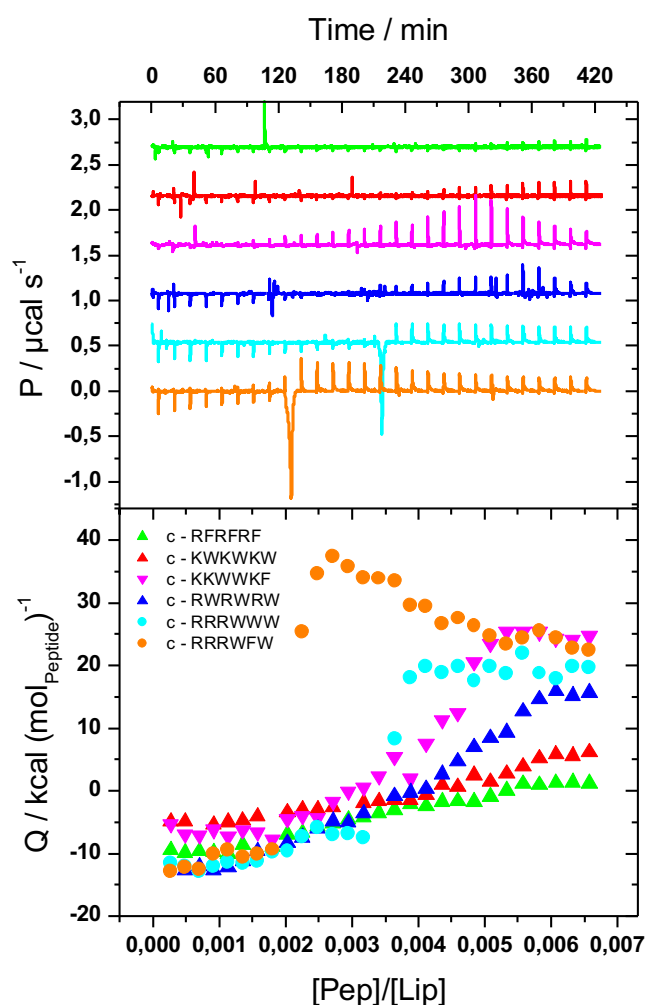


Figure 3-4-8 *top*: ITC titration curves (heating power vs. time) of 62 μM cyclic peptide titrated into a 2 mM DPPG/DPPE (1:1) vesicle suspension at 43 °C. *bottom*: integrated heats per mol injected peptide vs. peptide-lipid ratio. The high exothermic heats observed for the c-RRRWWW and c-RRRWFW titration are omitted for the sake of clarity.

Figure 3-4-8 displays a comparison of the titration curves and the measured heat at 43 °C of all six peptides as a function of peptide to lipid ratio. As already discussed above and shown in Figure 3-4-7 for the binding of c-RRRWWW and c-RWRWRW the appearance of endothermic reaction heats above a certain threshold ratio indicates the formation of liquid-crystalline PG cluster, therefore called the molten cluster state. These endothermic peaks are also visible for the binding of the other

peptides, but clear differences in the heights of the peaks are seen. Peptides which show less clustering efficiency, such as c-RFRFRF and c-KWKWKW display only weak endothermic peaks, whereas these peaks are more pronounced for c-RRRWWF, c-KKWWKF and c-RRRWWW. For c-RRRWWF the reaction heat is between 25 and 34 kcal mol⁻¹ of peptide. Assuming a stoichiometry of 3 and complete binding to DPPG in the mixed vesicle this would mean that the endothermic reaction heat is around 8-11 kcal mol⁻¹ per DPPG. This corresponds roughly to the heat of transition of pure DPPG at its transition temperature of 41°C. So, the binding data obtained by ITC support the DSC data, which show clustering of almost pure DPPG after peptide binding. For the other peptides the endothermic heats of binding are somewhat lower, meaning that either the stoichiometry is different or the degree of binding is lower; both resulting in a reduced clustering efficiency f_c . As the sudden increase in reaction enthalpy is less pronounced for the other peptides, weaker binding seems more likely.

The transition from the exothermic to endothermic heat pattern upon peptide titration occurs in a small peptide-lipid ratio range of ~0.001 for the block-peptides. The range of peptide-lipid ratio for this transition is increased for the semi-block-peptide c-KKWWKF. For the alternating peptide the transition range is the largest with ~0.005 ranging from a peptide-lipid ratio of ~0.001 to ~0.006. This shows that the induction of lipid clustering is also the most efficient for the block-peptides, i.e. only few additional peptides are needed to achieve the maximum of clustered lipids per peptide after the first cluster occur.

As the DSC results showed, the demixing phenomenon for PG/PE mixtures with both palmitoyl and myristoyl chains was similar. We now performed ITC experiments to see, whether the critical clustering ratio r_{cc} for the DMPG/DMPE mixture was different from the one observed for DPPG/DPPE. The peptide solutions were therefore titrated into the vesicle suspension of a DMPG/DMPE 1:1 mixture.

Figure 3-4-9 displays the titration of c-RWRWRW to a DMPG/DMPE 1:1 mixed membrane in the lipid gel phase at 10 °C, the titration to vesicles in the intermediate temperature of 27 °C and to vesicles in the liquid crystalline phase at 50 °C. In general, a similar sequence of heat effects is observed as described before for DPPG/DPPE 1:1 mixtures. The titration curve obtained for a temperature of 10 °C first shows exothermic peaks of decaying height until a sudden larger exothermic peak is observed at a peptide-lipid ratio of ca. 0.007. This larger exothermic peak is interpreted as the onset of a permeation event as discussed before. Therefore, a sudden burst of peptide binding to the inside lipids takes place leading to peaks with a high reaction enthalpy of -100 kcal mol⁻¹ of injected peptide. Consecutive further peptide addition leads to only small decaying exothermic peaks.

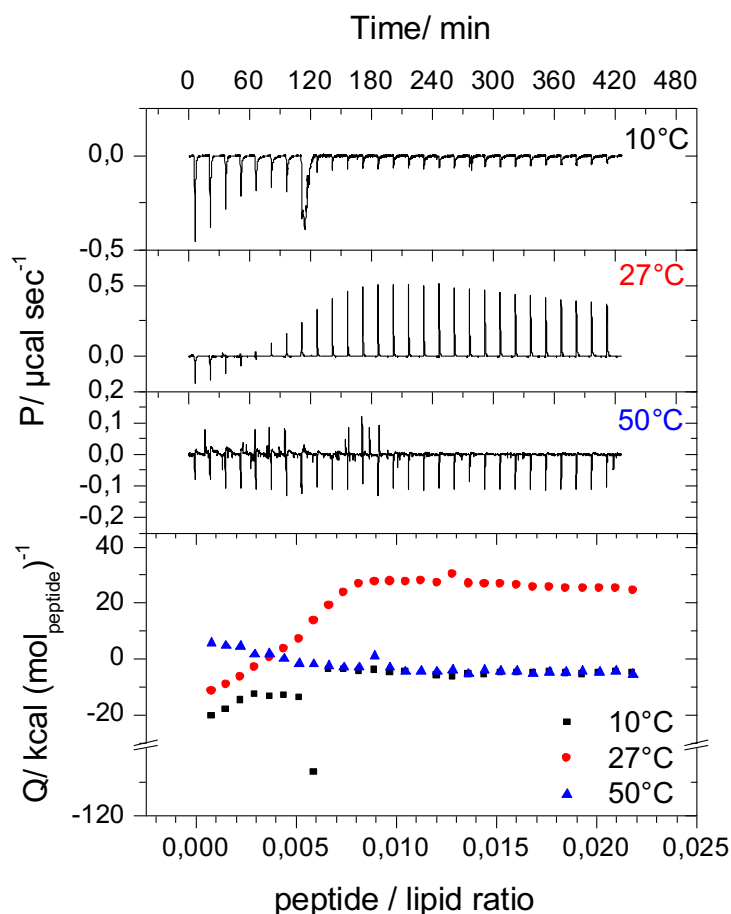


Figure 3-4-9 *top three panels*: ITC titration curves (heating power vs. time) of 62 μM c-RWRWRW titrated into a 600 μM DMPG/DMPE (1:1) vesicle suspension at the indicated temperatures. *bottom*: integrated heats per mol injected peptide vs. peptide-lipid ratio of the respective titration curve at 10 °C, 27 °C and 50 °C.

At a temperature of 27 °C, the titration peaks are initially also exothermic but become endothermic at a peptide-lipid ratio of 0.005, i.e. at a similar ratio as observed in the titration curve at 10°C. The following titration peaks become higher and then decay with increasing peptide concentration. Here, the interpretation is similar to the observation made at 43 °C for DPPG/DPPE 1:1 mixture: at a temperature of 27 °C, the mixed vesicles are still in the gel phase, but peptide binding leads to a permeation of the peptides to the inside of the vesicles and then immediately to the formation of already molten PG rich clusters. This cluster melting is an endothermic process and starts at a critical peptide-lipid ratio r_{cc} of ca. 0.005. It probably continues up to higher peptide-lipid ratios, as the endothermic peaks are still present at ratios > 0.02. The titration of c-RWRWRW to the mixed membrane in the liquid crystalline phase at 50 °C yield only small endo-exothermic peaks which decay at r_{cc} . This is expected as the bilayers are now in the liquid-crystalline phase at all peptide-lipid ratios as seen in the DSC curves in Figure 3-2-5 and this further indicates that clustering also takes place in the liquid crystalline phase. For the DPPG/DPPE 1:1 mixture, the critical ratio r_{cc} was found to be 0.004. Thus, no major differences are observed between the two systems and the chain length of the lipid seems to have no significant effect on the critical clustering ratio r_{cc} .

We then studied the reaction enthalpy observed in the first peptide injections as a function of temperature. For the first three injections, it can be assumed that only outside binding occurs due to the low peptide-lipid ratio of maximal 0.0024, i.e. a lipid/peptide ratio of ~ 400 . To this end, we averaged the reaction enthalpy values and plotted the average as a function of temperature as shown in Figure 3-4-10. For all peptides the binding enthalpy becomes less negative or even positive with increasing temperature.

The slope of the temperature dependence of the binding enthalpy Δ_{RC_P} yields information on changes in hydration. As discussed in the previous Section positive slopes correspond to a dehydration of hydrophilic and hydration of hydrophobic regions. Unfortunately, it is not easy to separate both contributions. The effect of headgroup dehydration on Δ_{RC_P} is approximately $10 \text{ cal mol}^{-1} \text{ K}^{-1}$ (181) and the dehydration of the peptide bond contributes with $14 \text{ cal mol}^{-1} \text{ K}^{-1}$ to the Δ_{RC_P} value (409). The hydration of a methylene group gives a Δ_{RC_P} value of ca. $15 \text{ cal mol}^{-1} \text{ K}^{-1}$ (407) and the hydration of the amino acid residue including the methylene group of the peptide chain is $72 \text{ cal mol}^{-1} \text{ K}^{-1}$ for tryptophan, $60,1 \text{ cal mol}^{-1} \text{ K}^{-1}$ for phenylalanine and $40 \text{ cal mol}^{-1} \text{ K}^{-1}$ for arginine and lysine (409). The heat capacity of aggregation ($\Delta_{agg}C_P$) is expected to make a negative contribution of ca. $-13 \text{ cal mol}^{-1} \text{ K}^{-1}$ per CH_2 group (411), as already discussed above. However, below r_{cc} no aggregation is expected but the insertion of hydrophobic moieties will disrupt the van-der-Waals interactions and might contribute to lipid chain separation and therefore a positive Δ_{RC_P} contribution could be expected.

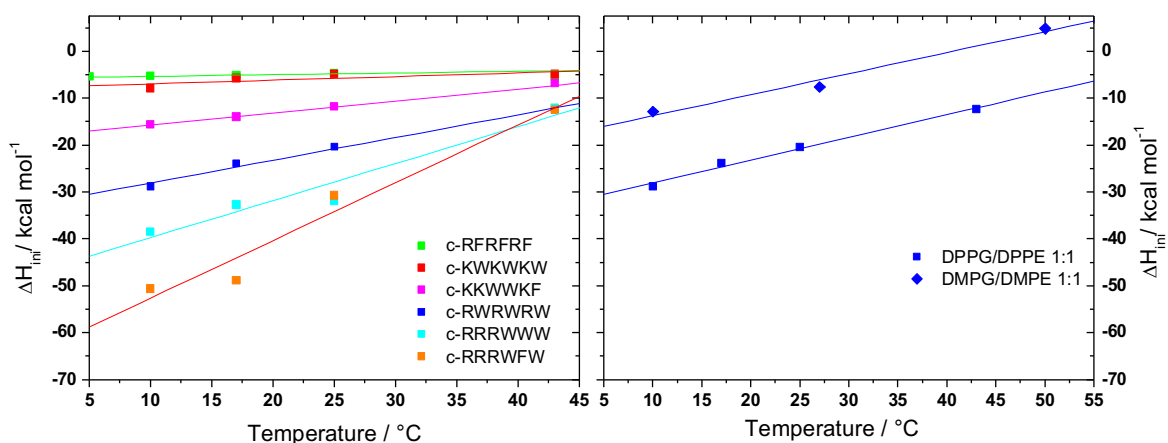


Figure 3-4-10 Averaged first three integrated heats of binding per mol of injected peptide for binding to DPPG/DPPE (1:1) vesicles (left) and comparison of c-RWRWRW binding to DPPG/DPPE 1:1 and DMPG/DMPE (1:1) vesicles (right) vs. temperature.

The reaction heats for c-RFRFRF binding to the DPPG/DPPE membranes are very small and also the Δ_{RC_P} value is very low with $4 \text{ cal mol}^{-1} \text{ K}^{-1}$. For c-RRRWFW binding the highest Δ_{RC_P} value was found with $1450 \text{ cal mol}^{-1} \text{ K}^{-1}$. This high value indicates that after binding many changes in hydration of the interacting partners occur. Extended hydrophobic surfaces are now accessible to water, probably caused by a perturbation of the bilayers by the bound peptide. The penetration of

the peptides into the lipid alkyl chain region seems to induce a local exposure of the lipid alkyl chains to water and disturb the lipid chain interactions. The Δ_{RC_P} values for the binding enthalpy of the other peptides lie between these two extremes. One can conclude that the ability to disturb the lipid chain packing by peptide insertion corresponds to the ability to induce lipid-peptide clusters. Furthermore the Δ_{RC_P} values of the different peptides correlate with their antimicrobial efficiency. The interaction with the mixed membrane is fundamentally different from the interaction with pure DPPG membrane as the Δ_{RC_P} values of peptide binding are around zero or negative (see Figure 3-4-3). This might be an effect of the smaller headgroup area and the therefore lower *c_{pp}* value for PE when compared to PG (Table S1-1-1) which allows a deeper penetration of the peptides into the mixed membrane interfacial area. This can lead to an increased hydration of hydrophobic moieties. The formation of PG-peptide clusters, however, results in dehydration as seen for the pure membrane displaying a negative Δ_{RC_P} .

The Δ_{RC_P} value of c-RWRWRW binding to DPPG/DPPE 1:1 membrane in comparison to the DMPG/DMPE 1:1 mixture is displayed in Figure 3-4-10 right. It is obvious that both Δ_{RC_P} values are almost the same with 450-480 cal mol⁻¹ K⁻¹. This shows again that the influence of lipid chain length is much smaller than the influence of peptide structure which indicates again that the largest contributions to Δ_{RC_P} occur from changes in structure and hydration in the membrane interface region due to the perturbation of the lipid packing.

The major differences between the two lipid systems are the absolute values of peptide binding. For DMPG/DMPE, the reaction enthalpies for peptide binding are 10-15 kcal mol⁻¹ less negative than for binding DPPG/DPPE bilayers. This difference is difficult to interpret as enthalpies of hydration of the membrane interface and the peptide, and the binding enthalpy can be of different sign, so that compensation effects can occur. However, as the hydration of a methylene group contributes about 7.2 kcal mol⁻¹ per CH₂ group to Δ_{RH}° and about 15 cal mol⁻¹ K⁻¹ to Δ_{RC_P} (407), the enthalpy offset and the small difference in Δ_{RC_P} of 30 cal mol⁻¹ K⁻¹ could be explained by the change of the hydration of two CH₂ groups.

We now addressed the question up to which maximal charge ratio the clustering effect of DMPG in mixed DMPG/DMPE membranes occurs by titrating two different peptides into a DMPG/DMPE 1:1 lipid mixture at the intermediate temperature of 27 °C. In Figure 3-4-11, the ITC results of titrations of c-RRRWWW and c-RWRWRW into a DMPG/DMPE 1:1 lipid suspension until an excess of peptide charge is reached are shown. For both peptides endothermic peaks are seen until a peptide-lipid ratio of 0.17, i.e. a charge ratio of ~1 is reached. This means that the formation of lipid clusters takes place until charge compensation occurs.

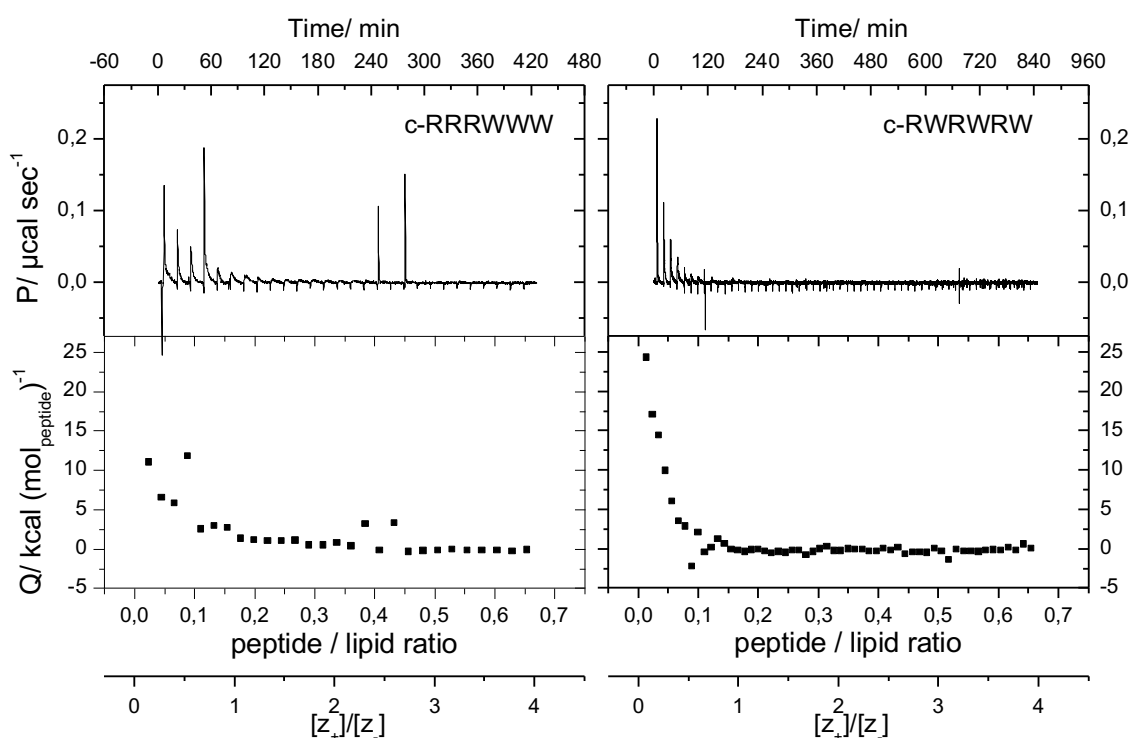


Figure 3-4-11 Titration of a 124 μM peptide solution into 40 μM DMPG/DMPE 1:1 lipid suspension (100 nm vesicle in phosphate buffer pH 7.2) at 27 $^{\circ}\text{C}$. c-RRRWWW (left, injection volume 10 μl) and c-RWRWRW (right, injection volume 5 μl).

Under the assumption that the change in reaction enthalpy as a function of peptide content is directly related to the peptide binding event followed by the clustering process, a binding constant can be formally determined from the decay of the endothermic reaction enthalpy. The binding constants determined in this way are in the order of 10^5 M^{-1} for c-RRRWWW and $10^6\text{-}10^7 \text{ M}^{-1}$ for c-RWRWRW. The latter one is in the same range as the binding constant determined for c-RRRWWW binding to POPG/POPE membrane at 25 $^{\circ}\text{C}$ (119), indicating that the initial assumption is probably correct. The observed binding stoichiometries are 0.07 - 0.12 for c-RRRWWW and 0.04 - 0.1 for c-RWRWRW, respectively. This leads to peptide-lipid charge ratios of $\sim 0.42 - 0.6$ and $\sim 0.24 - 0.6$, respectively. Therefore, the ITC binding experiments lead to similar conclusions as the DSC experiments, namely that the clustered PG domains are not charge compensated but contain more PG than calculated from the charge ratio.

We now studied the effect of changes in mixing ratio of the two lipids in the mixture on the binding and clustering induced by addition of a peptide. Figure 3-4-12 shows ITC titration curves for c-RRRWWW binding to DPPG/DPPE lipid vesicle suspension with different DPPG/DPPE ratios. In the lipid mixture containing 75% DPPG, only endothermic peaks are seen and no exothermic peak characteristic for the initial binding reaction. As mentioned above and seen in the DSC experiments, the DPPG/DPPE 3:1 mixture is the one where the peptides most efficiently induce clustering of DPPG-rich domains (see Section 3.2.2). This was interpreted as being caused by the specific properties of this mixture, namely being closer to a state of demixing than the other mixtures. Indeed,

Lohner et al. (238) found that both lipids are demixed at this lipid ratio under conditions of low ionic strength (10 mM phosphate buffer).

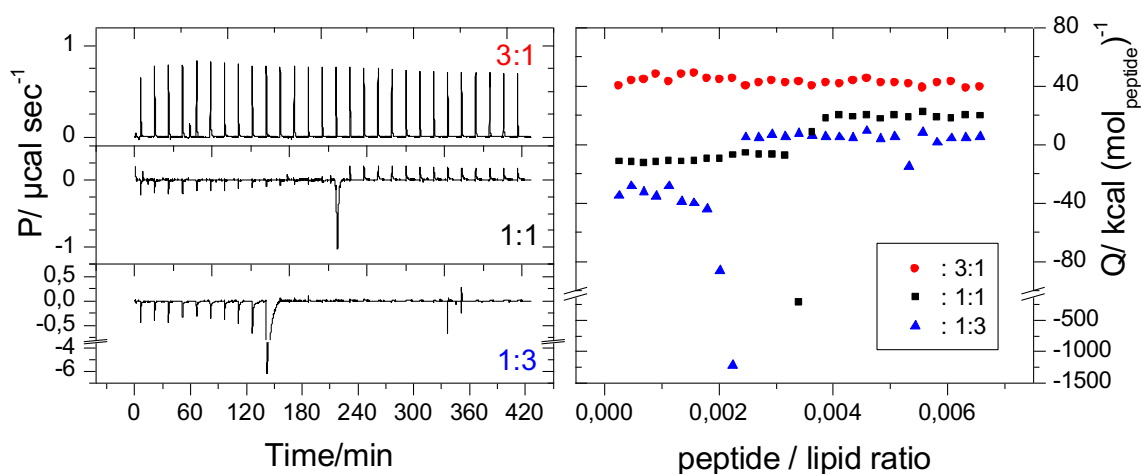


Figure 3-4-12: 62 μM c-RRRWWW titrated into 2 mM DPPG/DPPE 3:1, 1:1 and 1:3 lipid suspension (phosphate buffer, pH 7.2) at 43 $^{\circ}\text{C}$.

Under our conditions of higher ionic strength the pure membranes are not demixed, as the shapes of the DSC curves in Figure 3-2-8 show. The phase transitions at high PG content are clearly different and shifted to higher temperature compared to the published curves by Lohner et al. (414). However, the DSC curve in Figure 3-2-8 (left panel) shows that at a temperature of 43 $^{\circ}\text{C}$ melting of the mixture has already begun. Therefore, binding of peptides immediately leads to the formation of molten DPPG-rich clusters as seen in the DSC curves of Figure 3-2-8 (left panel). The exothermic heat of binding is thus overcompensated by the heat of melting so that only endothermic effects are seen in Figure 3-4-12 (top left).

For the 1:1 and 1:3 mixtures, the initial addition of peptides leads to exothermic binding events. Only after the inside of the vesicles become accessible to the peptides, indicated by the large exothermic peak for a single injection, endothermic peaks occur caused by the melting of clustered PG-rich domains. In case of excess of DPPE molecules in the DPPG/DPPE 1:3 mixture, the initial exothermic peaks indicating binding are higher than for the 1:1 mixture, i.e. $\sim 30 \text{ kcal mol}^{-1}$ compared to $-15 \text{ kcal mol}^{-1}$, respectively. In addition, the single exothermic peak indicating the sudden onset of inside binding is also higher in the 1:3 mixture and occurs at a lower critical peptide-lipid ratio r_{cc} of 0.002. From the charge density of the lipid vesicles alone, one would expect the opposite effect, i.e. less binding to 1:3 DPPG/DPPE vesicles due to their lower charge density. As the experiments show higher binding enthalpies and a lower ratio r_{cc} despite lower charge density, the electrostatic attraction is obviously not the only driving force for binding. Insertion of the peptides into the headgroup region of the bilayers has a major influence on the binding. This seems to depend on the mixing ratio of charged and uncharged lipids.

At the end of the titration curves at a peptide/lipid ratio of 0.0066, i.e. lipid-peptide ratio of ~ 150 , the endothermic reaction heats are clearly dependent on the lipid mixing ratio. The highest values

with ca. 40 kcal mol⁻¹ are observed for the 3:1 mixture with highest PG content. Thus, the endothermic contributions scale with the DPPG/DPPE ratio. The lowest reaction enthalpy is seen for the 1:3 mixture with only ~4.5 kcal mol⁻¹. The high reaction enthalpy of ca. 40 kcal mol⁻¹ of peptide for the 3:1 mixture indicates that ~4 - 5 lipids undergo a phase transition after binding of one c-RRRWWW molecule as the transition enthalpy of pure DPPG is ca. 9 - 10 kcal mol⁻¹ (252). The DSC-experiments (see Figure 3-2-8) and the data evaluation in Figure 3-2-9 gave similar results, namely that at a lipid-peptide ratio of 20:1 in the DPPG/DPPE 3:1 mixture, ca. 50 - 60% of DPPG were clustered and that the lipid to peptide charge ratio in the clusters was around 7.5:3. Both results show that more lipids are influenced than expected if only the charge ratio would play a role. In this case, a maximum of three DPPG molecules would melt after binding of one peptide. This is another indication that electrostatic charge compensation effects alone are not sufficient to describe the clustering effect.

For the mixtures with lower PG content, clearly less PG molecules are melting per additional peptide. For the 1:1 and the 1:3 mixture, the clustering ability of the added peptide is clearly reduced as the lower reaction enthalpies show. This agrees with the results of the analysis of the DSC curves for the transition enthalpy of the PG-enriched domains as a function of peptide content shown in Figure 3-2-9 (left panel). This analysis also showed, that the endothermic low temperature transition scales with the PG content of the mixture, being the highest for the 3:1 DPPG/DPPE mixture.

For mixtures with high PG content also peptide binding takes place until charge compensation occurs as can be seen from Figure S3-4-11 of the supplementary data where the block-peptide c-RRRWWF is titrated to a DPPG/DPPE 3:1 mixture at 20 °C. As the lipid is in the gel phase only exothermic peaks occur and a binding constant of $1.3 \cdot 10^5 \text{ M}^{-1}$ could be determined which is in the same order as for the block-peptide c-RRRWWW binding to the DMPG/DMPE 1:1 membrane ($2.3 \cdot 10^5 \text{ M}^{-1}$) in the molten cluster state at 27 °C (Figure 3-4-11). This indicates that the difference in surface potential of both lipid mixtures does not affect the binding constant.

In Figure 3-4-13 the titration of c-RRRWWW and c-RWRWRW into lipid suspension of a DMPG/DMPE 1:3 and DMPG/DPPE 1:3 lipid mixture at 27 °C is shown. As a result of the difference in chain length the non-ideality parameter in the DMPG/DPPE mixture is increased (215). The 1:3 lipid ratio is used to ensure a mixed lipid state before the peptides are added. All curves show the expected first exothermic heat until a certain peptide-lipid ratio is reached thenceforward endothermic heat contributions occur.

In case of c-RRRWWW the peptide-lipid ratio at which the clustering occurs is shifted from 1:300 to 1:500 upon increasing non-ideality. Nevertheless, in case of c-RWRWRW endothermic heat contributions only occur after a peptide-lipid ratio of 1:200 is reached for DMPG/DPPE mixture compared to 1:500 ratio for the DMPG/DMPE mixture. Therefore, no systematic dependence of r_{cc} on the non-ideality parameter can be observed.

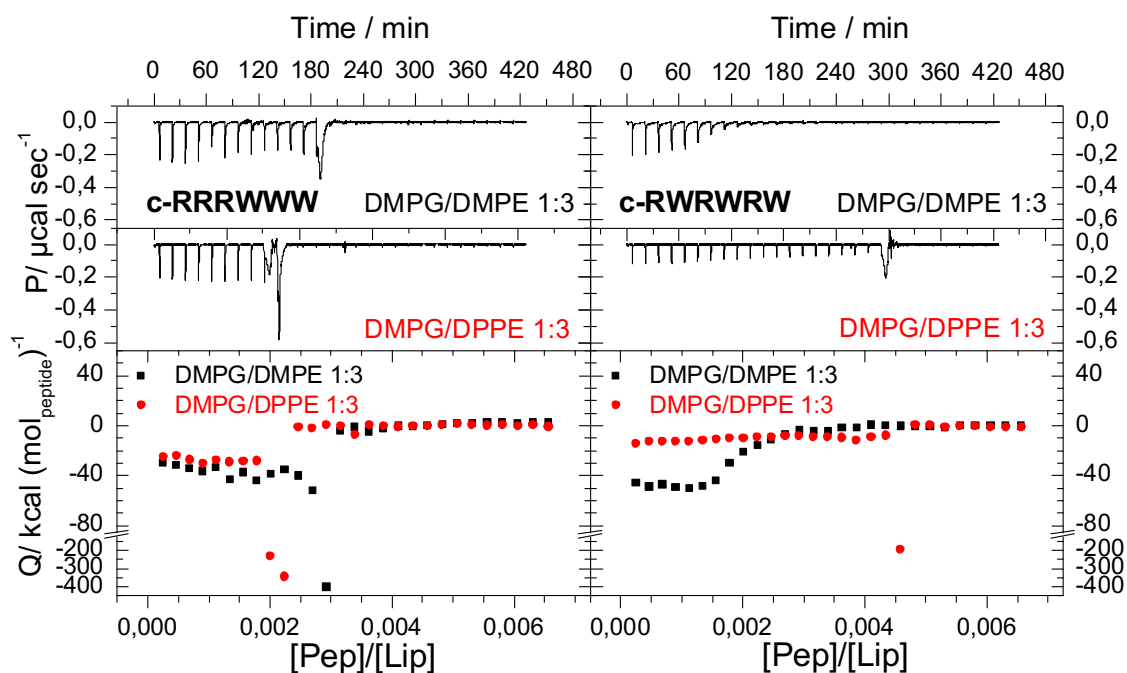


Figure 3-4-13 31 μM peptide solution titrated into 1 mM lipid suspension (100 nm vesicles in phosphate buffer pH 7.2) at 27 $^{\circ}\text{C}$. c-RRRWWW (left) and c-RWRWRW (right).

$\Delta_{\text{R}}H^{\circ}$ of the first binding of $\sim -40 \text{ kcal mol}^{-1}$ is similar for c-RRRWWW binding to both membranes and of the same value for c-RWRWRW binding to the DMPG/DMPE membrane. Here, the comparison to the 1:1 mixture displayed in Figure 3-4-9 shows that the enthalpy of the first binding of c-RWRWRW to the DMPG/DMPE mixture decreases from $\sim -15 \text{ kcal mol}^{-1}$ to $\sim -40 \text{ kcal mol}^{-1}$ from 1:1 to a 1:3 mixture at 27 $^{\circ}\text{C}$ as it was observed for c-RRRWWW binding to DPPG/DPPE 1:1 and 1:3 mixtures at 43 $^{\circ}\text{C}$ (Figure 3-4-12). This indicates that the enthalpy of first binding is peptide specific (Figure 3-4-8 and 3-4-10) but the relative changes resulting from the reduction of PG content in the membrane are independent of the peptide and the lipid chain length.

However, c-RWRWRW shows a heat of first binding of only $\sim -10 \text{ kcal mol}^{-1}$ upon binding to the DMPG/DPPE membrane, meaning that the alteration of the lipid chains is less pronounced for the DMPG/DPPE mixture. This can be due to the fact that the additional methyl groups from the C_{16} chains from the PE moiety can better compensate for the change in lipid chain area of the mixed membrane, due to the peptide insertion. For the deeper penetrating peptide c-RRRWWW this is not the case.

Altogether, the non-ideality of the lipid mixture, resulting from different lipid chain length does not largely effect the critical clustering ratio r_{cc} and the clustering efficiency as it was already discussed for the DSC results of the peptide interacting with DMPG/DMPE 1:1 and DMPG/DPPE 1:1 mixture, respectively (see Figure 3-2-9).

3.4.3 TMCL/DMPE mixture

A similar behaviour as observed for PG/PE membranes is observed for the peptides interacting with a TMCL/DMPE 1:1 mixed membrane. In Figure 3-4-14 the titration of c-RRRWWW (left) and c-RWRWRW (right) solution into a TMCL/DMPE 1:1 suspension is displayed. In both cases, a first exothermic peptide binding is observed, which transforms into an endothermic heat of reaction after the critical clustering ratio r_{cc} is reached. At 27 °C, the lipid-peptide system is in the molten cluster state, meaning that the addition of peptide has led to the formation of clusters with disordered lipid chains consisting solely of TMCL as shown by ATR-IR experiments (see Figure 3-3-11).

When compared to the DMPG/DMPE 1:1 mixture at 27 °C (Figure 3-4-9), the r_{cc} value, i.e. the peptide-lipid ratio where endothermic peaks occur, is increased by about 2 - 4. Also, $\Delta_R H^\circ$ of peptide binding at peptide-lipid ratios below and above r_{cc} is decreased which indicates that the clustering efficiency f_c of c-RRRWWW and c-RWRWRW is decreased when DMPG is replaced by TMCL.

The titration experiments with c-KWKWKW and c-RFRFRF binding to TMCL/DMPE 1:1 also display a r_{cc} value between 0.01 and 0.02 (Figure S3-4-12 and S3-4-13) which confirms the finding that the r_{cc} value is independent of the peptide structure.

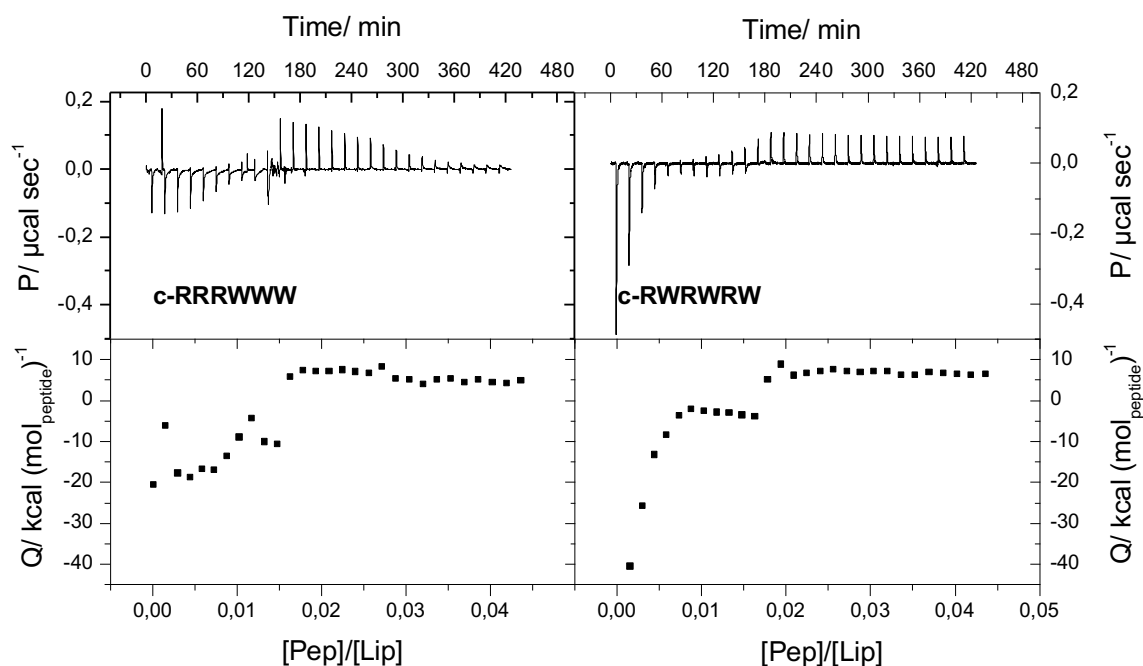


Figure 3-4-14 31 μ M peptide solution titrated into a 1 mM TMCL/DMPE 1:1 suspension (phosphate buffer, pH 7.2) at 27 °C. c-RRRWWW (left) and c-RWRWRW (right).

For the alternating peptide, an additional first process below a peptide-lipid ratio of 0.01 is distinguishable by a decay of even more exothermic heats of ~ -40 kcal mol⁻¹. Neglecting these contributions, the heat of binding is with ~ -18 kcal mol⁻¹ more exothermic for c-RRRWWW than for c-RWRWRW with only ~ -3 kcal mol⁻¹. The difference of ~ 15 kcal mol⁻¹ for the first binding of both peptides is similarly observed for binding to DPPG/DPPE membranes at a temperature of 25 °C

(Figure 3-4-10). The endothermic $\Delta_R H^\circ$ values at peptide-lipid ratios above r_{cc} are in a similar range for both peptides with $\sim 7 \text{ kcal mol}^{-1}$. This means that the overall difference in enthalpy below and above r_{cc} is $\sim 25 \text{ kcal mol}^{-1}$ for c-RRRWWW, but only $\sim 10 \text{ kcal mol}^{-1}$ for c-RWRWRW. These values are strongly decreased when compared to the difference of $\sim 40 \text{ kcal mol}^{-1}$ for the PG/PE 1:1 mixtures. For the TMCL/DMPE mixture the endothermic heat pattern upon peptide titration is reached in peptide-lipid ratio range of ~ 0.02 for both peptides. This is in agreement with the observation made for PG/PE mixtures that r_{cc} is independent of the peptide structure.

Whereas $\Delta_R H^\circ$ for first binding for c-RRRWWW is constant until r_{cc} is reached the peaks occurring for c-RWRWRW binding to TMCL/DMPE 1:1 membrane show a first binding process at peptide-lipid ratio of 0.005, which is at a similar peptide-lipid ratio and similar enthalpies when compared to PG/PE mixtures. This difference in binding between the two peptides might be due to different orientation of the peptides. Where c-RRRWWW adopts only one orientation upon membrane binding, c-RWRWRW might establish different orientations. The first binding might lead to a deeper penetration of the membrane. Additional peptide binding, which leads to an increased chain packing density in the membrane interface region, results in a decrease in penetration depth leading to a decrease in hydration and therefore displaying a decreased exothermic heat of binding. The decrease in penetration depth might be stabilised by a guanidinium-indole interaction (Figure 3-3-13 and 3-3-14) which might further contribute the change in $\Delta_R H^\circ$. Moreover, this indicates that the process involved in the very first binding is similar for the TMCL/DMPE and DMPG/DMPE mixture, but does not directly lead to a lipid clustering in case of TMCL/DMPE mixture. This supports the notion that the origin of lipid clustering is not due to direct peptide-lipid interactions but is related to alteration of the lipid mixing (see Section 2.1.3). The DMPG/DMPE mixture shows an ideal mixing behaviour whereas the TMCL/DMPE mixture displays a phase diagram with an azeotropic maximum (see Section 2.3.1 and 2.3.3) indicating a preferred lipid interaction in the gel phase. This difference in non-ideality increases the difference to the critical non-ideality at which clustering occurs, leading to a shift in r_{cc} value to higher peptide-lipid ratios.

For the TMCL/DMPE mixture the clustering also takes place until charge compensation occurs. This can be seen from the titration of $31 \mu\text{M}$ c-RFRFRF into $120 \mu\text{M}$ lipid suspension, i.e. excess of peptide, shown in Figure S3-4-13 of the supplementary data. The decay of cluster formation with increasing peptide concentration takes place until charge ratio of ~ 1 is reached. Here, the apparent binding constant of $\sim 5 \cdot 10^5 \text{ M}^{-1}$ is slightly below the values observed for the arginine-tryptophan containing peptides binding to DMPG/DMPE membrane.

Altogether, the peptide binding to TMCL/DMPE membrane when compared to DMPG/DMPE membrane, displays an increased value and a decreased clustering efficiency as already discussed for the DSC data in Section 3.2.3. However, from the increased surface potential of the TMCL/DMPE 1:1 mixture when compared to DMPG/DMPE 1:1 mixture (Figure 2-1-4), an

increased peptide binding to the TMCL/DMPE mixture is expected. Therefore, the reduced clustering efficiency and increased r_{cc} value seem to be an effect of decreased non-ideality of the lipid mixture.

3.4.4 Summary

The interaction of peptides with pure DPPG and pure TMCL vesicles is different. For binding to DPPG two interaction processes are observed, whereas for TMCL only one binding process was detected. For binding to DPPG the $\Delta_R H^\circ$ and the $\Delta_R C_P$ value is negative for RW containing peptides in both lipid phases. The $\Delta_R H^\circ$ -values are even more exothermic when the RW containing peptides bind to a liquid crystalline TMCL membrane. However, binding to the gel-phase TMCL membranes leads to endothermic $\Delta_R H^\circ$ -values with a large positive $\Delta_R C_P$ which can be explained by the binding induced transition from subgel to gel phase and the hydration of the alkyl chains. The $\Delta_R G^\circ$ is about 1.6 kcal mol⁻¹ lower when c-RWRWRW binds to the TMCL membrane. As the charge density is similar for the pure DPPG and the pure TMCL membrane (Figure 2-1-4), this increase in z_{eff} results from increased hydrophobic interactions of the peptides with the TMCL membrane. This increase is thought to result from different free headgroup space, which is larger for TMCL, leading to fewer steric hinderances when the peptides interact with the membrane core. Additional peptide-peptide interactions might as well result from the missing glycerol moieties in TMCL, which increases the chance of guanidinium and indole groups to interact with each other.

The peptide interactions with both pure lipid membranes show that the lipid-peptide stoichiometry of the alternating peptides is governed by the number of charges. The block-peptides, however, show a reduced stoichiometry. This indicates that only outside binding occurs for the block-peptide. Another possibility is that the lipid charges are screened more efficiently by the higher charge density of the block-peptide when its bound somewhat tilted to the membrane plane.

For the peptide binding to mixed membrane the ITC measurements show that a critical peptide-lipid ratio r_{cc} exists, at which lipid clusters are formed. The r_{cc} value remains the same for a given binary lipid mixture and is independent of the peptide sequence and the lipid chain length. Until r_{cc} is reached only outside binding with exothermic reaction heats occurs except for the DPPG/DPPE 3:1 mixture at an intermediate temperature above the T_m -value of pure DPPG indicating the immediate formation of molten DPPG-rich clusters. For TMCL/DMPE mixture and PG/PE mixture with PG content of 50 mol% PG or less the binding of peptides at an intermediate temperature above the T_m -value of pure charged component leads to endothermic peaks above r_{cc} indicating the simultaneous formation and melting of the pure charged lipid clusters. For a r_{cc} value of 0.004 and a concentration of 2 mM lipid, the peptide concentration would amount to 8 μ M, a value well within the range of MIC values observed for the various peptides (see Figure 3-1-1).

The r_{cc} value is increased for TMCL/DMPE mixtures when compared to PG/PE mixtures, which can be explained by the reduced non-ideality of the mixture and the critical packing parameter of the individual lipids. As demixing occurs once a critical non-ideality is reached, one would expect a lower r_{cc} value for mixtures that display a non-ideality already closer to the critical demixing value than for ideal lipid mixtures or mixtures with negative non-ideality (see Section 2.1.3). This explains the shift in r_{cc} , when cyclic peptides induce clusters in the TMCL/DMPE mixtures that display an azeotropic maximum when compared to PG/PE mixtures that tend to demix at PG fractions above 65-75% (see Section 2.3).

However, the effect of non-ideality on r_{cc} is not observed for PG/PE mixtures when the non-ideality of the mixture is altered by combining components with different chain lengths. The increased non-ideality is a result of hydrophobic mismatch and potentially reduced PG-PE headgroup interactions. Peptide insertion might compensate for the hydrophobic mismatch and the resulting perturbation of chain packing and change in lipid chain area can be compensated for by both, longer and shorter chains of both lipid moieties. Therefore, we conclude that the main influence on r_{cc} and clustering efficacy from the non-ideality of mixing results from lipid headgroup interaction and not hydrophobic mismatch of lipid chains.

The clustering ends for all observed lipid mixtures when charge compensation occurs. This means that the peptide-lipid ratio in which the clustering takes place is independent of the peptide structure and the lipid chain length and only depends on the lipid headgroup composition and peptide charge. Moreover, the endothermic heat above r_{cc} at temperatures above T_m of the clustered component confirm the finding from DSC results that the antimicrobial efficiency of the peptides correlates to the clustering efficacy. Additionally, to the DSC results, the Δ_{RC_p} values of the initial binding show that below r_{cc} the penetration into the lipid alkyl chain region correlates to the amount of clustered lipids and the antimicrobial efficiency meaning that the peptides with higher antimicrobial efficiency penetrate deeper into the lipid membrane leading to higher Δ_{RC_p} values and increased difference in enthalpy of binding below and above r_{cc} .

4

Conclusions

4.1 Lipid clustering mechanism

Binding of trivalent cyclic hexapeptides leads to a lipid segregation into domains of pure anionic lipids and a remaining lipid matrix depleted in anionic lipids (Figure 3-3-8, 3-3-10 and 3-3-11). Two parameters describe the lipid clustering: The critical clustering ratio r_{cc} and the clustering efficiency f_c . Both parameters were analysed with respect to changes in peptide sequence and lipid membrane parameters.

The critical clustering ratio r_{cc} is the peptide to lipid ratio at which clustering occurs. It is independent of the peptide sequence (Figure 3-4-8) and unaffected by changes in chain non-ideality of a given lipid mixture (Figure 3-4-13). However, it was shown that r_{cc} increases for a given peptide by exchanging DMPG with TMCL in a 1:1 mixture with DMPE. With this change the critical packing parameter and the non-ideality of mixing is altered. Therefore, it still remains unclear how large the contribution of both parameters on the critical clustering ratio is.

The clustering efficiency f_c refers to the amount of clustered lipid per peptide. It is determined by the temperature upshift of the remaining lipid mixture, depleted in clustered lipid. The efficiency of the cyclic peptides correlates to a deeper membrane penetration (Figure 3-2-4, 3-2-5 and 3-2-6). This is further supported by ITC results (Figure 3-4-8 and 3-4-10). The ATR results (Figures 3-3-2, 3-3-5, 3-3-8, 3-3-11 and Figure 3-3-15) confirm a deeper penetration of peptides binding to mixed membranes than to pure lipid membranes. For comparison, tetravalent polyamines binding to the lipid headgroup region show no clustering (Figure 3-2-3). Moreover, the clustering efficiency is influenced by the chain non-ideality of the lipid mixture (Figure 3-2-7 and 3-2-9). The clustering efficiency of the alternating arginine containing peptide decreases for TMCL/DMPE 1:1 membrane when compared to the DMPG/DMPE 1:1 membrane but not significantly for the alternating lysine containing peptide (Figure 3-2-13). This indicates a dependence of f_c on cpp and/or the non-ideality of lipid mixing for the arginine but not lysine containing peptide. Surprisingly, the clustering efficiency scales with the molar fraction of charged lipids (Figure 3-2-10). This indicates that the number of clustered lipids for a given peptide and lipid mixture is constant and only scales with the amount of bound peptides in dependence of the surface potential, i.e. the number of anionic lipids.

Concluding all obtained results, two main models explaining the origin of lipid clustering can be summarised.

4.1.1 The stress release model

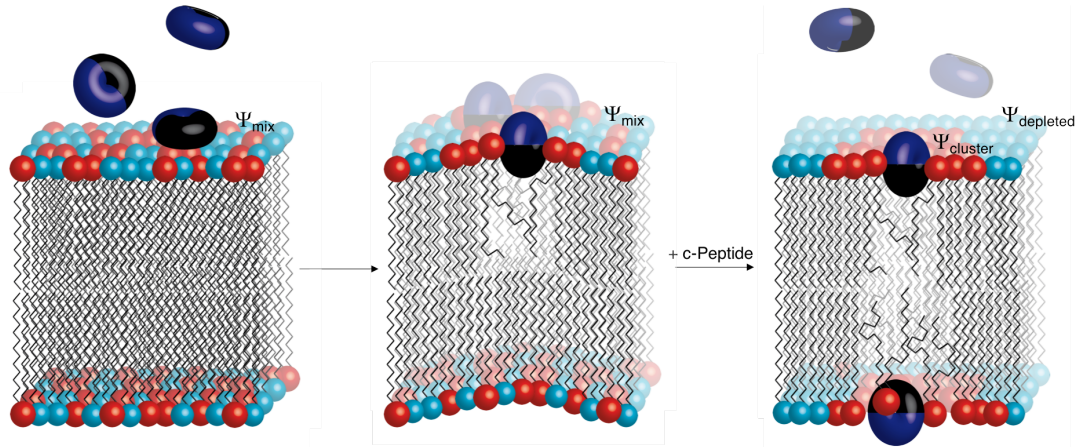


Figure 4-1-1 The stress release model for lipid cluster formation: The insertion of the peptides leads to membrane stress, depicted are curvature induction and the accessibility of hydrophobic lipid surface to water (middle). The formation of clusters (right) leads to an increased surface potential of the pure lipid for the clusters and a reduced surface potential of the mixture depleted in charged lipids. The sum of both surface potentials is below the one for the mixed membrane which leads to a decreased binding constant and therefore reduced membrane stress.

In the stress release model the lipid clustering results from the stress the membrane experiences by binding of the peptides and the insertion of the peptide side groups. The volume of one tryptophan inserting into the membrane is 228 \AA^3 (The DPPC headgroup volume is 319 \AA^3 (125)). This can create free volume in the fatty acyl chain region increasing the hydration of the hydrophobic lipid chains. Furthermore, this will lead to changes in the lateral pressure profile or to curvature stress, as the peptides binding to the outer monolayer increase the area per lipid which is also discussed as the “detergent-like manner” (See Section 1.2.2). Clustering decreases this stress by decreasing the number of bound peptides to the membrane. This happens because the overall membrane surface potential is reduced when instead of a mixed membrane a cluster with a slightly higher surface potential and a remaining mixture with a strongly decreased surface potential coexist. As the membrane surface potential does not scale linearly with the molar fraction of charged lipids (see Figure 2.1.4) this occurs when sufficient lipids are clustered into a domain that the surface potential of remaining lipid mixture depleted in charged lipids is further below the surface potential of the mixed membrane than the cluster potential is above.

$$\Psi_{0cluster} + \Psi_{0depleted} < \Psi_{0mix} \quad (4.1)$$

Figure 4-1-1 depicts schematically the binding of the peptides and the membrane insertion leading to membrane stress. The stress is decreased by a release in bound peptides, resulting from changes in overall surface potential.

The cyclic peptides with larger hydrophobic surfaces show an increased binding constant already to pure charged lipid membranes (Figure 3-4-4 and Table 3-4-2 and 3-4-3). This indicates that binding to mixed membrane is also increased, leading to higher membrane stress. Additionally, the deeper penetration of the more potent antimicrobial peptides leads to increased stress by increased hydrophobic surfaces in contact with water resulting from the perturbation of lipid chains by insertion of hydrophobic moieties as it was observed by ITC (Figure 3-4-10).

Therefore, the clustering efficiency for the deeper membrane penetrating peptides is increased as more bound peptides need to be released. This could also explain the difference in clustering observed between TMCL/DMPE and PG/PE mixtures. The stress induction in TMCL/DMPE mixtures is reduced when compared to PG/PE mixtures because the headgroup volume is lower for TMCL when compared to DMPG.

However, within this model one would expect a dependence of the critical clustering ratio r_{cc} on the peptide structure. As this is not the case, the process leading to cluster formation might be more complicated. For example, positive curvature could also support the assembly of lipids with c_{pp} values <1 which might compensate for the membrane stress but additionally support the demixing. Moreover, the surface potential will also be altered by binding of trivalent in place of monovalent counter ions. According to the Grahame equation already small amounts of di- and trivalent ions lead to a decrease in surface potential (34, 415) which might additionally reduce the charge contributions to lipid mixing entropy.

4.1.2 The model of macroion induced lipid clustering

The correlation of peptide penetration depth and clustering efficiency supports the model of macroion induced clustering by May et al. (170) discussed in Section 2.1.3. In this model lipid clustering is a result of macroion charge, the number of bound macroions on the membrane surface, the size of the macroion and depends additionally on the number of lipids in the affected membrane area. Figure 4-1-2 displays schematically the membrane penetration by hydrophobic peptide sidechains leading to an increased lipid area, meaning the number of lipids in the affected membrane area decreases. This means that the peptide lipid area ratio σ_A ($\sigma_A = A_P/A_L$) decreases and hence changing the lipid composition by increasing the number of charged molecules in the peptide affected area ϕ_p ($\phi_p = z_p/\sigma_A$) which in turn leads to a decrease of the critical minimal non-ideality parameter χ_c . As the critical non-ideality calculates by $\chi_c = \frac{2}{\phi_p^2 \sqrt{\sigma_A}}$, the increase in ϕ_p is more

dominant on the decrease in χ_c than the decrease in σ_A (the effect of increasing σ_A on χ at constant z_p is displayed in Figure 2-1-7). In other words, the fewer lipids fit into the peptide affected area to screen the peptide charges, the higher is the tendency of demixing which explains the increased clustering efficiency of the antimicrobial peptides showing the highest lipid penetration.

The observed shift in r_{cc} when DMPG is replaced by TMCL could be attributed to the change in non-ideality of mixing (Figure 2-3-4). An increased membrane-coverage by the peptides is therefore required to compensate for the increased difference to the critical non-ideality at which clustering occurs. Another reason for the observed difference in r_{cc} is a reduced expansion of the interfacial area by the peptide insertion for the TMCL/DMPE mixture caused by the different headgroup structure of the charged lipid component.

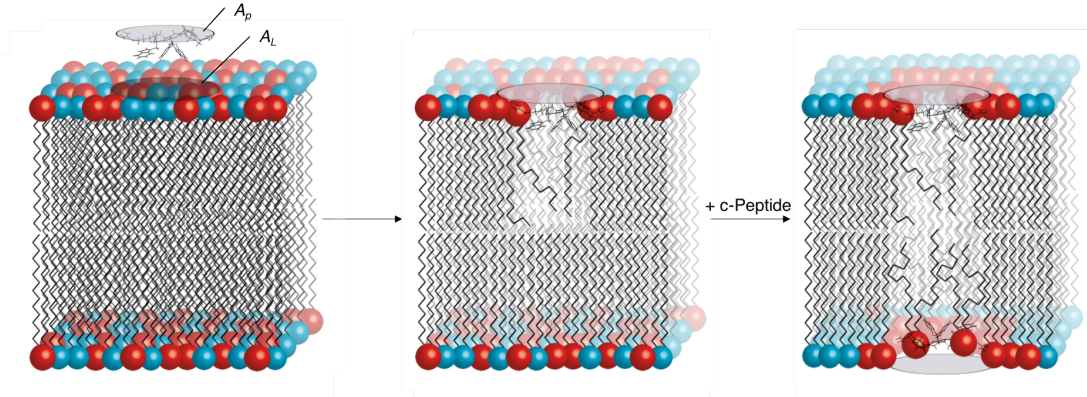


Figure 4-1-2 Schematic representation of the adsorption of cyclic hexapeptides (here c-RRRWWF) from solution onto a binary gel phase membrane, inducing lipid clustering. The area of peptide is depicted by A_p and the lipid membrane area affected by the adsorption of a single macroion by A_L .

However, we observe only minor effects of peptide structure and penetration depth on the critical clustering ratio r_{cc} . Here, the main contributing factor to the formation of small seed clusters at the critical clustering ratio r_{cc} might be the line energy. The aggregation of individual peptide lipid interaction sides into larger clusters would minimize the perimeter length leading to increasing cluster sizes. The critical value therefore depends also on the line energy between the cluster and the remaining mixture. As described by May et al. (170), the line energy calculates

$$\Lambda = \sqrt{\sigma_A} \chi (\phi_P - \phi_L)^2. \quad (4.2)$$

This also explains the observed differences in r_{cc} between PG/PE and TMCL/DMPE mixture which could occur from different line energy between the cluster and the remaining mixed membrane resulting from different lipid non-idealities. The peptide-lipid membrane area ratio only scales by $\sigma_A^{1/2}$, which explains why the differences in r_{cc} between the peptides binding to PG/PE mixtures are negligible. Once the clusters of certain size are formed the determined binding constant of the clustering process at r_{cc} again correlates with the amphipathicity of the peptides, which might than be mostly driven by the changes $\Delta\phi$.

Altogether, the model of macroion induced clustering can qualitatively well describe the observed effects. However, to further proof the validity of this model a better quantification of bound peptides in different membrane states needs to be assessed.

4.1.3 Direct lipid-peptide and peptide-peptide interactions that induce lipid demixing

Besides the already mentioned general model of lipid clustering the impact of additional intermolecular interactions on the clustering efficiency is discussed. As presented in Section 3.1, arginine was shown to form up to five and lysine up to three hydrogen bonds. In case of the arginine containing peptide c-RRWRF a complex with eight lipid molecules was shown to be formed by MD simulation (270). If the binding occurs preferentially to negatively charged molecules as they are attracted by the positive charge only three charges are compensated in direct contact. This means the complex formation leads to a negative net charge of the complex attracting again more positively charged peptides resulting in a bigger complex formation. Upon membrane binding to DMPG-containing membranes and mixed TMCL/DMPE membranes, the ratio of the guanidinium vibration peak intensities is shifted due to interactions with other moieties than solvent molecules when compared to the pure peptide in solution (Figure 3-3-9 and S3-3-3). The alternating peptides c-RWRWRW and c-RFRFRF, however, show only small changes when bound to pure TMCL membrane (Figure 3-3-6) meaning that the arginine-lipid membrane interaction cannot be generalised for the different peptide-lipid interactions.

Another reason for the observed increased clustering ability of arginine-tryptophane containing peptide as a result of increased penetration depth could be due to specific guanidinium–indole group interactions. A correlation of changes in vibration frequency intensity and wavenumber of guanidinium and indole group, respectively, was observed for c-RWRWRW binding to TMCL/DMPE mixtures but not for DMPG/DMPE mixtures (Figure 3-3-13, 3-3-14 and 3-3-15). This could explain the observed differences of arginine and lysine containing peptides but not the differences in clustering efficacy of both lysine containing peptides c-KWKWKW and c-KKWWKF.

Another contributor are lipid-peptide charge interactions. For lysine with a localised charge at the amine group, these contributions are considered to be higher than for the delocalised charge in the guanidinium group of arginine. The interactions with the negatively charged phosphate group are emphasised by a dehydration of the lipid headgroup area and therefore a decrease in dielectric constant meaning that the shielding of the charges is decreased and distance and strength of charge interactions is increased.

Altogether, no direct correlation of clustering ability and the observed structural changes could be deduced from stoichiometry or spectroscopic measurements. Therefore, we can state that direct intermolecular interaction might influence the clustering ability of a given peptide by e.g. influencing the penetration depth but direct peptide-lipid interactions are not the origin of lipid clustering.

4.2 Consequences for lipid clustering as a model of antimicrobial action

Within this study we showed that the peptides with the highest antimicrobial effect also show the highest impact on clustering efficiency.

The relation of clustering to the antimicrobial effect is extensively discussed in Section 1.2.2.1. Lipid clustering might contribute as an initial step in peptide pore formation or it might alter the lipid-protein interplay influencing protein adsorption or insertion kinetics, inhibiting membrane protein functionality, affecting cell homeostasis like cell division (119), metabolism, communication to the cell environment, structural integrity, taxis or growth.

Wenzel et al. (144) observed a glutamate release upon binding of the linear RWRWRW attributed to an activation of the mechanosensitive channel MscL. As MscL is sensitive to changes in the lipid headgroup and interfacial area (125) this finding underlines the assumption that lipid membrane perturbation also takes place in bacteria membrane. Besides the delocalisation of membrane- and membrane-bound proteins like MurG, MinD, cytochrome c, the activity of cell membrane synthesis proteins like PgsA and PlsX, and cell division proteins like FtsZ and DivIVA (a comprehensive overview can be found in the respective literature (144, 148, 416)) is affected by the occurrence of membrane domains which has been shown in vivo by Ormadien et al. (416, 417) and Scheinpflug et al. (119, 145).

Also, the difference in activity of each peptide against *B. subtilis* and *E. coli* is only marginal and can partially be attributed to the presence of a second membrane in *E. coli* as the MIC values are roughly twice as high (see Figure 3-1-1). However, according to our results obtained with binary and ternary lipid mixtures, the clustering in *B. subtilis* with a charged lipid content of about 65% is expected to be higher than for *E. coli* with only 9% charged lipid in the outer and 18% in the inner membrane (see Table 1-1-1). This indicates that different amounts of lipids need to be clustered to induce a lethal event. In these cases, clustering seems to have no direct impact on the lethality of the bacteria but alters the lipid-protein interplay leading to bacteria cell death.

In case cyclic polymyxin also acts via lipid clustering, the membrane composition of the polymyxin producing *Bacillus polymyxa* is 60% PE and only 11% charged lipid partitioned into 3% PG and 8% CL (see Table 1-1-1). The remaining lipids are not conclusively identified as PA, lyso-PC, lyso-PE, lyso-PS, and other not further specified neutral lipids (418).

In a study with polymyxin sensitive and resistant strain of *Pseudomonas aeruginosa* which also has 60% zwitterionic PE content but 33% of charged lipids with 21% PG and 11% CL about 65% of the phospholipids are replaced by uncharged or zwitterionic phospholipids and the overall amount of charged lipids is reduced to 17.5% (15.5% CL and 2% PG) to obtain polymyxin resistance (25). This examples imply that resistance against lipid clustering can be obtained by decreased amount of charged lipids most likely to reduce the binding constant of antimicrobial peptides meaning that the

critical clustering concentration is not reached. However, this interpretation of the beforementioned study is not in line with our result that r_{cc} is independent of the amount of charged lipids.

Therefore, it is more likely that not r_{cc} alone but in combination with the clustering efficiency fc predicts the antimicrobial efficacy of a given peptide and bacteria membrane. At a certain amount of formed clusters the protein functionality is altered in a manner that a lethal event takes place. Furthermore, the study also showed that the number of unsaturated lipid chains increases upon acquisition of polymyxin resistance. The concomitant increase in lipid area is additionally expected to lower the change in lipid area upon peptide insertion and therefore decreasing the membrane stress, supporting the stress release model.

Although the data insinuates that the lethal event of lipid clustering is the alteration of lipid-protein interaction, a direct proof that not the clustering itself or the membrane penetration by the peptides causes the lethal event is still missing. To understand the relation of lipid clustering and antimicrobial action, further investigations should focus on the impact of chain distribution between lipid headgroups including unsaturated chains on lipid clustering and protein activity in vitro and in vivo. Moreover, to better quantify the impact of clustering on membrane protein activity and detachment of membrane bound peptides, the clustering effect should be investigated on reconstituted proteins in model membranes.

5

Summary/ Zusammenfassung

5.1 English version

In this work we investigated the phenomenon of peptide induced lipid demixing, so-called lipid clustering. Within this section we summarise the key findings:

- As a model system for bacterial membranes the thermotropic behaviour of ternary lipid mixtures of DMPG, DMPE and TMCL was investigated (Chapter 2).
 - It was shown that, although all lipids contain alkyl chains of the same length, a gel phase demixing for DMPG contents >60% occurs.
 - The binary TMCL/DMPE mixture displays an azeotropic maximum for high DMPE content.
- The binding constant of the trivalent hexapeptides interacting with pure lipid membranes is higher than expected for trivalent counter ions indicating a contribution of hydrophobic amino acids to the binding strength. Furthermore, the binding constant of the peptides interacting with the TMCL membrane is about one order of magnitude higher when compared to the peptides binding to pure PG membrane.
- Tri- and tetravalent polyamines do not induce clustering in PG/PE membranes. All investigated cyclic trivalent hexapeptides, however, induce lipid clustering. Moreover, lipid clustering efficiency, i.e. the amount of clustered lipid per peptide, correlates with the membrane penetration depth of the peptides with the block-peptides showing the highest penetration (Section 3.2, 3.3 and 3.4). Therefore, we conclude that lipid clustering is a combined effect of counter ion charge and penetration depth of the peptides into the membranes.
- The efficacy of the different trivalent cyclic hexapeptides to induce lipid clustering in PG/PE membranes reasoned from the DSC (Section 3.2) and ITC (Section 3.4) results correlates with their antimicrobial potency.
- A critical clustering peptide-lipid ratio r_{cc} , at which the induction of lipid clusters occurs, exists (Section 3.4).

- r_{cc} is about 1:500-1:200 for PG/PE mixtures and independent of peptide structure and chain length variations. The value for the TMCL/DMPE mixture displaying an azeotropic mixing behaviour is about 1:100-1:50.
- These low peptide-lipid ratios correlate to the low MIC values observed for the antimicrobial activity of the peptide. This further supports the model of lipid clustering for the antimicrobial effect. However, as r_{cc} is independent of peptide structure, the occurrence of the lethal event is also dependent on the clustering efficiency.
- Lipid clustering takes place until equilibrium between lipid and peptide charges occurs (Section 3.4).
- The extent of clustered lipid increases with higher PG content in the PG/PE mixed membrane.
- The non-ideality of the lipid mixture has an impact on the clustering efficiency if the non-ideality is a result of headgroup interactions and not alkyl chain variations (Section 3.2. and Section 3.4).
- Different peptide-lipid and peptide-peptide interactions are observed for the different peptides, indicating a different orientation of the block-peptides with respect to the lipid membrane when compared to the alternating peptides. However, no correlation of these interactions to the clustering efficiency could be identified (Section 3.3). Together with the high stoichiometry values at r_{cc} this indicates that lipid clustering cannot be a result of specific lipid-lipid or lipid-peptide interaction.
- The lipid-peptide ratio within the clusters varies in dependence of the lipid mixture (Section 3.2. and 3.4). Therefore, the achievement of charge equilibrium in clusters is not the driving force behind the observed clustering effect.
- Our observations of the boundary conditions in peptide structure and lipid miscibility affecting the lipid clustering behaviour can be best described by two models:
 - The model of macroion induced clustering by May et al. (170) describes the reduction of the critical non-ideality parameter by macroion binding. It predicts a decrease in critical non-ideality parameter with increasing lipid area. This means that due to the insertion of the hydrophobic side groups and therefore the increase in lipid area, the critical non-ideality is lowered which, if sufficient, leads to membrane demixing.
 - The stress release model explains the clustering effect by an increase in ΔG due to peptide binding, e.g. the deeper penetration of water molecules into the membrane core. As the surface potential dependence of the membrane on the molar fraction of charged lipid is non-linear (Figure 2-1-4), demixing could lead to a decrease of the

overall surface potential and therefore reduce the number of bound peptides. This reduction, in turn, decreases the membrane stress and reduces ΔG .

5.2 German version

In dieser Arbeit wurde das Phänomen der peptidinduzierten Lipidentmischung, dem sogenannten “lipid-clustering”, untersucht. In diesem Abschnitt möchten wir kurz die wichtigsten Ergebnisse zusammenfassen:

- Als Modellsystem für die Bakterienlipidmembran wurde eine ternäre Mischung aus DMPG, DMPE und TMCL untersucht (Kapitel 2):
 - Wir konnten zeigen, dass die Lipidmembran sich in der Gelphase mit einem DMPG-Anteil $>60\%$ entmischt, obwohl alle Lipide die gleiche Alkylkettenlänge besitzen.
 - Die binäre TMCL/DMPE Mischung zeigt ein azeotropes Maximum bei hohem DMPE-Gehalt.
- Die Bindungskonstante der Bindung der trivalenten Peptide an reine Lipidmembranen ist höher als für trivalente Gegenionen erwartet, was den Beitrag der hydrophoben Aminosäuren zur Bindungskonstante bestätigt. Weiterhin ist die Bindungskonstante für die Bindung der Peptide an die reine TMCL-Membran, verglichen mit reiner PG-Membran, um etwa eine Zehnerpotenz erhöht.
- Tri- und Tetraivalente Polyamine induzieren kein “lipid-clustering” in PG/PE Mischmembranen, wohingegen alle trivalenten Peptide ein “lipid clustering” zeigen. Die Effizienz der Lipidentmischung, die sich aus der Menge der entmischten Lipide pro Peptid ergibt, korreliert mit der Eindringtiefe der Peptide in die Lipidmembran und ist für die Blockpeptide am stärksten ausgeprägt (Abschnitt 3.2, Abschnitt 3.3 und Abschnitt 3.4). Daraus kann geschlossen werden, dass “lipid clustering” als Ergebnis aus Gegenionenladung und der Eindringtiefe der Gegenionen in die Lipidmembran resultiert.
- Die “Clustering”-Effizienz der trivalenten zyklischen Hexapeptide an PG/PE Membranen, die aus den DSC (Abschnitt 3.2) und ITC Ergebnissen (Abschnitt 3.4) abgeleitet werden konnte, korreliert mit der antimikrobiellen Effizienz der Peptide.
- “Lipid clustering” tritt erst oberhalb eines kritischen Peptid-Lipid Verhältnisses r_{cc} auf (Abschnitt 3.4).
 - Für PG/PE Membranen konnten wir ein r_{cc} Wert von etwa 1:500-1:200 bestimmen, der unabhängig von Peptidstruktur und Kettenlängenvariationen der Lipide ist. Der r_{cc} Wert für die TMCL/DMPE Mischung mit azeotropem Maximum ist 1:100-1:50.
 - Die niedrigen Peptid-Lipid-Verhältnisse korrelieren mit den niedrigen MIC Werten der antimikrobiellen Aktivität. Dies stützt die Annahme, dass die peptidinduzierte

Membranentmischung ursächlich für die antimikrobielle Aktivität ist. Da jedoch die r_{cc} Werte unabhängig von der Peptidstruktur sind, ist der Eintritt des letalen Ereignisses auch von der Clustering Effizienz der Peptide abhängig.

- Das “lipid-clustering” findet bis zum Ladungsausgleich zwischen Lipiden und Peptiden statt (Abschnitt 3.4).
- Die Menge an geclustertem Lipid steigt mit höherem PG-Gehalt in der PG/PE Mischmembran.
- Wenn aufgrund von Lipid-Kopfgruppen-Interaktionen die Nichtidealität der Lipidmischung beeinflusst wird, so resultiert daraus auch eine Änderung der “Clustering”-Effizienz der Peptide (Abschnitt 3.2 und Abschnitt 3.4).
- Die unterschiedlichen Peptidstrukturen beeinflussen Peptid-Peptid und Peptid-Lipid-Interaktionen und resultieren in einer unterschiedlichen Orientierung zwischen den Block-Peptiden und den Peptiden mit alternierender Aminosäuresequenz an der Lipidmembran. Jedoch konnte keine Korrelation dieses unterschiedlichen Bindungsverhaltens zu der Clustering-Effizienz identifiziert werden (Abschnitt 3.3). Zusammen mit den hohen Stöchiometrieverhältnissen zu Beginn des “Clusterings” bei r_{cc} lässt sich schlussfolgern, dass “lipid clustering” nicht auf eine bestimmte Peptid-Peptid oder Peptid-Lipid Wechselwirkungen zurückgeführt werden kann.
- Da das Lipid-Peptid-Verhältnis eines Lipidclusters in Abhängig der Mischungszusammensetzung variiert (Abschnitt 3.2 und Abschnitt 3.4) und somit auch nicht notwendigerweise ein Ladungsausgleich der Lipidcluster erzeugt wird, kann dies als treibende Kraft des “lipid clusterings” ebenfalls ausgeschlossen werden.
- Aufgrund der gemachten Beobachtungen welche Randbedingungen der Peptid-Struktur und Mischbarkeit der Lipidmembran das Clustering-Verhalten beeinflussen, kann das “lipid clustering” durch zwei Modelle beschrieben werden:
 - Das Modell des Makroionen induzierten “Clusterings” geht auf May et al. (170) zurück und beschreibt die Erniedrigung des kritischen Nicht-Idealitätsparameters der Lipidmischung durch die Bindung von Makroionen. Das Modell sagt eine Erniedrigung des kritischen Nicht-Idealitätsparameters mit Vergrößerung der Lipidfläche unter dem bindenden Makroion voraus. Das bedeutet, durch die Insertion der hydrophoben Seitenketten des Peptids in die Lipidmembran wird die Lipidfläche vergrößert und durch ausreichende Erniedrigung des kritischen Nicht-Idealitätsparameters erfolgt eine Entmischung.
 - Das “Stress-Release”-Modell erklärt das “lipid-clustering” durch eine Erhöhung von ΔG resultierend aus der Peptidbindung, beispielsweise durch erhöhter Eindringtiefe des Wassers in die Lipidmembran. Da die Abhängigkeit des

Oberflächenpotentials vom Molenbruch des geladenen Lipids nicht-linear ist (Abbildung 2-1-4), führt die Entmischung zu einer Reduktion des Oberflächenpotentials und somit zu einer Reduktion an gebundenem Peptid, was wiederum den Membranstress reduziert und zu einer Erniedrigung in ΔG führt.

6

Materials and Methods

6.1 Material

6.1.1 Chemicals

6.1.1.1 Lipids

The lipids 1,2-dimyristoyl-*sn*-glycero-3-phosphoglycerol (DMPG), 1,2-dipalmitoyl-*sn*-glycero-3-phosphoglycerol (DPPG), 1,2-dimyristoyl-*sn*-glycero-3-phosphoethanolamine (DMPE) and 1,2-dipalmitoyl-*sn*-glycero-3-phosphoethanolamine (DPPE) were purchased from Genzyme (Neu-Isenburg, Germany). 1',3'-bis[1,2-dimyristoyl-*sn*-glycero-3-phospho]-glycerol (TMCL) and the deuterated lipids 1,2-dimyristoyl- d_{54} -*sn*-glycero-3-phosphoglycerol (DMPG- d_{54}) and 1,2-dimyristoyl- d_{54} -*sn*-glycero-3-phosphoethanolamine (DMPE- d_{54}) were purchased from Avanti polar lipids (Alabasta, Alabama, USA).

6.1.1.2 Peptides

The synthetic cyclic peptides c-RWRWRW, c-RRRWWW, c-RRRWWF, c-RRWWRF and c-KKWWKF were synthesized as described before (250, 254) and provided by Margitta Dathe (FMP Berlin). The peptides c-RFRFRF and c-KWKWKW were purchased from Genecust (Dudelange, Luxembourg) with a purity >98% as shown by HPLC.

6.1.1.3 Polyamines

Ethylenediamine (1,2-diaminoethane dihydrochloride), propylenediamine (1,3-diaminopropane), putrescine (1,4-diaminobutanedihydrochloride), cadaverine (1,5-diaminobutane dihydrochloride) and spermine (N,N'-Bis(3-aminopropyl)butane-1,4-diaminetetrahydrochloride) were purchased

from Sigma-Aldrich (Steinheim, Germany) with a purity higher than 98%. Propylenediamine was titrated with HCl (Sigma-Aldrich, Steinheim, Germany) to pH 6.2 before further use. All samples were prepared in a 100 mM NaCl solution and titrated to a pH of 5.8 - 6.2.

6.1.2 Vesicle preparation

All samples for calorimetric measurements were prepared in 20 mM aqueous phosphate buffer (pH 7.2) with 100 mM NaCl. The peptides were weighed after lyophilisation, dissolved in phosphate buffer solution, diluted to the required concentration. The sample was then degassed in a vacuum chamber before further use.

Binary and ternary lipid mixtures were prepared by dissolving each single lipid in chloroform/methanol 2:1 and mixing appropriate volumes of each stock solution. The organic solvent was removed by applying a gentle N₂ stream. The remaining lipid film was dried overnight under vacuum at 40 °C. The lipids were then dispersed in the required buffer solution, vortexed above the respective phase transition temperature of the lipid, and the coarse lipid dispersions were then extruded 17 times through a 100 nm diameter polycarbonate filter at a temperature higher than the respective phase transition temperature of the lipid by using an Avanti Mini Extruder (Avanti Polar Lipids, Alabaster, Alabama, USA). The obtained lipid concentration of the stock suspension was 2 mM. The vesicle size was checked by dynamic light scattering (DLS) using an ALV-NIBS/HPPS DLS instrument (ALV-Laser Vertriebsgesellschaft, Langen, Germany). Dispersions of pure lipids were extruded in a similar way after weighing and dissolving them in buffer.

Samples for IR-spectroscopy measurements were prepared in the same way but 100 mM NaCl solution in H₂O or D₂O (from Sigma-Aldrich, Steinheim, Germany) titrated to a pH or pD of 6.8 - 7.2 was used to ensure no infrared absorbance from the phosphate buffer.

6.2. Methods

6.2.1 Differential Scanning Calorimetry (DSC)

DSC measurements were performed using a VP-DSC microcalorimeter (MicroCal, Northampton, Massachusetts, USA). The applied scanning rate was 60°C/h. The reference cell was filled with the appropriate aqueous phosphate buffer solution. Several heating and cooling scans were performed to check for reproducibility. If not stated differently, only the last heating scan is displayed in the figures.

Lipid vesicles to study the phase behaviour of binary and ternary mixtures were prepared as described above. However, some samples were already measured before extrusion to investigate the

effect of MLV and LUV on the phase behaviour as indicated in the text and displayed in supplementary data. The lipid concentration was 2 mM.

To study the effect of the cyclic peptides on the phase transition temperature of phosphatidylglycerols and cardiolipin and their respective mixtures with phosphatidylethanolamines the lipid suspension was mixed with aliquots of freshly prepared peptide solution to obtain the desired lipid to peptide ratio and a lipid concentration of 1 mM.

6.2.2 Isothermal Titration Calorimetry (ITC)

To determine the thermodynamic parameters of the peptide lipid interaction, ITC measurements were performed with a MicroCal VP-ITC microcalorimeter (Microcal, Northampton, Massachusetts, USA). The lipid vesicle suspension was either titrated into a peptide solution in the cell or *vice versa*. For instance, a 62 μM peptide solution was added in 10 μL aliquots into the reaction cell ($V = 1.4591 \text{ mL}$) containing a 2 mM lipid dispersion with an injection duration of 20 s. In some cases, also 5 μL aliquots were titrated as stated in the text or Figures. The equilibration time between each titration step was 15 minutes. The first titration of 2 μL was disregarded to ensure that a premixing of both solutions during the equilibration time does not affect the first titration step. During the experiment the stirring speed of the injection syringe was 286 rpm. The reversed titration experiments were performed similarly. The respective concentrations of peptide and vesicle solution, respectively, are given in the figure captions.

6.2.3 Attenuated Total Reflection Infrared (ATR-IR) spectroscopy (Bio-ATR)

We obtained temperature dependent ATR-Fourier Transform IR spectroscopy spectra with a spectral resolution of 2 cm^{-1} using a Bruker Tensor 27 spectrophotometer equipped with an N₂-cooled MCT detector and a BioATR II unit (Bruker Optics, Ettlingen, Germany). The internal reflection element (IRE) of the BioATR II unit is Si-crystal with about 4 mm in diameter. The thin Si-crystal layer is placed on a ZnSe-crystal so that the light reaches a reflection angle $\varphi = 45^\circ$ with about 9 - 12 internal reflections in the 4 mm Si-crystal layer (Figure 6-2-1). The desired temperature was set by a computer-controlled circulating water bath (Haake C25P Phoenix II, Karlsruhe, Germany).

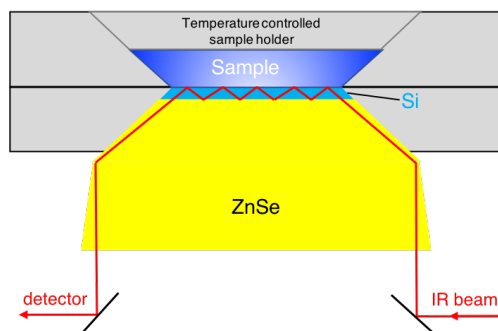


Figure 6-2-1 Schematic cross section of the BioATR II unit from Bruker Optics. The sample is placed on the Si crystal which is mounted on a ZnSe crystal and surrounded by a temperature controlled casing.

Each single channel spectrum is an average of 256 scans. The final absorbance spectra for each temperature were calculated by $A = -\log_{10}(I/I_0)$. The spectrum of pure water at each temperature was used as a reference spectrum. The sample consisted of extruded lipid vesicles of 100 nm in diameter and the peptide solutions. Defined aliquots of the peptide and vesicle solutions were mixed above the respective lipid phase transition temperature directly on the crystal surface of the cell to obtain a lipid concentration of 1 mM. If not otherwise mentioned a lipid-peptide ratio of 2:1 was used, i.e. in most cases but pure TMCL a peptide-lipid charge ratio of 1 or higher to achieve high amounts of clustered phase at overall comparable signal intensities. Before recording spectra, one heating and cooling scan was performed to ensure equilibration of the system. Spectra were recorded in 2 °C intervals within the temperature range of interest after temperature equilibration in a temperature interval (ΔT) of ± 0.1 °C for 15 min was ensured. The temperature was measured inside the cover plate of the sample holder by a Pt100 resistor (Omega Newport, Deckenpfronn, Germany). For further data analysis absorbance spectra were shifted to a zero baseline in a spectral region where no vibrational peak occurred. To determine the position of the CH₂ vibrational bands in a certain wavenumber interval by calculating the second derivative of the spectra, we used the ‘peak picking’ function included in the Bruker OPUS software. For comparison of peak position and intensity ratios, the spectra were normalized in intensity at the amide I band at 1640 cm⁻¹ or at the lipid carbonyl stretching vibration at 1742 cm⁻¹ when peptides were bound to lipid vesicles.

7

Supplementary

7.1 Supplementary to Chapter 1

Lipid	$a_0 / \text{\AA}^2$	$d_{hh} / \text{\AA}$	$V_{hc} / \text{\AA}^3$	$V_{hg} / \text{\AA}^3$	$\theta / ^\circ$	c_{pp}
POPG	48 (173)	51	930 (419)	257 (420)		0.92
DMPG	48 (173)	45.3 (421)	730 (419)	257 (420)	29 (421)	0.82
DPPG	48 (173)	51.1 (173)	840 (420)	257 (420)	32 (173)	0.81
DSPG	48 (173)	60.0 (173)	930 (419)	257 (420)	27 (420)	0.76
DMPA	43.2 (421)	40.1 (421)	730 (419)	220 (422)	31 (421)	1.04
DMPS	51.3 (423)	44.3 (424)	735 (424)	244 (424)	0 (424)	0.70
TMCL	78.9 (197)	42.8 (226)	1460 (419)	480 (422)	15 (226)	1.03
DPPC	47.9 (425)	47.8 (425)	825 (419)	319 (419)	32 (426)	0.94
DLPE	41 (187)	50.6 (187)	611 (419)	252 (187)	0 (33)	0.87

Table S1-1-1 Lipid head group area, lipid chain length and volume and the resulting critical packing parameter are given for different lipid species in gel phase. Adapted from (427).

Peptide Amino acid sequence	PDB	Escherichia coli [μg/ml]	Pseudomonas aeruginosa [μg/ml]	Staphylococcus aureus [μg/ml]	Reference
<i>α-helical</i>					
Magainin2 GIGKFLHSAKKFGKAFVGEIMNS	2MAG	5	100	50	(428)
MSI-78 GIGKFLKAKKFGKAFVKILKK		8	8	32	(429)
PGLa GMSKAGAIAGKIAKVALKAL		10-50	200-500	50-100	(430)
Melittin GIGAVLKVLTGLPALISWIKRKRQQ	2MLT	5	64-128	25	(431-433)
LL-37 LLGDFFRKSKEKIGKEFKRIVQRIKDF LRNLVPRTES	2K6O	5	32-128	31	(431, 434, 435)
<i>β-turn/ β-sheet</i>					
Tritrpticidin VRRFPWWPFLRR	ID6X	32	32	16	(436)
Protegrin-1 RGGRLCYCRRRFCVCVGR	1PG1	0.12	0.5		(437)
<i>cyclic</i>					
Polymyxin B DabTDabDabDabFLDabDabT		<1	<1	50-100	(438, 439)

Table S1-2-1 Minimal inhibitory concentrations taken from the given reference

7.2 Supplementary to Chapter 2

7.2.1 Supplementary to Chapter 2.3

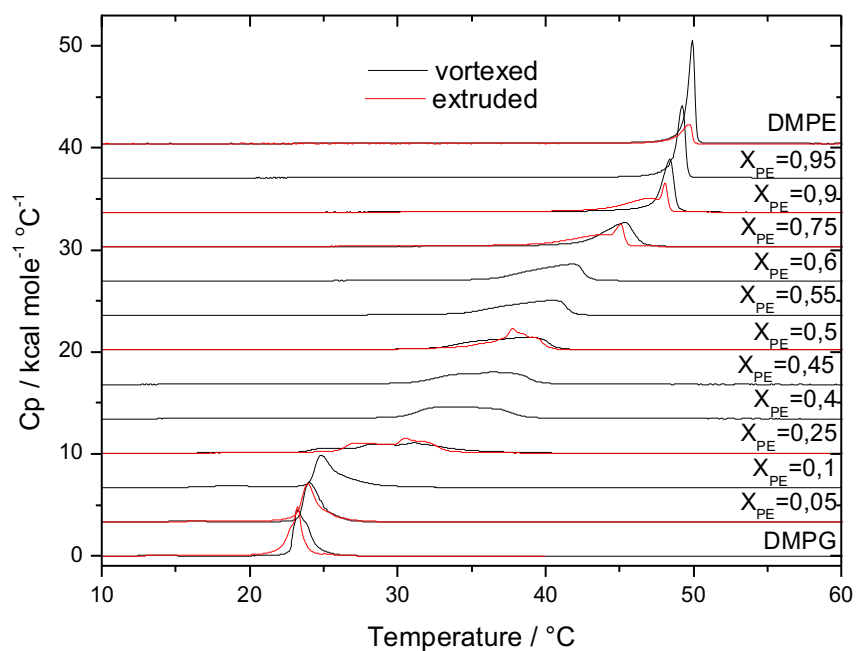


Figure S2-3-1 DSC heating thermograms of DMPG/DMPE mixtures with varying molar ratios

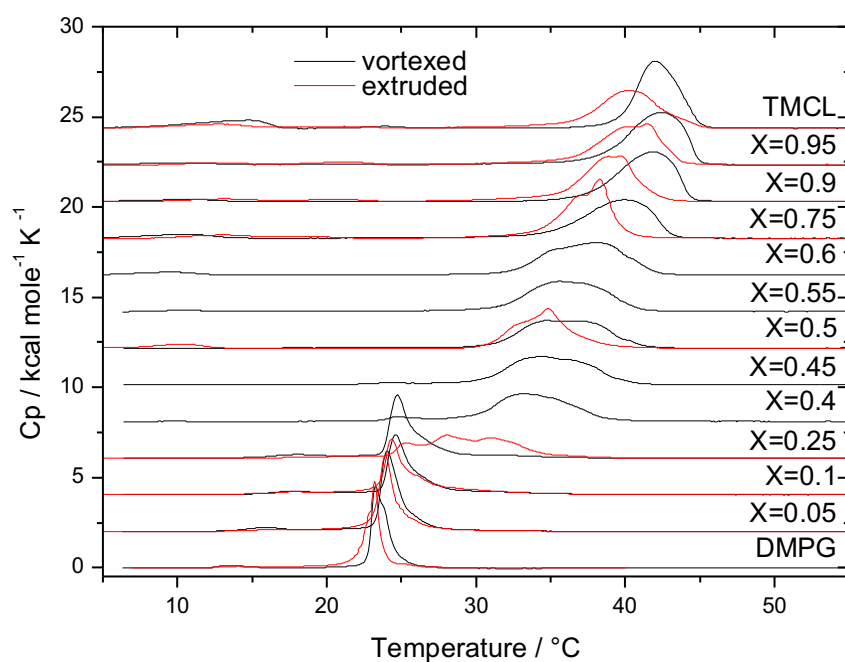


Figure S2-3-2 DSC heating thermograms of DMPG/TMCL mixtures with varying molar ratios

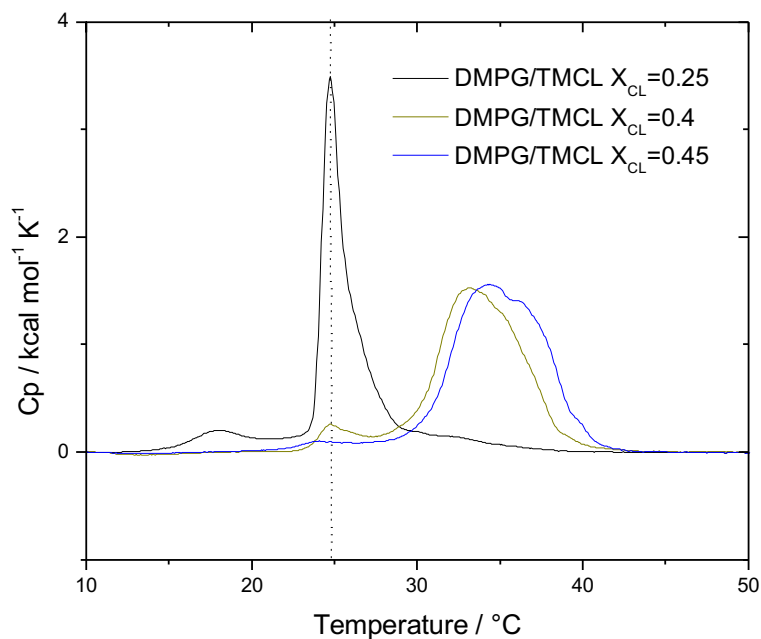


Figure S2-3-3 DSC curves of DMPG/TMCL mixtures of $X_{TMCL}=0.25, 0.4$ and 0.45 .

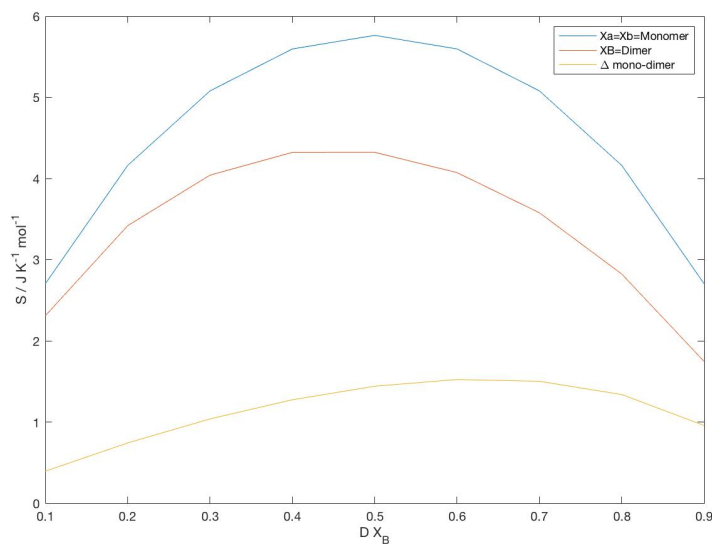


Figure S2-3-4 Entropy of mixing vs molar fraction for two monomers (blue) and a mono-dimer-mixture (red) wherein B is the dimer. The green line displays the difference between both mixing entropies.

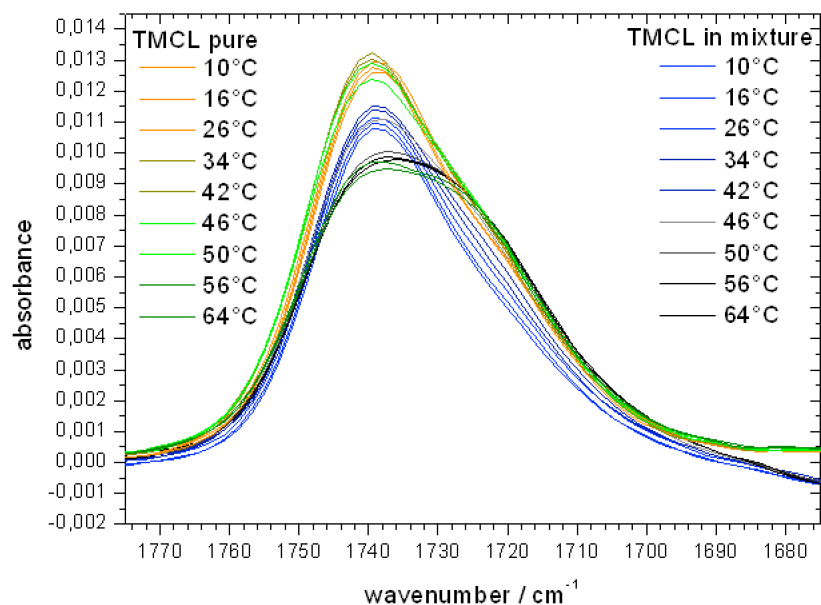


Figure S2-3-5 ATR-IR (Bio-ATR) temperature dependent lipid vesicle measurements. Selected spectra of C=O vibration of TMCL bilayer (orange to green) and DMPE-d₅₄/TMCL 1:1 mixture (blue to black) from 10 °C to 64 °C in D₂O (100 mM NaCl).

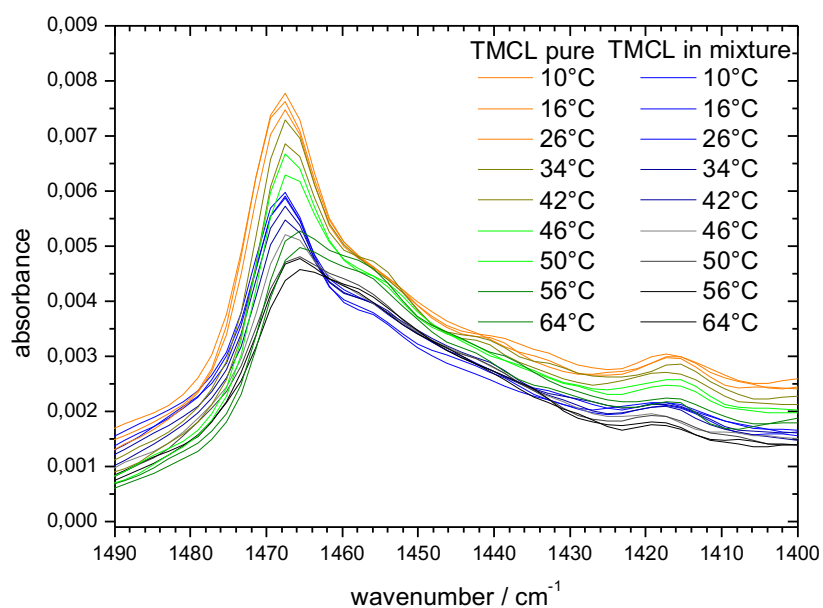


Figure S2-3-6 ATR-IR (Bio-ATR) temperature dependent lipid vesicle measurements. Selected spectra of CH₂ scissoring vibration of pure TMCL bilayer (orange to green) and DMPE-d₅₄/TMCL 1:1 mixture (blue to black) from 10 °C to 64 °C in D₂O (100 mM NaCl).

7.2.2 Supplementary to Chapter 2.4

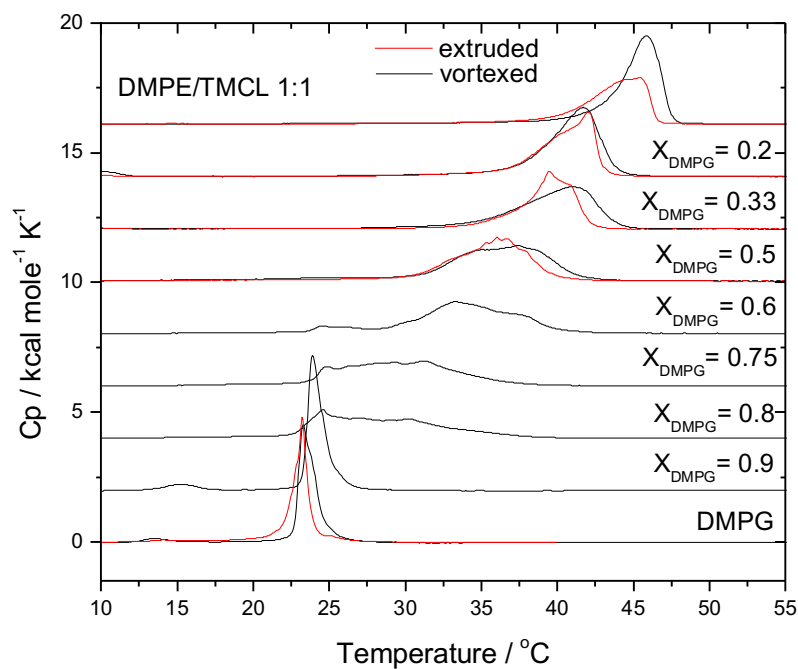


Figure S2-4-1 DSC thermograms of multilamellar (vortexed) and unilamellar (extruded) vesicles of ternary mixtures with increasing DMPG content in a DMPE/TMCL 1:1 mixture. For comparison the thermogram of the DMPE/TMCL 1:1 binary mixture and the pure DMPG is shown on top and bottom, respectively.

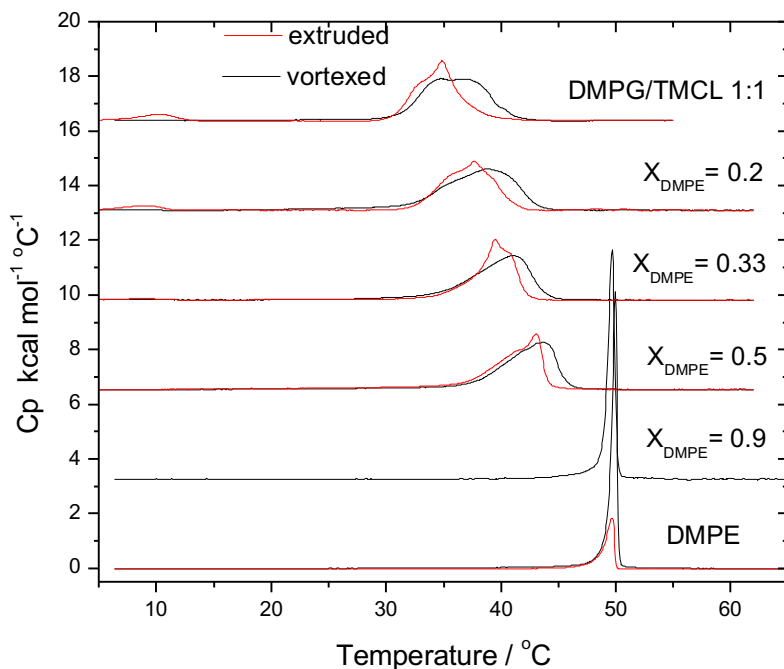


Figure S2-4-2 DSC thermograms of multilamellar (vortexed) and unilamellar (extruded) vesicles of ternary mixtures with increasing DMPE content in a DMPG/TMCL 1:1 mixture. For comparison the thermogram of the DMPG/TMCL 1:1 binary mixture and the pure DMPE is shown on top and bottom, respectively.

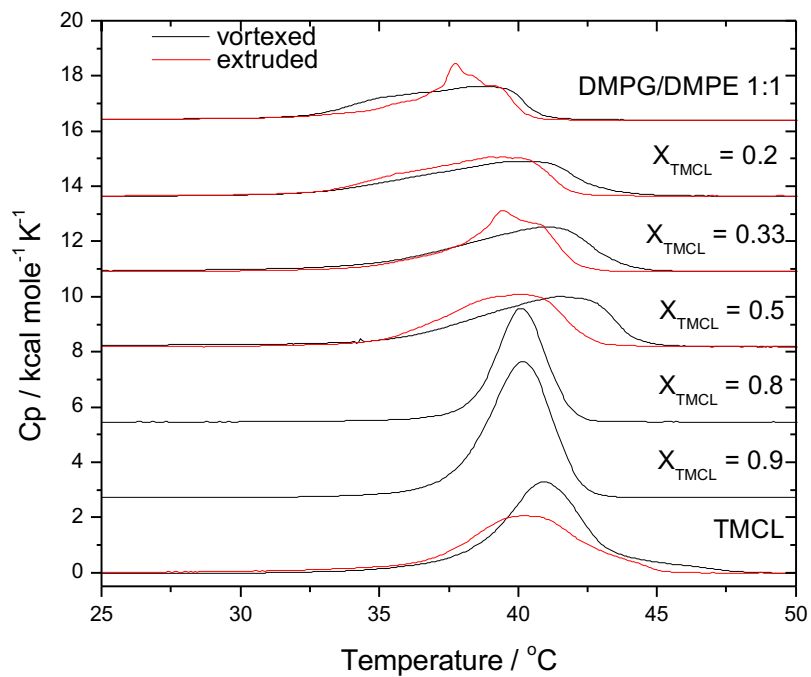


Figure S2-4-3 DSC thermograms of multilamellar vesicles of ternary mixtures with increasing TMCL content in a DMPG/DMPE 1:1 mixture. For comparison the thermogram of the DMPG/DMPE 1:1 binary mixture and the pure TMCL is shown on top and bottom, respectively.

7.3 Supplementary to Chapter 3

7.3.1 Supplementary to Chapter 3.1

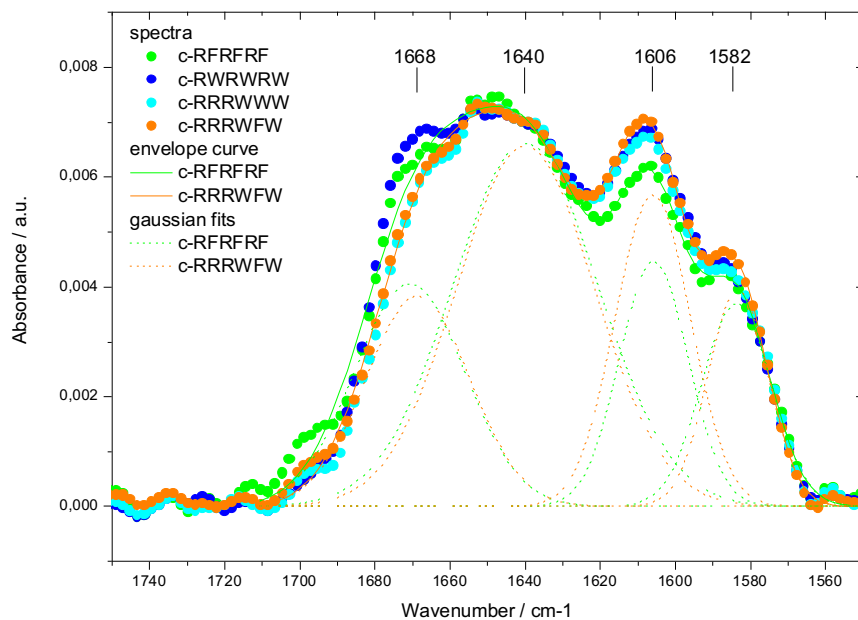


Figure S3-1-1 Amide I and Guanidinium bands of the different peptides at 10 °C in 100 mM NaCl pH 6.8 recorded using ATR-IR spectroscopy (circles). The curve fit subbands at 1668 cm^{-1} (1670 cm^{-1}), 1640 cm^{-1} , 1606 cm^{-1} and 1582 cm^{-1} are displayed for c-RFRFRF and c-RRRWFW (dashed lines). The line is resulting fitted envelope curve.

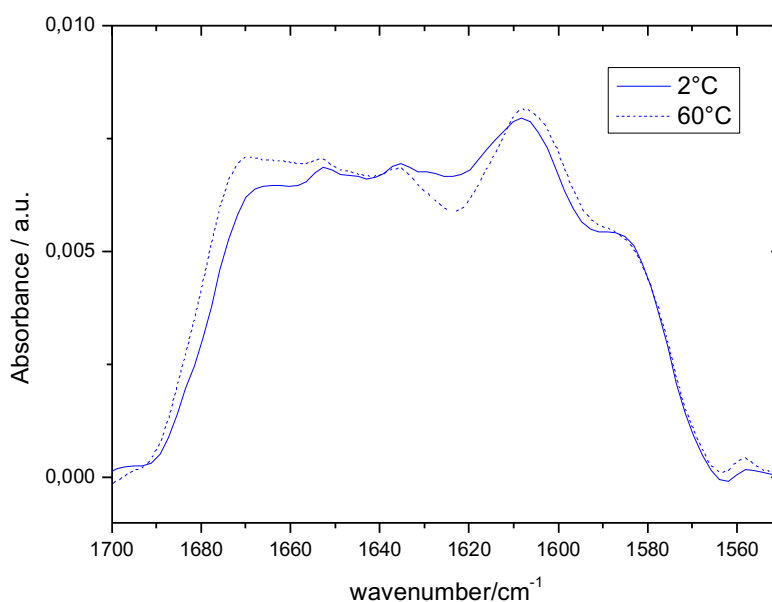


Figure S3-1-2 ATR-IR spectra of c-RWRWRW in D_2O NaCl 100mM at 2 °C and 60 °C. The spectra have been normalized at 1640 cm^{-1} .

Structure	Dihedral angle n+1		Dihedral angle n+2		Infrared absorption wavenumber	Occurrence within this turn-type
	Φ	Ψ	Φ	Ψ		
β -turn I	-60	-30	-90	0		38.2 %
β -turn I'	60	30	90	0		4.1 %
β -turn II	-60	120	80	0		11.8 %
β -turn II'	60	-120	-80	0		2.5 %
β -turn III	-60	-30	-60	-30		
β -turn III'	60	30	60	30	All β -turns show one absorption peak at 1690-1660 cm⁻¹ and one at 1645-1635 cm⁻¹	
β -turn IV ₁	-120	130	55	41		
β -turn IV ₂	-85	-15	-125	55		
β -turn IV ₃	-71	-30	-72	-47		
β -turn IV ₄	-97	-2	-117	-11		
β -turn IV _{misc.}						16.4 %
β -turn VI _{a1}	-60	120	-90	0		0.7 %
β -turn VI _{a2}	-120	120	-60	0		0.2 %
β -turn VI _b	-135	135	-75	160		0.9 %
β -turn VIII	-60	-30	-120	120		9.9 %
γ -turn	70 to 85	-60 to -70			For H-bonded γ -turns ~1625 cm⁻¹ and for non-H-bonded ≥1645 cm⁻¹	
reverse γ -turn	-70 to -85	60 to 70				

Table S3-1-1 Dihedral angles of the amino acid n+1 and n+2 in the respective turn structure (n is the 1←4 or 1←3 hydrogen bond forming amino acid, respectively) taken from de Brevern (265) and Kaur et al. (440). The infrared absorption wavenumbers were taken from Vass et al. (273, 275) and the percentages of occurring β -turn structures from de Brevern (265), respectively.

7.3.2 Supplementary to Chapter 3.2

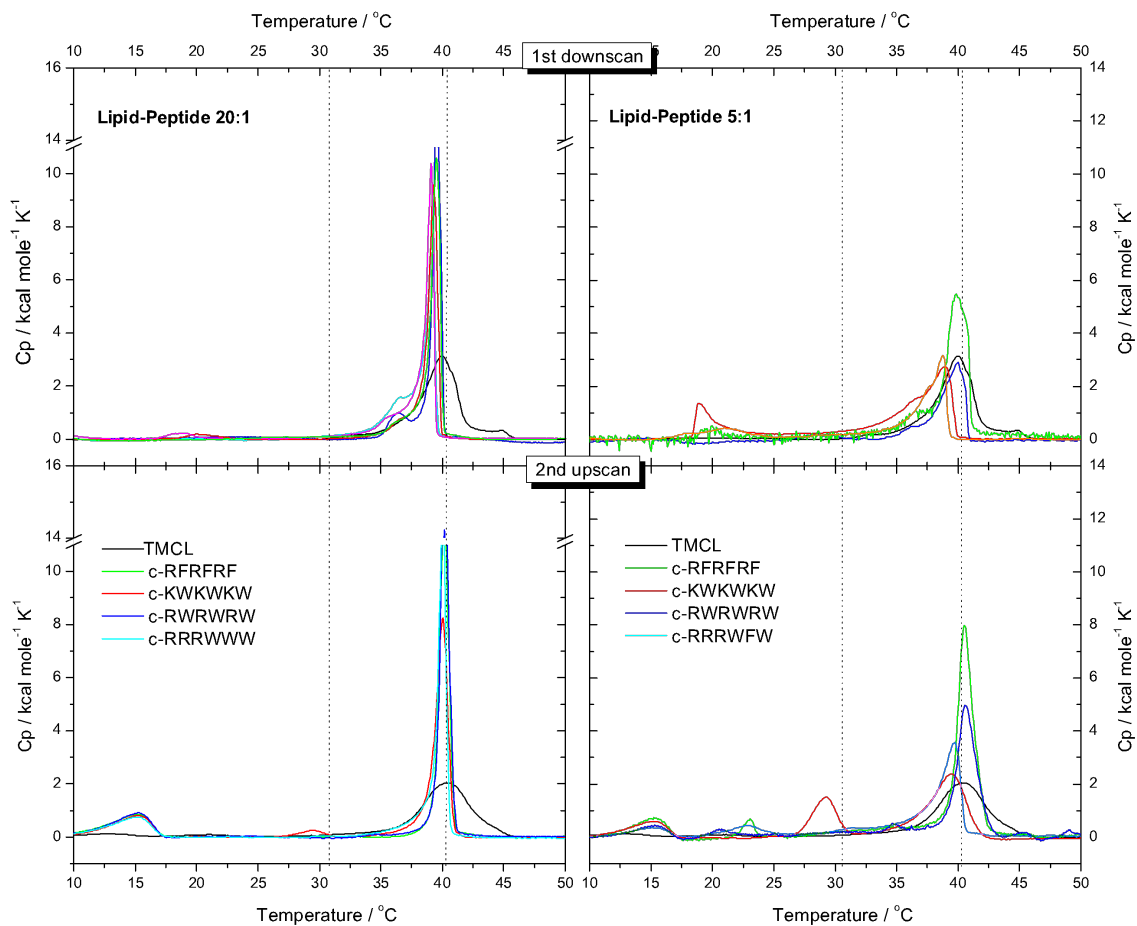


Figure S3-2-1 DSC thermograms of vesicles of TMCL (black) and TMCL after addition of the cyclic hexapeptides at a lipid-peptide ratio of 20:1 (left) and 5:1 (right). The first downscan (up) and second upscan (bottom) is shown. The dotted black line at the phase transition temperatures of pure TMCL should guide the eye.

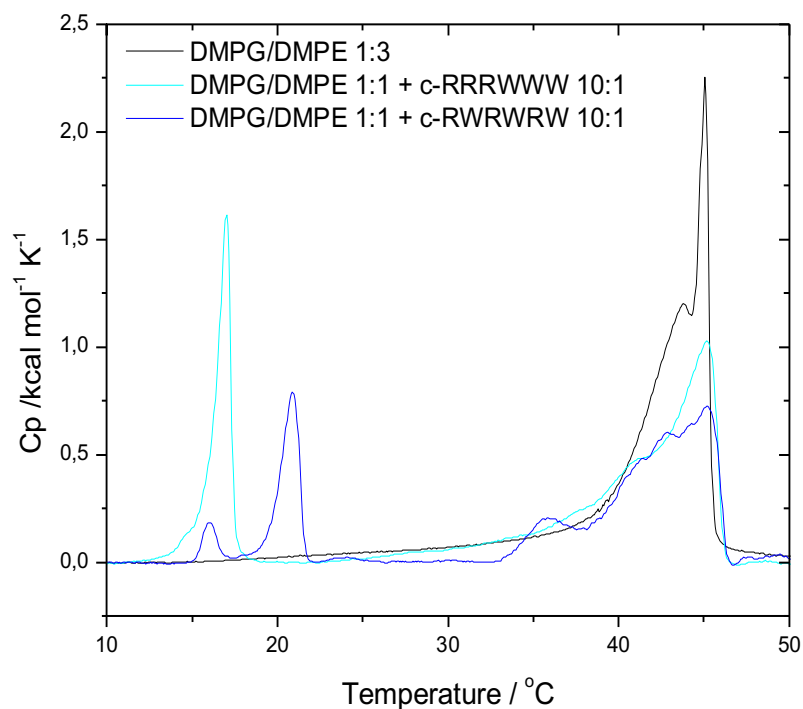


Figure S3-2-2 DSC thermograms of DMPG/DMPE 1:1 mixture with added c-RWRWRW and c-RRRWWW in a 10:1 lipid-peptid ratio, respectively, and pure DMPG/DMPE 3:1 mixture for comparison.

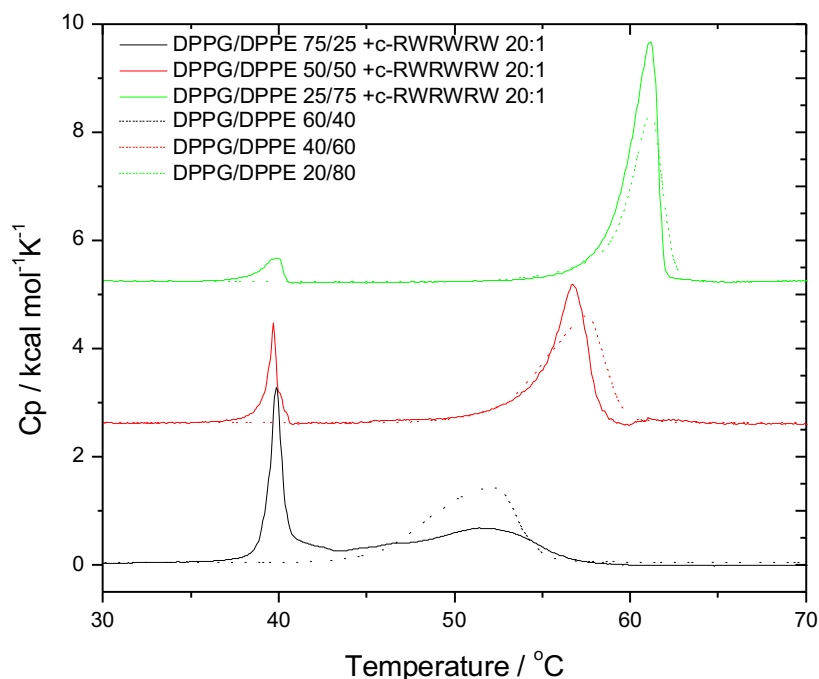


Figure S3-2-3 DSC thermograms of DPPG/DPPE 3:1, 1:1 and 1:3 mixtures with added c-RWRWRW in a 20:1 lipid-peptid ratio (solid lines) and pure DPPG/DPPE mixtures of 3:2, 2:3 and 1:4 ratio for comparison (dotted line).

7.3.3 Supplementary to Chapter 3.3

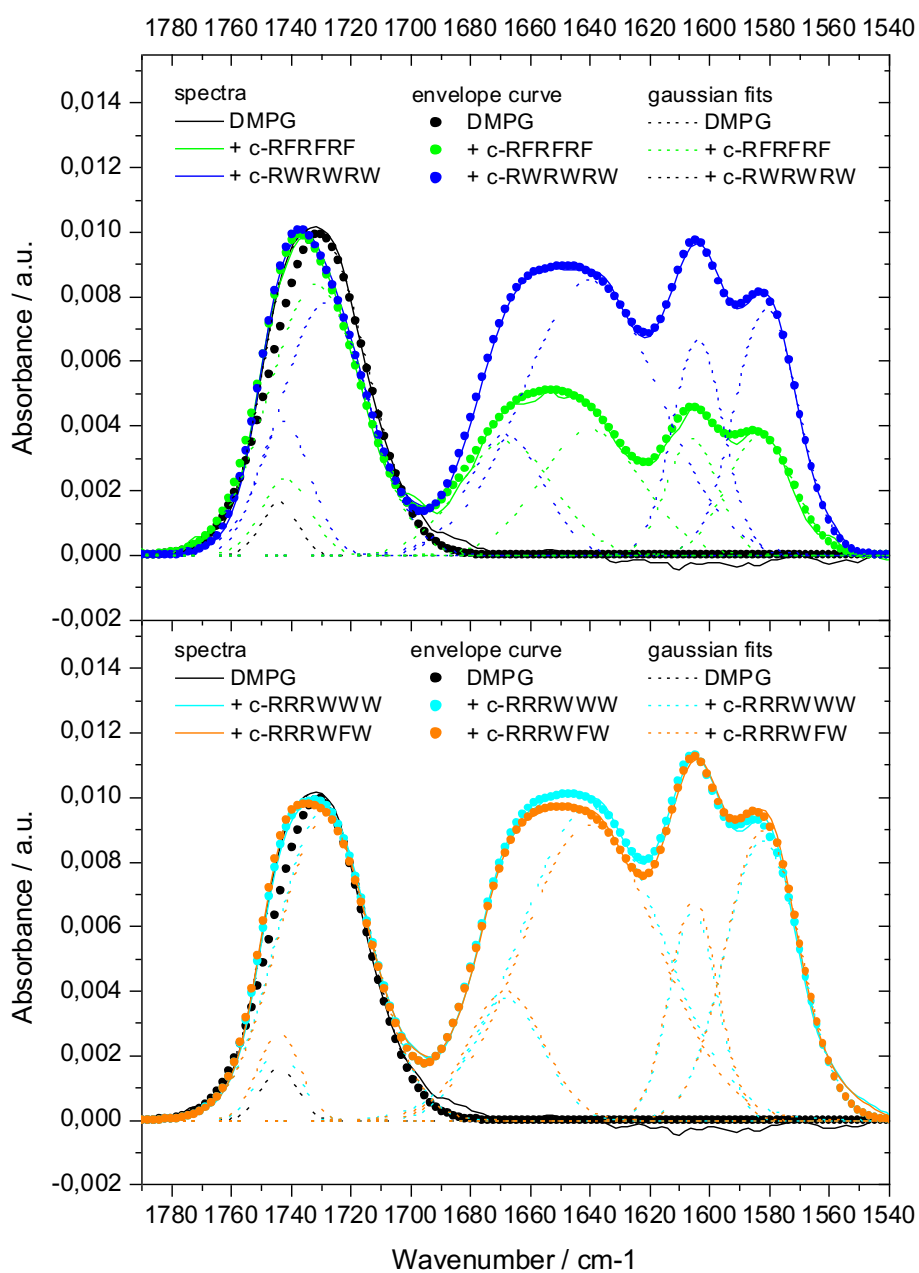


Figure S3-3-1 Carbonyl band of DMPG (pure in black), amide I and guanidinium bands of the different peptides bound to DMPG at 10 °C in 100 mM NaCl pH 6.8 recorded using ATR-IR spectroscopy (lines). The curves were fitted with subbands at 1668 cm^{-1} (1670 cm^{-1}), 1640 cm^{-1} , 1605 cm^{-1} and 1585 cm^{-1} (dashed lines). The resulting fitted curve is plotted in dots.

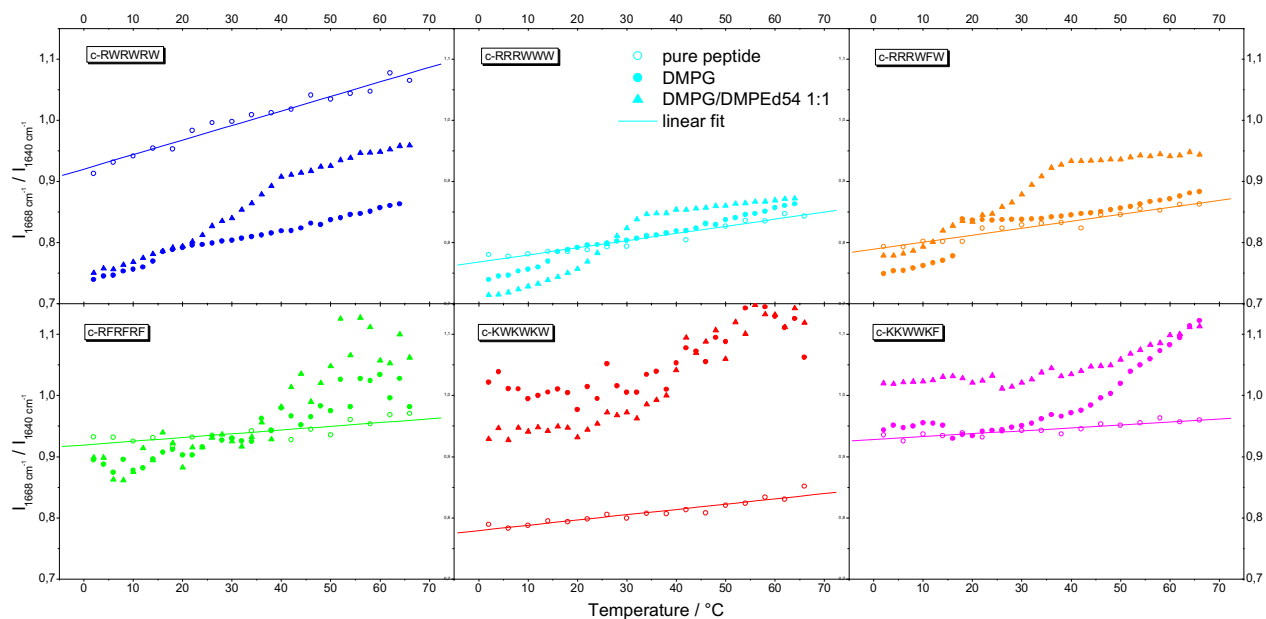


Figure S3-3-2 Temperature dependence of the amide I band intensity ratio at $1668\text{ cm}^{-1}/1640\text{ cm}^{-1}$ of the various peptides pure (open circles) with the respective linear fit (line) and bound to DMPG (filled circles) and DMPG/DMPE-d₅₄ 1:1 mixture (filled triangles). The lipid-peptide ratio was 2:1.

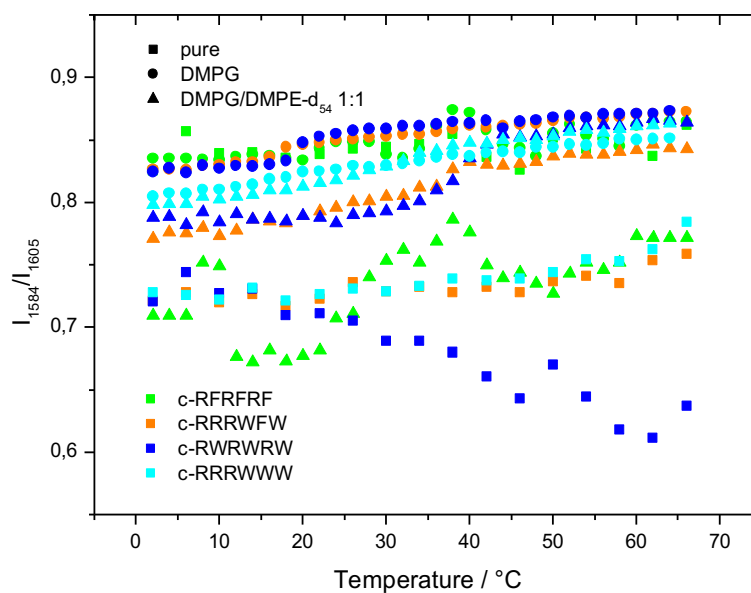


Figure S3-3-3 Temperature dependence of the guanidinium band intensity ratio at $1584\text{ cm}^{-1}/1605\text{ cm}^{-1}$ of the various peptides pure, bound to DMPG and DMPG/DMPE-d₅₄ 1:1 mixture. The lipid-peptide ratio was 2:1. The data of c-RFRFRF bound to DMPG and DMPG/DMPE-d₅₄ 1:1 mixture was averaged using Savitzky-Golay 5 point averaging method implemented in Origin software.

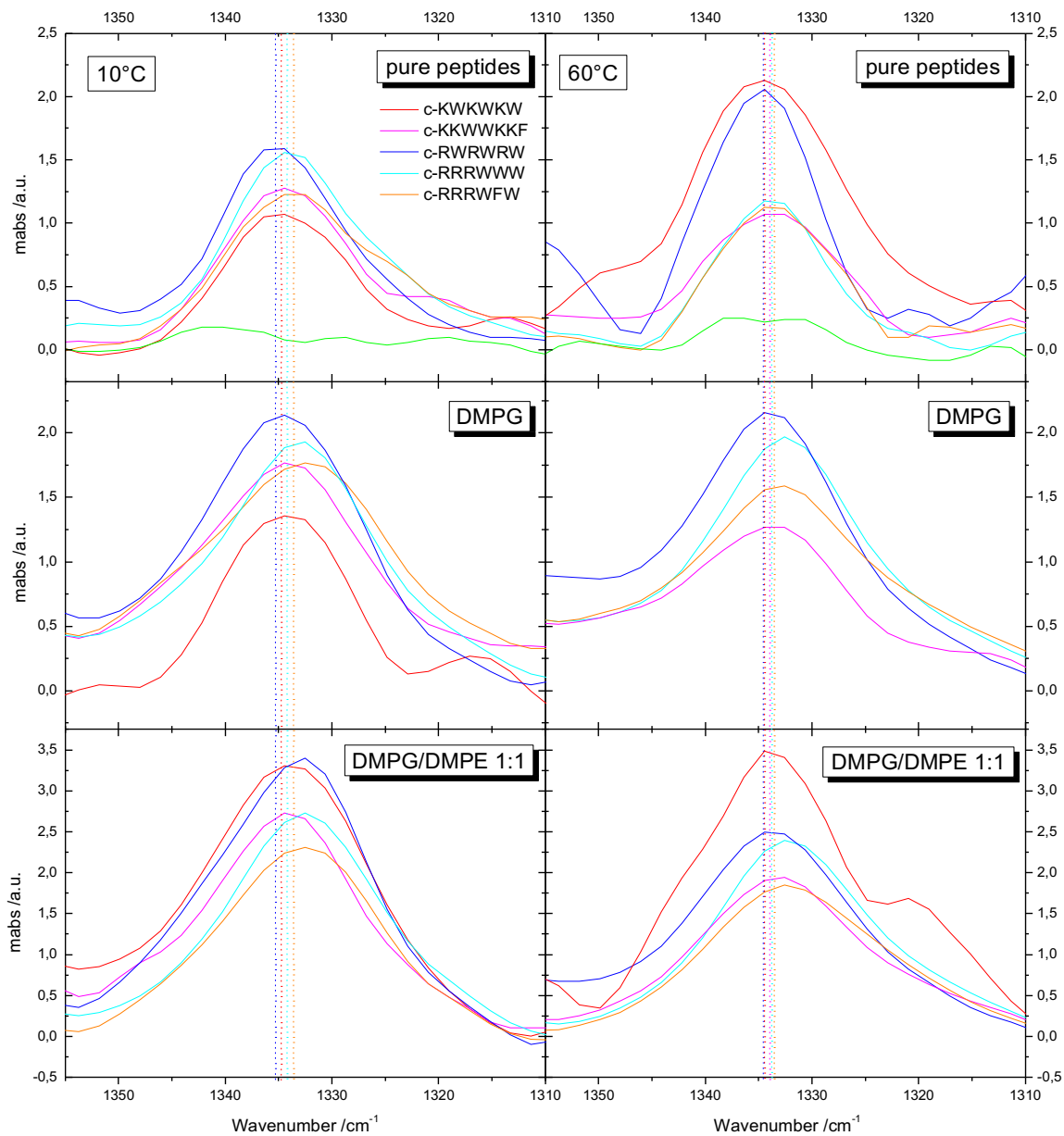


Figure S3-3-4 Tryptophan band at 1333 cm^{-1} of the different peptides in solution (top), bound to DMPG (middle) and interacting with DMPG/DMPE- d_{54} 1:1 mixture (bottom) at $10\text{ }^{\circ}\text{C}$ (left) and $60\text{ }^{\circ}\text{C}$ (right). The lipid-peptide ratio was 2:1. The dotted lines depict the peak maximum of the peptides in solution to guide the eye.

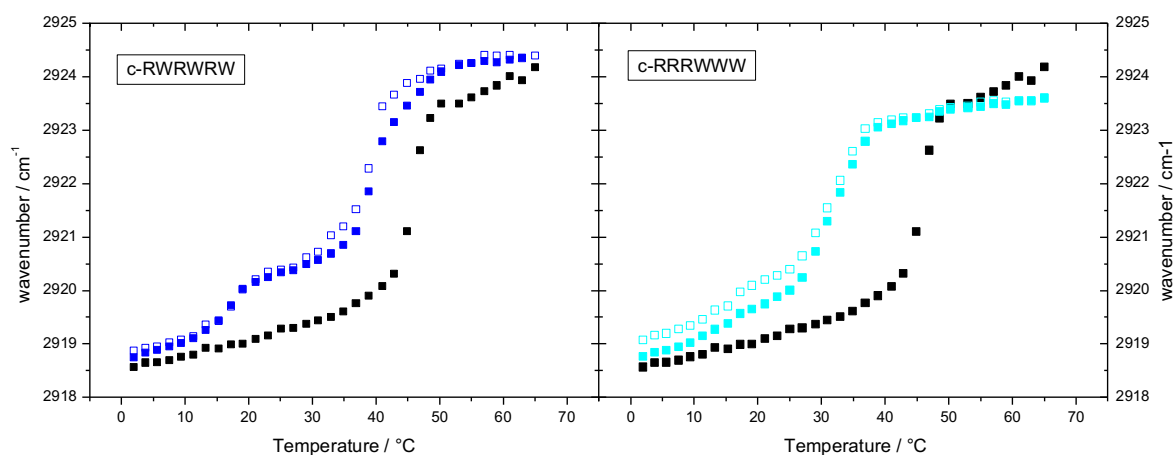


Figure S3-3-5 ATR-IR temperature dependent measurements. Antisymmetric CH_2 vibrational band of TMCL in a pure TMCL/DMPE- d_{54} 1:1 mixture (black) and interacting with c-RWRWRW (left) and c-RRRWWW (right). The 1st (open squares) and 2nd (filled squares) upscans are displayed. The lipid-peptide ratio was 2:1.

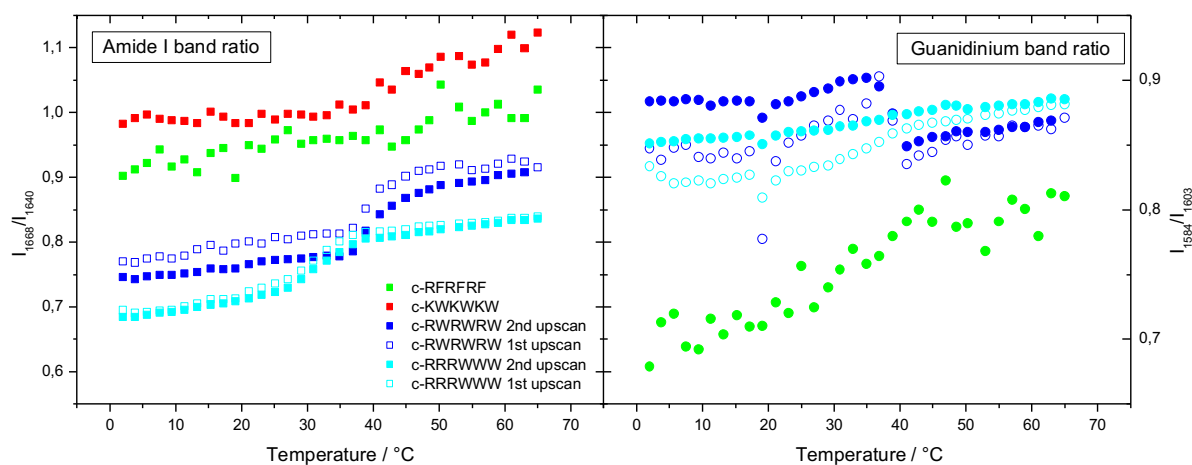


Figure S3-3-6 ATR-IR temperature dependent measurement of the amide I band intensity ratio I_{1668}/I_{1640} (left) and the guanidinium band intensity ratio at I_{1584}/I_{1603} (right) of the different peptides interacting with the TMCL/DMPE- d_{54} 1:1 mixture. The lipid-peptide ratio was 2:1.

7.3.4 Supplementary to Chapter 3.4

Peptide	Charge	Lipid	T/°C	K/M ⁻¹	$\Delta H/\text{kcal mol}^{-1}$	$\Delta G/\text{kcal mol}^{-1}$	T $\Delta S/\text{kcal mol}^{-1}$	Ref.
GL13K GKIKLKASLKLL	+4	DOPG	22	$10^6\text{-}10^7$	1.5	-19	20.5	(441)
		DOPC	22	No interaction	-	-	-	
Gramicidin S e-(VOLdFP) ₂	+2	POPG	25	$9.6 \cdot 10^4\text{-}$ $9.3 \cdot 10^5$	2.6	-12.1	14.7	(442)
		POPC	25	$1.5 \cdot 10^3\text{-}$ $1.4 \cdot 10^4$	2.7	-11	13.8	
		POPG/POPC 1:3	25	$1.5 \cdot 10^4\text{-}$ $2.4 \cdot 10^5$	2.6	-10.9	13.5	
Tritrpticidin VRRFPWWPFLRR	+4	POPC	37	$1.2 \cdot 10^4$	-11	-5.8	-5.2	(443)
		POPG/POPE 3:7		$1.4 \cdot 10^6$	-4.7	-8.7	4.0	
Gomesin ZCRLCYKQRCVTYCR GR-NH ₂	+6	POPG/POPC 1:1	25	$5 \cdot 10^5$	-7	-10.1	-3.1	(444)
		POPG/POPC 1:3	25	$1 \cdot 10^4$	-5.6	-7.8	2.2	
HHC-36 KRWWKWWRR	+5	POPG/POPC 1:1	37	$6.9 \cdot 10^5$	-16	-10.7	-5.3	(445)
		POPG/POPE 1:1		$7.5 \cdot 10^5$	-7.2	-10.8	3.6	
PGLa GMASKAGAIAGKIAKV ALKAL-NH ₂	+4	POPC	30	$8 \cdot 10^2$	-11	-6.4	-4.6	(446)
		POPG/POPC 1:3	15	$1.4 \cdot 10^3$	-12.3	-6.5	-5.8	
			30	$1.5 \cdot 10^3$	-12.3	-6.8	-5.5	
	45	$1.3 \cdot 10^3$	-14.6	-7.1	-7.5			

Table S3-4-1 Thermodynamic parameters of different antimicrobial peptides interacting with model lipid membranes determined by ITC measurements.

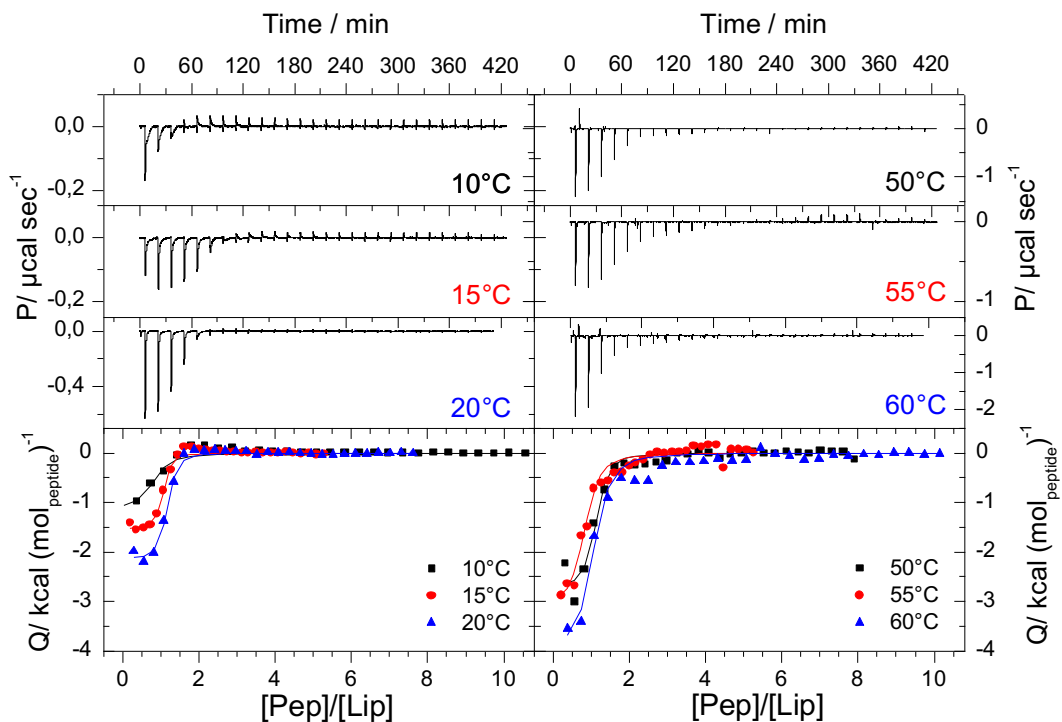


Figure S3-4-1 ITC titration curves of DPPG vesicle suspension titrated into 40 μM c-RRWRF solution. 10 $^{\circ}\text{C}$ and 60 $^{\circ}\text{C}$: 2 mM DPPG. 15 $^{\circ}\text{C}$ and 55 $^{\circ}\text{C}$: 1 mM DPPG. 20 $^{\circ}\text{C}$ and 50 $^{\circ}\text{C}$: 1.5 mM DPPG. All solutions contained 20 mM phosphate buffer (pH 7.2, $I = 100$ mM). Bottom figures: Heat of binding Q in kcal mol^{-1} of lipid vs. lipid-peptide ratio (left: 10 $^{\circ}\text{C}$ - 20 $^{\circ}\text{C}$, right: 50 $^{\circ}\text{C}$ - 60 $^{\circ}\text{C}$).

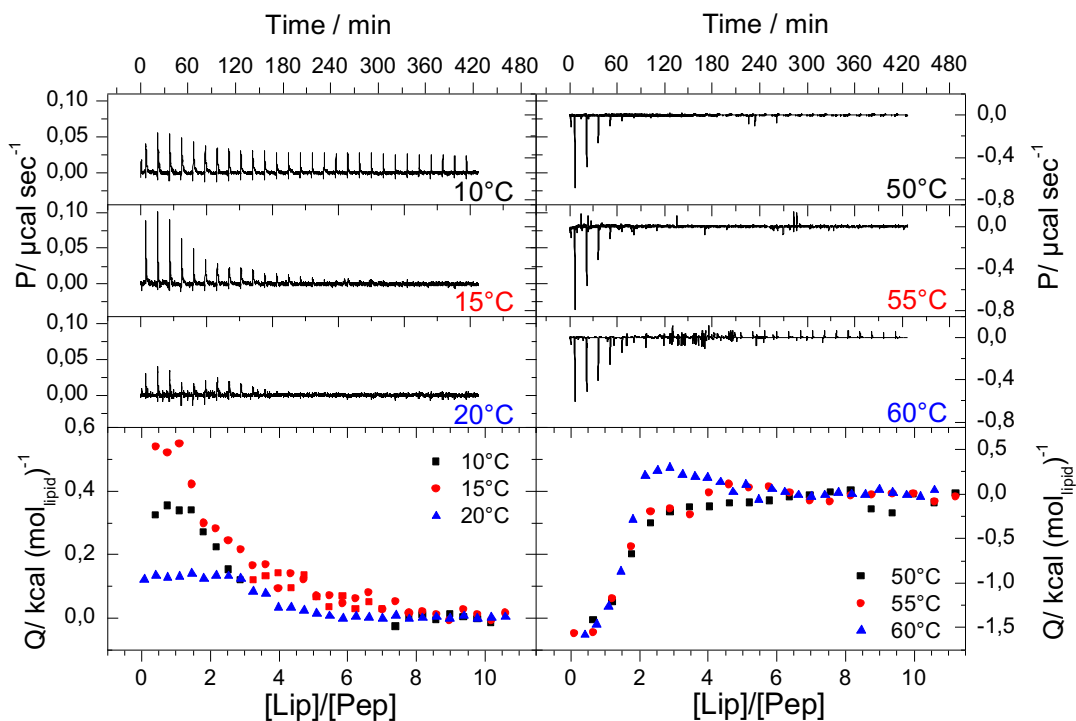


Figure S3-4-2 ITC titration curves of DPPG vesicle suspension titrated into 20 μM c-RFRFRF solution. 10 $^{\circ}\text{C}$, 15 $^{\circ}\text{C}$, 20 $^{\circ}\text{C}$ and 50 $^{\circ}\text{C}$: 1 mM DPPG. 55 $^{\circ}\text{C}$ and 60 $^{\circ}\text{C}$: 1.6 mM DPPG. All solutions contained 20 mM phosphate buffer (pH 7.2, $I = 100$ mM). Bottom figures: Heat of binding Q in kcal mol^{-1} of lipid vs. lipid-peptide ratio (left: 10 $^{\circ}\text{C}$ - 20 $^{\circ}\text{C}$, right: 50 $^{\circ}\text{C}$ - 60 $^{\circ}\text{C}$).

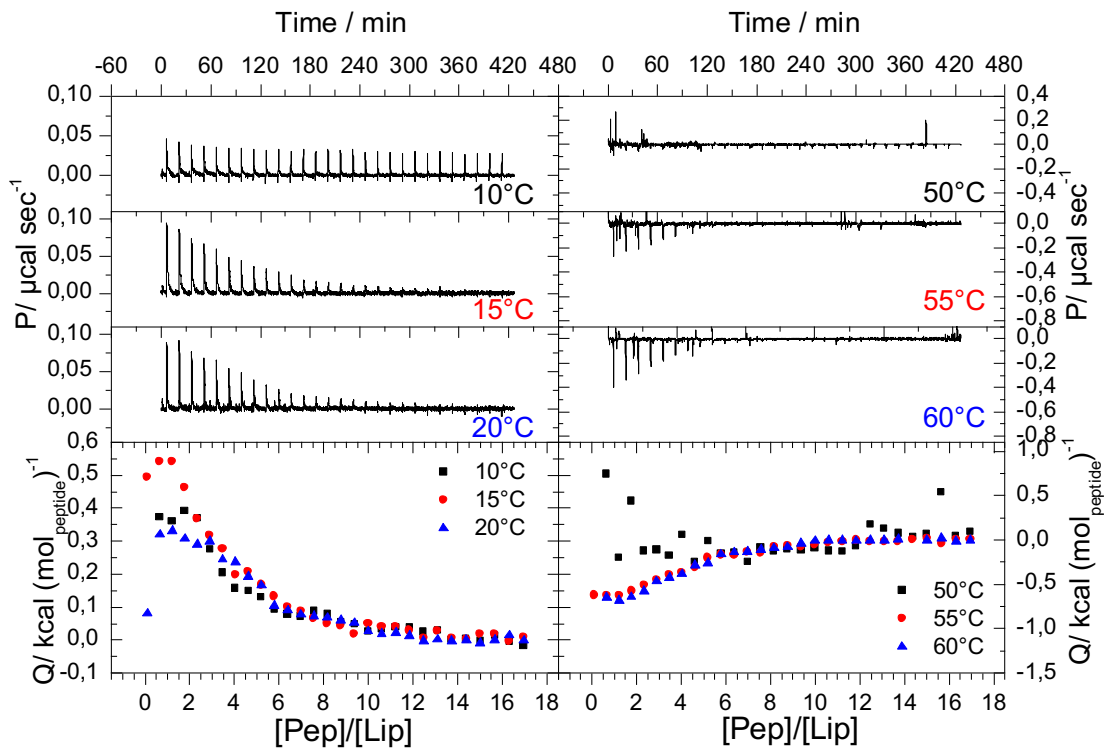


Figure S3-4-3 ITC titration curves of DPPG vesicle suspension titrated into c-KWKWKW solution. At 10 °C 0.8 mM DPPG are titrated into 10 μM c-RFRFRF solution. At 15 °C, 20 °C, 50 °C, 55°C and 60 °C 1.6 mM DPPG are titrated in 20 μM c-RFRFRF solution. All solutions contained 20 mM phosphate buffer (pH 7.2, I = 100 mM) with 100 mM NaCl. Bottom figures: Heat of binding Q in kcal mol⁻¹ of lipid vs. lipid-peptide ratio (left: 10 °C - 20 °C, right: 50 °C - 60 °C).

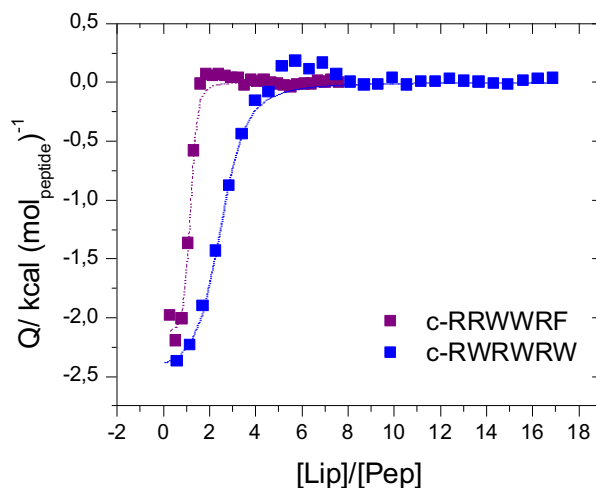


Figure S3-4-4 Heat of binding vs. lipid-peptide ratio at 20 °C of 1.5 mM DPPG titrated into 40 μM c-RRWRF and 0.8 mM DPPG titrated into 10 μM c-RWRWRW solution.

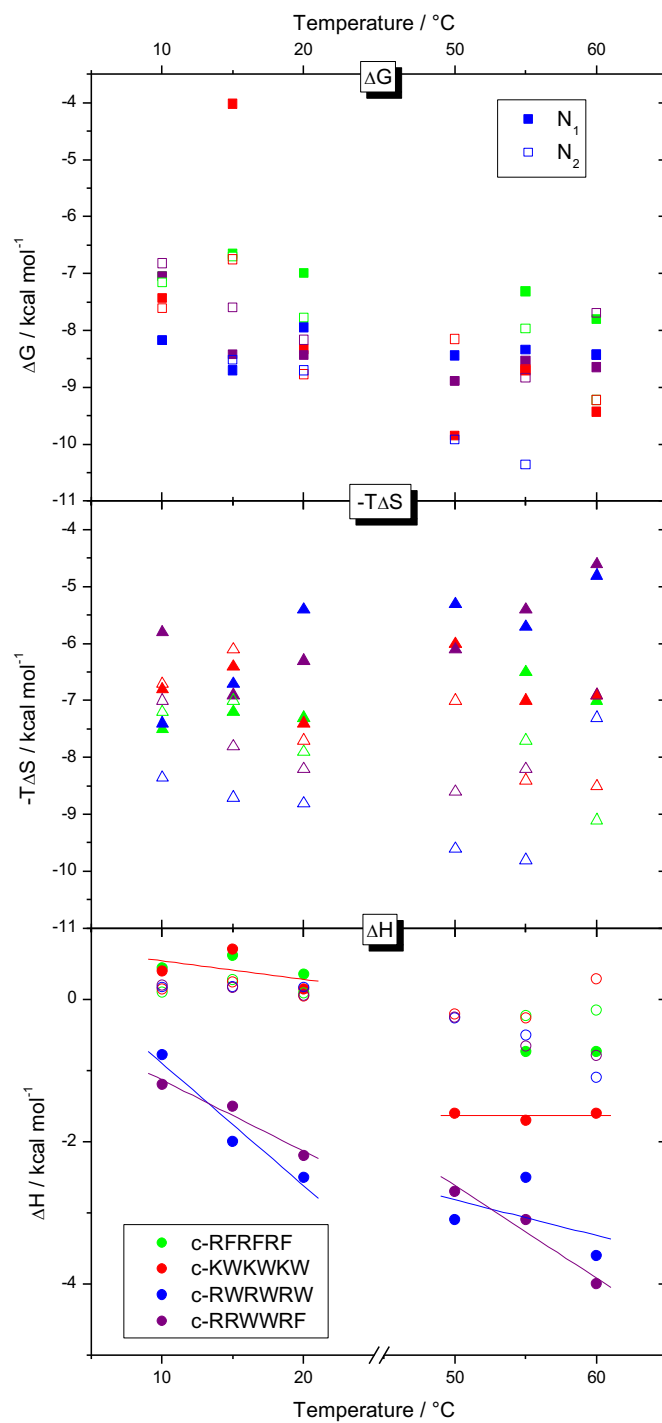


Figure S3-4-5 Temperature dependence of ΔG° , $-T\Delta S^\circ$ and ΔH° of c-RFRFRF, c-KWKWKW, c-RWRWRW and c-RRWWRW for the two processes with the stoichiometry value N1 (filled data points) and N2 (open data points).

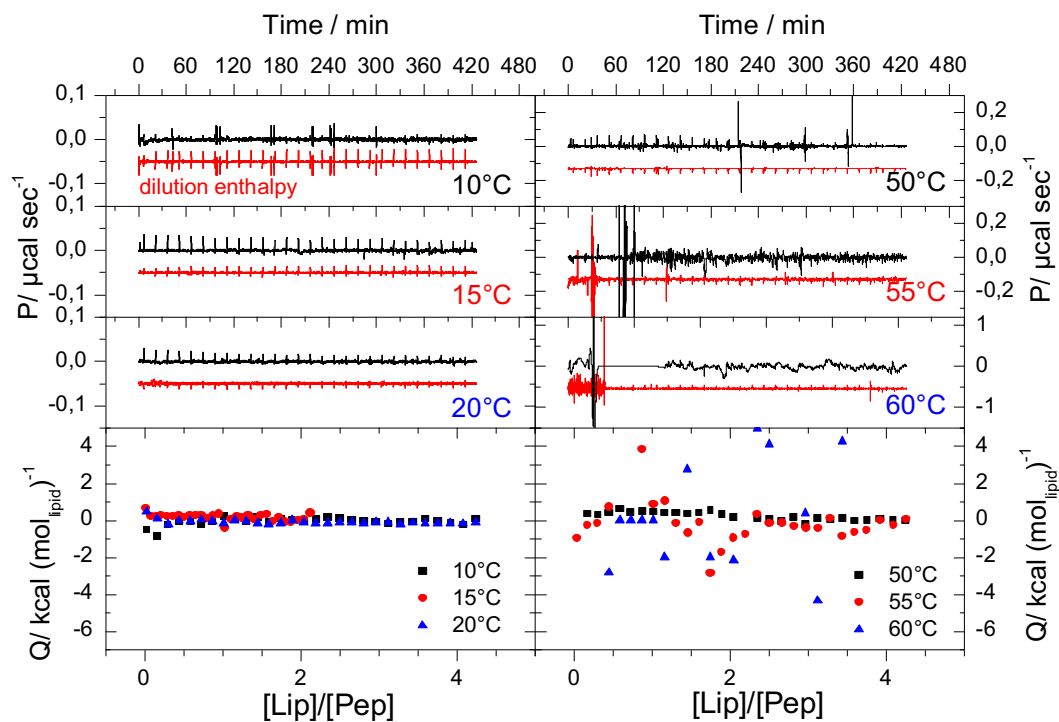


Figure S3-4-6 ITC titration curves of 400 μM TMCL vesicle suspension (100 nm vesicles in phosphate buffer pH 7.2, $I = 100$ mM) titrated into 20 μM c-RFRFRF solution at 10 $^{\circ}\text{C}$, 20 $^{\circ}\text{C}$, 50 $^{\circ}\text{C}$, 55 $^{\circ}\text{C}$ and 60 $^{\circ}\text{C}$ and 40 μM at 15 $^{\circ}\text{C}$. Bottom figures: Heat of binding Q in kcal mol^{-1} of lipid vs. lipid-peptide ratio.

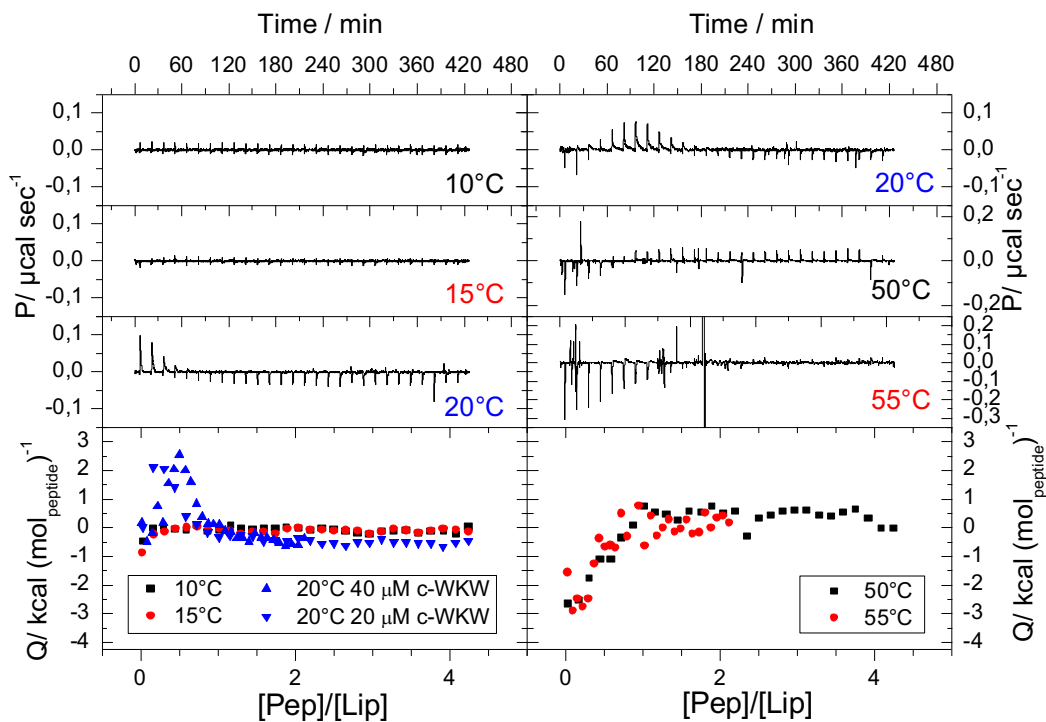


Figure S3-4-7 400 μM TMCL suspension (100nm vesicles in phosphate buffer pH 7.2, $I = 100$ mM) titrated into 20 μM c-KWKWKW solution at 10 $^{\circ}\text{C}$, 15 $^{\circ}\text{C}$, 20 $^{\circ}\text{C}$ and 50 $^{\circ}\text{C}$ and 40 μM c-KWKWKW solution at 20 $^{\circ}\text{C}$ and 55 $^{\circ}\text{C}$. Top three left and right: Titration curves. Bottom left: Heat of binding vs. lipid-peptide ratio at 10 $^{\circ}\text{C}$ - 20 $^{\circ}\text{C}$. Bottom right: Heat of binding vs. lipid-peptide ratio at 50 $^{\circ}\text{C}$ and 55 $^{\circ}\text{C}$.

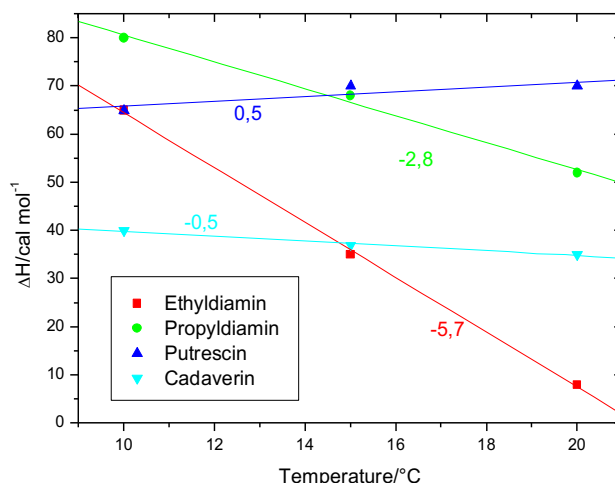


Figure S3-4-8 Temperature dependence of the averaged first five integrated heats of binding per mol of 10 mM DPPG solution injected in to the respective 150 μM polyamine solution. The slope ($\Delta R C_p$) values are depicted in the Figure.

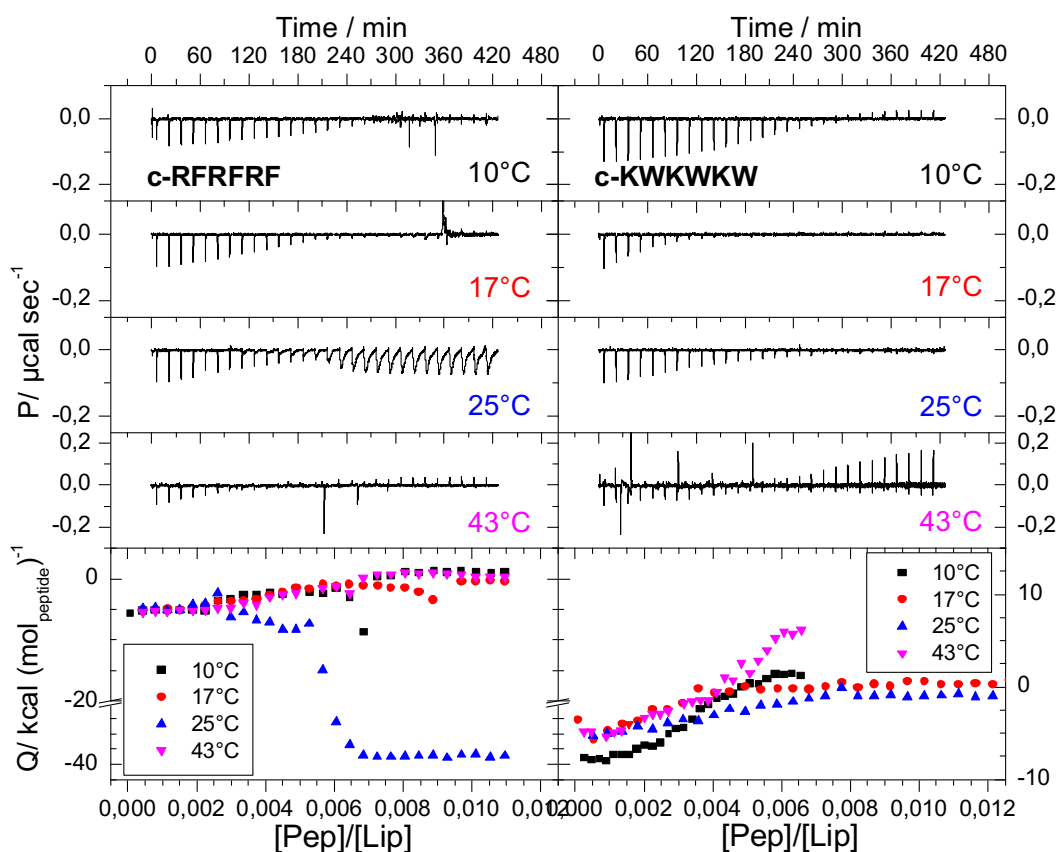


Figure S3-4-9 *top*: ITC titration curves (heating power vs. time) of 62 μM c-RFRFRF (left panels) titrated into a 1.2 mM and c-KWKWKW (right panels) titrated into 2 mM (10 $^{\circ}\text{C}$ and 43 $^{\circ}\text{C}$) and 1 mM (17 $^{\circ}\text{C}$ and 25 $^{\circ}\text{C}$) DPPG/DPPE (1:1) vesicle suspension at the indicated temperatures. *bottom*: integrated heats per mol injected peptide vs. peptide-lipid ratio of the respective titration curve at 10 $^{\circ}\text{C}$ (square), 17 $^{\circ}\text{C}$ (circle), 25 $^{\circ}\text{C}$ (triangle) and 43 $^{\circ}\text{C}$ (inverse triangle).

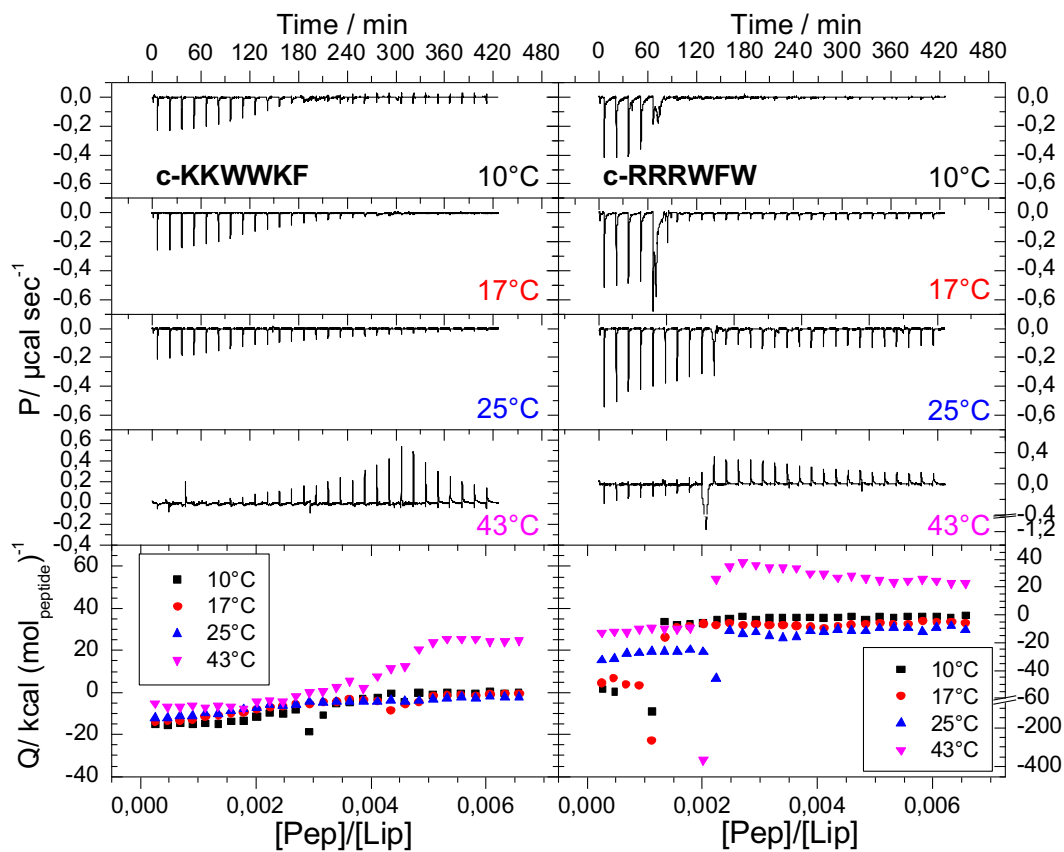


Figure S3-4-10 *top*: ITC titration curves (heating power vs. time) of 62 μM c-KKWWKF (left panels) and c-RRRWWF (right panels) titrated into a 2 mM DPPG/DPPE (1:1) vesicle suspension at the indicated temperatures. *bottom*: integrated heats per mol injected peptide vs. peptide-lipid ratio of the respective titration curve at 10 °C (square), 17 °C (circle), 25 °C (triangle) and 43 °C (inverse triangle).

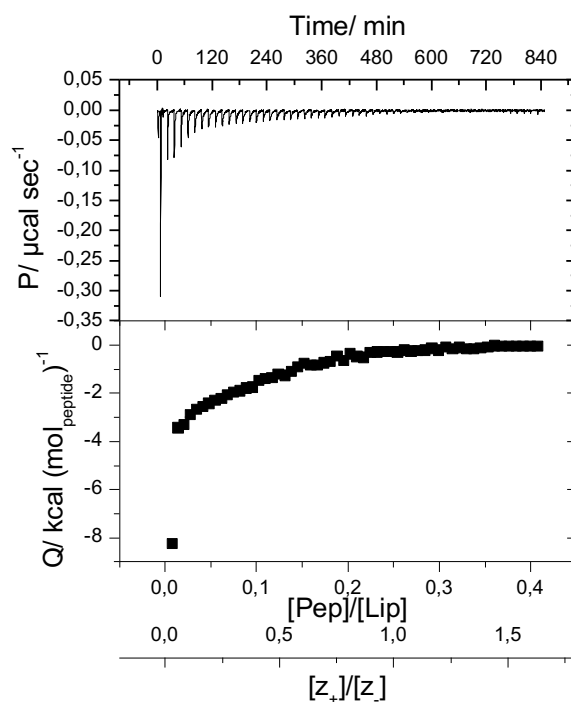


Figure S3-4-11 Titration of 400 μM c-RRRWFW into 250 μM DPPG/DPPE 3:1 at 20 $^{\circ}\text{C}$ (phosphate buffer pH 7.2, I = 100 mM). Top: Titration curve. Bottom: Heat of binding vs. lipid-peptide ratio (square) and the respective fit (line).

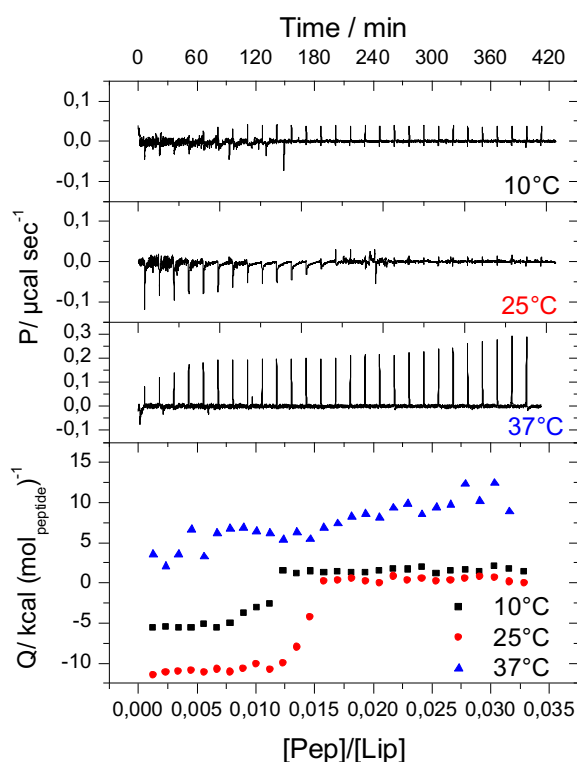


Figure S3-4-12top: ITC titration curves of 62 μM c-KWKWKW solution into 400 μM TMCL/DMPE 1:1 vesicle suspension at 10 $^{\circ}\text{C}$, 25 $^{\circ}\text{C}$ and 37 $^{\circ}\text{C}$. All solutions contained 20 mM phosphate buffer (pH 7.2, I = 100 mM). Bottom: integrated heats per mol injected peptide vs. peptide-lipid ratio of the respective titration curve at 10 $^{\circ}\text{C}$ (square), 25 $^{\circ}\text{C}$ (circle), 37 $^{\circ}\text{C}$ (triangle).

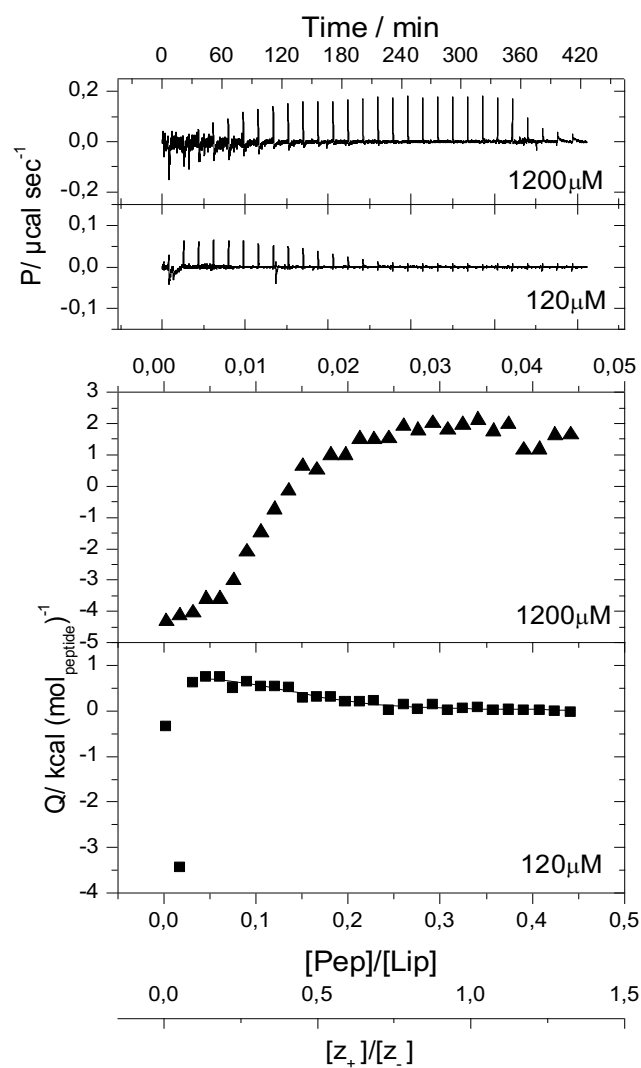


Figure S3-4-13 250 μM c-RFRFRF solution titrated into 1.2 mM and 120 μM TMCL/DMPE 1:1 lipid suspension (100 nm vesicles in phosphate buffer pH 7.2, I = 100 mM) at 27 $^{\circ}\text{C}$.

8

Bibliography

1. Luisi, P. L., P. Walde, and T. Oberholzer. 1999. Lipid vesicles as possible intermediates in the origin of life. *Current Opinion in Colloid & Interface Science* 4:33-39.
2. Walde, P., R. Wick, M. Fresta, A. Mangone, and P. L. Luisi. 1994. Autopoietic self-reproduction of fatty-acid vesicles. *Journal of the American Chemical Society* 116:11649-11654.
3. Trevors, J. T. 2003. Early assembly of cellular life. *Progress in Biophysics and Molecular Biology* 81:201-217.
4. Heimburg, T. 2007. *Thermal biophysics of membranes*. Wiley-VCH, Weinheim.
5. Jensen, M. Ø., and O. G. Mouritsen. 2004. Lipids do influence protein function—the hydrophobic matching hypothesis revisited. *Biochimica et Biophysica Acta (BBA) - Biomembranes* 1666:205-226.
6. Celesia, G. G. 2001. Disorders of membrane channels or channelopathies. *Clinical Neurophysiology* 112:2-18.
7. Florent-Béchar, S., C. Desbène, P. Garcia, A. Allouche, I. Youssef, M.-C. Escanyé, V. Koziel, M. Hanse, C. Malaplate-Armand, C. Stenger, B. Kriem, F. T. Yen-Potin, J. L. Olivier, T. Pillot, and T. Oster. 2009. The essential role of lipids in alzheimer's disease. *Biochimie* 91:804-809.
8. Kosicek, M., and S. Hecimovic. 2013. Phospholipids and alzheimer's disease: Alterations, mechanisms and potential biomarkers. *International Journal of Molecular Sciences* 14:1310-1322.
9. Yadav, R. S., and N. K. Tiwari. 2014. Lipid integration in neurodegeneration: An overview of alzheimer's disease. *Molecular Neurobiology* 50:168-176.
10. Mouritsen, O. G. 2011. Lipidology and lipidomics—quo vadis? A new era for the physical chemistry of lipids. *Physical Chemistry Chemical Physics* 13:19195-19111.
11. Danielli, J., and H. Davson. 1935. A contribution to the theory of permeability of thin films. *Journal of Cellular and Comparative Physiology* 5.
12. Goñi, F. M. 2014. The basic structure and dynamics of cell membranes: An update of the singer–nicolson model. *Biochimica et Biophysica Acta (BBA) - Biomembranes* 1838:1467-1476.
13. Singer, S. J., and G. L. Nicolson. 1972. The fluid mosaic model of the structure of cell membranes. *Science* 175:720-731.
14. Mouritsen, O. G., and M. Bloom. 1984. Mattress model of lipid-protein interactions in membranes. *Biophysical Journal* 46:141-153.
15. Nicolson, G. L. 2014. The fluid-mosaic model of membrane structure: Still relevant to understanding the structure, function and dynamics of biological membranes after more than 40 years. *Biochimica et Biophysica Acta (BBA) - Biomembranes* 1838:1451-1466.
16. Lundbæk, J. A., A. M. Maer, and O. S. Andersen. 1997. Lipid bilayer electrostatic energy, curvature stress, and assembly of gramicidin channels. *Biochemistry* 36:5695-5701.

17. Escribá, P. V., J. M. González-Ros, F. M. Goñi, P. K. J. Kinnunen, L. Vigh, L. Sánchez-Magraner, A. M. Fernández, X. Busquets, I. Horváth, and G. Barceló-Coblijn. 2008. Membranes: A meeting point for lipids, proteins and therapies. *Journal of Cellular and Molecular Medicine* 12:829-875.
18. Seddon, J. M. 1996. Lyotropic phase behaviour of biological amphiphiles. *Berichte der Bunsengesellschaft für physikalische Chemie* 100:380-393.
19. Ratledge, C., and S. G. Wilkinson. 1988. *Microbial lipids*. Academic Press, London.
20. Batrakov, S. G., A. G. Panosyan, I. V. Konova, and L. D. Bergelson. 1974. Diol lipids: XXVI. Identification of a threo-butane-2,3-diol phospholipid from *actinomyces olivaceus*. *Biochimica et Biophysica Acta (BBA) – Molecular and Cell Biology of Lipids* 337:29-40.
21. Stodola, F. H., M. H. Deinema, and J. F. Spencer. 1967. Extracellular lipids of yeasts. *Bacteriological Reviews* 31:194-213.
22. Henriksen, J., A. C. Rowat, E. Brief, Y. W. Hsueh, J. L. Thewalt, M. J. Zuckermann, and J. H. Ipsen. 2006. Universal behavior of membranes with sterols. *Biophysical Journal* 90:1639-1649.
23. Wei, J. H., X. Yin, and P. V. Welander. 2016. Sterol synthesis in diverse bacteria. *Frontiers in Microbiology* 7:259-219.
24. Schmitt, P., R. D. Rosa, and D. Destoumieux-Garzón. 2015. An intimate link between antimicrobial peptide sequence diversity and binding to essential components of bacterial membranes. *Biochimica et Biophysica Acta (BBA) - Biomembranes* 1858:958-970.
25. Conrad, R. S., and H. E. Gilleland. 1981. Lipid alterations in cell envelopes of polymyxin-resistant *pseudomonas aeruginosa* isolates. *Journal of Bacteriology* 148:487-497.
26. Poralla, K., E. Kannenberg, and A. Blume. 1980. A glycolipid containing hopane isolated from the acidophilic, thermophilic *bacillus acidocaldarius*, has a cholesterol-like function in membranes. *FEBS Letters* 113:107-110.
27. de Almeida, R. F. M., A. Fedorov, and M. Prieto. 2003. Sphingomyelin/phosphatidylcholine/cholesterol phase diagram: Boundaries and composition of lipid rafts. *Biophysical Journal* 85:2406-2416.
28. Seddon, J. M., and R. H. Templer. 1995. Polymorphism of lipid-water systems. In *Structure and dynamics of membranes*. E. Sackmann, and R. Lipowsky, editors. Elsevier. 97-160.
29. Seddon, J. M. 1990. Structure of the inverted hexagonal (HII) phase, and non-lamellar phase transitions of lipids. *Biochimica et Biophysica Acta (BBA) - Biomembranes* 1031:1-69.
30. Heimburg, T. 2000. A model for the lipid pretransition: Coupling of ripple formation with the chain-melting transition. *Biophysical Journal* 78:1154-1165.
31. de Vries, A. H., S. Yefimov, A. E. Mark, and S. J. Marrink. 2005. Molecular structure of the lecithin ripple phase. *Proceedings of the National Academy of Sciences of the United States of America* 102:5392-5396.
32. Winter, R., and F. Noll. 1998. *Methoden der biophysikalischen Chemie*. B. G. Teubner, Stuttgart.
33. Janiak, M. J., D. M. Small, and G. G. Shipley. 1979. Temperature and compositional dependence of the structure of hydrated dimyristoyl lecithin. *The Journal of Biological Chemistry* 254:6068-6078.
34. Israelachvili, J. N. 2011. *Intermolecular and surface forces*. Elsevier Academic Press, New York.
35. Jähnig, F. 1996. What is the surface tension of a lipid bilayer membrane? *Biophysical Journal* 71:1348-1349.
36. Marsh, D. 2012. Lateral order in gel, subgel and crystalline phases of lipid membranes: Wide-angle x-ray scattering. *Chemistry and Physics of Lipids* 165:59-76.
37. Heerklotz, H. 2008. Interactions of surfactants with lipid membranes. *Quarterly Reviews of Biophysics* 41:205-264.
38. Boni, L. T., and S. W. Hui. 1983. Polymorphic phase behaviour of dilinoleoylphosphatidylethanolamine and palmitoyllecithin mixtures:

- Structural changes between hexagonal, cubic and bilayer phases. *Biochimica et Biophysica Acta (BBA) - Biomembranes* 731:177-185.
39. Trnobranski, P. H. 1998. Are we facing a 'post-antibiotic era' ? – a review of the literature regarding antimicrobial drug resistance. *Journal of Clinical Nursing* 7:392-400.
 40. Lohner, K. 2017. Membrane-active antimicrobial peptides as template structures for novel antibiotic agents. *Current Topics in Medicinal Chemistry* 17:508-519.
 41. WHO. 2014. Antimicrobial resistance - global report on surveillance, world health organisation
 42. Brandenburg, K., and T. Schürholz. 2015. Lack of new antiinfective agents: Passing into the pre-antibiotic age? *World Journal of Biological Chemistry* 6:71-78.
 43. Hoffmann, J. A. 2013. Jules A. Hoffmann - Nobel lecture: The host defense of insects: A paradigm for innate immunity. *Nobel Lecture*:1-33.
 44. Wang, G., X. Li, and Z. Wang. 2016. Apd3: The antimicrobial peptide database as a tool for research and education. *Nucleic Acids Research* 44:D1087-D1093.
 45. Dathe, M., H. Nikolenko, J. Meyer, and M. Beyermann. 2001. Optimization of the antimicrobial activity of magainin peptides by modification of charge. *FEBS Letters* 501:146-150.
 46. Dathe, M., T. Wieprecht, H. Nikolenko, L. Handel, W. L. Maloy, D. L. MacDonald, M. Beyermann, and M. Bienert. 1997. Hydrophobicity, hydrophobic moment and angle subtended by charged residues modulate antibacterial and haemolytic activity of amphipathic helical peptides. *FEBS Letters* 403:208-212.
 47. Blondelle, S. E., E. Takahashi, K. T. Dinh, and R. A. Houghten. 1995. The antimicrobial activity of hexapeptides derived from synthetic combinatorial libraries. *The Journal of Applied Bacteriology* 78:39-46.
 48. Fjell, C. D., J. A. Hiss, R. E. W. Hancock, and G. Schneider. 2011. Designing antimicrobial peptides: Form follows function. *Nature Reviews Drug Discovery* 11:37-51.
 49. Wessolowski, A., M. Bienert, and M. Dathe. 2004. Antimicrobial activity of arginine- and tryptophan-rich hexapeptides: The effects of aromatic clusters, D-amino acid substitution and cyclization. *Journal of Peptide Research* 64:159-169.
 50. Giuliani, A., G. Pirri, and S. Nicoletto. 2007. Antimicrobial peptides: An overview of a promising class of therapeutics. *Open Life Sciences* 2:1-33.
 51. Jamali, H., K. Krylova, and C. M. Dozois. 2018. The 100 top-cited scientific papers focused on the topic of bacteriocins. *International Journal of Peptide Research and Therapeutics* 36:119.
 52. Zhou, P., and J. Huang. 2015. Computational peptidology.
 53. Epanand, R. M., and H. J. Vogel. 1999. Diversity of antimicrobial peptides and their mechanisms of action. *Biochimica et Biophysica Acta (BBA) - Biomembranes* 1462:11-28.
 54. Ganz, T. 2003. Defensins: Antimicrobial peptides of innate immunity. *Nature Reviews Immunology* 3:710-720.
 55. Zhao, L., and W. Lu. 2014. Defensins in innate immunity. *Current Opinion in Hematology* 21:37-42.
 56. Gallo, R. L., M. Murakami, T. Ohtake, and M. Zaiou. 2002. Biology and clinical relevance of naturally occurring antimicrobial peptides. *Journal of Allergy and Clinical Immunology* 110:823-831.
 57. Kościuczuk, E. M., P. Lisowski, J. Jarczak, N. Strzałkowska, A. Józwick, J. Horbańczuk, J. Krzyżewski, L. Zwierzchowski, and E. Bagnicka. 2012. Cathelicidins: Family of antimicrobial peptides. A review. *Molecular Biology Reports* 39:10957-10970.
 58. Wimley, W. C., and K. Hristova. 2011. Antimicrobial peptides: Successes, challenges and unanswered questions. *The Journal of Membrane Biology* 239:27-34.
 59. Seelig, J., and P. Ganz. 1991. Nonclassical hydrophobic effect in membrane binding equilibria. *Biochemistry* 30:9354-9359.
 60. Wimley, W. C., and S. H. White. 1993. Membrane partitioning - distinguishing bilayer effects from the hydrophobic effect. *Biochemistry* 32:6307-6312.

61. Ulmschneider, J. P., J. C. Smith, S. H. White, and M. B. Ulmschneider. 2011. In silico partitioning and transmembrane insertion of hydrophobic peptides under equilibrium conditions. *Journal of the American Chemical Society* 133:15487-15495.
62. Fernández-Vidal, M., S. H. White, and A. S. Ladokhin. 2010. Membrane partitioning: “Classical” and “nonclassical” hydrophobic effects. *The Journal of Membrane Biology* 239:5-14.
63. Nguyen, L. T., E. F. Haney, and H. J. Vogel. 2011. The expanding scope of antimicrobial peptide structures and their modes of action. *Trends in Biotechnology* 29:464-472.
64. Yang, L., T. M. Weiss, R. I. Lehrer, and H. W. Huang. 2000. Crystallization of antimicrobial pores in membranes: Magainin and protegrin. *Biophysical Journal* 79:2002-2009.
65. Irudayam, S. J., and M. L. Berkowitz. 2012. Binding and reorientation of melittin in a POPC bilayer: Computer simulations. *Biochimica et Biophysica Acta (BBA) - Biomembranes* 1818:2975-2981.
66. Huang, H. W. 2006. Molecular mechanism of antimicrobial peptides: The origin of cooperativity. *Biochimica et Biophysica Acta (BBA) - Biomembranes* 1758:1292-1302.
67. Irudayam, S. J., T. Pobandt, and M. L. Berkowitz. 2013. Free energy barrier for melittin reorientation from a membrane-bound state to a transmembrane state. *The Journal of Physical Chemistry B* 117:13457-13463.
68. Santo, K. P., S. J. Irudayam, and M. L. Berkowitz. 2013. Melittin creates transient pores in a lipid bilayer: Results from computer simulations. *The Journal of Physical Chemistry B* 117:5031-5042.
69. Ramadurai, S., R. Durkens, V. V. Krasnikov, and B. Poolman. 2010. Lateral diffusion of membrane proteins: Consequences of hydrophobic mismatch and lipid composition. *Biophysical Journal* 99:1482-1489.
70. Ren, J., S. Lew, Z. Wang, and E. London. 1997. Transmembrane orientation of hydrophobic α -helices is regulated both by the relationship of helix length to bilayer thickness and by the cholesterol concentration. *Biochemistry* 36:10213-10220.
71. Ren, J., S. Lew, J. Wang, and E. London. 1999. Control of the transmembrane orientation and interhelical interactions within membranes by hydrophobic helix length. *Biochemistry* 38:5905-5912.
72. Webb, R. J., J. M. East, R. P. Sharma, and A. G. Lee. 1998. Hydrophobic mismatch and the incorporation of peptides into lipid bilayers: A possible mechanism for retention in the golgi. *Biochemistry* 37:673-679.
73. Finkelstein, A. 1973. Aqueous pores created in thin lipid membranes by the antibiotics nystatin, amphotericin B and gramicidin A: Implications for pores in plasma membranes. In *Drugs and Transport Processes*. B. A. Callingham, editor. Palgrave, London. 241-250.
74. Baumann, G., and P. Mueller. 1974. A molecular model of membrane excitability. *Journal of Supramolecular Structure* 2:538-557.
75. Ehrenstein, G., and H. Lecar. 1977. Electrically gated ionic channels in lipid bilayers. *Quarterly Reviews of Biophysics* 10:1-34.
76. Shai, Y., and Z. Oren. 2001. From “carpet” mechanism to de-novo designed diastereomeric cell-selective antimicrobial peptides. *Peptides* 22:1629-1641.
77. Yang, L., T. A. Harroun, T. M. Weiss, L. Ding, and H. W. Huang. 2001. Barrel-stave model or toroidal model? A case study on melittin pores. *Biophysical Journal* 81:1475-1485.
78. Brogden, K. A. 2005. Antimicrobial peptides: Pore formers or metabolic inhibitors in bacteria? *Nature Reviews Microbiology* 3:238-250.
79. Vogel, H. 1987. Comparison of the conformation and orientation of alamethicin and melittin in lipid membranes. *Biochemistry* 26:4562-4572.
80. Rahaman, A., and T. Lazaridis. 2014. A thermodynamic approach to alamethicin pore formation. *Biochimica et Biophysica Acta (BBA) - Biomembranes* 1838:98-105.
81. Keller, S. L., S. M. Bezrukov, S. M. Gruner, M. W. Tate, I. Vodyanoy, and V. A. Parsegian. 1993. Probability of alamethicin conductance states varies with nonlamellar tendency of bilayer phospholipids. *Biophysical Journal* 65:23-27.

82. Oliynyk, V., M. Jäger, T. Heimbürg, V. Buckin, and U. Kaatz. 2008. Lipid membrane domain formation and alamethicin aggregation studied by calorimetry, sound velocity measurements, and atomic force microscopy. *Biophysical Chemistry* 134:168-177.
83. He, K., S. J. Ludtke, D. L. Worcester, and H. W. Huang. 1996. Neutron scattering in the plane of membranes: Structure of alamethicin pores. *Biophysical Journal* 70:2659-2666.
84. Song, C., C. Weichbrodt, E. S. Salnikov, M. Dynowski, B. O. Forsberg, B. Bechinger, C. Steinem, B. L. de Groot, U. Zachariae, and K. Zeth. 2013. Crystal structure and functional mechanism of a human antimicrobial membrane channel. *Proceedings of the National Academy of Sciences of the United States of America* 110:4586-4591.
85. Matsuzaki, K., O. Murase, a. Nobutaka Fujii, and K. Miyajima. 1996. An antimicrobial peptide, magainin 2, induced rapid flip-flop of phospholipids coupled with pore formation and peptide translocation. *Biochemistry* 35:11361-11368.
86. Hirsh, D. J., J. Hammer, W. L. Maloy, J. Blazyk, and J. Schaefer. 1996. Secondary structure and location of a magainin analogue in synthetic phospholipid bilayers. *Biochemistry* 35:12733-12741.
87. Bechinger, B., M. Zasloff, and S. J. Opella. 1993. Structure and orientation of the antibiotic peptide magainin in membranes by solid-state nuclear magnetic resonance spectroscopy. *Protein Science* 2:2077-2084.
88. Hallock, K. J., D.-K. Lee, and A. Ramamoorthy. 2003. MSI-78, an analogue of the magainin antimicrobial peptides, disrupts lipid bilayer structure via positive curvature strain. *Biophysical Journal* 84:3052-3060.
89. Ludtke, S. J., K. He, W. T. Heller, T. A. Harroun, L. Yang, and H. W. Huang. 1996. Membrane pores induced by magainin. *Biochemistry* 35:13723-13728.
90. Leontiadou, H., A. E. Mark, and S. J. Marrink. 2006. Antimicrobial peptides in action. *Journal of the American Chemical Society* 128:12156-12161.
91. Sengupta, D., H. Leontiadou, A. E. Mark, and S.-J. Marrink. 2008. Toroidal pores formed by antimicrobial peptides show significant disorder. *Biochimica et Biophysica Acta (BBA) - Biomembranes* 1778:2308-2317.
92. Sancho-Vaello, E., P. Franois, E.-J. Bonetti, H. Lilie, S. Finger, F. Gil-Ortiz, D. Gil-Carton, and K. Zeth. 2017. Structural remodeling and oligomerization of human cathelicidin on membranes suggest fibril-like structures as active species. *Scientific Reports* 7:15371-15382.
93. Pouny, Y., D. Rapaport, A. Mor, P. Nicolas, and Y. Shai. 1992. Interaction of antimicrobial dermaseptin and its fluorescently labeled analogs with phospholipid membranes. *Biochemistry* 31:12416-12423.
94. Helenius, A., and K. Simons. 1975. Solubilization of membranes by detergents. *Biochimica et Biophysica Acta (BBA) - Biomembranes* 415:29-79.
95. Keller, M., A. Kerth, and A. Blume. 1997. Thermodynamics of interaction of octyl glucoside with phosphatidylcholine vesicles: Partitioning and solubilization as studied by high sensitivity titration calorimetry. *Biochimica et Biophysica Acta (BBA) - Biomembranes* 1326:178-192.
96. Hildebrand, A., R. Neubert, P. Garidel, and A. Blume. 2002. Bile salt induced solubilization of synthetic phosphatidylcholine vesicles studied by isothermal titration calorimetry. *Langmuir* 18:2836-2847.
97. Bechinger, B., and K. Lohner. 2006. Detergent-like actions of linear amphipathic cationic antimicrobial peptides. *Biochimica et Biophysica Acta (BBA) - Biomembranes* 1758:1529-1539.
98. Bechinger, B. 2009. Rationalizing the membrane interactions of cationic amphipathic antimicrobial peptides by their molecular shape. *Current Opinion in Colloid & Interface Science* 14:349-355.
99. Lee, T.-H., D. J. Hirst, and M. I. Aguilar. 2015. New insights into the molecular mechanisms of biomembrane structural changes and interactions by optical biosensor technology. *Biochimica et Biophysica Acta (BBA) - Biomembranes* 1848:1868-1885.

100. Mattila, J.-P., K. Sabatini, and P. K. J. Kinnunen. 2008. Oxidized phospholipids as potential molecular targets for antimicrobial peptides. *Biochimica et Biophysica Acta (BBA) - Biomembranes* 1778:2041-2050.
101. Epanand, R. F., L. Maloy, A. Ramamoorthy, and R. M. Epanand. 2010. Amphipathic helical cationic antimicrobial peptides promote rapid formation of crystalline states in the presence of phosphatidylglycerol: Lipid clustering in anionic membranes. *Biophysical Journal* 98:2564-2573.
102. Wadhvani, P., R. F. Epanand, N. Heidenreich, J. Bürck, A. S. Ulrich, and R. M. Epanand. 2012. Membrane-active peptides and the clustering of anionic lipids. *Biophysical Journal* 103:265-274.
103. Latal, A., G. Degovics, R. F. Epanand, R. M. Epanand, and K. Lohner. 1997. Structural aspects of the interaction of peptidyl-glycylleucine-carboxamide, a highly potent antimicrobial peptide from frog skin, with lipids. *European Journal of Biochemistry* 248:938-946.
104. Kwon, B., A. J. Waring, and M. Hong. 2013. A 2H solid-state NMR study of lipid clustering by cationic antimicrobial and cell-penetrating peptides in model bacterial membranes. *Biophysical Journal* 105:2333-2342.
105. Lohner, K., A. Latal, R. I. Lehrer, and T. Ganz. 1997. Differential scanning microcalorimetry indicates that human defensin, HNP-2, interacts specifically with biomembrane mimetic systems. *Biochemistry* 36:1525-1531.
106. Hartmann, W., H. J. Galla, and E. Sackmann. 1978. Polymyxin binding to charged lipid membranes. An example of cooperative lipid-protein interaction. *Biochimica et Biophysica Acta (BBA) - Biomembranes* 510:124-139.
107. Theretz, A., J. L. Ranck, and J. F. Tocanne. 1983. Polymyxin B-induced phase separation and acyl chain interdigitation in phosphatidylcholine/phosphatidylglycerol mixtures. *Biochimica et Biophysica Acta (BBA) - Biomembranes* 732:499-508.
108. Aroui, A., M. Dathe, and A. Blume. 2009. Peptide induced demixing in PG/PE lipid mixtures: A mechanism for the specificity of antimicrobial peptides towards bacterial membranes? *Biochimica et Biophysica Acta (BBA) - Biomembranes* 1788:650-659.
109. Aroui, A. 2009. Interaction of antimicrobial peptides with model lipid membranes. Doctoral Thesis. Naturwissenschaftliche Fakultät II - Chemie und Physik. Martin-Luther-Universität Halle-Wittenberg, Halle/Saale.
110. Epanand, R. M., R. F. Epanand, C. J. Arnusch, B. Papahadjopoulos-Sternberg, G. Wang, and Y. Shai. 2010. Lipid clustering by three homologous arginine-rich antimicrobial peptides is insensitive to amino acid arrangement and induced secondary structure. *Biochimica et Biophysica Acta (BBA) - Biomembranes* 1798:1272-1280.
111. Vanounou, S., A. H. Parola, and I. Fishov. 2003. Phosphatidylethanolamine and phosphatidylglycerol are segregated into different domains in bacterial membrane. A study with pyrene-labelled phospholipids. *Molecular Microbiology* 49:1067-1079.
112. Epanand, R. F., G. Wang, B. Berno, and R. M. Epanand. 2009. Lipid segregation explains selective toxicity of a series of fragments derived from the human cathelicidin LL-37. *Antimicrobial Agents and Chemotherapy* 53:3705-3714.
113. Mason, A. J., I. N. H. Chotimah, P. Bertani, and B. Bechinger. 2009. A spectroscopic study of the membrane interaction of the antimicrobial peptide pleurocidin. *Molecular Membrane Biology* 23:185-194.
114. Miteva, M., M. Andersson, A. Karshikoff, and G. Otting. 1999. Molecular electroporation: A unifying concept for the description of membrane pore formation by antibacterial peptides, exemplified with NK-lysin. *FEBS Letters* 462:155-158.
115. Epanand, R. M., S. Rotem, A. Mor, B. Berno, and R. F. Epanand. 2008. Bacterial membranes as predictors of antimicrobial potency. *Journal of the American Chemical Society* 130:14346-14352.
116. Epanand, R. M., and R. F. Epanand. 2009. Lipid domains in bacterial membranes and the action of antimicrobial agents. *Biochimica et Biophysica Acta (BBA) - Biomembranes* 1788:289-294.

117. Auvynet, C., P. Joanne, J. Bourdais, P. Nicolas, C. Lacombe, and Y. Rosenstein. 2009. Dermaseptin DA4, although closely related to dermaseptin B2, presents chemotactic and gram-negative selective bactericidal activities. *The FEBS Journal* 276:6773-6786.
118. Epand, R. F., W. L. Maloy, A. Ramamoorthy, and R. M. Epand. 2010. Probing the "charge cluster mechanism" in amphipathic helical cationic antimicrobial peptides. *Biochemistry* 49:4076-4084.
119. Scheinpflug, K., O. Krylova, H. Nikolenko, C. Thurm, and M. Dathe. 2015. Evidence for a novel mechanism of antimicrobial action of a cyclic R-, W-rich hexapeptide. *PloS one* 10:e0125056.
120. Beyer, K., and M. Klingenberg. 1985. ADP/ATP carrier protein from beef heart mitochondria has high amounts of tightly bound cardiolipin, as revealed by phosphorus-31 nuclear magnetic resonance. *Biochemistry* 24:3821-3826.
121. Palsdottir, H., and C. Hunte. 2004. Lipids in membrane protein structures. *Biochimica et Biophysica Acta (BBA) - Biomembranes* 1666:2-18.
122. Shinzawa-Itoh, K., H. Aoyama, K. Muramoto, H. Terada, T. Kurauchi, Y. Tadehara, A. Yamasaki, T. Sugimura, S. Kurono, K. Tsujimoto, T. Mizushima, E. Yamashita, T. Tsukihara, and S. Yoshikawa. 2007. Structures and physiological roles of 13 integral lipids of bovine heart cytochrome c oxidase. *The EMBO Journal* 26:1713-1725.
123. Zhou, M., N. Morgner, N. P. Barrera, A. Politis, S. C. Isaacson, D. Matak-Vinkovic, T. Murata, R. A. Bernal, D. Stock, and C. V. Robinson. 2011. Mass spectrometry of intact V-type ATPases reveals bound lipids and the effects of nucleotide binding. *Science* 334:380-385.
124. Lee, A. G. 2003. Lipid-protein interactions in biological membranes: A structural perspective. *Biochimica et Biophysica Acta (BBA) - Biomembranes* 1612:1-40.
125. Lee, A. G. 2004. How lipids affect the activities of integral membrane proteins. *Biochimica et Biophysica Acta (BBA) - Biomembranes* 1666:62-87.
126. Salas-Estrada, L. A., N. Leioatts, T. D. Romo, and A. Grossfield. 2018. Lipids alter rhodopsin function via ligand-like and solvent-like interactions. *Biophysical Journal* 114:355-367.
127. Pfeiffer, K., V. Gohil, R. A. Stuart, C. Hunte, U. Brandt, M. L. Greenberg, and H. Schagger. 2003. Cardiolipin stabilizes respiratory chain supercomplexes. *The Journal of Biological Chemistry* 278:52873-52880.
128. Acehan, D., A. Malhotra, Y. Xu, M. Ren, D. L. Stokes, and M. Schlame. 2011. Cardiolipin affects the supramolecular organization of ATP synthase in mitochondria. *Biophysical Journal* 100:2184-2192.
129. Böttinger, L., S. E. Horvath, T. Kleinschroth, C. Hunte, G. Daum, N. Pfanner, and T. Becker. 2012. Phosphatidylethanolamine and cardiolipin differentially affect the stability of mitochondrial respiratory chain supercomplexes. *Journal of Molecular Biology* 423:677-686.
130. Baldwin, P. A., and W. L. Hubbell. 1985. Effects of lipid environment on the light-induced conformational changes of rhodopsin. 2. Roles of lipid chain length, unsaturation, and phase state. *Biochemistry* 24:2633-2639.
131. Pilot, J. D., a. J Malcolm East, and A. G. Lee. 2001. Effects of bilayer thickness on the activity of diacylglycerol kinase of escherichia coli. *Biochemistry* 40:8188-8195.
132. Starling, A. P., J. M. East, and A. G. Lee. 1993. Effects of phosphatidylcholine fatty acyl chain length on calcium binding and other functions of the calcium-magnesium-ATPase. *Biochemistry* 32:1593-1600.
133. Cornelius, F. 2001. Modulation of Na, K-ATPase and Na-ATPase activity by phospholipids and cholesterol. I. Steady-state kinetics. *Biochemistry* 40:8842-8851.
134. Starling, A. P., J. M. East, and A. G. Lee. 1995. Evidence that the effects of phospholipids on the activity of the Ca²⁺-ATPase do not involve aggregation. *Biochemical Journal* 308:343-346.
135. Pilot, J. D., a. J Malcolm East, and A. G. Lee. 2001. Effects of phospholipid headgroup and phase on the activity of diacylglycerol kinase of escherichia coli. *Biochemistry* 40:14891-14897.

136. Mitchell, D. C., M. Straume, J. L. Miller, and B. J. Litman. 1990. Modulation of metarhodopsin formation by cholesterol-induced ordering of bilayer lipids. *Biochemistry* 29:9143-9149.
137. Litman, B. J., and D. C. Mitchell. 1996. Rhodopsin structure and function. Volume 2 Rhodopsin and G-protein linked receptors, Lee, A.G, editor, JAI Press Inc.
138. Lindahl, E., and O. Edholm. 2000. Spatial and energetic-entropic decomposition of surface tension in lipid bilayers from molecular dynamics simulations. *The Journal of Chemical Physics* 113:3882-3893.
139. Marsh, D. 1996. Lateral pressure in membranes. *Biochimica et Biophysica Acta (BBA) - Biomembranes* 1286:183-223.
140. Cantor, R. S. 1997. Lateral pressures in cell membranes: A mechanism for modulation of protein function. *The Journal of Physical Chemistry B* 101:1723-1725.
141. Cantor, R. S. 1999. The influence of membrane lateral pressures on simple geometric models of protein conformational equilibria. *Chemistry and Physics of Lipids* 101:45-56.
142. Cantor, R. S. 1999. Lipid composition and the lateral pressure profile in bilayers. *Biophysical Journal* 76:2625-2639.
143. Rietveld, A., T. J. J. M. van Kemenade, T. Hak, A. J. Verkleij, and B. d. Kruijff. 1987. The effect of cytochrome c oxidase on lipid polymorphism of model membranes containing cardiolipin. *European Journal of Biochemistry* 164:137-140.
144. Wenzel, M., A.-I. Chiriac, A. Otto, D. Zweytick, C. May, C. Schumacher, R. Gust, H. B. Albada, M. Penkova, U. Krämer, R. Erdmann, N. Metzler-Nolte, S. K. Straus, E. Bremer, D. Becher, H. Brötz-Oesterhelt, H.-G. Sahl, and J. E. Bandow. 2014. Small cationic antimicrobial peptides delocalize peripheral membrane proteins. *Proceedings of the National Academy of Sciences of the United States of America* 111:E1409-1418.
145. Scheinflug, K., M. Wenzel, O. Krylova, J. E. Bandow, M. Dathe, and H. Strahl. 2017. Antimicrobial peptide cWFW kills by combining lipid phase separation with autolysis. *Scientific Reports* 7:44332.
146. Hamill, O. P., and B. Martinac. 2001. Molecular basis of mechanotransduction in living cells. *Physiological Reviews* 81:685-740.
147. Albada, H. B., P. Prochnow, S. Bobersky, S. Langklotz, P. Schriek, J. E. Bandow, and N. Metzler-Nolte. 2012. Tuning the activity of a short arg-trp antimicrobial peptide by lipidation of a C- or N-terminal lysine side-chain. *ACS Medicinal Chemistry Letters* 3:980-984.
148. Wenzel, M., P. Schriek, P. Prochnow, H. B. Albada, N. Metzler-Nolte, and J. E. Bandow. 2015. Influence of lipidation on the mode of action of a small RW-rich antimicrobial peptide. *Biochimica et Biophysica Acta (BBA) - Biomembranes* 1858:1004-1011.
149. Lee, A. 1991. Lipids and their effects on membrane proteins: Evidence against a role for fluidity. *Progress In Lipid Research* 30:323-348.
150. Lee, K. C., S. Huo, and T. A. Cross. 1995. Lipid-peptide interface: Valine conformation and dynamics in the gramicidin channel. *Biochemistry* 34:857-867.
151. Chiu, S.-W., S. Subramaniam, and E. Jakobsson. 1999. Simulation study of a gramicidin/lipid bilayer system in excess water and lipid. I. Structure of the molecular complex. *Biophysical Journal* 76:1929-1938.
152. Polyansky, A. A., R. Ramaswamy, P. E. Volynsky, I. F. Sbalzarini, S. J. Marrink, and R. G. Efremov. 2010. Antimicrobial peptides induce growth of phosphatidylglycerol domains in a model bacterial membrane. *The Journal of Physical Chemistry Letters* 1:3108-3111.
153. Gause, G. F., and M. G. Brazhnikova. 1944. Gramicidin S and its use in the treatment of infected wounds. *Nature* 154:703-703.
154. Sieprawska-Lupa, M., P. Mydel, K. Krawczyk, K. Wójcik, M. Puklo, B. Lupa, P. Suder, J. Silberring, M. Reed, J. Pohl, W. Shafer, F. McAleese, T. Foster, J. Travis, and J. Potempa. 2004. Degradation of human antimicrobial peptide LL-37 by *Staphylococcus aureus*-derived proteinases. *Antimicrobial Agents and Chemotherapy* 48:4673-4679.
155. Larock, C. N., and V. Nizet. 2015. Cationic antimicrobial peptide resistance mechanisms of streptococcal pathogens. *Biochimica et Biophysica Acta (BBA) - Biomembranes* 1848:3047-3054.

156. Nuri, R., T. Shprung, and Y. Shai. 2015. Defensive remodeling: How bacterial surface properties and biofilm formation promote resistance to antimicrobial peptides. *Biochimica et Biophysica Acta (BBA) - Biomembranes* 1848:3089-3100.
157. Matamouros, S., and S. I. Miller. 2015. *S. typhimurium* strategies to resist killing by cationic antimicrobial peptides. *Biochimica et Biophysica Acta (BBA) - Biomembranes* 1848:3021-3025.
158. Tzeng, Y.-L., and D. S. Stephens. 2015. Antimicrobial peptide resistance in *Neisseria meningitidis*. *Biochimica et Biophysica Acta (BBA) - Biomembranes* 1848:3026-3031.
159. Saar-Dover, R., A. Bitler, R. Nezer, L. Shmuel-Galia, A. Firon, E. Shimoni, P. Trieu-Cuot, and Y. Shai. 2012. D-alanylation of lipoteichoic acids confers resistance to cationic peptides in group B streptococcus by increasing the cell wall density. *PLoS Pathogens* 8:e1002891.
160. Lewis, L. A., B. Choudhury, J. T. Balthazar, L. E. Martin, S. Ram, P. A. Rice, D. S. Stephens, R. Carlson, and W. M. Shafer. 2009. Phosphoethanolamine substitution of lipid A and resistance of *Neisseria gonorrhoeae* to cationic antimicrobial peptides and complement-mediated killing by normal human serum. *Infection and Immunity* 77:1112-1120.
161. Roy, H., and M. Ibba. 2008. RNA-dependent lipid remodeling by bacterial multiple peptide resistance factors. *Proceedings of the National Academy of Sciences of the United States of America* 105:4667-4672.
162. Andra, J., T. Goldmann, C. M. Ernst, A. Peschel, and T. Gutschmann. 2011. Multiple peptide resistance factor (MPRF)-mediated resistance of *Staphylococcus aureus* against antimicrobial peptides coincides with a modulated peptide interaction with artificial membranes comprising lysyl-phosphatidylglycerol. *The Journal of Biological Chemistry* 286:18692-18700.
163. Kilelee, E., A. Pokorny, M. R. Yeaman, and A. S. Bayer. 2010. Lysyl-phosphatidylglycerol attenuates membrane perturbation rather than surface association of the cationic antimicrobial peptide 6W-RP-1 in a model membrane system: Implications for daptomycin resistance. *Antimicrobial Agents and Chemotherapy* 54:4476-4479.
164. Sackmann, E., and R. Merkel. 2010. *Lehrbuch der Biophysik*. Wiley-VCH, Weinheim.
165. Garidel, P. 1997. The negatively charged phospholipids phosphatidic acid and phosphatidylglycerol. Doctoral Thesis. Fachbereich Chemie. Universität Kaiserslautern, Kaiserslautern, Germany.
166. Saunders, N., and A. P. Miodownik, editors. 1998. *Calphad: Calculation of phase diagrams - a comprehensive guide*. Elsevier.
167. Träuble, H., M. Teubner, P. Woolley, and H. Eibl. 1976. Electrostatic interactions at charged lipid membranes: I. Effects of pH and univalent cations on membrane structure. *Biophysical Chemistry* 4:319-342.
168. Gelbart, W. M., and R. Bruinsma. 1997. Compositional-mechanical instability of interacting mixed lipid membranes. *Physical Review E* 55:831-835.
169. Hill, T. L. 1986. *Introduction to statistical thermodynamics*.
170. May, S., D. Harries, and A. Ben-Shaul. 2002. Macroion-induced compositional instability of binary fluid membranes. *Physical Review Letters* 89:268102.
171. Watts, A., K. Harlos, W. Maschke, and D. Marsh. 1978. Control of the structure and fluidity of phosphatidylglycerol bilayers by pH titration. *Biochimica et Biophysica Acta (BBA) - Biomembranes* 510:63-74.
172. Garidel, P., W. Richter, G. Rapp, and A. Blume. 2001. Structural and morphological investigations of the formation of quasi-crystalline phases of 1,2-dimyristoyl- sn -glycero-3-phosphoglycerol (DMPG). *Physical Chemistry Chemical Physics* 3:1504-1513.
173. Watts, A., K. Harlos, and D. Marsh. 1981. Charge-induced tilt in ordered-phase phosphatidylglycerol bilayers. Evidence from X-ray diffraction. *Biochimica et Biophysica Acta (BBA) - Biomembranes* 645:91-96.
174. Pascher, I., S. Sundell, K. Harlos, and H. Eibl. 1987. Conformation and packing properties of membrane lipids: The crystal structure of sodium dimyristoylphosphatidylglycerol. *Biochimica et Biophysica Acta (BBA) - Biomembranes* 896:77-88.

175. Blaurock, A. E., and T. J. McIntosh. 1986. Structure of the crystalline bilayer in the subgel phase of dipalmitoylphosphatidylglycerol. *Biochemistry* 25:299-305.
176. Kinoshita, M., S. Kato, and H. Takahashi. 2008. Effect of bilayer morphology on the subgel phase formation. *Chemistry and Physics of Lipids* 151:30-40.
177. Kinoshita, M., S. Kato, and H. Takahashi. 2009. NaCl-dependent formation of the highly crystalline phase in sufficiently hydrated dimyristoylphosphatidylglycerol bilayers. *Chemistry and Physics of Lipids* 161:1-10.
178. Kodama, M., H. Aoki, and T. Miyata. 1999. Effect of Na⁺ concentration on the subgel phases of negatively charged phosphatidylglycerol. *Biophysical Chemistry* 79:205-217.
179. Lotta, T. I., I. S. Salonen, J. A. Virtanen, K. K. Eklund, and P. K. J. Kinnunen. 1988. Fourier transform infrared study of fully hydrated dimyristoylphosphatidylglycerol. Effects of sodium on the sn-1' and sn-3' headgroup stereoisomers. *Biochemistry* 27:8158-8169.
180. Zhang, Y.-P., R. N. A. H. Lewis, and R. N. McElhaney. 1997. Calorimetric and spectroscopic studies of the thermotropic phase behavior of the n-saturated 1,2-diacylphosphatidylglycerols. *Biophysical Journal* 72:779-793.
181. Garidel, P., and A. Blume. 1999. Interaction of alkaline earth cations with the negatively charged phospholipid 1,2-dimyristoyl-sn-glycero-3-phosphoglycerol: A differential scanning and isothermal titration calorimetric study. *Langmuir* 15:5526-5534.
182. Garidel, P., A. Blume, and W. Hübner. 2000. A fourier transform infrared spectroscopic study of the interaction of alkaline earth cations with the negatively charged phospholipid 1, 2-dimyristoyl-sn-glycero-3-phosphoglycerol. *Biochimica et Biophysica Acta (BBA) - Biomembranes* 1466:245-259.
183. Garidel, P., G. Förster, W. Richter, B. H. Kunst, G. Rapp, and A. Blume. 2000. 1,2-dimyristoyl-sn-glycero-3-phosphoglycerol (DMPG) divalent cation complexes: An X-ray scattering and freeze-fracture electron microscopy study. *Physical Chemistry Chemical Physics* 2:4537-4544.
184. Garidel, P., and A. Blume. 2005. 1,2-dimyristoyl-sn-glycero-3-phosphoglycerol (DMPG) monolayers: Influence of temperature, pH, ionic strength and binding of alkaline earth cations. *Chemistry and Physics of Lipids* 138:50-59.
185. Seddon, J. M., G. Cevc, and D. Marsh. 1983. Calorimetric studies of the gel-fluid (L_β-L_α) and lamellar-inverted hexagonal (L_α-HII) phase transitions in dialkyl- and diacylphosphatidylethanolamine. *Biochemistry* 22:1280-1289.
186. Lewis, R. N., and R. N. McElhaney. 1993. Calorimetric and spectroscopic studies of the polymorphic phase behavior of a homologous series of n-saturated 1,2-diacyl phosphatidylethanolamines. *Biophysical Journal* 64:1081-1096.
187. McIntosh, T. J., and S. A. Simon. 1986. Area per molecule and distribution of water in fully hydrated dilauroylphosphatidylethanolamine bilayers. *Biochemistry* 25:4948-4952.
188. McIntosh, T. J. 1980. Differences in hydrocarbon chain tilt between hydrated phosphatidylethanolamine and phosphatidylcholine bilayers. A molecular packing model. *Biophysical Journal* 29:237-245.
189. Pimthon, J., R. Willumeit, A. Lendlein, and D. Hofmann. 2009. All-atom molecular dynamics simulation studies of fully hydrated gel phase DPPG and DPPE bilayers. *Journal of Molecular Structure* 921:38-50.
190. Uppulury, K., P. S. Coppock, and J. T. Kindt. 2015. Molecular simulation of the DPPE lipid bilayer gel phase: Coupling between molecular packing order and tail tilt angle. *The Journal of Physical Chemistry B* 119:8725-8733.
191. Boehm, C., H. Möhwald, L. Leiserowitz, J. Als-Nielsen, and K. Kjaer. 1993. Influence of chirality on the structure of phospholipid monolayers. *Biophysical Journal* 64:553-559.
192. Dyck, M., P. Krüger, and M. Lösche. 2005. Headgroup organization and hydration of methylated phosphatidylethanolamines in Langmuir monolayers. *Physical Chemistry Chemical Physics* 7:150-156.
193. Blume, A. 1979. A comparative study of the phase transitions of phospholipid bilayers and monolayers. *Biochimica et Biophysica Acta (BBA) - Biomembranes* 557:32-44.

194. Gromelski, S., and G. Brezesinski. 2004. Adsorption of DNA to zwitterionic DMPE monolayers mediated by magnesium ions. *Physical Chemistry Chemical Physics* 6:5551-5556.
195. Kodama, M., H. Inoue, and Y. Tsuchida. 1995. The behavior of water molecules associated with structural changes in phosphatidylethanolamine assembly as studied by DSC. *Thermochimica Acta* 266:373-384.
196. Aoki, H., and M. Kodama. 1997. The behavior of water molecules in semi-crystalline bilayer structure of phosphatidylethanolamine. *Journal of Thermal Analysis and Calorimetry* 49:839-845.
197. Lewis, R. N. A. H., D. Zweytick, G. Pabst, K. Lohner, and R. N. McElhaney. 2007. Calorimetric, X-ray diffraction, and spectroscopic studies of the thermotropic phase behavior and organization of tetramyristoyl cardiolipin membranes. *Biophysical Journal* 92:3166-3177.
198. Tenchov, B., R. Koynova, and G. Rapp. 2001. New ordered metastable phases between the gel and subgel phases in hydrated phospholipids. *Biophysical Journal* 80:1873-1890.
199. Nagle, J. F. 1976. Theory of lipid monolayer and bilayer phase transitions: Effect of headgroup interactions. *The Journal of Membrane Biology* 27:233-250.
200. Rainier, S., M. K. Jain, F. Ramirez, and P. V. Ioannou. 1979. Phase transition characteristics of diphosphatidylglycerol (cardiolipin) and stereoisomeric phosphatidyl diacylglycerol bilayers: Mono- and divalent metal ion effects. *Biochimica et Biophysica Acta (BBA) - Biomembranes* 558:187-198.
201. Seddon, J. M., R. D. Kaye, and D. Marsh. 1983. Induction of the lamellar-inverted hexagonal phase transition in cardiolipin by protons and monovalent cations. *Biochimica et Biophysica Acta (BBA) - Biomembranes* 734:347-352.
202. Dahlberg, M. 2007. Polymorphic phase behavior of cardiolipin derivatives studied by coarse-grained molecular dynamics. *The Journal of Physical Chemistry B* 111:7194-7200.
203. Allegrini, P. R., G. Pluschke, and J. Seelig. 1984. Cardiolipin conformation and dynamics in bilayer-membranes as seen by deuterium magnetic-resonance. *Biochemistry* 23:6452-6458.
204. Kates, M., J.-Y. Syz, D. Gosser, and T. H. Haines. 1993. pH-dissociation characteristics of cardiolipin and its 2'-deoxy analogue. *Lipids* 28:877-882.
205. Haines, T. H., and N. A. Dencher. 2002. Cardiolipin: A proton trap for oxidative phosphorylation. *FEBS Letters* 528:35-39.
206. Hübner, W., H. H. Mantsch, and M. Kates. 1991. Intramolecular hydrogen bonding in cardiolipin. *Biochimica et Biophysica Acta (BBA) - Biomembranes* 1066:166-174.
207. Blume, A., and J. Tuchtenhagen. 1992. Thermodynamics of ion binding to phosphatidic acid bilayers. Titration calorimetry of the heat of dissociation of DMPA. *Biochemistry* 31:4636-4642.
208. Blume, A., and H. Eibl. 1979. Influence of charge on bilayer membranes - calorimetric investigations of phosphatidic-acid bilayers. *Biochimica et Biophysica Acta (BBA) - Biomembranes* 558:13-21.
209. Eibl, H., and A. Blume. 1979. Influence of charge on phosphatidic-acid bilayer membranes. *Biochimica et Biophysica Acta (BBA) - Biomembranes* 553:476-488.
210. Blume, A., and P. Garidel. Lipid model membranes and biomembranes. *The handbook of thermal analysis and calorimetry, from macromolecules to man*. R. Kemp, and P. Gallagher, editors. 109-173.
211. van Dijck, P. W. M., B. de Kruijff, A. J. Verkleij, L. L. M. van Deenen, and J. de Gier. 1978. Comparative studies on the effects of pH and Ca²⁺ on bilayers of various negatively charged phospholipids and their mixtures with phosphatidylcholine. *Biochimica et Biophysica Acta (BBA) - Biomembranes* 512:84-96.
212. Verkleij, A. J., B. De Kruijff, P. H. J. T. Ververgaert, J. F. Tocanne, and L. L. M. van Deenen. 1974. The influence of pH, Ca²⁺ and protein on the thermotropic behaviour of the negatively charged phospholipid, phosphatidylglycerol. *Biochimica et Biophysica Acta (BBA) - Biomembranes* 339:432-437.

213. MacDonald, R. C., S. A. Simon, and E. Baer. 1976. Ionic influences on the phase transition of dipalmitoylphosphatidylserine. *Biochemistry* 15:885-891.
214. Jacobson, K., and D. Papahadjopoulos. 1975. Phase transitions and phase separations in phospholipid membranes induced by changes in temperature, pH, and concentration of bivalent cations. *Biochemistry* 14:152-161.
215. Garidel, P., and A. Blume. 2000. Miscibility of phosphatidylethanolamine-phosphatidylglycerol mixtures as a function of pH and acyl chain length. *European Biophysics Journal* 28:629-638.
216. Garidel, P., C. Johann, L. Mennicke, and A. Blume. 1997. The mixing behavior of pseudobinary phosphatidylcholine-phosphatidylglycerol mixtures as a function of pH and chain length. *European Biophysics Journal* 26:447-459.
217. Prossnigg, F., A. Hickel, G. Pabst, and K. Lohner. 2010. Packing behaviour of two predominant anionic phospholipids of bacterial cytoplasmic membranes. *Biophysical Chemistry* 150:129-135.
218. Tamm, L., and S. A. Tatulian. 1997. Infrared spectroscopy of proteins and peptides in lipid bilayers. *Quarterly Reviews of Biophysics* 30:365-429.
219. Siminovitch, D. J., P. T. Wong, and H. H. Mantsch. 1987. High-pressure infrared spectroscopy of ether- and ester-linked phosphatidylcholine aqueous dispersions. *Biophysical Journal* 51:465-473.
220. Siminovitch, D. J., P. T. T. Wong, and H. H. Mantsch. 1987. High pressure infrared spectroscopy of lipid bilayers: New tests for interdigitation. *Biochimica et Biophysica Acta (BBA) - Biomembranes* 900:163-167.
221. Blume, A., W. Hübner, and G. Messner. 1988. Fourier transform infrared spectroscopy of ¹³C=O labeled phospholipids hydrogen bonding to carbonyl groups. *Biochemistry* 27:8239-8249.
222. Garidel, P., C. Johann, and A. Blume. 2011. Non-ideal mixing and fluid–fluid immiscibility in phosphatidic acid–phosphatidylethanolamine mixed bilayers. *European Biophysics Journal* 40:891-905.
223. Tuchtenhagen, J. 1994. Kalorimetrische und FT-IR-spektroskopische Untersuchungen an Phospholipidmodellmembranen. Doctoral Thesis. Fachbereich Chemie. Universität Kaiserslautern, Kaiserslautern.
224. Casal, H. L., H. H. Mantsch, and H. Hauser. 1989. Infrared and ³¹P-NMR studies of the interaction of Mg²⁺ with phosphatidylserines: Effect of hydrocarbon chain unsaturation. *Biochimica et Biophysica Acta (BBA) - Biomembranes* 982:228-236.
225. Lewis, R. N. A. H., and R. N. McElhaney. 2009. The physicochemical properties of cardiolipin bilayers and cardiolipin-containing lipid membranes. *Biochimica et Biophysica Acta (BBA) - Biomembranes* 1788:2069-2079.
226. Etienne, F., Y. Roche, P. Peretti, and S. Bernard. 2008. Cardiolipin packing ability studied by grazing incidence X-ray diffraction. *Chemistry and Physics of Lipids* 152:13-23.
227. Domènech, Ò., F. Sanz, M. T. Montero, and J. Hernández-Borrell. 2006. Thermodynamic and structural study of the main phospholipid components comprising the mitochondrial inner membrane. *Biochimica et Biophysica Acta (BBA) - Biomembranes* 1758:213-221.
228. Sennato, S., F. Bordi, C. Cametti, C. Coluzza, A. Desideri, and S. Rufini. 2005. Evidence of domain formation in cardiolipin–glycerophospholipid mixed monolayers. A thermodynamic and AFM study. *The Journal of Physical Chemistry B* 109:15950-15957.
229. Zhang, M., E. Mileykovskaya, and W. Dowhan. 2002. Gluing the respiratory chain together. Cardiolipin is required for supercomplex formation in the inner mitochondrial membrane. *The Journal of Biological Chemistry* 277:43553-43556.
230. Zhong, Q., V. M. Gohil, L. Ma, and M. L. Greenberg. 2004. Absence of cardiolipin results in temperature sensitivity, respiratory defects, and mitochondrial DNA instability independent of pet56. *The Journal of Biological Chemistry* 279:32294-32300.
231. Lacombe, M.-L., M. Tokarska-Schlattner, R. F. Epand, M. Boissan, R. M. Epand, and U. Schlattner. 2009. Interaction of NDPK-D with cardiolipin-containing membranes: Structural basis and implications for mitochondrial physiology. *Biochimie* 91:779-783.

232. Laage, S., Y. Tao, and A. E. McDermott. 2015. Cardiolipin interaction with subunit c of ATP synthase: Solid-state NMR characterization. *Biochimica et Biophysica Acta (BBA) - Biomembranes* 1848:260-265.
233. Klingenberg, M. 2009. Cardiolipin and mitochondrial carriers. *Biochimica et Biophysica Acta (BBA) - Biomembranes* 1788:2048-2058.
234. Jiang, F., M. T. Ryan, M. Schlame, M. Zhao, Z. Gu, M. Klingenberg, N. Pfanner, and M. L. Greenberg. 2000. Absence of cardiolipin in the *crd1* null mutant results in decreased mitochondrial membrane potential and reduced mitochondrial function. *The Journal of Biological Chemistry* 275:22387-22394.
235. Claypool, S. M. 2009. Cardiolipin, a critical determinant of mitochondrial carrier protein assembly and function. *Biochimica et Biophysica Acta (BBA) - Biomembranes* 1788:2059-2068.
236. Sorice, M., V. Manganelli, P. Matarrese, A. Tinari, R. Misasi, W. Malorni, and T. Garofalo. 2009. Cardiolipin-enriched raft-like microdomains are essential activating platforms for apoptotic signals on mitochondria. *FEBS Letters* 583:2447-2450.
237. Schug, Z. T., and E. Gottlieb. 2009. Cardiolipin acts as a mitochondrial signalling platform to launch apoptosis. *Biochimica et Biophysica Acta (BBA) - Biomembranes* 1788:2022-2031.
238. Lohner, K., A. Latal, G. Degovics, and P. Garidel. 2001. Packing characteristics of a model system mimicking cytoplasmic bacterial membranes. *Chemistry and Physics of Lipids* 111:177-192.
239. Pozo Navas, B., K. Lohner, G. Deutsch, E. Sevesik, K. A. Riske, R. Dimova, P. Garidel, and G. Pabst. 2005. Composition dependence of vesicle morphology and mixing properties in a bacterial model membrane system. *Biochimica et Biophysica Acta (BBA) - Biomembranes* 1716:40-48.
240. Uragami, M., T. Dewa, M. Inagaki, R. A. Hendel, and S. L. Regen. 1997. Influence of head group mismatch on the miscibility of phospholipids in the physiologically-relevant fluid phase: A nearest-neighbor recognition analysis. *Journal of the American Chemical Society* 119:3797-3801.
241. Benesch, M. G. K., R. N. A. H. Lewis, and R. N. McElhaney. 2015. On the miscibility of cardiolipin with 1,2-diacyl phosphoglycerides: Binary mixtures of dimyristoylphosphatidylglycerol and tetramyristoylcardiolipin. *Biochimica et Biophysica Acta (BBA) - Biomembranes* 1848:2878-2888.
242. Frias, M., M. G. K. Benesch, R. N. A. H. Lewis, and R. N. McElhaney. 2011. On the miscibility of cardiolipin with 1,2-diacyl phosphoglycerides: Binary mixtures of dimyristoylphosphatidylethanolamine and tetramyristoylcardiolipin. *Biochimica et Biophysica Acta (BBA) - Biomembranes* 1808:774-783.
243. Blondelle, S. E., and R. A. Houghten. 1996. Novel antimicrobial compounds identified using synthetic combinatorial library technology. *Trends in Biotechnology* 14:60-65.
244. Blondelle, S. E., E. Takahashi, R. A. Houghten, and E. Pérez-Payá. 1996. Rapid identification of compounds with enhanced antimicrobial activity by using conformationally defined combinatorial libraries. *Biochemical Journal* 313:141-147.
245. Blondelle, S. E., E. Pérez-Payá, and R. A. Houghten. 1996. Synthetic combinatorial libraries: Novel discovery strategy for identification of antimicrobial agents. *Antimicrobial Agents and Chemotherapy* 40:1067-1071.
246. Strøm, M. B., B. E. Haug, M. L. Skar, W. Stensen, T. Stiberg, and J. S. Svendsen. 2003. The pharmacophore of short cationic antibacterial peptides. *Journal of Medicinal Chemistry* 46:1567-1570.
247. Liu, Z., A. Brady, A. Young, B. Rasimick, K. Chen, C. Zhou, and N. R. Kallenbach. 2007. Length effects in antimicrobial peptides of the (RW)_n series. *Antimicrobial Agents and Chemotherapy* 51:597-603.
248. Mohan, K. V. K., S. S. Rao, and C. D. Atreya. 2010. Antiviral activity of selected antimicrobial peptides against vaccinia virus. *Antiviral Research* 86:306-311.

249. Mohan, K. V. K., S. S. Rao, and C. D. Atreya. 2010. Evaluation of antimicrobial peptides as novel bactericidal agents for room temperature-stored platelets. *Transfusion* 50:166-173.
250. Dathe, M., H. Nikolenko, J. Klose, and M. Bienert. 2004. Cyclization increases the antimicrobial activity and selectivity of arginine- and tryptophan-containing hexapeptides. *Biochemistry* 43:9140-9150.
251. Junkes, C. 2012. Strukturelle Grundlagen der antimikrobiellen Aktivität und Selektivität kleiner cyclischer Peptide. Doctoral Thesis. Fachbereich Biologie, Chemie, Pharmazie. FU Berlin, Berlin.
252. Finger, S., A. Kerth, M. Dathe, and A. Blume. 2015. The efficacy of trivalent cyclic hexapeptides to induce lipid clustering in PG/PE membranes correlates with their antimicrobial activity. *Biochimica et Biophysica Acta (BBA) - Biomembranes* 1848:2998-3006.
253. Appelt, C., A. K. Schrey, J. A. Söderhäll, and P. Schmieder. 2007. Design of antimicrobial compounds based on peptide structures. *Bioorganic & Medicinal Chemistry Letters* 17:2334-2337.
254. Junkes, C., R. D. Harvey, K. D. Bruce, R. Dölling, M. Bagheri, and M. Dathe. 2011. Cyclic antimicrobial R-, W-rich peptides: The role of peptide structure and E. coli outer and inner membranes in activity and the mode of action. *European Biophysics Journal* 40:515-528.
255. Speck, S., A. Courtiol, C. Junkes, M. Dathe, K. Müller, and M. Schulze. 2014. Cationic synthetic peptides: Assessment of their antimicrobial potency in liquid preserved boar semen. *PloS one* 9:e105949.
256. Arouri, A., V. Kiessling, L. Tamm, M. Dathe, and A. Blume. 2011. Morphological changes induced by the action of antimicrobial peptides on supported lipid bilayers. *The Journal of Physical Chemistry B* 115:158-167.
257. Hancock, R. E. W., and A. Rozek. 2002. Role of membranes in the activities of antimicrobial cationic peptides. *FEMS Microbiology Letters* 206:143-149.
258. Ramachandran, G. N., C. Ramakrishnan, and V. Sasisekharan. 1963. Stereochemistry of polypeptide chain configurations. *Journal of Molecular Biology* 7:95-99.
259. Corey, R. B., and L. Pauling. 1953. Fundamental dimensions of polypeptide chains. *Proceedings of the Royal Society of London B: Biological Sciences* 141:10-20.
260. Anfinsen, C. B. 1973. Principles that govern the folding of protein chains. *Science* 181:223-230.
261. Rose, G. D., P. J. Fleming, J. R. Banavar, and A. Maritan. 2006. A backbone-based theory of protein folding. *Proceedings of the National Academy of Sciences of the United States of America* 103:16623-16633.
262. McMorran, L. M., D. J. Brockwell, and S. E. Radford. 2014. Mechanistic studies of the biogenesis and folding of outer membrane proteins in vitro and in vivo: What have we learned to date? *Archives of Biochemistry and Biophysics* 564:265-280.
263. Hagen, S. J., J. Hofrichter, A. Szabo, and W. A. Eaton. 1996. Diffusion-limited contact formation in unfolded cytochrome c: Estimating the maximum rate of protein folding. *Proceedings of the National Academy of Sciences of the United States of America* 93:11615-11617.
264. Krieger, F., B. Fierz, O. Bieri, and M. Drewello. 2003. Dynamics of unfolded polypeptide chains as model for the earliest steps in protein folding. *Journal of Molecular Biology* 332:265-274.
265. de Brevern, A. G. 2016. Extension of the classical classification of β -turns. *Scientific Reports* 6:205.
266. Panasik, N., P. J. Fleming, and G. D. Rose. 2005. Hydrogen-bonded turns in proteins: The case for a recount. *Protein Science* 14:2910-2914.
267. Smith, J. A., L. G. Pease, and K. D. Kopple. 1980. Reverse turns in peptides and protein. *Critical Reviews in Biochemistry* 8:315-399.

268. Appelt, C., A. Wessolowski, M. Dathe, and P. Schmieder. 2008. Structures of cyclic, antimicrobial peptides in a membrane-mimicking environment define requirements for activity. *Journal of Peptide Science* 14:524-527.
269. Appelt, C., A. Wessolowski, J. A. Söderhäll, M. Dathe, and P. Schmieder. 2005. Structure of the antimicrobial, cationic hexapeptide cyclo(RRWRF) and its analogues in solution and bound to detergent micelles. *ChemBioChem* 6:1654-1662.
270. Appelt, C., F. Eisenmenger, R. Kühne, P. Schmieder, and J. A. Söderhäll. 2005. Interaction of the antimicrobial peptide cyclo(RRWRF) with membranes by molecular dynamics simulations. *Biophysical Journal* 89:2296-2306.
271. Krimm, S., and J. Bandekar. 1986. Vibrational spectroscopy and conformation of peptides, polypeptides, and proteins. *Advances in Protein Chemistry* 38:181-364.
272. Vass, E., U. Strijowski, K. Wollschläger, I. M. Mándity, G. Szilvágyi, M. Jewgiński, K. Gaus, S. Royo, Z. Majer, N. Sewald, and M. Hollósi. 2010. VCD studies on cyclic peptides assembled from L- α -amino acids and a trans-2-aminocyclopentane- or trans-2-aminocyclohexane carboxylic acid. *Journal of Peptide Science* 16:613-620.
273. Vass, E., M. Hollósi, F. Besson, and R. Buchet. 2003. Vibrational spectroscopic detection of beta- and gamma-turns in synthetic and natural peptides and proteins. *Chemical Reviews* 103:1917-1954.
274. Vass, E., S. Holly, Z. Majer, J. Samu, I. Laczko, and M. Hollósi. 1997. FT-IR and CD spectroscopic detection of H-bonded folded polypeptide structures. *Journal of Molecular Structure* 408:47-56.
275. Vass, E., E. Lang, J. Samu, and Z. Majer. 1998. Vibrational spectroscopic detection of H-bonded β - and γ -turns in cyclic peptides and glycopeptides. *Journal of Molecular Structure* 440:59-71.
276. Hilario, J., J. Kubelka, and T. A. Keiderling. 2003. Optical spectroscopic investigations of model β -sheet hairpins in aqueous solution. *Journal of the American Chemical Society* 125:7562-7574.
277. Kolano, C., J. Helbing, M. Kozinski, W. Sander, and P. Hamm. 2006. Watching hydrogen-bond dynamics in a β -turn by transient two-dimensional infrared spectroscopy. *Nature* 444:469-472.
278. Merten, C., F. Li, K. Bravo-Rodriguez, E. Sanchez-Garcia, Y. Xu, and W. Sander. 2014. Solvent-induced conformational changes in cyclic peptides: A vibrational circular dichroism study. *Physical Chemistry Chemical Physics* 16:5627-5633.
279. Ferré, G., F. Besson, and R. Buchet. 1997. Conformational studies of the cyclic L,D-lipopeptide surfactin by fourier transform infrared spectroscopy. *Spectrochimica Acta Part A: Molecular and Biomolecular Spectroscopy* 53:623-635.
280. Bredenbeck, J., J. Helbing, A. Sieg, T. Schrader, W. Zinth, C. Renner, R. Behrendt, L. Moroder, J. Wachtveitl, and P. Hamm. 2003. Picosecond conformational transition and equilibration of a cyclic peptide. *Proceedings of the National Academy of Sciences of the United States of America* 100:6452-6457.
281. Mantsch, H. H., A. Perczel, M. Hollósi, and G. D. Fasman. 1993. Characterization of β -turns in cyclic hexapeptides in solution by fourier transform IR spectroscopy. *Biopolymers* 33:201-207.
282. Chirgadze, Y. N., O. V. Fedorov, and N. P. Trushina. 1975. Estimation of amino acid residue side-chain absorption in the infrared spectra of protein solutions in heavy water. *Biopolymers*.
283. Bandekar, J. 1993. Amide modes of reverse turns. *Vibrational Spectroscopy* 5:143-173.
284. Bandekar, J. 1992. Amide modes and protein conformation. *Biochimica et Biophysica Acta (BBA) - Proteins and Proteomics* 1120:123-143.
285. Shaw, R. A., A. Perczel, and H. H. Mantsch. 1994. Turns in small cyclic peptides—can infrared spectroscopy detect and discriminate amongst them? *Journal of Molecular Structure* 324:143-150.
286. Bouř, P., J. Kim, J. Kapitan, R. P. Hammer, R. Huang, L. Wu, and T. A. Keiderling. 2008. Vibrational circular dichroism and IR spectral analysis as a test of theoretical conformational modeling for a cyclic hexapeptide. *Chirality* 20:1104-1119.

287. Brauner, J. W., C. Dugan, and R. Mendelsohn. 2000. ^{13}C isotope labeling of hydrophobic peptides. Origin of the anomalous intensity distribution in the infrared amide I spectral region of β -sheet structures. *Journal of the American Chemical Society* 122:677-683.
288. Kubelka, J., and T. A. Keiderling. 2001. Differentiation of β -sheet-forming structures: Ab initio-based simulations of IR absorption and vibrational CD for model peptide and protein β -sheets. *Journal of the American Chemical Society* 123:12048-12058.
289. Barth, A. 2000. The infrared absorption of amino acid side chains. *Progress in Biophysics and Molecular Biology* 74:141-173.
290. Rahmelow, K., W. Hübner, and T. Ackermann. 1998. Infrared absorbances of protein side chains. *Analytical Biochemistry* 257:1-11.
291. Vorobyev, D. Y., C.-H. Kuo, D. G. Kuroda, J. N. Scott, J. M. Vanderkooi, and R. M. Hochstrasser. 2010. Water-induced relaxation of a degenerate vibration of guanidinium using 2D IR echo spectroscopy. *The Journal of Physical Chemistry B* 114:2944-2953.
292. Ghosh, A., M. J. Tucker, and R. M. Hochstrasser. 2011. Identification of arginine residues in peptides by 2D-IR echo spectroscopy. *The Journal of Physical Chemistry A* 115:9731-9738.
293. Hong, Z., J. Wert, and S. A. Asher. 2013. UV resonance Raman and DFT studies of arginine side chains in peptides: Insights into arginine hydration. *The Journal of Physical Chemistry B*.
294. Bagchi, S., C. Falvo, S. Mukamel, and R. M. Hochstrasser. 2009. 2d-IR experiments and simulations of the coupling between amide-I and ionizable side chains in proteins: Application to the villin headpiece. *The Journal of Physical Chemistry B* 113:11260-11273.
295. Hernández, B., F. Pflüger, and N. Derbel. 2010. Vibrational analysis of amino acids and short peptides in hydrated media. VI. Amino acids with positively charged side chains: L-lysine and l-arginine. *The Journal of Physical Chemistry B* 114:1077-1088.
296. Drozd, M. 2008. New complexes of guanidine with acetic, trichloroacetic and trifluoroacetic acids. *Spectrochimica Acta Part A: Molecular and Biomolecular Spectroscopy* 69:1223-1234.
297. Braiman, M. S., D. M. Briercheck, and K. M. Kriger. 1999. Modeling vibrational spectra of amino acid side chains in proteins: Effects of protonation state, counterion, and solvent on arginine C–N stretch frequencies. *The Journal of Physical Chemistry B* 103:4744-4750.
298. Huerta-Viga, A., S. Amirjalayer, S. R. Domingos, H. Meuzelaar, A. Rupenyan, and S. Woutersen. 2015. The structure of salt bridges between arg⁺ and glu⁻ in peptides investigated with 2D-IR spectroscopy: Evidence for two distinct hydrogen-bond geometries. *The Journal of Chemical Physics* 142:212444.
299. Liberato, M. S., S. Kogikoski Jr., E. R. Silva, M. D. Coutinho-Neto, L. P. B. Scott, R. H. Silva, V. X. Oliveira Jr., R. A. Ando, and W. A. Alves. 2013. Self-assembly of arg–phe nanostructures via the solid–vapor phase method. *The Journal of Physical Chemistry B* 117:733-740.
300. Drozd, M. 2007. Molecular structure and infrared spectra of guanidinium cation. *Materials Science and Engineering: B* 136:20-28.
301. Huerta-Viga, A., S. R. Domingos, and S. Amirjalayer. 2014. A salt-bridge structure in solution revealed by 2D-IR spectroscopy. *Physical Chemistry Chemical Physics* 16:15784-15786.
302. Fabian, H., C. Schultz, J. Backmann, and U. Hahn. 1994. Impact of point mutations on the structure and thermal stability of ribonuclease T1 in aqueous solution probed by fourier transform infrared spectroscopy. *Biochemistry* 33:10725-10730.
303. Ten, G. N., A. A. Yakovleva, T. G. Burova, V. I. Berezin, and V. I. Baranov. 2010. Modeling vibrational spectra of indole in water. *Journal of Applied Spectroscopy* 77:502-509.
304. Hernández, B. n., F. Pflüger, A. Adenier, S. G. Kruglik, and M. Ghomi. 2010. Vibrational analysis of amino acids and short peptides in hydrated media. VIII. Amino acids with aromatic side chains: L-phenylalanine, L-tyrosine, and L-tryptophan. *The Journal of Physical Chemistry B* 114:15319-15330.

305. Harada, I., T. Miura, and H. Takeuchi. 1986. Origin of the doublet at 1360 and 1340 cm^{-1} in the Raman spectra of tryptophan and related compounds. *Spectrochimica Acta Part A: Molecular and Biomolecular Spectroscopy* 42:307-312.
306. Takeuchi, H., and I. Harada. 1986. Normal coordinate analysis of the indole ring. *Spectrochimica Acta Part A: Molecular and Biomolecular Spectroscopy* 42:1069-1078.
307. Efremov, R. G., A. V. Feofanov, and I. R. Nabiev. 1992. Effect of hydrophobic environment on the resonance Raman-spectra of tryptophan residues in proteins. *Journal of Raman Spectroscopy* 23:69-73.
308. de Kruijff, B., A. Rietveld, and N. Telders. 1985. Molecular aspects of the bilayer stabilization induced by poly (L-lysines) of varying size in cardiolipin liposomes. *Biochimica et Biophysica Acta (BBA) - Biomembranes* 820:295-304.
309. Ben-Tal, N., B. Honig, R. M. Peitzsch, G. Denisov, and S. McLaughlin. 1996. Binding of small basic peptides to membranes containing acidic lipids: Theoretical models and experimental results. *Biophysical Journal* 71:561-575.
310. Kim, J., M. Mosior, L. A. Chung, H. Wu, and S. McLaughlin. 1991. Binding of peptides with basic residues to membranes containing acidic phospholipids. *Biophysical Journal* 60:135-148.
311. Momo, F., S. Fabris, and R. Stevanato. 2000. Interaction of linear mono- and diamines with dimyristoylphosphatidylcholine and dimyristoylphosphatidylglycerol multilamellar liposomes. *Archives of Biochemistry and Biophysics* 382:224-231.
312. Finger, S., C. Schwieger, A. Arouri, A. Kerth, and A. Blume. 2014. Interaction of linear polyamines with negatively charged phospholipids: The effect of polyamine charge distance. *Biological Chemistry* 395:769-778.
313. Ladokhin, A. S., and S. H. White. 2001. Protein chemistry at membrane interfaces: Non-additivity of electrostatic and hydrophobic interactions. *Journal of Molecular Biology* 309:543-552.
314. Wimley, W. C., and S. H. White. 1996. Experimentally determined hydrophobicity scale for proteins at membrane interfaces. *Nature Structural Biology* 3:842-848.
315. Jing, W., H. N. Hunter, J. Hagel, and H. J. Vogel. 2003. The structure of the antimicrobial peptide Ac-RRWRF-NH₂ bound to micelles and its interactions with phospholipid bilayers. *Journal of Peptide Research* 61:219-229.
316. Li, L., I. Vorobyov, and T. W. Allen. 2013. The different interactions of lysine and arginine side chains with lipid membranes. *The Journal of Physical Chemistry B* 117:11906-11920.
317. Wender, P. A., W. C. Galliher, E. A. Goun, L. R. Jones, and T. H. Pillow. 2003. The design of guanidinium-rich transporters and their internalization mechanisms. *Advanced Drug Delivery Reviews* 60:452-472.
318. Calnan, B. J., B. Tidor, S. Biancalana, D. Hudson, and A. D. Frankel. 1991. Arginine-mediated RNA recognition: The arginine fork. *Science* 252:1167-1171.
319. Sakai, N., T. Takeuchi, S. Futaki, and S. Matile. 2005. Direct observation of anion-mediated translocation of fluorescent oligoarginine carriers into and across bulk liquid and anionic bilayer membranes. *ChemBioChem* 6:114-122.
320. Hamelberg, D., T. Shen, and J. A. McCammon. 2007. A proposed signaling motif for nuclear import in mRNA processing via the formation of arginine claw. *Proceedings of the National Academy of Sciences of the United States of America* 104:14947-14951.
321. Vondrásek, J., P. E. Mason, J. Heyda, K. D. Collins, and P. Jungwirth. 2009. The molecular origin of like-charge arginine-arginine pairing in water. *The Journal of Physical Chemistry B* 113:9041-9045.
322. Mason, P. E., G. W. Neilson, J. E. Enderby, M.-L. Saboungi, C. E. Dempsey, A. D. MacKerell, and J. W. Brady. 2004. The structure of aqueous guanidinium chloride solutions. *Journal of the American Chemical Society* 126:11462-11470.
323. Frigyes, D., F. Alber, S. Pongor, and P. Carloni. 2001. Arginine-phosphate salt bridges in protein-DNA complexes: A Car-Parrinello study. *Journal of Molecular Structure* 574:39-45.

324. Schwieger, C., and A. Blume. 2009. Interaction of poly(L-arginine) with negatively charged DPPG membranes: Calorimetric and monolayer studies. *Biomacromolecules* 10:2152-2161.
325. Schwieger, C., and A. Blume. 2006. Interaction of poly(L-lysines) with negatively charged membranes: An FT-IR and DSC study. *European Biophysics Journal* 36:437-450.
326. Schwieger, C. 2008. Electrostatic and non-electrostatic interactions of positively charged polypeptides with negatively charged lipid membranes. Doctoral Thesis. Naturwissenschaftliche Fakultät II - Chemie und Physik. Martin-Luther-Universität Halle-Wittenberg, Halle/Saale.
327. Wu, Z., Q. Cui, and A. Yethiraj. 2013. Why do arginine and lysine organize lipids differently? Insights from coarse-grained and atomistic simulations. *The Journal of Physical Chemistry B* 117:12145-12156.
328. Schmidt, N. W., A. Mishra, G. H. Lai, M. Davis, L. K. Sanders, D. Tran, A. Garcia, K. P. Tai, P. B. McCray, A. J. Ouellette, M. E. Selsted, and G. C. L. Wong. 2011. Criterion for amino acid composition of defensins and antimicrobial peptides based on geometry of membrane destabilization. *Journal of the American Chemical Society* 133:6720-6727.
329. Perkins, S. J. 1986. Protein volumes and hydration effects - the calculations of partial specific volumes, neutron-scattering matchpoints and 280-nm absorption-coefficients for proteins and glycoproteins from amino-acid-sequences. *European Journal of Biochemistry* 157:169-180.
330. Millero, F. J., A. Lo Surdo, and C. Shin. 1978. The apparent molal volumes and adiabatic compressibilities of aqueous amino acids at 25 °C. *The Journal of Physical Chemistry* 82:784-792.
331. Ulmschneider, M. B., M. Sansom, and A. Di Nola. 2005. Properties of integral membrane protein structures: Derivation of an implicit membrane potential. *Proteins: Structure, Function, and Bioinformatics* 59:252-265.
332. Braun, P., and G. von Heijne. 1999. The aromatic residues trp and phe have different effects on the positioning of a transmembrane helix in the microsomal membrane. *Biochemistry* 38:9778-9782.
333. Norman, K. E., and H. Nymeyer. 2006. Indole localization in lipid membranes revealed by molecular simulation. *Biophysical Journal* 91:2046-2054.
334. Yau, W. M., W. C. Wimley, K. Gawrisch, and S. H. White. 1998. The preference of tryptophan for membrane interfaces. *Biochemistry* 37:14713-14718.
335. Jacobs, R. E., and S. H. White. 1989. The nature of the hydrophobic binding of small peptides at the bilayer interface: Implications for the insertion of transbilayer helices. *Biochemistry* 28:3421-3437.
336. Schibli, D. J., R. F. Epand, H. J. Vogel, and R. M. Epand. 2002. Tryptophan-rich antimicrobial peptides: Comparative properties and membrane interactions. *Biochemistry and Cell Biology* 80:667-677.
337. Kachel, K., E. Asuncion-Punzalan, and E. London. 1995. Anchoring of tryptophan and tyrosine analogs at the hydrocarbon-polar boundary in model membrane vesicles. *Biochemistry* 34:15475-15479.
338. Meulendijks, G. H. W. M., T. Sonderkamp, J. E. Dubois, R. J. Nielen, J. A. Kremers, and H. M. Buck. 1989. The different influences of ether and ester phospholipids on the conformation of gramicidin A. A molecular modelling study. *Biochimica et Biophysica Acta (BBA) - Biomembranes* 979:321-330.
339. Petersen, F. N. R., M. Ø. Jensen, and C. H. Nielsen. 2005. Interfacial tryptophan residues: A role for the cation- π effect? *Biophysical Journal* 89:3985-3996.
340. Hu, W., K. C. Lee, and T. A. Cross. 1993. Tryptophans in membrane proteins: Indole ring orientations and functional implications in the gramicidin channel. *Biochemistry* 32:7035-7047.
341. van der Wel, P. C. A., E. Strandberg, J. A. Killian, and R. E. Koeppe II. 2002. Geometry and intrinsic tilt of a tryptophan-anchored transmembrane α -helix determined by ^2H NMR. *Biophysical Journal* 83:1479-1488.

342. Lazo, N. D., W. Hu, and T. A. Cross. 1992. Probing lipid-protein interactions by solid-state NMR spectroscopy of fast frozen samples. *Journal of the Chemical Society, Chemical Communications* 20:1529-1531.
343. Chaudhuri, A., S. Haldar, H. Sun, R. E. Koeppe, and A. Chattopadhyay. 2014. Importance of indole N-H hydrogen bonding in the organization and dynamics of gramicidin channels. *Biochimica et Biophysica Acta (BBA) - Biomembranes* 1838:419-428.
344. van der Wel, P. C. A., N. D. Reed, D. V. Greathouse, and R. E. Koeppe. 2007. Orientation and motion of tryptophan interfacial anchors in membrane-spanning peptides. *Biochemistry* 46:7514-7524.
345. Esbjörner, E. K., C. E. B. Caesar, B. Albinsson, P. Lincoln, and B. Nordén. 2007. Tryptophan orientation in model lipid membranes. *Biochemical and Biophysical Research Communications* 361:645-650.
346. Persson, S., J. Antoinette Killian, and G. Lindblom. 1998. Molecular ordering of interfacially localized tryptophan analogs in ester- and ether-lipid bilayers studied by 2H-NMR. *Biophysical Journal* 75:1365-1371.
347. Dougherty, D. A. 1996. Cation- π interactions in chemistry and biology: A new view of benzene, phe, tyr, and trp. *Science* 271:163-168.
348. Gallivan, J. P., and D. A. Dougherty. 1999. Cation- π interactions in structural biology. *Proceedings of the National Academy of Sciences of the United States of America* 96:9459-9464.
349. Dougherty, D. A. 2012. The cation- π interaction. *Accounts of Chemical Research* 46:885-893.
350. Ma, J. C., and D. A. Dougherty. 1997. The cation- π interaction. *Chemical Reviews* 97:1303-1324.
351. Sanderson, J. M., and E. J. Whelan. 2004. Characterisation of the interactions of aromatic amino acids with diacetyl phosphatidylcholine. *Physical Chemistry Chemical Physics* 6:1012-1017.
352. Chan, D. I., E. J. Prenner, and H. J. Vogel. 2006. Tryptophan- and arginine-rich antimicrobial peptides: Structures and mechanisms of action. *Biochimica et Biophysica Acta (BBA) - Biomembranes* 1758:1184-1202.
353. Khandelia, H., and Y. N. Kaznessis. 2007. Cation- π interactions stabilize the structure of the antimicrobial peptide indolicidin near membranes: Molecular dynamics simulations. *The Journal of Physical Chemistry B* 111:242-250.
354. Aliste, M. P., J. L. MacCallum, and D. P. Tieleman. 2003. Molecular dynamics simulations of pentapeptides at interfaces: Salt bridge and cation- π interactions. *Biochemistry* 42:8976-8987.
355. Adamian, L., and J. Liang. 2001. Helix-helix packing and interfacial pairwise interactions of residues in membrane proteins. *Journal of Molecular Biology* 311:891-907.
356. Glaser, F., D. M. Steinberg, I. A. Vakser, and N. Ben-Tal. 2001. Residue frequencies and pairing preferences at protein-protein interfaces. *Proteins: Structure, Function, and Bioinformatics* 43:89-102.
357. Mitchell, J. B. O., C. L. Nandi, I. K. McDonald, J. M. Thornton, and S. L. Price. 1994. Amino/aromatic interactions in proteins: Is the evidence stacked against hydrogen bonding? *Journal of Molecular Biology* 239:315-331.
358. Polyansky, A. A., P. E. Volynsky, A. S. Arseniev, and R. G. Efremov. 2009. Adaptation of a membrane-active peptide to heterogeneous environment. I. Structural plasticity of the peptide. *The Journal of Physical Chemistry B* 113:1107-1119.
359. Heinrichs, G., S. Kubik, J. Lacour, and L. Vial. 2005. Matched/mismatched interaction of a cyclic hexapeptide with ion pairs containing chiral cations and chiral anions. *Journal of Organic Chemistry* 70:4498-4501.
360. Haino, T., D. M. Rudkevich, and J. Rebek. 1999. Kinetically stable caviplaxes in water. *Journal of the American Chemical Society* 121:11253-11254.
361. Lhoták, P., and S. Shinkai. 1997. Cation- π interactions in Calix[n]Arene and related systems. *Journal of Physical Organic Chemistry* 10:273-285.

362. Meyer, E. A., R. K. Castellano, and F. Diederich. 2003. Interactions with aromatic rings in chemical and biological recognition. *Angewandte Chemie International Edition* 42:1210-1250.
363. Kubik, S., and R. Goddard. 2001. Fine tuning of the cation affinity of artificial receptors based on cyclic peptides by intramolecular conformational control. *European Journal of Organic Chemistry* 2001:311-322.
364. Kubik, S., and R. Goddard. 2000. Intramolecular conformational control in a cyclic peptide composed of alternating L-proline and substituted 3-aminobenzoic acid subunits. *Chemical Communications* 7:633-634.
365. Kubik, S. 1999. Large increase in cation binding affinity of artificial cyclopeptide receptors by an allosteric effect. *Journal of the American Chemical Society* 121:9001-9007.
366. Remko, M., and S. Soralova. 2012. Effect of water coordination on competition between pi and non-pi cation binding sites in aromatic amino acids: L-phenylalanine, L-tyrosine, and L-tryptophan Li⁺, Na⁺, and K⁺ complexes. *Journal of Biological Inorganic Chemistry* 17:621-630.
367. Schibli, D. J., P. M. Hwang, and H. J. Vogel. 1999. Structure of the antimicrobial peptide tritripticin bound to micelles: A distinct membrane-bound peptide fold. *Biochemistry* 38:16749-16755.
368. Gramse, G., A. Dols-Perez, M. A. Edwards, L. Fumagalli, and G. Gomila. 2013. Nanoscale measurement of the dielectric constant of supported lipid bilayers in aqueous solutions with electrostatic force microscopy. *Biophysical Journal* 104:1257-1262.
369. Nymeyer, H., and H.-X. Zhou. 2008. A method to determine dielectric constants in nonhomogeneous systems: Application to biological membranes. *Biophysical Journal* 94:1185-1193.
370. Stern, H. A., and S. E. Feller. 2003. Calculation of the dielectric permittivity profile for a nonuniform system: Application to a lipid bilayer simulation. *The Journal of Chemical Physics* 118:3401-3412.
371. Zhou, F., and K. Schulten. 1995. Molecular-dynamics study of a membrane water interface. *The Journal of Physical Chemistry* 99:2194-2207.
372. Gawrisch, K., D. Ruston, J. Zimmerberg, V. A. Parsegian, R. P. Rand, and N. Fuller. 1992. Membrane dipole potentials, hydration forces, and the ordering of water at membrane surfaces. *Biophysical Journal* 61:1213-1223.
373. Marrink, S. J., and H. J. C. Berendsen. 1996. Permeation process of small molecules across lipid membranes studied by molecular dynamics simulations. *The Journal of Physical Chemistry* 100:16729-16738.
374. Eklund, K. K., and P. Kinnunen. 1986. Effects of polyamines on the thermotropic behaviour of dipalmitoylphosphatidylglycerol. *Chemistry and Physics of Lipids* 39:109-117.
375. Hädicke, A., and A. Blume. 2016. Binding of cationic peptides (KX)₄K to DPPG bilayers. Increasing the hydrophobicity of the uncharged amino acid X drives formation of membrane bound β -sheets: A DSC and FT-IR study. *Biochimica et Biophysica Acta (BBA) - Biomembranes* 1858:1196-1206.
376. Hörnke, M., C. Schwieger, A. Kerth, and A. Blume. 2012. Binding of cationic pentapeptides with modified side chain lengths to negatively charged lipid membranes: Complex interplay of electrostatic and hydrophobic interactions. *Biochimica et Biophysica Acta (BBA) - Biomembranes* 1818:1663-1672.
377. Hörnke, M. 2008. Wechselwirkung von Oligopeptiden mit Lipidmembranmodellen. Naturwissenschaftliche Fakultät II - Chemie und Physik. Martin-Luther-Universität Halle-Wittenberg, Halle/Saale.
378. Malanovic, N., R. Leber, M. Schmuck, M. Kriechbaum, R. A. Cordfunke, J. W. Drijfhout, A. de Breij, P. H. Nibbering, D. Kolb, and K. Lohner. 2015. Phospholipid-driven differences determine the action of the synthetic antimicrobial peptide OP-145 on gram-positive bacterial and mammalian membrane model systems. *Biochimica et Biophysica Acta (BBA) - Biomembranes* 1848:2437-2447.

379. Pabst, G., S. L. Grage, S. Danner-Pongratz, W. Jing, A. S. Ulrich, A. Watts, K. Lohner, and A. Hickel. 2008. Membrane thickening by the antimicrobial peptide PGLa. *Biophysical Journal* 95:5779-5788.
380. Andrushchenko, V. V., H. J. Vogel, and E. J. Prenner. 2007. Interactions of tryptophan-rich cathelicidin antimicrobial peptides with model membranes studied by differential scanning calorimetry. *Biochimica et Biophysica Acta (BBA) - Biomembranes* 1768:2447-2458.
381. Pirc, K., and N. P. Ulrih. 2015. A-synuclein interactions with phospholipid model membranes: Key roles for electrostatic interactions and lipid-bilayer structure. *Biochimica et Biophysica Acta (BBA) - Biomembranes* 1848:2002-2012.
382. Heimburg, T. 1998. Mechanical aspects of membrane thermodynamics. Estimation of the mechanical properties of lipid membranes close to the chain melting transition from calorimetry. *Biochimica et Biophysica Acta (BBA) - Biomembranes* 1415:147-162.
383. Schneider, M. F., D. Marsh, W. Jahn, B. Kloesgen, and T. Heimburg. 1999. Network formation of lipid membranes: Triggering structural transitions by chain melting. *Proceedings of the National Academy of Sciences of the United States of America* 96:14312-14317.
384. Heimburg, T., and R. L. Biltonen. 1994. Thermotropic behavior of dimyristoylphosphatidylglycerol and its interaction with cytochrome-c. *Biochemistry* 33:9477-9488.
385. Alakoskela, J.-M. I., and P. K. J. Kinnunen. 2007. Thermal phase behavior of DMPG: the exclusion of continuous network and dense aggregates. *Langmuir* 23:4203-4213.
386. Alakoskela, J.-M., M. J. Parry, and P. K. J. Kinnunen. 2010. The intermediate state of DMPG is stabilized by enhanced positive spontaneous curvature. *Langmuir* 26:4892-4900.
387. Riske, K. A., L. Q. Amaral, and M. T. Lamy. 2009. Extensive bilayer perforation coupled with the phase transition region of an anionic phospholipid. *Langmuir* 25:10083-10091.
388. Riske, K. A., H.-G. Döbereiner, and M. T. Lamy-Freund. 2001. Gel-fluid transition in dilute versus concentrated DMPG aqueous dispersions. *The Journal of Physical Chemistry B* 106:239-246.
389. Riske, K. A., L. Q. Amaral, and M. T. Lamy-Freund. 2001. Thermal transitions of DMPG bilayers in aqueous solution: SAXS structural studies. *Biochimica et Biophysica Acta (BBA) - Biomembranes* 1511:297-308.
390. Cevc, G. 1990. Membrane electrostatics. *Biochimica et Biophysica Acta (BBA) - Biomembranes* 1031:311-382.
391. Laroche, G., E. J. Dufourc, J. Dufourcq, and M. Pezolet. 1991. Structure and dynamics of dimyristoylphosphatidic acid/calcium complexes by deuterium NMR, infrared, and Raman spectroscopies and small-angle X-ray diffraction. *Biochemistry* 30:3105-3114.
392. Teixeira, V., M. J. Feio, and M. Bastos. 2012. Role of lipids in the interaction of antimicrobial peptides with membranes. *Progress in Lipid Research* 51:149-177.
393. Junkes, C., A. Wessolowski, S. Farnaud, R. W. Evans, L. Good, M. Bienert, and M. Dathe. 2008. The interaction of arginine- and tryptophan-rich cyclic hexapeptides with *Escherichia coli* membranes. *Journal of Peptide Science* 14:535-543.
394. Schibli, D. J., P. M. Hwang, and H. J. Vogel. 1999. The structure of the antimicrobial active center of lactoferricin B bound to sodium dodecyl sulfate micelles. *FEBS Letters* 446:213-217.
395. Boggs, J. M., E. Jo, I. V. Polozov, R. F. Epand, G. M. Anantharamaiah, J. Blazyk, and R. M. Epand. 2001. Effect of magainin, class L, and class A amphipathic peptides on fatty acid spin labels in lipid bilayers. *Biochimica et Biophysica Acta (BBA) - Biomembranes* 1511:28-41.
396. Leclair, S., P. Baillargeon, R. Skouta, D. Gauthier, Y. Zhao, and Y. L. Dory. 2004. Micrometer-sized hexagonal tubes self-assembled by a cyclic peptide in a liquid crystal. *Angewandte Chemie International Edition* 43:349-353.
397. Montenegro, J., M. R. Ghadiri, and J. R. Granja. 2013. Ion channel models based on self-assembling cyclic peptide nanotubes. *Accounts of Chemical Research* 46:2955-2965.

398. Ghadiri, M. R., J. R. Granja, and L. K. Buehler. 1994. Artificial transmembrane ion channels from self-assembling peptide nanotubes. *Nature* 369:301-304.
399. Kim, H. S., J. D. Hartgerink, and M. R. Ghadiri. 1998. Oriented self-assembly of cyclic peptide nanotubes in lipid membranes. *Journal of the American Chemical Society* 120:4417-4424.
400. Ghadiri, M. R., J. R. Granja, R. A. Milligan, D. E. McRee, and N. Khazanovich. 1993. Self-assembling organic nanotubes based on a cyclic peptide architecture. *Nature* 366:324-327.
401. Scheinpflug, K., H. Nikolenko, I. Komarov, M. Rautenbach, and M. Dathe. 2013. What goes around comes around - a comparative study of the influence of chemical modifications on the antimicrobial properties of small cyclic peptides. *Pharmaceuticals* 6:1130-1144.
402. Jing, W., A. R. Demcoe, and H. J. Vogel. 2003. Conformation of a bactericidal domain of puroindoline A: Structure and mechanism of action of a 13-residue antimicrobial peptide. *Journal of Bacteriology* 185:4938-4947.
403. Montich, G., S. Scarlata, S. McLaughlin, R. Lehrmann, and J. Seelig. 1993. Thermodynamic characterization of the association of small basic peptides with membranes containing acidic lipids. *Biochimica et Biophysica Acta (BBA) - Biomembranes* 1146:17-24.
404. Seelig, J. 2004. Thermodynamics of lipid-peptide interactions. *Biochimica et Biophysica Acta (BBA) - Biomembranes* 1666:40-50.
405. Blume, A. 1988. Applications of calorimetry to lipid model membranes. Springer, Boston, MA, Boston, MA. 71-121.
406. Aroui, A., A. Kerth, M. Dathe, and A. Blume. 2011. The binding of an amphipathic peptide to lipid monolayers at the air/water interface is modulated by the lipid headgroup structure. *Langmuir* 27:2811-2818.
407. Gill, S. J., and I. Wadsö. 1976. An equation of state describing hydrophobic interactions. *Proceedings of the National Academy of Sciences of the United States of America* 73:2955-2958.
408. Madan, B., and K. Sharp. 1997. Molecular origin of hydration heat capacity changes of hydrophobic solutes: Perturbation of water structure around alkanes. *The Journal of Physical Chemistry B* 101:11237-11242.
409. Makhatadze, G. I., and P. L. Privalov. 1993. Contribution of hydration to protein folding thermodynamics. I. The enthalpy of hydration. *Journal of Molecular Biology* 232:639-659.
410. Beschiasvili, G., and H.-D. Baeuerle. 1991. Effective charge of melittin upon interaction with POPC vesicles. *Biochimica et Biophysica Acta (BBA) - Biomembranes* 1068:195-200.
411. Matulis, D. 2001. Thermodynamics of the hydrophobic effect. III. Condensation and aggregation of alkanes, alcohols, and alkylamines. *Biophysical Chemistry* 93:67-82.
412. Matulis, D., and V. A. Bloomfield. 2001. Thermodynamics of the hydrophobic effect. I. Coupling of aggregation and pKa shifts in solutions of aliphatic amines. *Biophysical Chemistry* 93:37-51.
413. May, S., D. Harries, and A. Ben-Shaul. 2000. Lipid demixing and protein-protein interactions in the adsorption of charged proteins on mixed membranes. *Biophysical Journal* 79:1747-1760.
414. Lohner, K., A. Latal, G. Degovics, and P. Garidel. 2001. Packing characteristics of a model system mimicking cytoplasmic bacterial membranes. *Chem. Phys. Lipids* 111:177-192.
415. Grahame, D. C. 1953. Diffuse double layer theory for electrolytes of unsymmetrical valence types. *The Journal of Chemical Physics* 21:1054-1060.
416. Omardien, S., J. W. Drijfhout, F. M. Vaz, M. Wenzel, L. W. Hamoen, S. A. J. Zaat, and S. Brul. 2018. Bactericidal activity of amphipathic cationic antimicrobial peptides involves altering the membrane fluidity when interacting with the phospholipid bilayer. *Biochimica et Biophysica Acta (BBA) - Biomembranes* 1860:2404-2415.

417. Ouardien, S., J. W. Drijfhout, S. A. Zaat, and S. Brul. 2018. Cationic amphipathic antimicrobial peptides perturb the inner membrane of germinated spores thus inhibiting their outgrowth. *Frontiers in Microbiology* 9:4541-4513.
418. Matches, J. R., H. W. Walker, and J. C. Ayres. 1964. Phospholipids in vegetative cells and spores of bacillus polymyxa. *Journal of Bacteriology* 87:16-23.
419. Nagle, J. F., and S. Tristram-Nagle. 2000. Structure of lipid bilayers. *Biochimica et Biophysica Acta (BBA) - Biomembranes* 1469:159-195.
420. Pabst, G., S. Danner, S. Karmakar, G. Deutsch, and V. A. Raghunathan. 2007. On the propensity of phosphatidylglycerols to form interdigitated phases. *Biophysical Journal* 93:513-525.
421. Pascher, I., M. Lundmark, P.-G. Nyholm, and S. Sundell. 1992. Crystal structures of membrane lipids. *Biochimica et Biophysica Acta (BBA) - Biomembranes* 1113:339-373.
422. Armen, R. S., O. D. Uitto, and S. E. Feller. 1998. Phospholipid component volumes: Determination and application to bilayer structure calculations. *Biophysical Journal* 75:734-744.
423. Pedersen, U. R., C. Leidy, P. Westh, and G. H. Peters. 2006. The effect of calcium on the properties of charged phospholipid bilayers. *Biochimica et Biophysica Acta (BBA) - Biomembranes* 1758:573-582.
424. Petrache, H. I., S. Tristram-Nagle, K. Gawrisch, D. Harries, V. A. Parsegian, and J. F. Nagle. 2004. Structure and fluctuations of charged phosphatidylserine bilayers in the absence of salt. *Biophysical Journal* 86:1574-1586.
425. Nagle, J. F., R. Zhang, S. Tristram-Nagle, W. Sun, H. I. Petrache, and R. M. Suter. 1996. X-ray structure determination of fully hydrated L alpha phase of dipalmitoylphosphatidylcholine bilayers. *Biophysical Journal* 70:1419-1431.
426. Tristram-Nagle, S., R. Zhang, R. M. Suter, C. R. Worthington, W. J. Sun, and J. F. Nagle. 1993. Measurement of chain tilt angle in fully hydrated bilayers of gel phase lecithins. *Biophysical Journal* 64:1097-1109.
427. Hädicke, A. 2016. Interactions of cationic peptides with anionic lipid bilayers and monolayers. Doctoral Thesis. Naturwissenschaftliche Fakultät II - Chemie, Physik und Mathematik. Martin-Luther-Universität Halle-Wittenberg, Halle/Saale.
428. Zasloff, M. 1987. Magainins, a class of antimicrobial peptides from *Xenopus* skin: Isolation, characterization of two active forms, and partial cDNA sequence of a precursor. *Proceedings of the National Academy of Sciences of the United States of America* 84:5449-5453.
429. Fuchs, P. C., A. L. Barry, and S. D. Brown. 1998. In vitro antimicrobial activity of MSI-78, a magainin analog. *Antimicrobial Agents and Chemotherapy* 42:1213-1216.
430. Soravia, E., G. Martini, and M. Zasloff. 2001. Antimicrobial properties of peptides from *Xenopus* granular gland secretions. *FEBS Letters* 228:337-340.
431. Dosler, S., and E. Karaaslan. 2014. Inhibition and destruction of *Pseudomonas aeruginosa* biofilms by antibiotics and antimicrobial peptides. *Peptides* 62:32-37.
432. Oren, Z., and Y. Shai. 1997. Selective lysis of bacteria but not mammalian cells by diastereomers of melittin: Structure–function study. *Biochemistry* 36:1826-1835.
433. Blondelle, S. E., and R. A. Houghten. 1991. Hemolytic and antimicrobial activities of the twenty-four individual omission analogs of melittin. *Biochemistry* 30:4671-4678.
434. Johansson, J., G. H. Gudmundsson, M. n. E. Rottenberg, K. D. Berndt, and B. Agerberth. 1998. Conformation-dependent antibacterial activity of the naturally occurring human peptide LL-37. *The Journal of Biological Chemistry* 273:3718-3724.
435. Bals, R., X. R. Wang, M. Zasloff, and J. M. Wilson. 1998. The peptide antibiotic LL-37/hCAP-18 is expressed in epithelia of the human lung where it has broad antimicrobial activity at the airway surface. *Proceedings of the National Academy of Sciences of the United States of America* 95:9541-9546.
436. Yang, S.-T., S. Yub Shin, Y.-C. Kim, Y. Kim, K.-S. Hahm, and J. I. Kim. 2002. Conformation-dependent antibiotic activity of tritricin, a cathelicidin-derived antimicrobial peptide. *Biochemical and Biophysical Research Communications* 296:1044-1050.

437. Wang, G. The antimicrobial peptide database.
438. Zavascki, A. P., L. Z. Goldani, J. Li, and R. L. Nation. 2007. Polymyxin B for the treatment of multidrug-resistant pathogens: A critical review. *Journal of Antimicrobial Chemotherapy* 60:1206-1215.
439. Sabath, L. D., C. Garner, C. Wilcox, and M. Finland. 1976. Susceptibility of *Staphylococcus aureus* and *Staphylococcus epidermidis* to 65 antibiotics. *Antimicrobial Agents and Chemotherapy* 9:962-969.
440. Kaur, H., and G. P. S. Raghava. 2004. A neural network method for prediction of beta-turn types in proteins using evolutionary information. *Bioinformatics* 20:2751-2758.
441. Balhara, V., R. Schmidt, S.-U. Gorr, and C. DeWolf. 2013. Membrane selectivity and biophysical studies of the antimicrobial peptide GL13K. *Biochimica et Biophysica Acta (BBA) - Biomembranes* 1828:2193-2203.
442. Abraham, T., R. N. A. H. Lewis, R. S. Hodges, and R. N. McElhaney. 2005. Isothermal titration calorimetry studies of the binding of the antimicrobial peptide gramicidin S to phospholipid bilayer membranes. *Biochemistry* 44:11279-11285.
443. Andrushchenko, V. V., M. H. Aarabi, L. T. Nguyen, E. J. Prenner, and H. J. Vogel. 2008. Thermodynamics of the interactions of tryptophan-rich cathelicidin antimicrobial peptides with model and natural membranes. *Biochimica et Biophysica Acta (BBA) - Biomembranes* 1778:1004-1014.
444. Domingues, T. M., K. R. Perez, A. Miranda, and K. A. Riske. 2015. Comparative study of the mechanism of action of the antimicrobial peptide gomesin and its linear analogue: The role of the β -hairpin structure. *Biochimica et Biophysica Acta (BBA) - Biomembranes* 1848:2414-2421.
445. Nichols, M., M. Kuljanin, M. Nategholeslam, T. Hoang, S. Vafaei, B. Tomberli, C. G. Gray, L. DeBruin, and M. Jelokhani-Niaraki. 2013. Dynamic turn conformation of a short tryptophan-rich cationic antimicrobial peptide and its interaction with phospholipid membranes. *The Journal of Physical Chemistry B* 117:14697-14708.
446. Wieprecht, T., O. Apostolov, M. Beyermann, and J. Seelig. 2000. Membrane binding and pore formation of the antibacterial peptide PGLa: Thermodynamic and mechanistic aspects. *Biochemistry* 39:442-452.

9

Acknowledgement

As finishing this work seemed often unattainable throughout its development, I would like to thank those essential to its completion.

Of foremost, I would like to thank Prof. Dr. Alfred Blume for supervising this work and especially for his scientific and personal support throughout the whole time and I sincerely hope to continue this inspirational relationship.

I thank Dr. Margitta Dathe (Forschungsinstitut für Molekulare Pharmakologie, Berlin) for the provision of the peptides and the successful cooperation.

I am extremely grateful to have been given the opportunity to be a member of the DFG Graduiertenkolleg 1026 “Conformational transitions in macromolecular interactions”. I enjoyed the vivid discussions throughout the weekly meetings and especially throughout the biannual conferences. Here, I would like to thank Prof. Milton Stubbs in particular for his major contributions to the scientifically stimulating atmosphere.

I owe my gratitude to the best work group I could have imagined. The regular discussions, the generous support, the constant encouragement and valuable advice created an atmosphere where colleagues became friends. Here, I especially would like to thank Dr. Andreas Kerth for his kind and thorough supervision, Dr. Christian Schwieger for his introduction to the topic and the lively and intellectually refreshing discussions, Dr. Maria Hörnke for the productive contributions and critical reviews on the clustering model, Dr. Martin Schiewek for his help with the IR experiments and setup, PD Dr. Annette Meister for her kind help with CryoTEM measurements, Dr. Bob-Dan Lechner for sharing the work, laughs and music inside and outside the lab, Dr. André Hädicke for solving many everyday problems, Anja Huster and Dr. Waquar Shah for giving the best everyday support with their loveliness. I thank Andreas Lonitz for being Andreas Lonitz.

Thanks to the monks from La Grande Chartreuse for sharing their bodacious green liqueur with the entire world enabling the rise of supportive thoughts through deep discussions.

The technical assistance of Mrs. Bettina Fölting, and Mrs. Edith Brendel is highly appreciated.

My sincere thanks are due to Dr. Günter Förster and Dr Ute Baumeister. Only due to their patience and ability to teach the basics of physical chemistry I was able to conduct this work.

The financial support from Deutsche Forschungsgemeinschaft (DFG) is gratefully acknowledged.

I thank Theresa Windorffer, Paul Ahlert, Jan Ebenhahn and Sven Zimmermann for their contributions to this work.

I thank Dr. Andreas Kerth, Dr. Maria Hörnke and Dr. Yana Hristova for carefully proofreading.

Finally, a very special debt of gratitude goes to my beloved family and friends. Thanks to Flavie for sharing a home of one's own, my parents and my brothers and sister for their undivided love and Vesal for everything. I want to thank all my friends for being there. I consider myself lucky to know you.

10

Curriculum vitae

10.1 Personal data

Surname: Finger

First name: Sebastian

Date of birth: 13.06.1982

Place of birth: Frankenberg/Eder

10.2. Education and research experience

Since 2016 *Material research scientist at the Research & Development center of Continental AG, Hannover, Germany.*

2014-2016 *Platform development engineer at the Research & Development center of Continental AG, Hannover, Germany.*

2009-2014 *PhD candidate at the Physical Chemistry Department at Martin-Luther-Universität Halle-Wittenberg within the Graduate college GRK1026, Halle/Saale, Germany.*

Title: Interaction of cyclic antimicrobial hexapeptides with model lipid membranes. Supervisor: Prof. Dr. Alfred Blume

2003-2009 *Student at Martin-Luther-Universität Halle-Wittenberg, Halle/Saale, Germany.*

Studies in Biology and Chemistry for teaching A-level students, first state examination, grade: 2.0

Exam thesis title: Interaction of linear polyamines with negatively charged lipid membranes.

grade: 1.0

Supervisor: Prof. Dr. Alfred Blume

2002-2003 *Editor assistant, Berlin, Germany*

„Kroko“, 90min, Sylke Enders, Editor: Frank Brummundt.

„Hab mich lieb“, 90min, Sylke Enders, Editor: Frank Brummundt.

2001-2002 *Student at Philipps University, Marburg, Germany*

Study in Chemistry (diploma)

1992-2001 *Abitur at Edertalschule, Frankenberg/Eder, Germany.*

10.2.1 Scientific Publications

Natarajan, T.S., S. Finger, J. Lacayo-Pineda, E. S. Bhagavatheswaran, S. S. Banerjee, G. Heinrich, and A. Das. 2020. Robust Triboelectric Generators by All-in-One Commercial Rubbers. *ACS Applied Electronic Materials* 12:4054-4064

Finger, S, A. Kerth, M. Dathe, and A. Blume. 2020. The impact of non-ideality of lipid mixing on peptide induced lipid clustering. *Biochimica et biophysica acta (BBA) - Biomembranes* 1862:1832-1848

Sancho-Vaello, E., P. Franois, E.-J. Bonetti, H. Lilie, S. Finger, F. Gil-Ortiz, D. Gil-Carton, and K. Zeth. 2017. Structural remodeling and oligomerization of human cathelicidin on membranes suggest fibril-like structures as active species. *Scientific Reports* 7:15371-15382.

Finger, S., A. Kerth, M. Dathe, and A. Blume. 2015. The efficacy of trivalent cyclic hexapeptides to induce lipid clustering in PG/PE membranes correlates with their antimicrobial activity. *Biochimica et biophysica acta (BBA) - Biomembranes* 1848:2998-3006.

Finger, S., C. Schwieger, A. Arouri, A. Kerth, and A. Blume. 2014. Interaction of linear polyamines with negatively charged phospholipids: the effect of polyamine charge distance. *Biological Chemistry* 395:769-778.

Meister, A.; S. Finger, G.Hause, and A. Blume. 2014. Morphological Changes of Bacterial Model Membrane Vesicles. *European Journal of Lipid Science and Technology* 116:1228–1233.

Khanal, B. P., E. Grimm, S. Finger, A. Blume, and M. Knoche. 2013. Intracuticular Wax Fixes and Restricts Strain in Leaf and Fruit Cuticles. *The New Phytologist* 200:134–143.

10.2.2 Patents published

Sebastian Finger; Martin Kurz; Monika Nawrocka-Herczynska; Tobias Ehmke; Nils Walter Hojdis *Radio unit and device with a radio unit*, **DE102018222380-A1**, Continental Reifen Deutschland GmbH

Sebastian Finger; Martin Kurz; Monika Nawrocka-Herczynska; Tobias Ehmke *Active RFID transponder*, **EP3671527-A1**, Continental Reifen Deutschland GmbH

Sebastian Finger; Nils Walter Hojdis; Menglong Huang *Secondary galvanic cell*, **EP3671932-A1**, Continental Reifen Deutschland GmbH

Fabian Peters; Dieter Jeromin; Mathias Plückers; Sebastian Finger *Vehicle Tire*, **WO2020043407-A1**, Continental Reifen Deutschland GmbH

Sebastian Finger; Frank Fleck; Carla Recker *Crosslinked polymer blends*, **EP3597698-A1**, Continental Reifen Deutschland GmbH

Martin Kurz; Monika Nawrocka-Herczynska; Tobias Ehmke; Sebastian Finger *Electromagnetic transmitter and receiving device*, **EP-3578395-A1**, Continental Reifen Deutschland GmbH

Sebastian Finger; Jorge Lacayo-Pineda; Amit Das; Tamil Natarjan *Pneumatic tire comprising a device for measuring a mechanical force and use of the device*, **WO-2019192809-A1**, Continental Reifen Deutschland GmbH

Emily Baird Anderson, John Dayton Baker, JR., Terri Roxanne Carvagno, Judicael Jacques Chapelet, Wei Min Cheng, Liu Deng, Jacobus Gillis de Hullu, Sebastian Finger, Hubert Hirschlag, Christopher Lee Lester, Wentao Li, Mutombo Joseph Muvundamina, Mark Stanley Pavlin, Fabian Peters, Carla Recker, Christopher Thomas Scilla *Functionalized resin having a polar linker*, **US-2018291124-A1**, Eastman Chemical Company

Emily Baird Anderson, John Dayton Baker, JR., Terri Roxanne Carvagno, Judicael Jacques Chapelet, Wei Min Cheng, Liu Deng, Jacobus Gillis de Hullu, Sebastian Finger, Hubert Hirschlag, Christopher Lee Lester, Wentao Li, Mutombo Joseph Muvundamina, Mark Stanley Pavlin, Fabian Peters, Carla Recker, Christopher Thomas Scilla *Functionalized resin having a polar linker*, **WO-2018191187-A8**, Continental Reifen Deutschland GmbH

Emily Baird Anderson, John Dayton Baker, JR., Terri Roxanne Carvagno, Judicael Jacques Chapelet, Wei Min Cheng, Liu Deng, Jacobus Gillis de Hullu, Sebastian Finger, Hubert Hirschlag, Christopher Lee Lester, Wentao Li, Mutombo Joseph Muvundamina, Mark Stanley Pavlin, Fabian Peters, Carla Recker, Christopher Thomas Scilla *Functionalized resin having a polar linker*, **WO-2018191186-A1**, Eastman Chemical Company

Emily Baird Anderson, John Dayton Baker, JR., Terri Roxanne Carvagno, Judicael Jacques Chapelet, Wei Min Cheng, Liu Deng, Jacobus Gillis de Hullu, Sebastian Finger, Hubert Hirschlag, Christopher Lee Lester, Wentao Li, Mutombo Joseph Muvundamina, Mark Stanley Pavlin, Fabian

Peters, Carla Recker, Christopher Thomas Scilla *Functionalized resin having a polar linker*, **WO-2018191185-A8**, Continental Reifen Deutschland GmbH, Eastman Chemical Company

Mark Arigo, Terri Roxanne Carvagno, Jacobus Gillis de Hullu, Sebastian Finger, Hubert Hirschlag, Janine Klomp, Fabian Peters, Carla Recker, Christopher George Robertson, Peter Versluijs *Modified resins and uses thereof*, **US-2018282444-A1**, Eastman Chemical Company

Mark Arigo, Terri Roxanne Carvagno, Jacobus Gillis de Hullu, Sebastian Finger, Hubert Hirschlag, Janine Klomp, Fabian Peters, Carla Recker, Christopher George Robertson, Peter Versluijs *Modified resins and uses thereof*, **WO-2018187250-A1**, Continental Reifen Deutschland GmbH

Mark Arigo, Terri Roxanne Carvagno, Jacobus Gillis de Hullu, Sebastian Finger, Hubert Hirschlag, Janine Klomp, Fabian Peters, Carla Recker, Christopher George Robertson, Peter Versluijs *Modified resins and uses thereof*, **WO-2018187249-A1**, Continental Reifen Deutschland GmbH, Eastman Chemical Company

Mark Arigo, Terri Roxanne Carvagno, Jacobus Gillis de Hullu, Sebastian Finger, Hubert Hirschlag, Janine Klomp, Fabian Peters, Carla Recker, Christopher George Robertson, Peter Versluijs *Modified resins and uses thereof*, **WO-2018187243-A1**, Eastman Chemical Company

Martin Kurz, Ralf Komischke, Joachim Busche, Norbert Kendziorra, Jens Winkler, Marian Rostek, Sebastian Finger *Vehicle tyre with integrated conductor paths*, **WO-2018095615-A1**, Continental Reifen Deutschland GmbH

Martin Kurz, Holger Dietrich, Tobias Ehmke, Daniel Mohr, Mathias Wenckel, Benjamin Bröker, Sebastian Finger *A device for reading out data, their uses and a pneumatic vehicle tire comprising the device and a method for producing a pneumatic vehicle tire comprising the device*, **DE-102017209552-A1**, Continental Reifen Deutschland GmbH

Martin Kurz, Joachim Busche, Ralf Komischke, Norbert Kendziorra, Jens Winkler, Marian Rostek, Sebastian Finger *Vehicle tire with a tire sensor*, **DE-102017203409-A1**, Continental Reifen Deutschland GmbH

Martin Kurz, Joachim Busche, Ralf Komischke, Norbert Kendziorra, Jens Winkler, Marian Rostek, Sebastian Finger *Vehicle tires*, **DE-102016223298-A1**, Continental Reifen Deutschland GmbH

Martin Kurz, Joachim Busche, Ralf Komischke, Norbert Kendziorra, Jens Winkler, Marian Rostek, Sebastian Finger *Vehicle tires*, **DE-102016222535-A1**, Continental Reifen Deutschland GmbH

11

Statement of originality

Herewith I confirm that this work has not been previously submitted at any university. This thesis is entirely my own work and has been written without any help of others. Where passages from other authors are used the respective sources are cited accordingly.

Sebastian Finger
Hannover, March 2021